Order Number 9334912

Techniques for hydroelastic analysis of very large floating structures

Che, Xiling, Ph.D.

University of Hawaii, 1993

U·M·I
300 N. Zeeb Rd.
Ann Arbor, MI 48106

TECHNIQUES FOR HYDROELASTIC ANALYSIS OF VERY LARGE FLOATING STRUCTURES

A DISSERTATION SUBMITTED TO THE GRADUATE DIVISION OF THE
UNIVERSITY OF HAWAII IN PARTIAL FULFILLMENT
OF THE REQUIREMENTS FOR THE DEGREE OF

DOCTOR OF PHILOSOPHY
IN
OCEAN ENGINEERING

AUGUST 1993

By

Xiling Che

Dissertation Committee:

H. Ronald Riggs, Chairman
R. Cengiz Ertekin
Ronald H. Knapp
Hans-Jürgen Krock
Ludwig H. Seidl

To my dear wife Li Xu

and my son Chunyu Kevin Che

ACKNOWLEDGEMENTS

I would like to express my deepest appreciation to Professor H. Ronald Riggs, my advisor and committee Chairman, without whom this dissertation could never have been completed. I am very fortunate to have Professor H. Ronald Riggs as my advisor during my Ph.D. degree study. I thank him for his extensive guidance, constructive suggestions, and enthusiastic encouragement. I have learned a lot from him, both professionally and personally. I benefitted very much from his knowledge during the daily discussion we have had. His kindness, patience, and support will never be forgotten.

I am grateful to my academic advisor, Professor R. Cengiz Ertekin, for his enthusiastic encouragement, constant inspiration, professional interest, and kind help. I have learned very much from his extensive knowledge in ocean engineering from both the classes he taught and the discussion we have had. I thank him very much for his valuable opinions, suggestions, and comments on this dissertation.

I am also grateful to the other members of my dissertation committee: Professor Ronald H. Knapp, Professor Hans-Jürgen Krock and Professor Ludwig H. Seidl for their advice, suggestions and comments on both my study and dissertation. The comments on this dissertation received from Professor Yingzhong Liu during his visit of the Department of Ocean Engineering in 1993 is appreciated.

The financial support for this study provided by the U.S. National Science Foundation and partially from the Hawaii Natural Energy Institute are acknowledged. The financial support from U.S. National Science Foundation under Grant No. BCS-8911099 and BCS 9200655 has made the dissertation possible. Additional support has also been received from NSF, Grant No. BCS-8958346.

I also wish to acknowledge several people with whom I have worked in the same

research group. They are: Professor Yousheng Wu, my fellow students Shuangxing Du, Dayun Wang and Minglun Wang. Their tremendous contributions to the project benefitted me very much in this study.

Special thanks to Ms. Edith Katada, Secretary of the Department of Ocean Engineering, for her thoughtful help during my stay here. Her patience and enthusiasm made things positively different.

Finally, this dissertation could not have been completed without my wife, Li Xu, who has always encouraged me and has been so patient.

ABSTRACT

Very Large Floating Structures (VLFSs) have been proposed for a number of applications. However, significant amounts of experimental and analytical work are still required before reliable designs of VLFSs can be made. The theme of this study is the development of analytical techniques for hydroelastic analysis of VLFSs in regular waves. Three efficient methods are developed and presented herein.

First, an improved method for two-dimensional hydroelastic analysis is developed by using a formulation consistent with the finite element method. Strip theory is used to calculate the hydrodynamic coefficients and wave exciting forces. The structure below the still water plane is modeled, by the finite element method, as a nonuniform beam subjected to hydrodynamic forces. Above the water surface, a three-dimensional model of the structure is possible.

Second, an efficient method for three-dimensional "hydroelastic" analysis incorporating frame elements with Morison's equation is developed. This approach is applicable to structures which consist of tubular members below the still water line, although there is no restriction on the upper part of the structure. This method is an efficient method for VLFSs which use columns and pontoons below the still water line.

Third, a composite 2D/3D method of hydroelastic analysis is developed for slender VLFSs. The method combines an accurate description of the structure by a three-dimensional structural model and the computational efficiency of a two-dimensional fluid model. The three-dimensional responses can be obtained by this method. In addition, the three-dimensional incident wave exciting force and more accurate

definition of normal vectors are used to improve the results calculated by using two-dimensional potential theory. This method is very useful for analysis of some twin-hull VLFSs with respect to their lower structure. Furthermore, this method is useful for SWATH ship design.

The methods discussed have been implemented in the **HYDRAS** series of computer programs and applied to three floating structures (a multi-module VLFS; a simple, twin-hull structure; and a SWATH ship). The comparisons of the results between the present methods and three-dimensional hydroelasticity are encouraging and show a significant reduction in computations compared with a complete three-dimensional analysis. Therefore, these methods are believed to be useful analytical tools for VLFS design.

TABLE OF CONTENTS

LIST OF TABLES

LIST OF FIGURES

LIST OF SYMBOLS

a_{kj} = sectional two-dimensional hydrodynamic coefficients

C_{fkj} = hydrodynamic damping coefficients

$[C_s]$ = structural damping matrix

$[C_s]^*$ = modal structural damping matrix

$[C_f]^*$ = modal hydrodynamic damping matrix

C = wetted surface of the cross-section

[D] = basic mode shape at a point

$[D_s]$ = basic mode shape of the cross-section

{D} = $ndof \times 1$ nodal displacement vector in global coordinate system

D = two-dimensional fluid domain

{d} = $n_e \times 1$ nodal displacement vector in element local coordinate system

{F} = structural internal force vector

$\{F_c\}$ = distributed surface force vector in the local coordinates

$\{F_f\}$ = fluid load vector

$\{F_f\}^*$ = generalized wave exciting force vector

$\{F_r\}$ = hydrostatic restoring force vector

$\{F_r\}^*$ = modal hydrostatic restoring forces

$\{F_s\}$ = structural load vector that is assembled by the element nodal force vectors

$[F_\Psi]$ = modal force matrix

{f} = generalized cross-sectional wave exciting force vector

$G(P, Q)$ = Green function

g = gravitational acceleration

[k] = element stiffness matrix that is equal to

$[K_s]$ = structural stiffness matrix

$[K_s]^*$ = modal structural stiffness

$[K_f]^*$ = modal hydrostatic restoring matrix

k = wave number

L = length between perpendiculars

L_e = length of beam element

$[\bar{m}]$ = element mass density matrix (can be other density matrix)

$[m]$ = element mass matrix

$[M_f]$ = modal hydrodynamic added mass matrix

M_{fkj} = added mass coefficient

$[M_s]$ = structural mass matrix

$[M_s]^*$ = modal structural mass matrix

M_x = bending moment of the element about x-axis

M_y = bending moment of the element about y-axis

$[N]$ = Shape function matrix which is satisfied $\{u\}=[N]\{d\}$

N_x = membrane force of the element in x-direction

N_y = membrane force of the element in y-direction

ndof = the total number of displacement degrees of freedom

n_e = the number of displacement degrees of freedom of the element

$\{n\}$ = normal vector of wetted surface

$\{n\}^*$ = generalized normal vector

$\{n_b\}^*$ = generalized normal vector for basic modes

$\{p\}$ = principle coordinates

p = fluid pressure

$\{\bar{r}^{ext}\}$ = equivalent nodal force vector in the local coordinates

$\{r^{ext}\}$ = global nodal force vector that satisfies $\{r^{ext}\} = [T]^T \{\bar{r}^{ext}\}$

R = wetted surface area of the right hull of the cross-section

$[S_s]$ = transfer matrix from principal modes to basic modes of the cross-section

t = time

$[T_1]$ = transformation matrix of a general three-dimensional vector $\{A\}$, if $\{\bar{A}\}$ is the same vector in the local coordinate system, one has

$$\{\bar{A}\} = [T_1]\{A\}$$

$[T]$ = transformation matrix, if $\{d_g\}$ is the element displacement vector in the global coordinate system, then $\{d\} = [T]\{d_g\}$

$\{u\}$ = $\{u, v, w\}^T$ the displacement field at a point within an element in local coordinate system

u = horizontal flexible displacement in x-direction

v = horizontal flexible displacement in y-direction

w = vertical flexible displacement in z-direction

x,y,z = coordinates in global coordinate system

y_G, z_G = coordinate y and z of the center of gravity

y^*, z^* = coordinate y and z of the joints between deck and struts

z_w = z-coordinate of the still water plane

z' = $z_w - z$

α = wave amplitude

β = angle between incident wave and structural heading

Γ = wet surface of the structure

γ^j = the ratio of the length between two vectors

θ^j = the angle between two vectors

λ_{kj} = two dimensional sectional hydrodynamic damping coefficient

μ_{kj} = two dimensional sectional added mass coefficient

$\{\zeta\}$ = principle coordinates of basic modes

ρ = water density

$\{\sigma\}$ = structural stress vector

$[\Sigma_\Psi]$ = modal stress matrix

Φ_T = total velocity potential

Φ = time independent part of total potential

ϕ_I = incident wave potential

ϕ_D = diffraction wave potential

ϕ_j = jth radiation wave potential

$[\psi]$ = 'dry' mode shapes at any point in global coordinate system

$[\bar{\psi}]$ = 'dry' mode shapes at any point in local coordinate system

$\{\psi_j^c\}$ = jth 'dry' mode shape at the center of quadrilateral element in global coordinate system (only contains three translational components)

$\{\bar{\psi}_j^c\}$ = jth 'dry' mode shape at the center of quadrilateral element in local coordinate system (only contains three translational components)

$[\bar{\psi}_n]$ = element nodal 'dry' mode shapes in local coordinate system

$[\Psi]$ = structural mode shapes

ω = wave frequency

ϖ = natural frequency of undamped structure

CHAPTER 1

INTRODUCTION

1.1 Overview

Numerous proposals have been made for very large floating structures (VLFSs) for ocean space utilization and ocean resource development. Proposed uses include floating airports and runways (Takarada, 1984; Lemke, 1987; Baschieri and Bellincioni, 1991; Chow et al., 1991); wave power generation (Katory, 1977); deep ocean miming (Winkler et al., 1990; Cruickshank, 1991); ocean thermal energy conversion (OTEC) (Nihous and Vega, 1993); and floating 'cities' (St. Denis, 1974; Yoshida et al., 1991). The largest of all VLFS applications would likely be a floating airport, which might have plan dimensions on the order of $1,000 \text{ m} \times 3,000 \text{ m}$. By comparison, the plan dimensions of the largest floating platforms used in the offshore oil industry are approximately $100 \text{ m} \times 100 \text{ m}$.

VLFSs, whether for public use (for example, airport or floating city) or for industrial facilities (for example, OTEC or deep ocean miming), will have a long service life, and their safety, reliability, and survivability are vital for their economic feasibility. Both experimental data and analytical methods will be very important for the design of a VLFS. The development of analytical tools and experimental methods which are reliable and robust is likely to require a considerable amount of time (Wilkins et al., 1992). The work described here concentrates on the development of analytical methodologies for the hydroelastic analysis of VLFSs.

The analysis of VLFSs differs substantially from that of a conventional structure because the motion of the latter is usually determined based on rigid body dynamics. This approach is insufficient for the much larger VLFS. Hence, much of the

methodology has either not been developed, needs further development, or is not oriented toward large scale systems (Riggs, 1991).

The size of a VLFS requires an alternative analysis methodology than that used for conventional floaters. Two basic characteristics of a VLFS must be considered in the methodologies for VLFSs: the flexibility and the huge dimensions. VLFSs, whether constructed from a series of modules hinged together or rigidly connected together, will behave in the open ocean as a flexible body, and the structural displacements as a result of the deformational response will generate significant hydrodynamic forces on the structure. Hence, traditional hydrodynamic theory based on rigid body motion is no longer sufficient for dynamic analysis of VLFSs. Instead, hydroelasticity theory must be used to determine the structural displacements and forces induced by wave action. Since a VLFS must be modeled as a flexible structure, the number of degrees of freedom will become huge. A very large computational problem for the fluid dynamics also results from the large dimensions. Therefore, efficient methodologies for hydroelastic analysis of VLFSs need to be developed.

The techniques developed in this work will reflect the above two basic characteristics. All the techniques treat the structure as a flexible body and hydroelasticity theory is involved. Efficiency is the basic feature of the methods developed in this work. While all techniques are oriented toward VLFSs, they are also applicable to general floating structures and other offshore structures.

1.2 Very large floating structures

VLFSs, when constructed, will be the largest and most expensive structures ever built. Physically, a VLFS will have large dimensions to accommodate significant human activity. A proposed floating city, shown in Figs. 1.1 and 1.2, requires 1,100,000 m^2 to allow 30,000 people to work and live on it (Yoshida et al., 1991). Proposed floating

airports, such as in Fig. 1.3, have varied from a few hundred meters in length to several thousand meters.

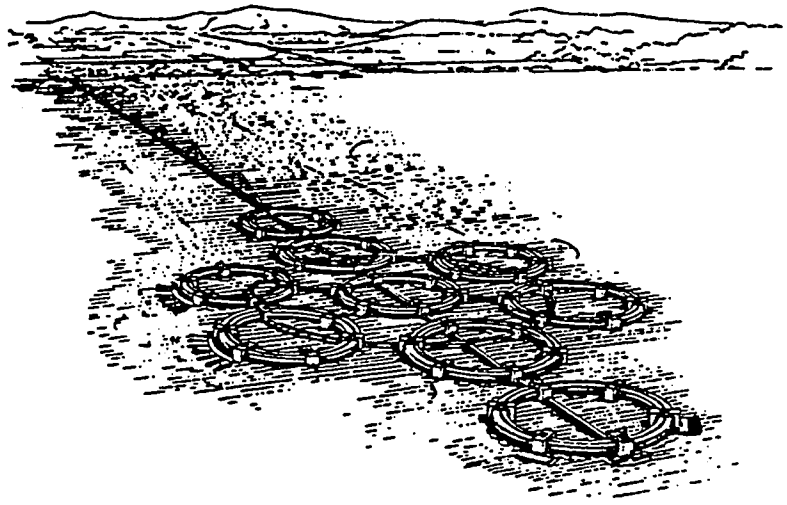

Figure 1.1 Business floating city complex by using ring-like semisubmersible (Yoshida et al., 1991)

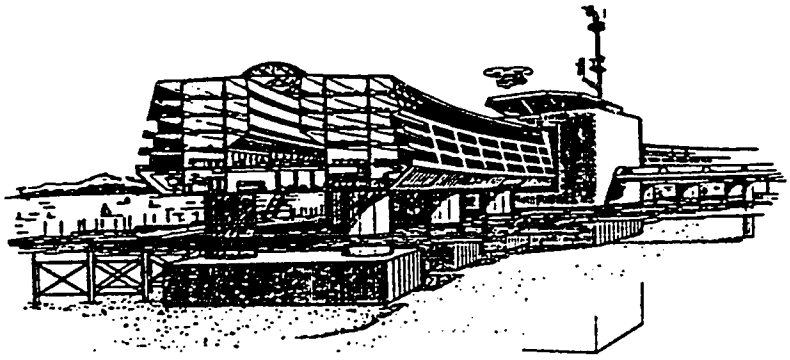

Figure 1.2 Section of ring-like semisubmersible (Yoshida et al., 1991)

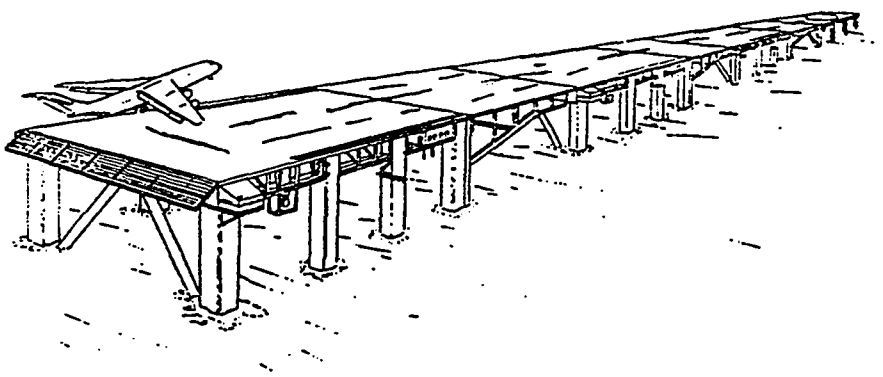

Figure 1.3 Floating airfield (Bretz et al., 1991)

The huge size is one of the significant characteristics of VLFSs. Based on data for existing semisubmersibles, a 'module' of 100 m × 100 m plan dimensions may be considered within the capability of existing floating structure technology, exemplified by modern floating drilling units. They usually use a semisubmersible hull design, which have two or more pontoons to provide buoyancy and columns to provide stability and support the superstructure. These shapes have smaller wave forces and motions than ships have because of their transparency and the relatively small hull area near the water surface. The successes of semisubmersibles make them candidates for constructing VLFSs. To provide a large space, a VLFS may be built-up from multiple modules connected side by side. Winkler et al. (1990) developed a basic module design (Fig. 1.4), 100 m × 100 m, which could be used to assemble alternative VLFSs, depending on the application.

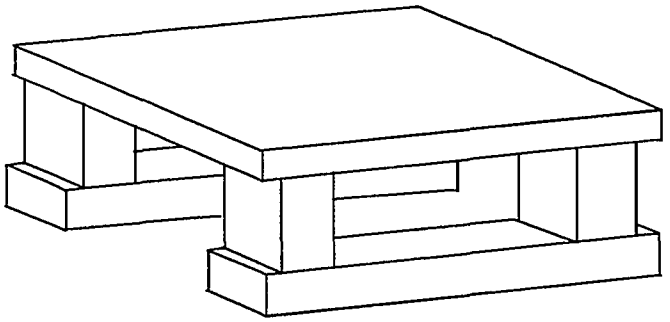

Figure 1.4 Schematic of a basic module design

The large size of a VLFS means the flexibility will be increased as compared to smaller, more 'rigid' structures. Hence, as mentioned before, the flexibility is another significant characteristic of a VLFS.

There is not a well-accepted definition of what constitutes a very large floating structure. Since this work focuses on development of methodologies, the definition proposed by Riggs (1991) is adopted: A VLFS is a floating structure whose characteristics, especially its size and flexibility, require for its design, construction, and operation special consideration not required by conventional-size floating structures. The techniques of analysis of VLFS developed in this work will be based on this definition.

1.3 Previous work on hydroelastic analysis of VLFS

Conventional hydrodynamics theory assumes that the structural motion as a result of deformational response does not affect hydrodynamic forces. While this assumption is most likely appropriate for many 'small size' structures, it will tend to breakdown as

structures increase in size and flexibility. Therefore, the formulation of hydrodynamics based on rigid-body motion is unsuitable for VLFSs. The size and flexibility of VLFSs require an alternative analysis methodology than that used for conventional floating structures.

Substantial work has been carried out in the last twenty years on the development of two-dimensional and three-dimensional hydroelasticity theories. Two-dimensional hydroelasticity is primarily applied to ship structures (Bishop and Price, 1979). Due to the huge dimensions, efficient two-dimensional hydroelasticity is attractive for the dynamic analysis of VLFS. Early application of two-dimensional hydroelasticity theory to large floating structures can be found in Okamoto et al. (1985) and Masuda et al. (1987).

The first application of strip theory to a multi-hull and multi-module VLFS appears to be by Che et al. (1990), and Ertekin et al. (1990). In their work, the rigid module, flexible connector model (RMFC) is proposed for the case in which the module is much stiffer than the connector. Application of using two-dimensional strip theory to VLFSs are then reported by Ertekin et al. (1991), Hamida and Webster (1991), Riggs et al. (1991), Wang et al. (1991), and Riggs and Ertekin (1993). A deficiency in this method is that because two-dimensional flow is assumed, the out-of-plane fluid forces, which may be particularly important for semisubmersible hulls, are not modeled, which can result in substantial error. Riggs and Ertekin (1993) used Morison's equation to represent the out-of-plane fluid forces to improve significantly the results. Another method to improve two-dimensional hydroelasticity considers the transverse deformation of the cross-section by a hybrid approach (Wang, 1991).

Three-dimensional hydroelasticity theory has also been applied to VLFSs. Che et al. (1990) and Ertekin et al. (1990) used the RMFC model and the three-dimensional

hydrodynamic coefficients and wave exciting forces for a single module, ignoring the fluid interaction between modules. Du and Ertekin (1991), Wang et al. (1991), and Ertekin et al. (1993) extended this approach to include the hydrodynamic interaction between modules. This approach was used for the hydroelastic analysis of a 100m × 1600m airfield by Ertekin et al. (1993), which appears to be the largest floating structure considered in a three-dimensional analysis. To reduce the computational requirements, the single-symmetry and double-symmetry of the structure were exploited by using the single-plane and double-plane composite source distribution method (Wu et al., 1993). In the single-plane composite source distribution method, the calculation domain of the fluid problem only involves one-half of the wetted surface (Wu, 1984), while in the double-plane composite source distribution method, only one-quarter of the wetted surface is considered.

Using single or double symmetry source distribution methods can reduce significantly the computational effort. Another efficient method to improve the three-dimensional source distribution method, called iterative source distribution technique, was proposed by Seidl (1991). The method allows, in principle, any number of surface facets to be employed in the analysis. Initially a coarse grid is employed. Consecutive iterations are performed (automatically) by subdividing a certain number of facets with each iteration.

A useful resource for detailed information on recent developments in VLFS-related work can be found in the Proceedings of the First International Workshop on Very Large Floating Structures (Ertekin and Riggs, 1991).

1.4 Objective and scope of work

The objective of this research is to develop efficient techniques for hydroelastic analysis of very large floating structures. Several different structural and fluid models

are involved for the different types of VLFSs. Based on the above definition of a VLFS, these techniques will specially consider the size and flexibility.

The well-developed hydrodynamic theory is the fundamental theory for solving the hydrodynamic fluid problems. Existing two-dimensional and three-dimensional hydroelasticity theories provide a basis for the hydroelastic analysis of flexible floating structures. Therefore, they are reviewed in Chapter 2.

The fundamental formulations of structural mechanics, fluid dynamics and their coupling, the key to hydroelasticity, are reviewed in Chapter 3.

The basic concept and formulation for three-dimensional hydroelasticity and the general formulation for three-dimensional hydrostatic restoring coefficients are given in Chapter 4. As mentioned previously, three-dimensional hydroelasticity theory is the most general and accurate theory to date. Therefore, this theory is also described in this work for completeness, specially for the coupling problem between structure and fluid. As an example, quadrilateral fluid panels are coupled with quadrilateral thin shell elements for the structure. The computer program **HYDRAS3D-I**, which performs the coupling between structure and fluid, has been developed. The brief description of this program can be found in Section B.5.

In Chapter 5, an alternative analysis method for two-dimensional hydroelasticity is developed by using a consistent formulation for both hydrodynamic forces and hydrostatic restoring coefficients. Strip theory is used to calculate the hydrodynamic coefficients and wave exciting forces. The structure below the still water plane is modeled, by the finite element method, as a nonuniform beam subjected to hydrodynamic forces. Above the water surface, a three-dimensional model of the structure is possible. Hydrodynamic matrices for added mass and damping, and wave exciting force vectors are formed directly in the same manner as the structural mass

matrix and structural force vector. The resulting coupled equations of motion are solved directly. The method is applicable to slender VLFSs with any stiffness distribution. This method is applicable to several different structural models, such as a fully elastic model; a rigid module, flexible connector model (RMFC); or elastic module, flexible connector model (EMFC). In addition, the hydrostatic restoring stiffness for the beam element is also derived. The method has been implemented in the computer program **HYDRAS-2D**. The brief description of this program can be found in Section B.1. The method is applied to a multi-module VLFS model.

In Chapter 6, a three-dimensional frame model to incorporate the elasticity of the structure is introduced. Morison's equation (Morison et al., 1950) is used to determine the fluid loading. This approach is applicable to structures which consist of tubular members below the still water line. There is no restriction on the upper part of the structure. Morison's equation includes the effects of fluid acceleration and viscous form drag in terms of empirically determined coefficients. Since the three-dimensional potential problem is avoided, Morison's equation is an efficient method for VLFSs which use tubular columns and pontoons below the still water line. In addition, the hydrostatic restoring stiffness matrix for a frame element is also derived. The method has been implemented in the computer program **HYDRAS-MORISON**. The brief description of this program can be found in Section B.2. The method is applied to a multi-module VLFS model.

In Chapter 7, a composite 2-D/3-D hydroelasticity approach is developed for slender VLFSs. A three-dimensional structural model and a two-dimensional fluid model are combined to obtain a new, efficient method. The method includes an accurate description of the structure by a three-dimensional structural model and the computational efficiency of a two-dimensional fluid model. Therefore, the responses are

not limited to the beam-like response of traditional two-dimensional hydroelasticity. In addition, since a three-dimensional structural model is used, some modifications to the two-dimensional flow problem can be made. For example, the three-dimensional incident wave exciting force can be obtained based on the three-dimensional structural model. This new method is very useful for the analysis of some twin-hull VLFSs. Furthermore, this method is also useful for SWATH (Small Water plane Area Twin-Hull) ship design. The method has been implemented in the computer program **HYDRAS-COMPOSITE**. The brief description of this program can be found in Section B.3. The method is applied to a simple, twin-hull structure and a SWATH ship.

Chapter 8 discusses three VLFS models for which the methods developed herein are applied. These structural models include a multi-module VLFS; an idealized twin-hull structure used to verify the composite 2-D/3-D method; and a SWATH ship model. The results obtained with the methods developed in this work, together with a comparison with the results from general three-dimensional hydroelasticity, can be found in Chapter 9. Conclusions and recommendations for future work are made in Chapter 10.

CHAPTER 2

BASIC CONCEPTS IN HYDROELASTICITY

2.1 Hydroelasticity

A formal definition of hydroelasticity was proposed by Heller and Abramson (1959): "hydroelasticity is concerned with the phenomena involving mutual interaction among inertial, hydrodynamic, and elastic forces." The difference between this definition and the traditional hydrodynamics is that hydroelasticity theory includes the elasticity of the structure in the fluid-structure interaction problem. Therefore, two advantages can be found in hydroelasticity theory. First, additional to the rigid body motion, the elastic deformation of the structure is also considered in the wave generation. This reflects the real situation so that more accurate results can be expected. Second, the coupled structural dynamics and hydrodynamics problems are solved simultaneously. This overcomes the disadvantage of the traditional two-step solution process (Ogilvie, 1971). Hence, even for stiffer structures, hydroelasticity theory provides a general and unified approach for dynamic analysis of ocean structures.

Briefly, the basic approach of hydroelasticity is to model the structure as an elastic body (e.g., with the finite element method). The linear potential theory is used to obtain the dynamic fluid pressure caused by waves and structural motion and deformation. The structural and fluid problems are interfaced by the kinematic continuity condition on the structural wetted surface. The hydrodynamic and hydrostatic pressures can be used to form the fluid loads. The structural responses can then be obtained by solving the coupled equations of motion.

Two solution techniques are used to determine hydroelastic response. One technique is based on modal superposition. In this approach, the structural motion is represented

by a linear combination of the normal modes of vibration of the structure in air ('dry modes'). The radiation potential is obtained as a linear combination of the radiation potentials for each mode. Modal structural properties and fluid properties are used to form the modal equations. The second approach may be called a direct approach. In this approach, the distribution of fluid forces are defined. Similar to that in the finite element method, these distribution of fluid forces can be used to form consistent fluid coefficient matrices and force vectors. The equations of motion are directly solved to obtain the physical responses.

Although hydroelasticity theory has many advantages over conventional hydrodynamics, this theory has not been widely applied in the design of floating structures. In addition, for a VLFS, numerically efficient techniques for hydroelastic analysis need to be developed.

2.2 Basic assumptions

In this work, linear structural dynamics theory is used for the structure. Methods based on both the linear potential theory (ideal fluid) and Morison's equation method are developed. The following assumptions are made.

The structure is assumed to respond linearly, which implies that the stiffness matrix and the load vector are independent of the displacements. This assumption requires both linear, elastic material and (infinitesimally) small displacements. Linear structural dynamics is applicable.

The structure is assumed to be freely floating and stationary (that is, with zero forward speed). A global coordinate system (x-y-z), with the z-axis directed upward, is used to describe the geometry and position. The hydrodynamic forces result from a train of regular waves with a crest at x=0 (at time t=0), an incidence angle of β about the x-axis, and propagating in the +x-direction, and also from the resultant motion of the

structure. For linear potential theory, the structure is partially submerged in an incompressible and inviscid fluid undergoing irrotational flow in infinitely deep water. For Morison's equation, the viscous form drag in terms of empirically determined coefficients is considered.

2.3 Hydrodynamics

Hydrodynamics provides a basis for hydroelasticity. Hydrodynamics originated in the fields of ship design and marine technology. An in depth discussion of hydrodynamics in marine technology can be found in *Marine Hydrodynamics* by Newman (1977). Ship hydrodynamics has been extended to apply to offshore structures. Representative topics in this area can be found in *Hydrodynamics of Offshore Structures* by Chakrabarti (1987), which has an extensive list of references on the subject.

Hydrodynamics based on linear potential theory has been developed to a high level. In this area, two-dimensional hydrodynamics (strip theory) has been especially well-developed. Significant work includes the ordinary strip theory (Korvin-Kroukovsky and Jacobs, 1957; Jacobs, 1958), the rational strip theory (Ogilvie and Tuck, 1969), and the revised ordinary strip theory (Salvesen, Tuck and Faltinsen, 1970). Strip theory is widely accepted in naval architecture and offshore engineering because of its computational efficiency and satisfactory agreement with experiments for rigid-body motions, and it is still used to predict ship motions. However, since two-dimensional flow is assumed in strip theory, no interaction is considered in the longitudinal direction. Therefore, strip theory is only applicable to slender structures.

Three-dimensional linear potential theory has been developed and used in three-dimensional hydrodynamics. Three-dimensional linear potential theory is applicable to an arbitrary shaped body. The interactions between various parts of the whole structure are rigorously treated. That is, the diffraction and radiation fluid motions are based on

the entire structural body boundary. This leads to more accurate predictions of the hydrodynamic pressure distribution and the estimations of wave exciting forces and moments. Three-dimensional potential theory for rigid body motion has been discussed in detail by Newman (1978) and Wu (1984), for example.

An essential feature of all two-dimensional and three-dimensional hydrodynamics based on potential theory is that the structure is assumed to be rigid. Hence, only rigid body motions can be predicted by conventional hydrodynamics. The internal forces and stresses are determined by applying to the structure the fluid pressures and inertial forces calculated in the hydrodynamic analysis for rigid-body motion. Therefore, this theory is most likely appropriate for conventional structures but not for large, flexible structures.

2.4 Existing hydroelasticity theories

The concept of hydroelasticity, which was introduced in the late 1950's by analogy to aeroelasticity, has been discussed in several excellent monographs (Flax, 1960; Heller, 1964; Kito, 1970). The application of hydroelasticity in marine hydrodynamics has received more attention after Bishop and Price's work (1979). An extensive list of references on hydroelasticity theory may be found in Wu (1984).

A significant contribution to two-dimensional hydroelasticity was made by the research group of Bishop and Price. Two-dimensional hydroelasticity, based on strip theory, is first introduced by Betts, Bishop, and Price (1977) to represent the generalized hydrodynamic forces as an essential step in a unified dynamic analysis of ship response to waves. A relatively complete presentation of two-dimensional hydroelasticity is found in *Hydroelasticity of Ships* by Bishop and Price (1979).

Mode superposition is usually used in two-dimensional hydroelastic analysis. Before 1974, the 'wet modes' were employed. The calculation of 'wet modes' involves not only the mechanical properties of the structure but also the fluid actions which makes the

calculations more complicated. Later, Bishop and Price (1974) pointed out that by employing the structural mode shapes in air ('dry modes'), the calculations are simplified. In addition, the orthogonality of the 'dry modes' can be used to simplify the mode superposition procedure. In 1976, Bishop and Price (1976) examined the relationship between employing dry modes and wet modes.

Briefly, in two-dimensional hydroelasticity, as formulated by Bishop and Price (1979), the structure is modeled as a nonuniform Timoshenko beam, while the hydrodynamic forces are calculated from strip theory. The continuous beam structural displacement is represented by a set of mode shapes to reduce the degrees of freedom. The modal fluid forces are calculated for each mode and then applied to the structure to obtain the principal coordinates. Symmetric structural motions are excited by the vertical (heave) hydrodynamic forces and antisymmetric motions are excited by the horizontal (sway and roll) hydrodynamic forces.

An essential feature of two-dimensional hydroelasticity is that the structure is assumed to be 'beam-like'. Only beam-like motion, deformation, and corresponding forces and moments can be predicted by this theory. Another limitation is that the structure must be slender, because the hydrodynamic forces are calculated by two-dimensional strip theory. Therefore, this theory can not be applied to an arbitrary structure.

A general linear hydroelasticity theory was developed by Wu (1984). This theory is based on conventional three-dimensional hydrodynamic theory. Therefore, it is applicable to any arbitrary-shaped structure. An elastic structural model is used to represent the structural motion and deformation, for which the finite element method is used. Mode superposition is used, and the external fluid forces are expressed in terms of the generalized forces corresponding to a set of principal modes. The radiation

potentials resulting from structural deformation are first directly calculated in this theory. Three-dimensional hydroelasticity theory is the most general and accurate theory to date.

Although two-dimensional hydroelasticity has limitations, it is a very efficient method, especially for large structures. Therefore, at the early design stage, this theory can be used to provide basic data for design of slender structures. On the other hand, the calculation of the three-dimensional velocity potential is computationally very time consuming. It requires significant computer memory and CPU time. As such, it is probably most useful as a final design tool.

CHAPTER 3

FUNDAMENTAL FORMULATIONS FOR HYDROELASTICITY

3.1 Overview

It is well known that the interaction between the structure and the fluid may be very significant. The fluid forces come not only from waves and currents, but also from structural motions, and the behavior of the structure in water is much different from that in air. This interaction complicates the dynamic analysis of offshore structures.

Structural dynamics has been studied extensively as evidenced by the large number of textbooks and papers on the subject. The finite element method, which has been used in structural mechanics and structural dynamics for several decades, provides a powerful tool to establish the structural model in offshore structural analysis. The well-known structural mode-superposition method has been applied to simplify the analysis of large structural systems. These developments in structural dynamics provide the fundamental theory for hydroelastic analysis of offshore structures.

Hydrodynamics has also been well developed. The linear potential theory has been used in the motion response of offshore structures for many years. In addition, the principle of superposition has also been applied to the ship-motion problem (St. Denis and Pierson, 1953). The most difficult aspect of hydroelasticity is to determine the coupling of the fluid and structural problems.

The general formulations for hydroelasticity are given in this chapter. The pertinent aspects of structural mechanics are reviewed first. The fluid dynamics, in particular linear potential theory and Green function method, are then discussed for the purpose of determining the fluid loads for hydroelastic analysis. Finally, the coupling of structural dynamics and hydrodynamics is introduced.

3.2 Structural mechanics

The study of hydroelasticity of offshore structures is primarily for structural analysis and design. The goal of this study is to provide structural responses, such as structural motions and deformations, internal forces, and strains and stresses under the fluid actions, for engineering design. Therefore, the equations of structural mechanics are used to form the foundation, and the hydrodynamic forces are expressed such that they can be easily fitted into the formulations for structural analysis. In fact, very little work in hydrodynamics has been done from a structural design viewpoint. For this reason, the linear theory of structural dynamics, finite element formulations, and mode superposition method are discussed in this section.

3.2.1 Dynamic equations of motion

The finite element method is used for structural dynamic analysis. In this case, the equations of motion for the linear dynamic response of a structure can be written as

$$[M_s]\{\ddot{D}(t)\} + [C_s]\{\dot{D}(t)\} + [K_s]\{D(t)\} = \{F_f(t)\} + \{F_r(t)\} + \{F_s(t)\} \tag{3.1}$$

in which $[M_s]$, $[C_s]$, and $[K_s]$ are the $ndof \times ndof$ structural mass, damping, and stiffness matrices, respectively; $ndof$ is the number of displacement degrees-of-freedom; $\{\ddot{D}(t)\}$, $\{\dot{D}(t)\}$, and $\{D(t)\}$ are the $ndof \times 1$ vectors of nodal accelerations, nodal velocities, and nodal displacements, respectively; $\{F_f(t)\}$ is the $ndof \times 1$ vector of hydrodynamic forces; $\{F_r(t)\}$ is the $ndof \times 1$ vector of hydrostatic restoring forces; and $\{F_s(t)\}$ is the structural load vector (i.e., loads which are not fluid related, such as from machinery vibration). Structural weight and buoyancy forces, in equilibrium, are excluded from Eq. 3.1. That is, the displacements are measured from the static

equilibrium position.

Eq. 3.1 represents a system of linear, second order, ordinary differential equations which govern the motion in the time domain. Superposition can be used to decompose Eq. 3.1 into two equations: one related to structural loads, and the other to the fluid loads. In this study, only the equations which are related to the fluid loads are considered here

$$[M_s]\{\ddot{D}_f(t)\} + [C_s]\{\dot{D}_f(t)\} + [K_s]\{D_f(t)\} + [K_f]\{D_f(t)\} = \{F_f(t)\} \quad (3.2)$$

where $\{D_f(t)\}$ is the vector of nodal displacement vector caused by fluid loads. The restoring forces have been expressed by $\{F_r\} = -[K_f]\{D(t)\}$, where $[K_f]$ is the hydrostatic restoring stiffness matrix which will be discussed later. For convenience, $\{D_f(t)\}$ is replaced by $\{D(t)\}$ in the following.

The structure is assumed to be excited by a train of regular, long-crested waves with frequency ω and a crest at x=0 (at time t=0). The resulting linear fluid forces, $\{F_f(t)\}$, are most conveniently determined in the frequency domain. The response of a structure to regular, harmonic excitation of the form

$$\{F_f(t)\} = \{F_f\}e^{-i\omega t} \quad (3.3)$$

in which $i = \sqrt{-1}$, can be represented as

$$\{D(t)\} = \{D\}e^{-i\omega t} \quad (3.4)$$

$\{D\}$ and $\{F_f\}$ are time independent, and, in general, they are complex quantities. Substitution of Eqs. 3.3 and 3.4 into 3.2 results in

$$(-\omega^2[M_s] - i\omega[C_s] + [K_s] + [K_f])\{D\} = \{F_f\} \quad (3.5)$$

Eq. 3.5 will be considered first from a structural dynamics viewpoint and then from a hydrodynamics viewpoint.

3.2.2 Finite element formulation

The finite element method is firmly established as a powerful and popular analysis tool, especially for structural mechanics. Since the floating structure will be modeled by the finite element method for hydroelastic analysis, the basic concept and procedure of this method are reviewed here. The Euler-Bernoulli beam element is used as an example.

The most popular finite element approach is based on an assumed displacement field (see Cook et al., 1989). The most straightforward formulation of the equations is at the element level. As such, it is convenient to define a local (element) coordinate system $(\bar{x}, \bar{y}, \bar{z})$, as distinguished from the global (structural) coordinate system (x,y,z). The displacement vector $\{u\}$, which usually contains the three translational displacement components, is written in the local coordinate system as $\{u\} = \{u, v, w\}^T$. It is assumed that the displacements $\{u\}$ can be adequately interpolated from $\{d\}$, the vector of the element nodal displacements in the local coordinate system:

$$\{u\} = [N] \{d\} \tag{3.6}$$

where [N] is the matrix of interpolation functions. It should be pointed out here that Eq. 3.6 can be used to calculate the displacements at any point $(\bar{x}, \bar{y}, \bar{z})$ within the element provided that the nodal displacements $\{d\}$ have been obtained. (The displacements within the element will be required later to form the body boundary conditions for the fluid problem.) The interpolation functions depend on the element type, as does the dimension of the nodal displacement vector. At this point, the formulation is general and the particular element type need not be specified.

The velocity vector $\{\dot{u}\}$ can be written, noting that the interpolation functions are independent of time, as

$$\{\dot{u}\} = [N] \{\dot{d}\} \tag{3.7}$$

and the acceleration vector $\{\ddot{u}\}$ can be written as

$$\{\ddot{u}\} = [N] \{\ddot{d}\} \tag{3.8}$$

The element strain vector $\{\varepsilon\}$ is obtained from displacements by differentiation:

$$\{\varepsilon\} = [\partial] \{u\} \tag{3.9}$$

where $[\partial]$ is a differential operator matrix obtained from the strain-displacement relations. With Eq. 3.6, Eq. 3.9 yields

$$\{\varepsilon\} = [B] \{d\} \tag{3.10}$$

where [B] is the strain-displacement matrix:

$$[B] = [\partial] [N] \tag{3.11}$$

The constitutive relations are represented by

$$\{\varepsilon\} = [C] \{\sigma\} \quad \text{or as} \quad \{\sigma\} = [E] \{\varepsilon\} \tag{3.12}$$

where $\{\sigma\}$ is the element stress vector; [C] is a matrix of material compliances; [E] is a matrix of material stiffnesses, and $[E] = [C]^{-1}$.

Equations that govern the dynamic response of a structure or medium will be derived by using the principle of virtual displacements (see for example, Bathe and Wilson, 1976). This principle states that the equilibrium of the body requires that for any compatible, small virtual displacements, $\{\delta u\}$, imposed onto the body, the total

internal virtual work is equal to the total external virtual work.

To use the principle of virtual displacements, the inertial force and damping force need to be defined. If the diagonal matrix $[\bar{m}]$ is defined such that the three translational mass densities are on the diagonal, then the inertial force (per unit volume) can be written as $[\bar{m}]\{\ddot{u}\}$. The energy-loss mechanisms are not well understood and the actual damping mechanism is usually approximated by viscous damping. Thus, it is assumed that the structural damping forces are proportional to the relative structural velocities. If $[\kappa_d]$ is used as a material-damping parameter matrix analogous to viscosity, the structural linear damping forces (per unit volume) can be written as $[\kappa_d]\{\dot{u}\}$.

The principle of virtual displacements, for a single element, requires

$$\int_{V_e} \{\delta u\}^T \{F_b\}\, dV + \int_{S_e} \{\delta u\}^T \{F_c\}\, dS + \sum_{i=1}^{n} \{\delta u_i\}^T \{p_i\} + \{\delta d\}^T \{F_{int}\} = \int_{V_e} (\{\delta\varepsilon\}^T \{\sigma\} + \{\delta u\}^T [\bar{m}]\{\ddot{u}\} + \{\delta u\}^T [\kappa_d]\{\dot{u}\})\, dV \tag{3.13}$$

where $\{\delta u\}$, $\{\delta\varepsilon\}$ and $\{\delta d\}$ are small, arbitrary, compatible virtual displacement, strain and nodal displacement vectors, respectively; $\{F_b\}$ are the body forces; $\{F_c\}$ are the surface tractions; $\{p_i\}$ are concentrated loads that act at a total of n points on the element; $\{\delta u_i\}$ is the virtual displacement vector of the point at which load $\{p_i\}$ is applied; $\{F_{int}\}$ is the internal forces at the nodes; the volume integration is carried out over the element volume V_e; and the surface integral is carried out on the element surface S_e.

Substitution of Eqs. 3.6, 3.7, 3.8, 3.10, and 3.12 into Eq. 3.13 results in

$$\{\delta d\}^T [\int_{V_e} [B]^T [E] [B] dV \{d\} + \int_{V_e} [N]^T [\bar{m}] [N] dV \{\ddot{d}\} + \int_{V_e} [N]^T [\kappa_d] [N] dV \{d\}] = \{\delta d\}^T \left[\int_{V_e} [N]^T \{F_b\} dV + \int_{S_e} [N]^T \{F_c\} dS + \sum_{i=1}^{n} [N_i]^T \{p_i\} + \{F_{int}\} \right] \quad (3.14)$$

in which $[N_i]$ is the interpolation function matrix evaluated at the coordinates of the point at which load $\{p_i\}$ is applied. Since $\{\delta d\}$ is arbitrary, Eq. 3.14 can be written as

$$[m] \{\ddot{d}\} + [c] \{d\} + [k] \{d\} = \{r^{ext}\} + \{r^{int}\} \quad (3.15)$$

where the element mass matrix [m], damping matrix [c], and stiffness matrix [k], in the local coordinate system, are defined as

$$[m] = \int_{V_e} [N]^T [\bar{m}] [N] dV \quad (3.16)$$

$$[c] = \int_{V_e} [N]^T [\kappa_c] [N] dV \quad (3.17)$$

$$[k] = \int_{V_e} [B]^T [E] [B] dV \quad (3.18)$$

the external load vector $\{r^{ext}\}$ is defined as

$$\{r^{ext}\} = \int_{V_e} [N]^T \{F_b\} dV + \int_{S_e} [N]^T \{F_c\} dS + \sum_{i=1}^{n} [N_i]^T \{p_i\} \quad (3.19)$$

and the internal force vector $\{r^{int}\}$ is equal to $\{F_i\}$, which will be canceled when

elements are assembled.

The element mass matrix [m] and damping matrix [c] in Eqs. 3.16 and 3.17 are called the consistent mass and consistent damping matrices. These matrices are symmetric, as is the element stiffness matrix. Generally, the consistent matrices [m] and [c] are positive definite. That is, using the mass matrix as an example, the kinetic energy $\frac{1}{2}\{d\}^T[m]\{d\}$ is positive for any nonzero velocity vector $\{d\}$.

Often, the element matrices are formed in element local coordinates. Hence, the assembly of the element matrices to form the structural matrices includes the coordinate transformation from local coordinate $(\bar{x}, \bar{y}, \bar{z})$ to the global structural coordinates (x,y,z):

$$[m_e] = [T]^T[m][T] \qquad [c_e] = [T]^T[c][T] \qquad [k_e] = [T]^T[k][T] \tag{3.20}$$

where [T] is a transformation matrix. [T] is a block diagonal matrix with matrix $[T_1]$ on the diagonal. $[T_1]$ is defined such that

$$\{\bar{A}\} = [T_1]\{A\} \tag{3.21}$$

in which $\{\bar{A}\}$ and {A} are, respectively, the vectors of components in the local and global coordinate system of an arbitrary vector. $[m_e]$, $[c_e]$, and $[k_e]$ are element mass, damping and stiffness matrices, but in the global coordinate system. The local element load vectors can be transformed to the global element load vectors as

$$[r_e^{ext}] = [T]^T\{r^{ext}\} \tag{3.22}$$

The structural matrices [M], [C], and [K] are constructed by the conceptual expansion of element matrices $[m_e]$, $[c_e]$, and $[k_e]$ to 'structural size' followed by addition, which can be written symbolically as

$$[M_s] = \sum_{e=1}^{nelm} [m_e] \qquad [C_s] = \sum_{e=1}^{nelm} [c_e] \qquad [K_s] = \sum_{e=1}^{nelm} [k_e] \tag{3.23}$$

The global structural load vector $\{F\}$ can be assembled in the same manner from the element load vectors $\{r_e^{ext}\}$.

$$\{F\} = \sum_{e=1}^{nelm} \{r_e^{ext}\} \tag{3.24}$$

where *nelm* is the number of elements.

3.2.3 Three-dimensional frame element- an example

Since the three-dimensional frame element, shown in Fig. 3.1, is frequently used in the following chapters, it is discussed in detail here. $(\bar{x}, \bar{y}, \bar{z})$ is the element local coordinate system, in which the $\bar{x}$ axis is directed from node i to node j; and $\bar{y}$ and $\bar{z}$ are principal axes of the beam cross section. Each node has 6 displacement degrees of freedom. The nodal displacement vector $\{d\}$ can be written as

$$\{d\} = [d_1, d_2, d_3, d_4, d_5, d_6, d_7, d_8, d_9, d_{10}, d_{11}, d_{12}]^T \tag{3.25}$$

in which the components d_1, d_2, d_3 and d_7, d_8, d_9 are the translational displacements at nodes i and j, respectively; while d_4, d_5, d_6 and d_{10}, d_{11}, d_{12} are the rotational displacements at nodes i and j, respectively.

The displacement field vector $\{u\}$, in local coordinates, contains six components:

$$\{u\} = [u, v, w, \theta_{\bar{x}}, \theta_{\bar{y}}, \theta_{\bar{z}}]^T \tag{3.26}$$

where u, v, and w are, again, the three translational displacement components in the

$\bar{x}$, $\bar{y}$, $\bar{z}$ directions, respectively, and $\theta_{\bar{x}}$, $\theta_{\bar{y}}$, and $\theta_{\bar{z}}$ are the corresponding three rotational displacement components. The interpolation function [N] can be written as

$$[N] = [N_{at}] + [N_b] \tag{3.27}$$

where $[N_{at}]$ is a 6×12 matrix of interpolation functions for axial and torsional degrees of freedom; and N_b is a 6×12 matrix of interpolation functions for transverse displacements. These interpolation functions are given in Eq. A.2 and Eq. A.4 in Appendix A.

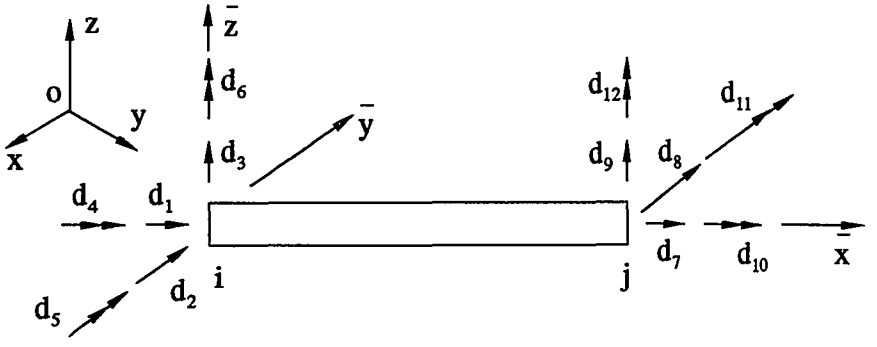

Figure 3.1 A frame element with 12 degrees-of-freedom

The mass density matrix $[\bar{m}]$ is usually defined as

$$[\bar{m}] = \begin{bmatrix} \bar{m}_{11} & 0 & 0 & 0 & 0 & 0 \\ 0 & \bar{m}_{22} & 0 & 0 & 0 & 0 \\ 0 & 0 & \bar{m}_{33} & 0 & 0 & 0 \\ 0 & 0 & 0 & \bar{m}_{44} & 0 & 0 \\ 0 & 0 & 0 & 0 & \bar{m}_{55} & 0 \\ 0 & 0 & 0 & 0 & 0 & \bar{m}_{66} \end{bmatrix} \tag{3.28}$$

where $\bar{m}_{11}$, $\bar{m}_{22}$, and $\bar{m}_{33}$ are translational mass densities in $\bar{x}$, $\bar{y}$, and $\bar{z}$ axis direction, respectively; and $\bar{m}_{44}$, $\bar{m}_{55}$, and $\bar{m}_{66}$ are rotational mass densities about $\bar{x}$, $\bar{y}$, and $\bar{z}$

axes, respectively. The mass densities are measured per unit length for the frame element. In this case, Eq. 3.16 for the element mass matrix [m] becomes

$$[m] = \int_{L_e} [N]^T [\bar{m}] [N] \, dL \tag{3.29}$$

where L_e is the element length. The 12×12 frame element mass matrix can be found in Eq. A.10 in Appendix A.

The element damping matrix can be obtained in a similar manner to the element mass matrix. However structural damping is often expressed in terms of damping ratios for each mode shape. Therefore, if the response is sought using the mode-superposition method, these damping ratios are introduced directly in the modal equations.

The element stiffness matrix [k] can be obtained by

$$[k] = \int_{L_e} [B]^T [E] [B] \, dL \tag{3.30}$$

The 12×12 element stiffness matrix can be found in Eq. A.11 in Appendix A.

When a beam element is subjected to an axial force in addition to a flexural load, the stiffness coefficients k_{ij} are modified by the presence of the axial force. The modification is known as the beam geometric stiffness k_{Gij}. The physical meaning of k_{Gij} can be explained as the force corresponding to degree of freedom i and caused by a change in orientation of the axial forces in the structure induced by a displacement at degree of freedom j. These coefficients can be evaluated by application of the principle of virtual displacements. The geometric stiffness coefficients may be expressed as

$$k_{Gij} = \int_{L_e} f_a(x) N'_i N'_j dL \qquad \text{for } i, j = 2, 3, 5, 6, 8, 9, 11, 12 \tag{3.31}$$

in which $f_a(x)$ is the axial force, which may vary along the element length; and N'_i and N'_j are the derivatives of the corresponding interpolation functions defined in Eq. 3.27. By using these interpolation functions to calculate the geometric stiffness coefficients, the result is the consistent geometric stiffness matrix. The beam element geometric stiffness matrix for the case where the axial force is constant can be found in Eq. A.14 in Appendix A.

The assembly of the system geometric stiffness matrix can be carried out exactly in the same manner as for assembly of the stiffness matrix. However a more efficient approach is to add the element stiffness matrix and element geometric stiffness matrix to form a combined stiffness matrix $[k_c]$:

$$[k_c] = [k] + [k_G] \tag{3.32}$$

$[k_c]$ is then transformed to the global coordinate system before adding the element combined stiffness matrix into the global stiffness matrix.

3.2.4 Mode-superposition method

In structural analysis, mode superposition is often used for dynamic analysis of large structural systems. If the structural motion can be approximately represented by q mode shapes, a large *ndof*-dimensional linear space of the displacements is reduced to a q-dimensional $(q \ll ndof)$ space of modal displacements. Such an approach is also useful for hydroelastic analysis. Only a few structural mode shapes corresponding to the lower natural frequencies need to be considered in hydroelasticity, because most of the wave energy is concentrated at relatively low frequencies compared to the structural natural frequencies. This reduction in dimensionality is especially important in the solution of the radiation problem. A radiation potential can be obtained for each mode shape, and

the total radiation potential can be obtained by superposing all radiation potentials for the reduced set of mode shapes.

As is common in hydroelasticity (Bishop and Price, 1976; Wu, 1984), the so-called 'dry' undamped structural normal modes are used to perform the mode superposition. The dry modes are obtained by solving the homogeneous, undamped form of Eq. 3.5:

$$[M_s]\{\ddot{D}(t)\} + [K_s]\{D(t)\} = 0 \tag{3.33}$$

The solution to Eq. 3.33 has the form

$$\{D\} = \{\psi\}e^{-i\varpi t} \tag{3.34}$$

and

$$\{\ddot{D}\} = -\varpi^2\{\psi\}e^{-i\varpi t} \tag{3.35}$$

where ϖ is the angular frequency (radians per second), $\{\psi\}$ is the vector of maximum values, or amplitudes, and it is time independent. With Eqs. 3.34 and 3.35, Eq. 3.33 becomes

$$([K] - \varpi^2[M])\{\psi\} = 0 \tag{3.36}$$

or

$$[K]\{\psi\} = \lambda[M]\{\psi\} \qquad \text{or} \qquad ([K] - \lambda[M])\{\psi\} = 0 \tag{3.37}$$

where $\lambda = \varpi^2$ and $([K] - \lambda[M])$ is the characteristic matrix of the structure. Eq. 3.37 is the so-called generalized eigenvalue problem. By solving Eq. 3.37, the eigenvalues λ_i and corresponding eigenvector $\{\psi_i\}$ can be obtained. Correspondingly, ϖ_i is called the ith natural frequency. For the first q eigenvalues, the generalized

eigenvalue problem can be written as

$$[K]\,[\Psi] = [M]\,[\Psi]\,[\Lambda] \tag{3.38}$$

in which $[\Psi]$ is the $ndof \times q$ mode-shape matrix with column i equal to $\{\psi_i\}$, and $[\Lambda]$ represents a $q \times q$ diagonal matrix with values of λ_i on the diagonal.

The eigenvector $\{\psi_i\}$ defines only the 'direction' of the mode shape in an *n*-dimensional space. That is, if α is a nonzero constant, then $\alpha\{\psi_i\}$ is also an eigenvector which corresponds to the same eigenvalue. Hence, for any ith mode shape $\{\bar{\psi}_i\}$, where

$$\{\bar{\psi}_i\}^T [M]\,\{\bar{\psi}_i\} = m_{ii} > 0 \tag{3.39}$$

it is possible to define a corresponding eigenvector $\{\psi_i\}$ as

$$\{\psi_i\} = \frac{1}{\sqrt{m_{ii}}}\{\bar{\psi}_i\} \tag{3.40}$$

such that

$$\{\psi_i\}^T [M]\,\{\psi_i\} = 1 \tag{3.41}$$

The process in Eqs. 3.39 and 3.40 is called mass-normalization of the eigenvectors. If not specially mentioned, the mass-normalized eigenvectors are used in the following. For mass-normalized eigenvectors, there are the following relationships:

$$\{\psi_i\}^T [M]\,\{\psi_j\} = \delta_{ij} \qquad (i, j = 1, 2, \ldots q) \tag{3.42}$$

$$\{\psi_i\}^T [K]\,\{\psi_j\} = \lambda_i \delta_{ij} \qquad (i, j = 1, 2, \ldots q) \tag{3.43}$$

where δ_{ij} is the Kronecker delta. Eq. 3.43 means that the eigenvectors are also [K]-orthogonal.

For a structure 'in-air', the first six zero frequency modes are defined here to be the usual rigid body modes in ship-motion theory, that is, surge, sway, heave, roll, pitch, and yaw, respectively. The corresponding rigid modal displacements $[\Psi_r]$ at any point (x,y,z) are given by

$$[\Psi_r] = \begin{bmatrix} 1 & 0 & 0 & 0 & (z-z_G) & -(y-y_G) \\ 0 & 1 & 0 & -(z-z_G) & 0 & (x-x_G) \\ 0 & 0 & 1 & (y-y_G) & -(x-x_G) & 0 \\ 0 & 0 & 0 & 1 & 0 & 0 \\ 0 & 0 & 0 & 0 & 1 & 0 \\ 0 & 0 & 0 & 0 & 0 & 1 \end{bmatrix} \tag{3.44}$$

where (x_G, y_G, z_G) is the coordinates of the center of gravity.

The actual nodal displacements {D} can be expressed in terms of the mode shapes $[\Psi]$ as

$$\{D\} = [\Psi]\{p\} \tag{3.45}$$

where {p} is the $q \times 1$ vector of principle coordinates. Given the modal displacements at the element nodes, the modal internal 'force' (forces and moments) matrix $[F_\Psi]$ and modal 'stress' matrix, $[\Sigma_\Psi]$, at a point within the element can be calculated. Therefore, the corresponding internal forces and stresses within the element can be calculated, respectively, by

$$\{F\} = [F_\Psi]\{p\} \tag{3.46}$$

and

$$\{\sigma\} = [\Sigma_\Psi]\{p\} \tag{3.47}$$

in which {F} is the internal forces and $\{\sigma\}$ is the stresses at any point within the element.

When Eq. 3.5 is premultiplied by $[\Psi]^T$ and Eq. 3.45 is substituted into Eq. 3.5, the result is

$$\left[-\omega^2 [M_s^*] - i\omega [C_s^*] + [K_s^*] + [K_f^*]\right] \{p\} = \{F_f^*\} \tag{3.48}$$

where

$$[M_s^*] = [\Psi]^T [M_s] [\Psi] = [I] \tag{3.49}$$

$$[C_s^*] = [\Psi]^T [C_s] [\Psi] \tag{3.50}$$

$$[K_s^*] = [\Psi]^T [K_s] [\Psi] = [M_s^*] [\Lambda] = [\Lambda] \tag{3.51}$$

$$[K_f^*] = [\Psi]^T [K_f] [\Psi] \tag{3.52}$$

$$\{F_f^*\} = [\Psi]^T \{F_f\} \tag{3.53}$$

where [I] is an identity matrix. Eq. 3.48 represents the q modal equations of motion, while Eqs. 3.49-3.53 define the structural modal mass, damping, and stiffness matrices, modal hydrostatic restoring stiffness matrix, and modal hydrodynamic forces.

3.3 Fluid dynamics

3.3.1 Fluid forces

When a structure is floating in an ideal fluid, the fluid pressure acting normal to the structural wetted surface will affect the motion. Therefore, to calculate the structural loads caused by fluid forces, the fluid pressure must be calculated first.

It is well known that for irrotational flow the total velocity field can be represented simply by the gradient of the total velocity potential Φ_T. In linear wave theory, the total

velocity potential is the summation of the incident wave potential ϕ_I, the diffraction wave potential ϕ_D, and radiation wave potentials ϕ_R. The total velocity potential satisfies Laplace's equation, which can be written as

$$\nabla^2 \Phi_T \equiv \frac{\partial^2 \Phi_T}{\partial x^2} + \frac{\partial^2 \Phi_T}{\partial y^2} + \frac{\partial^2 \Phi_T}{\partial z^2} = 0 \tag{3.54}$$

For irrotational, unsteady flow, the fluid pressure p_T can be calculated from Euler's integral, which can be written as

$$p_T = -\rho\left(\frac{\partial \Phi_T}{\partial t} + \frac{1}{2}|\nabla \Phi_T|^2 + gz'\right) \tag{3.55}$$

where ρ is the water density; g is the gravitational acceleration; $z' = z - z_w$; z is the vertical coordinate of the position at which the pressure is measured; and z_w is the vertical coordinate of the still-water plane. In Eq. 3.55, the first term is the hydrodynamic pressure, which comes from time-dependent flow; the second, nonlinear term is also hydrodynamic pressure, which is due to the flow velocity; and the third term is the hydrostatic pressure. In the linear theory, the higher-order nonlinear term is dropped.

The distributed pressure force $\{F_{cp}\}$ normal to the wetted element surface in local coordinates can be calculated from the pressure distribution as

$$\{F_{cp}\} = p_T \{\bar{n}\} \tag{3.56}$$

where $\{\bar{n}\}$ is the normal vector of the wetted surface at the point $(\bar{x}, \bar{y}, \bar{z})$ in the element local coordinate system. The vector $\{\bar{n}\}$ is directed out of the fluid, and it can be written as

$$\{\bar{n}\} = \left[\bar{n_x}\ \bar{n_y}\ \bar{n_z}\right]^T \tag{3.57}$$

The calculation of the normal vector in the local coordinate system will be discussed in Chapter 4.

Eq. 3.56 can be substituted in Eq. 3.19 to form the local external load vector for each element:

$$\{r_p^{ext}\} = \iint_{S_e} [N]^T \{F_{cp}\}\, dS \tag{3.58}$$

Eq. 3.58 will be used often. In the linear theory, for the sinusoidal wave the time-independent part of hydrodynamic forces can be written as

$$\{r_p^{ext}\} = i\omega\rho \iint_{S_e} [N]^T \{\bar{n}\}\, \Phi dS \tag{3.59}$$

The local external element load vector $\{r_p^{ext}\}$ must be transformed to the global coordinate system and then added to the global external load vector.

3.3.2 Linear Potential Theory

Based on the assumptions of an incompressible, inviscid fluid and irrotational flow, there exists a velocity potential $\Phi_T(x, y, z, t)$ which is a complex function of position and time. This potential function satisfies Laplace's equation in the fluid domain. In the three-dimensional case, it is written as

$$\Delta\Phi_T(x, y, z, t) = 0 \tag{3.60}$$

The fluid velocity vector, $\{V(x, y, z, t)\}$, is given by the gradient of the potential function

$$\{V(x, y, z, t)\} = \nabla\Phi_T(x, y, z, t) \tag{3.61}$$

where ∇ is the vector gradient operator:

$$\nabla = \left[\frac{\partial}{\partial x}\frac{\partial}{\partial y}\frac{\partial}{\partial z}\right]^T \tag{3.62}$$

If the wave height is very small compared with the wave length, the linear potential theory is applicable. The total potential Φ_T can be decomposed, if monochromatic waves are assumed, as

$$\Phi_T = \left(\phi_I + \phi_D + \sum_{j=1}^{q} p_j\phi_j\right)e^{-i\omega t} = \Phi e^{-i\omega t} \tag{3.63}$$

where ϕ_I is the incident wave potential; ϕ_D is the diffraction wave potential; ϕ_j is the radiation potential for the jth mode; p_j is the principal coordinate for mode j; and Φ is the time-independent part of the total velocity potential. ϕ_I is the potential for the case when there is no structure; ϕ_D is the modification to the potential due to a fixed structure. ϕ_j is the potential which results from the structure vibrating in the jth mode shape in an otherwise calm fluid. All the potentials must satisfy Laplace's equation in the fluid domain. In addition, they must satisfy the linear boundary conditions:

I. Linear free surface condition:

$$\frac{\partial^2\Phi_T}{\partial t^2} + g\frac{\partial\Phi_T}{\partial z} = 0 \quad \text{or} \quad \frac{\partial\phi}{\partial z} - k\phi = 0 \quad \text{on} \quad z = z_w \tag{3.64}$$

where $k = \omega^2/g$ is the wave number in infinitely deep fluid and $\phi = \phi_I$ or ϕ_D or ϕ_j.

II. Sea-floor condition:

$$\lim_{z \to -\infty} \frac{\partial \phi}{\partial z} = 0 \tag{3.65}$$

III. Radiation conditions (for the diffraction and radiation potentials):

Sommerfeld condition in three-dimensional problems:

$$\lim_{R \to \infty} \{R^{1/2} \left(\frac{\partial}{\partial R} - ik \right) \phi \} = 0 \tag{3.66}$$

where $R = \sqrt{x^2 + y^2}$ and k is the wave number, and for y-z plane two-dimensional flow

$$\lim_{y \to \pm\infty} \{ \frac{\partial}{\partial y} \mp ik \} \phi = 0 \tag{3.67}$$

IV. No-flux condition on the body wetted surface

$$\frac{\partial \phi}{\partial n} = \{\dot{u}\}^T \{n\} \tag{3.68}$$

where $\{\dot{u}\}$ is the velocity vector of the body wetted surface, which excludes $e^{-i\omega t}$ and $\{n\}$ is the normal vector of the fluid domain which is shown in Fig. 3.2. Eq. 3.68 becomes for the diffraction potential

$$\frac{\partial}{\partial n}(\phi_I + \phi_D) = 0 \qquad \text{or} \qquad \frac{\partial \phi_D}{\partial n} = -\frac{\partial \phi_I}{\partial n} \tag{3.69}$$

and for the jth radiation potential

$$\frac{\partial \phi_j}{\partial n} = \{\dot{u}_j\}^T \{n\} \tag{3.70}$$

The incident wave potential can be easily solved by using the method of separation of variables, and can be expressed for deep water as

$$\phi_I = -\frac{ig\alpha}{\omega} e^{ik(x\cos\beta + y\sin\beta)} e^{kz'} \tag{3.71}$$

The diffraction and radiation potentials may be solved by using the Green function method.

3.3.3 Green Function Method

The diffraction and radiation potentials can be solved by different methods. One of the most convenient methods is the Green function method (see for example, Frank, 1967; Yeung, 1973; Faltinsen and Michelsen, 1974; Garrison, 1977; and Garrison, 1984), which is based on Green's second identity.

In a three-dimensional fluid domain *V*, bounded by a closed surface *S*, if there are two scalar functions φ and G, which are second differentiable in *V*, and first differentiable on *S*, then Green's second identity states

$$\iint_S \left(\phi \frac{\partial G}{\partial n} - G\frac{\partial \phi}{\partial n}\right) dS = \iiint_V (\phi \nabla^2 G - G\nabla^2 \phi)\, dV \tag{3.72}$$

where $\frac{\partial}{\partial n}$ is the normal derivative, and the normal vector of the surface *S* is pointing out of the fluid domain. In this case, let ϕ be the velocity potential that satisfies Laplace's equation, and the second term on the right hand side of Eq. 3.72 will disappear.

If a suitable function G(*P*, *Q*) can be found, the right hand side of Eq. 3.72 can be expressed as

$$\iiint_V \phi(Q)\, \nabla^2 G(P, Q)\, dV = \alpha\phi(P) \tag{3.73}$$

where $P=P(x,y,z)$ is the field point in the domain *V* or on the surface *S*, $Q=Q(\xi, \eta, \zeta)$ is the source point (which will be explained later) in the domain *V* or on the surface *S*, and

α is a constant. If such a G(P, Q) can be found, Eq. 3.72 becomes

$$\iint_S \left(\phi(Q)\frac{\partial G(P,Q)}{\partial n} - G(P,Q)\frac{\partial \phi(Q)}{\partial n}\right) dS = \alpha\phi(P) \tag{3.74}$$

This means that the potential $\phi(P)$ at any point P in V or on S can be determined by the function and its normal derivative.

From Eq. 3.73, the function G(x,y,z) satisfies the following Poisson equation

$$\nabla^2 G(P,Q) = \alpha\delta(P-Q) \tag{3.75}$$

in which $\delta(P-Q)$ is the Dirac delta function. This function has the following property for a well-behaved function f(P)

$$\int_{-\infty}^{+\infty}\int\int f(P)\,\delta(P-Q)\,dV = f(Q) \tag{3.76}$$

One of the particular solutions of Eq. 3.75 is a Rankine source given by

$$\bar{G}(P,Q) = -\frac{1}{r(P,Q)} \tag{3.77}$$

where r(P, Q) is the distance between point P and point Q:

$$r(P,Q) = \sqrt{(x-\xi)^2 + (y-\eta)^2 + (z-\zeta)^2} = R \tag{3.78}$$

From Eq. 3.77, $\bar{G}(P,Q)$ will be singular when point Q approaches point P. Therefore, the Green function method is also called the singularity distribution method. It is also known that by definition of Eq. 3.77, $\bar{G}(P,Q)$ is a potential at any point P due to a unit source located at point Q, and $\frac{\partial \bar{G}(P,Q)}{\partial n}$ is also a potential at any point P due to a unit

dipole located at point Q and having its axis in the normal direction {n}.

It should be noted that if there is another function H(P, Q) which satisfies Laplace's equation in the fluid domain V, then

$$G(P, Q) = -\frac{1}{r(P, Q)} + H(P, Q) \tag{3.79}$$

is also a solution of Eq. 3.75. G(P, Q) defined in Eq. 3.79 is the Green function. The reason for adding this additional harmonic function is that if a suitable function H(P, Q) can be found such that the Green function satisfies all other boundary conditions except the body boundary condition, the surface integration in Eq. 3.72 need only be evaluated on the body surface.

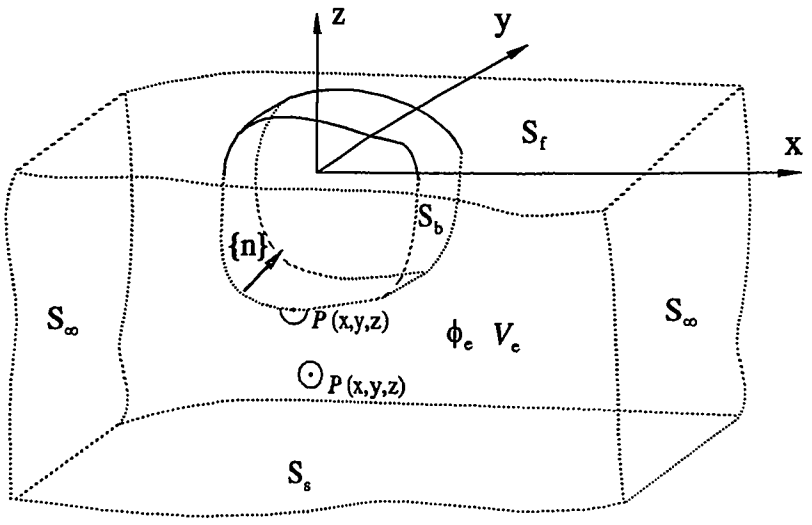

Figure 3.2 Three-dimensional fluid domain for velocity potential

Substitution of Eq. 3.79 into Eq. 3.73, if the singular point P(x,y,z) is isolated by enclosing it with a sphere of small radius ε (when P is in V) or a hemisphere of small radius ε (when P is on S), as shown in Fig. 3.2, then G(P, Q) will be harmonic outside

this isolated region and the volume integral, by knowing

$$\nabla^2 G = \nabla^2 \frac{1}{r(P,Q)} = \begin{cases} 0 & P \neq Q \\ \infty & P = Q \end{cases} \tag{3.80}$$

becomes

$$\iiint_V \phi \nabla^2 G \, dV = \begin{cases} -4\pi\phi(P) & P \in V \\ -2\pi\phi(P) & P \in S \\ 0 & P \notin V \cup S \end{cases} \tag{3.81}$$

Eq. 3.72, then can be written as

$$\iint_S \left(\phi(Q) \frac{\partial G(P,Q)}{\partial n} - G(P,Q) \frac{\partial \phi(Q)}{\partial n} \right) d(S) = \begin{cases} -4\pi\phi(P) & P \in V \\ -2\pi\phi(P) & P \in S \\ 0 & P \notin V \cup S \end{cases} \tag{3.82}$$

Eq. 3.82 is a general Green's third identity. Now, the potential at any field point can be written in a general form as

$$\phi(P) = \alpha \iint_S \left(\phi(Q) \frac{\partial G(P,Q)}{\partial n} - G(P,Q) \frac{\partial \phi(Q)}{\partial n} \right) dS \tag{3.83}$$

where α is a constant, which is equal to $-\frac{1}{4\pi}$ when P is in V, $-\frac{1}{2\pi}$ when P is on S, and 0 when P is outside the domain $V \cup S$. From Eq. 3.83 and the definition of the Green function $G(P, Q)$, it can be seen that the velocity potential $\phi(P)$ at any field point P inside the fluid domain V or on the surface S can be expressed by the sum of a distribution of sources on the surface S with the density $-\frac{\partial \phi(Q)}{\partial n}$ and a distribution of dipoles on the surface S with the density $\phi(Q)$. For this reason, $Q(\xi, \eta, \zeta)$ is called the

source point.

To obtain the fluid pressure forces, only the values of the potential located on the structural wetted surface need to be calculated. This means that the field point P will be limited to the wetted surface. For source point Q, if they are distributed on all surfaces, which include free surface S_f, sea bed surface S_s, infinite surface S_∞, and wetted structural surface S_b, it may be impossible to calculate velocity potential by using Eq. 3.83. If the additional term $H(P, Q)$ is chosen such that the Green function $G(P, Q)$ also can satisfy the free surface condition, sea bed boundary condition, and the radiation condition, then the velocity potential $\phi(P)$ must be calculated only on the structural body surface. To demonstrate this, Eq. 3.83 can be written as

$$\begin{aligned}\phi(P) &= \alpha \iint_S \left(\phi(Q)\frac{\partial G(P,Q)}{\partial n} - G(P,Q)\frac{\partial \phi(Q)}{\partial n}\right) dS \\ &= \alpha\left[\int_{S_b} + \int_{S_f} + \int_{S_\infty} + \int_{S_s}\right]\left(\phi(Q)\frac{\partial G(P,Q)}{\partial n} - G(P,Q)\frac{\partial \phi(Q)}{\partial n}\right) dS\end{aligned} \tag{3.84}$$

Consider each boundary separately:

1. When Q is on the sea bed, if the Green function satisfies $\frac{\partial G(P,Q)}{\partial n} = 0$, the integral on the sea bed surface will be zero since $\frac{\partial \phi(Q)}{\partial n} = 0$.

2. When Q is on the control boundary at infinity, from Eq. 3.66, the velocity potential satisfies $\lim_{R\to\infty}\{R^{1/2}\left(\frac{\partial}{\partial R} - ik\right)\phi\}$. When $R \to \infty$,

$$\begin{aligned}&\phi(Q)\frac{\partial G(P,Q)}{\partial n} - G(P,Q)\frac{\partial \phi(Q)}{\partial n} \\ &\propto R^{1/2} e^{-ikR}\frac{\partial G(P,Q)}{\partial n} - G(P,Q)R^{1/2}e^{-ikR}\left(-\frac{1}{2}R^{-1} - ik\right) \\ &= R^{1/2}e^{-ikR}\left(\frac{\partial G(P,Q)}{\partial n} + ikG(P,Q)\right) \qquad R\to\infty\end{aligned} \tag{3.85}$$

If the Green function satisfies the radiation condition

$$\lim_{R\to\infty} R^{1/2}\left(\frac{\partial G(P,Q)}{\partial n} + ikG(P,Q)\right) = 0 \tag{3.86}$$

then the integral on the infinite boundary will disappear.

3. When Q is on the free surface, from Eq. 3.64

$$\begin{aligned}\phi(Q)\frac{\partial G(P,Q)}{\partial n} - G(P,Q)\frac{\partial \phi(Q)}{\partial n} &= \phi(Q)\frac{\partial G(P,Q)}{\partial z} - G(P,Q)\frac{\partial \phi(Q)}{\partial z} \\ &= \left(\frac{\partial G(P,Q)}{\partial z} - kG(P,Q)\right)\phi(Q)\end{aligned} \tag{3.87}$$

If $G(P, Q)$ also satisfies the free surface boundary condition, the integral on free surface will disappear too. Therefore, if the Green function $G(P, Q)$ has been chosen such that it satisfies

$$\begin{aligned}&\nabla^2 G(P,Q) = \delta(P-Q) \qquad \text{in } V \\ &\frac{\partial G(P,Q)}{\partial z} - kG(P,Q) = 0 \qquad \text{on} \qquad z = z_w \\ &\lim_{z\to-\infty}\frac{\partial G(P,Q)}{\partial n} = 0 \\ &\lim_{R\to\infty} R^{1/2}\left(\frac{\partial G(P,Q)}{\partial n} + ikG(P,Q)\right) = 0\end{aligned} \tag{3.88}$$

then the velocity potential $\phi(P)$ at any field point can be obtained by integration only on the wetted surface S_b, leading to a Fredholm integral equation of the second kind:

$$\phi(P) = \alpha\iint_{S_b}\left(\phi(Q)\frac{\partial G(P,Q)}{\partial n} - G(P,Q)\frac{\partial \phi(Q)}{\partial n}\right)dS \tag{3.89}$$

In Eq. 3.89, the unknowns are the field velocity potential $\phi(P)$, the source density

$\phi(Q)$, and dipole density $\frac{\partial\phi(Q)}{\partial n}$. All of them are distributed on the wetted surface. Fortunately, the Green functions have been studied quite well; some are found in Weihausen and Laitone (1960).

3.3.4 Solution of the integral equation

In Eq. 3.89, the two 'densities' $\phi(Q)$ and $\frac{\partial\phi(Q)}{\partial n}$ must be determined. The unknowns can be reduced to one by constructing the interior problem (Newman, 1978). The interior domain V_i is the domain inside the structural body, Fig. 3.2. Mathematically, there exists a Green's third identity in the interior domain V_i and on the wetted surface S. It can be written as

$$\iint_{S_b}\left(\phi_i(Q)\frac{\partial G(P,Q)}{\partial n_i} - G(P,Q)\frac{\partial\phi_i(Q)}{\partial n_i}\right)dS = \begin{cases} -4\pi\phi_i(P) & P \in V_i \\ -2\pi\phi_i(P) & P \in S \\ 0 & P \notin V_i \cap S \end{cases} \tag{3.90}$$

where the normal vector $\{n_i\}$ is pointing out of the interior domain, and $\phi_i(P)$ is the field velocity potential in the interior domain. By definition, $\{n_i\} = -\{n_e\}$, where $\{n_e\}$ is the normal vector for the exterior domain, which is equal to the normal vector, $\{n\}$, defined before.

Eq. 3.82 can be rewritten for the exterior problem as

$$\iint_{S_b}\left(\phi_e(Q)\frac{\partial G(P,Q)}{\partial n_e} - G(P,Q)\frac{\partial\phi_e(Q)}{\partial n_e}\right)dS = \begin{cases} -4\pi\phi_e(P) & P \in V_e \\ -2\pi\phi_e(P) & P \in S \\ 0 & P \notin V_e \cap S \end{cases} \tag{3.91}$$

Eq. 3.90 and Eq. 3.91 are called interior and exterior problems, respectively. Subtracting Eq. 3.90 from Eq. 3.91, by knowing that the normal vectors $\{n_e\}$ and $\{n_i\}$ are equal but of opposite sign, results in

$$\phi(P) = \alpha \iint_{S_b} \left((\phi_i(Q) - \phi_e(Q)) \frac{\partial G(P,Q)}{\partial n} - G(P,Q) \left(\frac{\partial \phi_i(Q)}{\partial n} - \frac{\partial \phi_e(Q)}{\partial n} \right) \right) dS \qquad (3.92)$$

$$P \in S_b$$

in which $\alpha = \dfrac{1}{2\pi(\phi_i(P) + \phi_e(P))}$.

The basic two solution methods used to solve the potential from Eq. 3.92 are the source distribution method and the dipole distribution method, which are briefly discussed below.

3.3.4.1 Source distribution method

If the exterior and interior velocity potentials are set equal to each other, that is $\phi_e(Q) = \phi_i(Q)$, and the source density $\sigma(Q)$ is defined such that $\sigma(Q) = \dfrac{\partial \phi_i(Q)}{\partial n} - \dfrac{\partial \phi_e(Q)}{\partial n}$, then Eq. 3.92 becomes

$$\phi(P) = \frac{1}{4\pi} \iint_{S_b} G(P,Q)\,\sigma(Q)\,dS \qquad P \in S_b \qquad (3.93)$$

Eq. 3.93 means that the field velocity potential $\phi(P)$ can be expressed by the sum of the distribution of sources on the wetted surface S_b with the density $\sigma(Q)$. To obtain $\sigma(Q)$, the structural body boundary condition can be used. The normal derivative of Eq. 3.93, together with Eq. 3.70 and $\phi(P) = \dfrac{1}{2}(\phi_e(P) + \phi_i(P))$, results in

$$\frac{1}{2}\sigma(P) + \frac{1}{4\pi}\iint_{S_b}\sigma(Q)\frac{\partial G(P,Q)}{\partial n}dS = \frac{\partial \phi_e(P)}{\partial n} = \{\dot{u}\}^T\{n\} \tag{3.94}$$

Eq. 3.93 and Eq. 3.94 are the two basic equations used in the source distribution method.

3.3.4.2 Dipole distribution method

If the normal derivatives of the exterior and interior velocity potentials are set equal to each other, that is $\frac{\partial \phi_e(Q)}{\partial n} = \frac{\partial \phi_i(Q)}{\partial n}$, and the density m($Q$) is defined such that $m(Q) = \phi_i(Q) - \phi_e(Q)$, then Eq. 3.92 becomes

$$\phi(P) = \frac{1}{4\pi}\iint_{S_b}\frac{\partial G(P,Q)}{\partial n}m(Q)\,dS \qquad P \in S_b \tag{3.95}$$

Eq. 3.95 means that the field velocity potential $\phi(P)$ can be expressed by the sum of the distribution of dipoles on the wetted surface S_b with the density $m(Q)$.

3.4 Coupling of structural dynamics and hydrodynamics

From the above discussion, the coupling of structural dynamics and hydrodynamics for hydroelastic analysis of floating structures includes two key phases. First, the radiation wave potentials are obtained independently for each of the structural dry mode shapes required to represent the structural motion. The wetted surface boundary conditions for solving the radiation potentials are defined in terms of the modal normal velocity. Second, the hydrodynamic pressure from the incident, diffraction and radiation waves are calculated to determine the fluid loads acting on the structure.

3.4.1 Structural body boundary condition

The modal normal velocity at a point on the wetted surface is the velocity in the

normal direction for a particular mode shape. The modal velocity will be used in the wetted surface boundary condition to solve the radiation potential. To calculate the modal normal velocity, the structural normal vector, shown in Fig. 3.2, needs to be calculated first.

The structural normal vector $\{n\} = \{n_1, n_2, n_3\}^T$ can be calculated in the global coordinate system. The normal vector is a free vector for the plane, which means the vector can be located at any position within the plane. For the numerical calculation, the structural wetted surface is discretized by quadrilateral panels. The normal vector can be calculated by the vector cross product of the diagonal vectors, which can be formed from the coordinates of the four nodes. The vector cross product can then be normalized to obtain the unit normal vector. From Fig. 3.3, the diagonal vectors can be written as

$$\{r_{13}\} = \begin{bmatrix} (x_3 - x_1) \\ (y_3 - y_1) \\ (z_3 - z_1) \end{bmatrix} \tag{3.96}$$

and

$$\{r_{24}\} = \begin{bmatrix} (x_4 - x_2) \\ (y_4 - y_2) \\ (z_4 - z_2) \end{bmatrix} \tag{3.97}$$

The unit normal vector of the quadrilateral plane can be written as

$$\{n\} = \frac{\{r_{13}\} \times \{r_{24}\}}{|\{r_{13}\} \times \{r_{24}\}|} \tag{3.98}$$

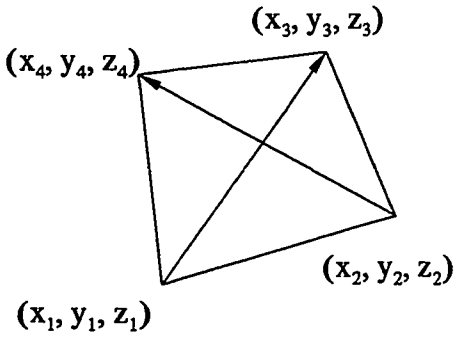

Figure 3.3 Normal vector of quadrilateral panel

For a curved panel, as long as the size of the panel is small enough, the method to calculate the unit normal vector for a plane panel can be used.

For each motion mode shape $\{\psi_j\}$, the normal component of the displacement is

$$n_j^* = \{\psi_j\}^T \{n\} \tag{3.99}$$

where $\{\psi_j\}$ is a mode shape vector containing the three translational displacements at the point (x,y,z) on the panel. Vector $\{n^*\}$, whose jth component is n_j^*, is defined as the generalized normal vector. The panel mode shape vector $\{\psi_j\}$ can be obtained from the global mode shape $[\Psi]$. For a sinusoidal wave, the modal normal velocity can be written as

$$\{\dot{u}_j\}^T \{n\} = -i\omega \{\psi_j\}^T \{n\} = -i\omega n_j^* \tag{3.100}$$

Eq. 3.100 can be used in Eq. 3.94 to determine the source densities for the jth radiation potential.

The generalized normal for the first six rigid body modes is obtained by substitution of Eq. 3.44 into Eq. 3.99:

$$\begin{bmatrix} n_1^* \\ n_2^* \\ n_3^* \\ n_4^* \\ n_5^* \\ n_6^* \end{bmatrix} = \begin{bmatrix} n_1 \\ n_2 \\ n_3 \\ -n_2(z-z_G)+n_3(y-y_G) \\ n_1(z-z_G)-n_3(x-x_G) \\ -n_1(y-y_G)+n_2(x-x_G) \end{bmatrix} \tag{3.101}$$

3.4.2 General formulation for modal hydrodynamic forces

The hydrodynamic forces result from the hydrodynamic pressures, and hence, only normal forces act on a structure in an ideal fluid. For the finite element method, the normal pressure force is treated as any other distributed force acting on the element. From Euler's integral, the linear time-independent part of the hydrodynamic distributed normal force at a point (x,y,z) on the wetted surface is, for a sinusoidal wave,

$$p\{n\} = i\omega\rho\Phi\{n\} \tag{3.102}$$

and the corresponding 'distributed' modal force becomes

$$\{f_f^*\} = i\omega\rho\Phi[\psi]^T\{n\} \tag{3.103}$$

where $[\psi]$ is the $3 \times q$ modal shape matrix at (x,y,z) with column j equal to $\{\psi_j\}$. The total modal hydrodynamic force $\{F_f\}^*$ is obtained by integration over the wetted surface:

$$\{F_f\}^* = \sum_{e=1}^{npanel} \iint_{S_e} i\omega\rho\Phi[\psi]^T\{n\}\,dS = \sum_{e=1}^{npanel} i\omega\rho \iint_{S_e} \Phi\{n\}^*\,dS \tag{3.104}$$

The $3 \times q$ modal shape matrix $[\psi]$ are modal displacements in global coordinates. In the finite element method, the displacements within the element are first calculated in the local coordinate system and then transformed to global coordinates as follows. First, the nodal mode shape matrix $[\psi_n]$ for an element can be extracted from the global mode shape $[\Psi]$ in the global coordinate system. The nodal mode shape matrix in the local coordinate system, $[\bar{\psi}_n]$, can be obtained by the transformation

$$[\bar{\psi}_n] = [T]\,[\psi_n] \tag{3.105}$$

The mode shape matrix $[\bar{\psi}]$ at the point (x,y,z) within an element in the local coordinate system can be obtain by interpolation as

$$[\bar{\psi}] = [N]\,[\bar{\psi}_n] \tag{3.106}$$

$[\psi]$ can be obtained by transforming $[\bar{\psi}]$ in the local coordinate system to the global coordinate system

$$[\psi] = [T_1]^T\,[\bar{\psi}] \tag{3.107}$$

If the pressure p is used in Eq. 3.104, one has

$$\{F_f\}^* = \sum_{e=1}^{npanel} \iint_{S_e} \{n\}^* p\,dS \tag{3.108}$$

Eq. 3.108 is the general formulation for the modal fluid force given the fluid pressure. It is also valid for the hydrostatic force calculation. The calculation of the generalized normals will be discussed in Chapter 4.

CHAPTER 4

THREE-DIMENSIONAL HYDROELASTICITY

4.1 Basic concept

Three-dimensional hydroelasticity theory (Wu, 1984; Price and Wu, 1985; Lee and Lou, 1989) uses a three-dimensional finite element structural model and a three-dimensional fluid model to describe the wave-induced motion problem, and mode superposition is used in coupling the interaction of structural and fluid motions. This method avoids the limitations of traditional three-dimensional hydrodynamics, which provides only rigid body motions, and two-dimensional hydroelasticity (Bishop and Price, 1979), which evaluates only beam-like motions and force resultants along the longitudinal axis of the structure. To date, three-dimensional hydroelasticity represents the most general and accurate theory for the hydroelastic analysis of very large floating structures.

Since three-dimensional hydroelasticity theory is the most general linear theory in hydroelasticity, the details of it will be discussed in this chapter with an example by using three-dimensional quadrilateral thin shell elements to model the structure and four node quadrilateral panels to model the fluid. The structural responses, such as motions and deformations, internal forces and moments, and strains and stresses, are of most interest to structural engineers for design. Therefore, this chapter explains three-dimensional hydroelasticity theory from a structural viewpoint and considers the hydrodynamic theory as a tool to obtain the fluid loads. In addition, the general formulations for the hydrostatic restoring coefficients are discussed.

4.1.1 Linear quadrilateral thin shell element

A finite element model is used to describe the structure for hydroelastic analysis of floating structures. Various types of elements, such as, beam, plate, shell, truss and solid elements, may be used to model the complex structure. The number of elements used to model the wetted structure depend on the accuracy of the structural motions and deformations required for the fluid-structure interaction problem.

To provide sufficient buoyancy for the structure, a large volume with relatively low weight is required for the part below the still-water plane. Such structures typically are 'shell-like'. Hence, one of the most useful finite elements used to model floating structures is the linear quadrilateral thin shell element. The formulation of a basic quadrilateral thin shell element is described in this section; many other formulations are possible.

A quadrilateral thin shell element is shown in Fig. 4.1 in the global coordinate system x-y-z. The element local coordinate system is denoted $\bar{x} - \bar{y} - \bar{z}$. The local $\bar{z}$ is directed in the same direction as the normal vector defined by the fluid panels, that is, it points into the structure.

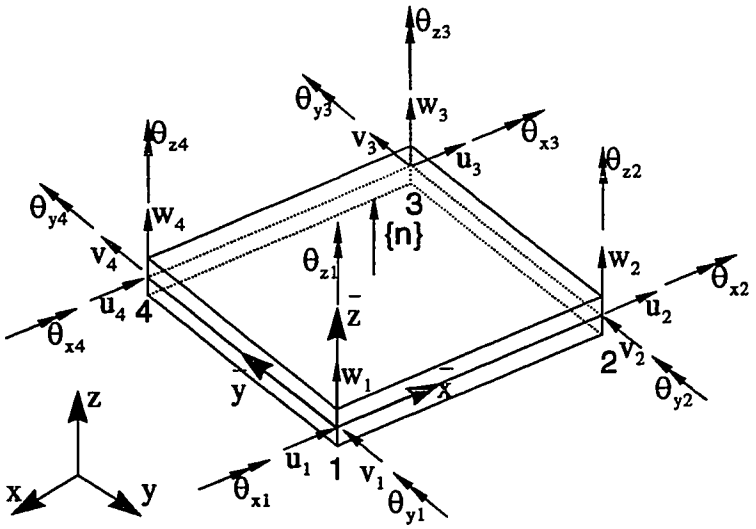

Figure 4.1 Quadrilateral thin shell element

The element has the capability to resist both membrane and bending loads. The 24×1 vector of element nodal displacements $\{d\}$ in the local coordinate system is

$$\{d\} = [u_1, v_1, w_1, \theta_{x1}, \theta_{y1}, \theta_{z1}, u_2, v_2, \ldots, u_4, v_4, w_4, \theta_{x4}, \theta_{y4}, \theta_{z4}]^T \quad (4.1)$$

and the corresponding nodal force vector is

$$\{\bar{r}^{ext}\} = [F_{x1}, F_{y1}, F_{z1}, M_{x1}, M_{y1}, M_{z1}, F_{x2}, F_{y2}, \ldots, F_{x4}, F_{y4}, F_{z4}, M_{x4}, M_{y4}, M_{z4}]^T \quad (4.2)$$

u_i, v_i i=1,2,3,4 refer to the in-plane displacements and F_{xi}, F_{yi} i=1,2,3,4 refer to the membrane forces. $w_i, \theta_{xi}, \theta_{yi}$ i=1,2,3,4 refer to the transverse displacements, and $F_{zi}, M_{xi}, M_{yi}, M_{zi}$ i=1,2,3,4 refer to transverse shear and bending moments. θ_{zi} i=1,2,3,4 do not contribute to the element forces and displacements. The element displacement field $\{u\}$ are interpolated from the nodal displacements by

$$\{u\} = [N]\{d\} \quad (4.3)$$

where [N] is a 3 × 24 matrix of interpolation functions.

To formulate a general quadrilateral thin shell element, it is convenient to define a natural coordinate system in the element plane, as shown in Fig. 4.2. For the local ξ, η (natural) coordinate system, the origin is taken as the intersection of lines joining the mid-points of the opposite sides, and the sides are defined by $\zeta = \pm 1$ and $\eta = \pm 1$.

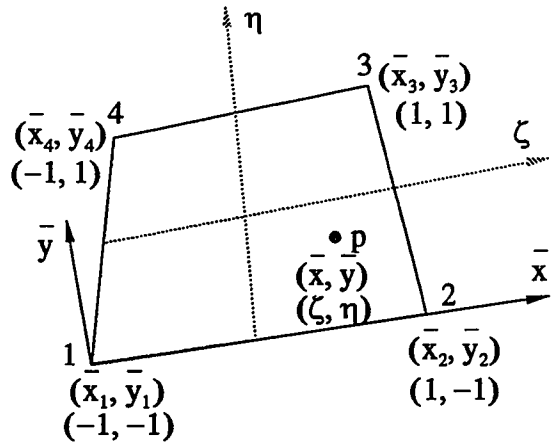

Figure 4.2 Natural coordinates for a quadrilateral element

The natural and cartesian coordinates are related by the interpolation function as:

$$\begin{bmatrix} \bar{x} \\ \bar{y} \end{bmatrix} = \begin{bmatrix} N_1 & 0 & N_2 & 0 & N_3 & 0 & N_4 & 0 \\ 0 & N_1 & 0 & N_2 & 0 & N_3 & 0 & N_4 \end{bmatrix} \begin{bmatrix} \bar{x}_1 \\ \bar{y}_1 \\ \bar{x}_2 \\ \bar{y}_2 \\ \bar{x}_3 \\ \bar{y}_3 \\ \bar{x}_4 \\ \bar{y}_4 \end{bmatrix} \tag{4.4}$$

where $(\bar{x}_i, \bar{y}_i)$ are the $(\bar{x}, \bar{y})$ coordinates of node i (i=1,2,3,4), and each interpolation

function is defined as (Rao, 1989)

$$N_i = \frac{1}{4}(1+\zeta\zeta_i)(1+\eta\eta_i) \qquad i = 1, 2, 3, 4 \tag{4.5}$$

(ζ_i, η_i) are the (ζ, η) coordinates of node i (i=1,2,3,4) and they are given by

$$\begin{aligned} (\zeta_1, \eta_1) &= (-1, -1) \qquad (\zeta_2, \eta_2) = (1, -1) \\ (\zeta_3, \eta_3) &= (1, 1) \qquad (\zeta_1, \eta_1) = (-1, 1) \end{aligned} \tag{4.6}$$

The same interpolation matrix is used to transform the nodal displacements to the displacement field in the element. For example, the in-plane displacements {u, v} are

$$\begin{bmatrix} u \\ v \end{bmatrix} = \begin{bmatrix} N_1 & 0 & N_2 & 0 & N_3 & 0 & N_4 & 0 \\ 0 & N_1 & 0 & N_2 & 0 & N_3 & 0 & N_4 \end{bmatrix} \begin{bmatrix} u_1 \\ v_1 \\ u_2 \\ v_2 \\ u_3 \\ v_3 \\ u_4 \\ v_4 \end{bmatrix} \tag{4.7}$$

Much work has been done on quadrilateral bending elements (e.g., Cook et al., 1989; Rao, 1989) and there are many possible formulations available. The vertical displacement field w can be interpolated by the nodal vertical displacements and rotations. Together with Eq. 4.7, the displacement field can be written as

$$\{u\} = \begin{Bmatrix} u \\ v \\ w \end{Bmatrix} = [N]\{d\} \tag{4.8}$$

where [N] is a 3 × 24 interpolation function matrix:

$$[N] = \begin{bmatrix} N_1 & 0 & 0 & 0 & 0 & 0 & N_2 & 0 & 0 & 0 & 0 & 0 & N_3 & 0 & 0 & 0 & 0 & 0 & N_4 & 0 & 0 & 0 & 0 & 0 \\ 0 & N_1 & 0 & 0 & 0 & 0 & 0 & N_2 & 0 & 0 & 0 & 0 & 0 & N_3 & 0 & 0 & 0 & 0 & 0 & N_4 & 0 & 0 & 0 & 0 \\ 0 & 0 & N_{11} & N_{12} & N_{13} & 0 & 0 & 0 & N_{21} & N_{22} & N_{23} & 0 & 0 & 0 & N_{31} & N_{32} & N_{33} & 0 & 0 & 0 & N_{41} & N_{42} & N_{43} & 0 \end{bmatrix} \quad (4.9)$$

where N_1, N_2, N_3, N_4 are given by Eq. 4.5. The other interpolation functions, which involve the vertical displacements, can be written, respectively, as (Rao, 1989)

$$\begin{aligned} N_{11} &= -\frac{1}{8}(-1+\zeta)(-1+\eta)(-2+\zeta+\zeta^2+\eta+\eta^2) \\ N_{21} &= \frac{1}{8}(1+\zeta)(-1+\eta)(-2-\zeta+\zeta^2+\eta+\eta^2) \\ N_{31} &= -\frac{1}{8}(1+\zeta)(1+\eta)(-2+\zeta+\zeta^2-\eta+\eta^2) \\ N_{41} &= \frac{1}{8}(-1+\zeta)(1+\eta)(-2+\zeta+\zeta^2-\eta+\eta^2) \end{aligned} \quad (4.10)$$

$$\begin{aligned} N_{12} &= -\frac{1}{8}(-1+\zeta)^2(1+\zeta)(-1+\eta) \\ N_{22} &= -\frac{1}{8}(-1+\zeta)(1+\zeta)^2(-1+\eta) \\ N_{32} &= \frac{1}{8}(-1+\zeta)(1+\zeta)^2(1+\eta) \\ N_{42} &= \frac{1}{8}(-1+\zeta)^2(1+\zeta)(1+\eta) \end{aligned} \quad (4.11)$$

$$
\begin{aligned}
N_{13} &= -\frac{1}{8}(-1+\zeta)(-1+\eta)^2(1+\eta) \\
N_{23} &= \frac{1}{8}(1+\zeta)(-1+\eta)^2(1+\eta) \\
N_{33} &= \frac{1}{8}(1+\zeta)(-1+\eta)(1+\eta)^2 \\
N_{43} &= -\frac{1}{8}(-1+\zeta)(-1+\eta)(1+\eta)^2
\end{aligned}
\tag{4.12}
$$

The element mass and stiffness matrices can be formed based on this interpolation function matrix by using Eqs. 3.16 and 3.18. The distributed element force can be transferred to the equivalent nodal force vector in element local coordinate system by using Eq. 3.19.

A mapping between the shell elements and the fluid panels is required to couple the structural and fluid models. The principle of the mapping between a structural element and fluid panel is that the structural motion must be related to the fluid motion through the boundary conditions. A one-to-one mapping between structural elements and panels is used herein, as it is the simplest approach and requires the least approximation.

4.1.2 The coordinate systems for quadrilateral element

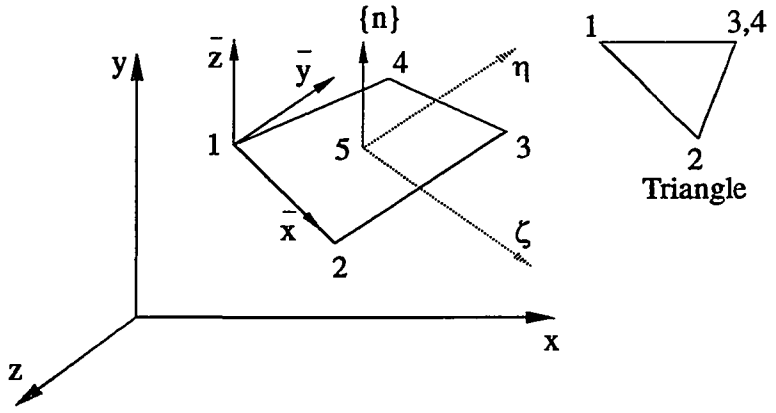

Figure 4.3 Global, local and natural coordinates for quadrilateral element

The definition of the global coordinate system x-y-z, the local element coordinate system $\bar{x}-\bar{y}-\bar{z}$, and the element natural coordinate system $\zeta-\eta$ are illustrated in Fig. 4.3. If a triangle element is necessary to fit the structural surface, the numbering of the four nodes are also shown in Fig. 4.3. The $\bar{x}$ axis is directed from node 1 to node 2, and the $\bar{z}$ axis is parallel to the normal vector of the quadrilateral element. The local $\bar{y}$ axis is then determined by the right hand rule.

The general vector {A}, with the components in the global coordinate system x-y-z, can be transferred to the same vector $\{\bar{A}\}$, with the components in the local coordinate system $\bar{x}-\bar{y}-\bar{z}$, by the transformation

$$\{\bar{A}\} = [T_1]\{A\} \tag{4.13}$$

or

$$\begin{bmatrix} \bar{x} \\ \bar{y} \\ \bar{z} \end{bmatrix} = \begin{bmatrix} \cos\bar{x}x & \cos\bar{x}y & \cos\bar{x}z \\ \cos\bar{y}x & \cos\bar{y}y & \cos\bar{y}z \\ \cos\bar{z}x & \cos\bar{z}y & \cos\bar{z}z \end{bmatrix} \begin{bmatrix} x \\ y \\ z \end{bmatrix} \tag{4.14}$$

where $[T_1]$ is the transformation matrix which contains the direction cosines. From the properties of the direction cosines, it can be easily shown that $[T_1]^T [T_1] = [I]$, where $[I]$ is an identity matrix. The procedure to calculate the direction cosines can be found in many references (for example, Paz, 1985, pp. 364-368). The transformation of the nodal displacement vectors involves the transformation of linear and angular displacement vectors at each node of the element. Therefore, a 4-node quadrilateral element requires the transformation of a total of eight displacement vectors. The transformation of 24×1 nodal displacement vector $\{d_g\}$ in the global coordinates to the displacement vector $\{d\}$ in local coordinates may be written in abbreviated form as

$$\{d\} = [T] \{d_g\} \tag{4.15}$$

in which

$$[T] = \begin{bmatrix} [T_1] & & & & & & & \\ & [T_1] & & & & & & \\ & & [T_1] & & & & & \\ & & & [T_1] & & & & \\ & & & & [T_1] & & & \\ & & & & & [T_1] & & \\ & & & & & & [T_1] & \\ & & & & & & & [T_1] \end{bmatrix} \tag{4.16}$$

Analogously, the transformation from nodal forces $\{r_g^{ext}\}$ in global coordinates to

nodal forces $\{r^{ext}\}$ in local coordinates is given by

$$\{r^{ext}\} = [T] \{r_g^{ext}\} \tag{4.17}$$

4.2 Three-dimensional fluid model

The three-dimensional velocity-potential problem has been described in Section 3.3.2. The incident wave potential in the fluid without a structure can be obtained easily by solving the Laplace equation subject to linear boundary conditions. The Green function method is introduced to solve the diffraction and radiation potentials, for which the structure is present. The volume integral in the three-dimensional domain is transferred to the two-dimensional surface integral by Green's identity. A Green function is selected which satisfies all boundary conditions, except on the structure, so that the integration is limited to the structural wetted surface under the still-water plane. The prescribed body motions, represented by the structural 'dry' mode shapes, are used to define the boundary conditions for the radiation potentials.

The Green function integral on the structural mean-wetted surface is calculated numerically. The structural wetted surface is discretized by a number of fluid panels. The structural and fluid motions are coupled by mapping the structural mode shapes for the structural elements onto the fluid panels. For simplicity, a constant velocity potential is assumed at each fluid panel. Therefore, the boundary condition is evaluated at the center of each fluid panel.

4.2.1 Fluid panels

The fluid panel method is used to solve numerically the velocity potentials by the source distribution method. Because a constant source distribution is assumed on each fluid panel, the panel size cannot be very large in general.

Four node quadrilateral panels are adopted as the fluid panels to describe the geometry of the structural wetted surface. If a triangular panel is necessary to fit the structural surface, a four node triangle element can be used as shown in Fig. 4.3. A one-to-one mapping between structural elements and fluid panels is used to couple the structural and fluid motions, that is the fluid panels exactly correspond to the structural shell elements on the wetted surface. Fig. 4.4 schematically shows the fluid panel distribution on a single module.

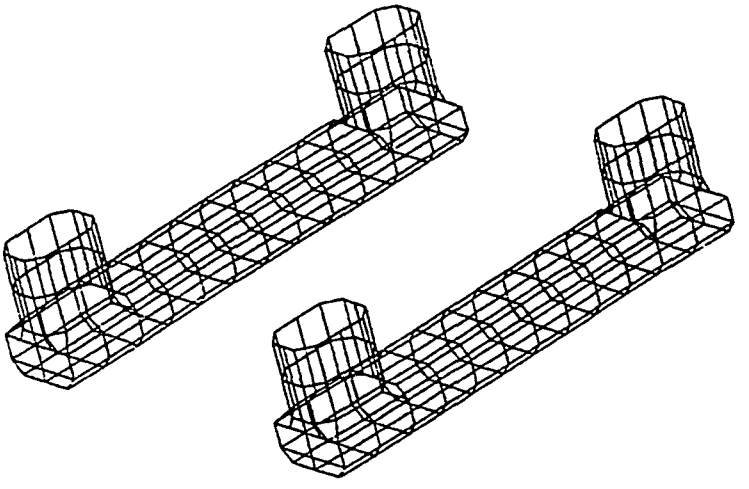

Figure 4.4 Quadrilateral panel distribution on a single module

The total fluid panel number is *npanel*. For each panel, the coordinates of the four nodes can be defined in the global coordinate system. Fig. 4.5 shows a fluid panel, in which

$$\{r_{ij}\} = \{(x_j - x_i), (y_j - y_i), (z_j - z_i)\} \qquad (i \neq j), i, j = 1, 2, 3, 4 \tag{4.18}$$

represents a vector from node i to node j; $\{n\}$ is the normal vector of the fluid panel; (x_i, y_i, z_i) $i = 1, 2, 3, 4$ are the coordinates of node i in the global coordinate system; (x_c, y_c, z_c) are the coordinates of the center of the fluid panel; $\bar{x} - \bar{y}$ is the local

coordinate system in the panel plane with $\bar{z}$ axis parallel to the normal vector {n}, which has the same definition as the local coordinate system of the shell element.

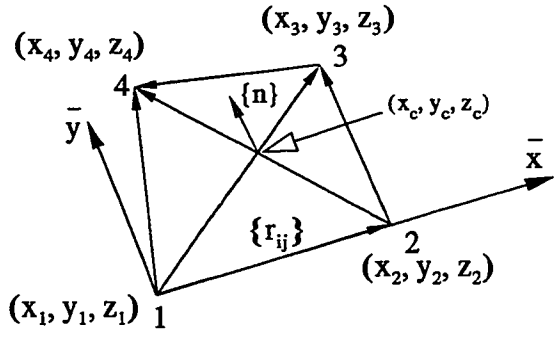

Figure 4.5 Fluid panel

The area of panel n, A_n, is the sum of two triangle areas:

$$A_n = \frac{1}{2}\left|\{r_{12}\} \times \{r_{23}\}\right| + \frac{1}{2}\left|\{r_{14}\} \times \{r_{34}\}\right| \tag{4.19}$$

The center coordinates of the fluid panel can be calculated by taking $\zeta = \eta = 0$ in Eq. 4.4 as

$$\begin{bmatrix}\bar{x}\\ \bar{y}\end{bmatrix} = \begin{bmatrix} N_1 & 0 & N_2 & 0 & N_3 & 0 & N_4 & 0 \\ 0 & N_1 & 0 & N_2 & 0 & N_3 & 0 & N_4 \end{bmatrix}_{\substack{\zeta=0 \\ \eta=0}} \begin{bmatrix} \bar{x}_1 \\ \bar{y}_1 \\ \bar{x}_2 \\ \bar{y}_2 \\ \bar{x}_3 \\ \bar{y}_3 \\ \bar{x}_4 \\ \bar{y}_4 \end{bmatrix} \tag{4.20}$$

The normal vector for each fluid panel is directed out of the fluid domain and into the structure, as mentioned in Section 3.3.2. The normal vector in global coordinates can be calculated by following the procedure in Section 3.4.1. The normal vector in local coordinates is, by definition,

$$\{\bar{n}\} = (0, 0, 1) \tag{4.21}$$

4.2.2 Generalized normal for three-dimensional panel

The generalized normal defined by Eq. 3.99 is in global coordinates. This generalized normal can be used in the body boundary condition in Eq. 3.100. It is straightforward to show that the generalized normal is the same whether calculated in the global or local coordinate system.

The normal vector {n} of a quadrilateral element in the global coordinate system is calculated at the center of the panel. From Eq. 4.13, the normal vector {n} has the relationship with the normal vector $\{\bar{n}\}$ in local coordinates

$$\{\bar{n}\} = [T_1]\{n\} \tag{4.22}$$

where $[T_1]$ has been defined in Eq. 4.14. $\{\psi_j^c\}$ is the displacement vector in the jth mode shape, which contains only three translational displacement components. $\{\bar{\psi}_j^c\}$ represents the same mode-shape vector but in the local coordinate system. $\{\bar{\psi}_j^c\}$ and $\{\psi_j^c\}$ have the relationship

$$\{\bar{\psi}_j^c\} = [T_1]\{\psi_j^c\} \tag{4.23}$$

So the generalized normal calculated in the local coordinate system can be written as

$$\bar{n}_j^* = \{\bar{\psi}_j^c\}^T \{\bar{n}\} = \{\psi_j^c\}^T [T_1]^T [T_1] \{n\} = \{\psi_j^c\}^T \{n\} = n_j^* \tag{4.24}$$

This means that the generalized normal can be calculated in either the local or global coordinate system. Since the mode displacement at a point is usually calculated in the local coordinate system, it may be more convenient to calculate the generalized normal in the local coordinate system.

The jth nodal mode shape $\{\psi_j\}$, a 24×1 vector in the global coordinate system, can be formed by extraction from the structural mode shapes $\{\Psi\}$. The jth local nodal mode shape $\{\bar{\psi}_j\}$ can be obtained by transforming $\{\psi_j\}$, i.e.

$$\{\bar{\psi}_j\} = [T] \{\psi_j\} \tag{4.25}$$

The jth mode shape vector at the center of the element in the local coordinate system, $\{\bar{\psi}_j^c\}$, can be interpolated from $\{\bar{\psi}_j\}$ by setting $\zeta = \eta = 0$ in the interpolation matrix [N] in Eq. 4.9

$$\{\bar{\psi}_j^c\} = [N]_{\substack{\zeta=0 \\ \eta=0}} \{\bar{\psi}_j\} \tag{4.26}$$

Finally, the generalized normal for each fluid panel can be calculated by

$$n_j^* = \{\bar{\psi}_j^c\}^T \{\bar{n}\} \tag{4.27}$$

By definition, the normal vector in the local coordinate system has only one nonzero component, a 1 for the $\bar{z}$ component. Therefore, the generalized normal can be simply obtained by taking the $\bar{z}$ component from the local mode shape $\{\bar{\psi}_j^c\}$.

4.2.3 Three-dimensional velocity potential

For a linear problem, the total velocity potential for a sinusoidal incoming wave can be decomposed, as in Eq. 3.63, into

$$\Phi_T = \Phi e^{-i\omega t} = (\phi_I + \phi_D + \phi_R) e^{-i\omega t} = \left(\phi_I + \phi_D + \sum_{j=1}^{q} p_j \phi_j\right) e^{-i\omega t} \tag{4.28}$$

in which ϕ_I is the incident wave potential; ϕ_D is the diffraction wave potential; and ϕ_j are the radiation wave potentials. The incident wave potential is given by

$$\phi_I = -\frac{ig\alpha}{\omega} e^{ik(x\cos\beta + y\sin\beta)} e^{kz'} \tag{4.29}$$

The diffraction and radiation velocity potentials need to be solved by using the Green function method. The source distribution method described in Section 3.3.4 is chosen to solve the velocity potentials. This method can be expressed by the following two equations:

$$\begin{aligned} \phi(P) &= \frac{1}{4\pi} \iint_{S_b} G(P, Q)\, \sigma(Q)\, dS \qquad P \in S_b \\ \frac{1}{2}\sigma(P) + \frac{1}{4\pi} \iint_{S_b} \sigma(Q) \frac{\partial G(P, Q)}{\partial n} dS &= \frac{\partial \phi_e(P)}{\partial n} = \dot{u}_n(P) \end{aligned} \tag{4.30}$$

in which $G(P, Q)$ is the Green function; $\sigma(Q)$ is the source density on the mean body surface S_b; $\dot{u}_n(P)$ is the normal velocity of the mean structural surface.

The structural surface below the still water line is discretized by quadrilateral fluid panels. Constant velocity potential (constant source density) at each fluid panel is assumed. The normal velocity at point P in each panel is taken at the center of the panel.

The jth normal modal velocity, which is equal to $-i\omega \{\psi_j^c\}^T \{n\} = -i\omega n_j^*$, is used as the body boundary condition to solve the jth radiation velocity potential. The generalized normal n_j^* can be calculated in the panel local coordinate system as mentioned in Section 4.2.2. Therefore, by using the constant fluid panel method, Eq. 4.30 can be written for the jth radiation potential as

$$\phi_n^j(P_n) = \frac{1}{4\pi} \sum_{\substack{i=1 \\ i \neq n}}^{npanel} \sigma_i^j(Q_i) \iint_{\Delta S_i} G(P_n, Q_i)\, dS$$

$$\frac{1}{2}\sigma_n^j(P_n) + \frac{1}{4\pi} \sum_{\substack{i=1 \\ i \neq n}}^{npanel} \sigma_i^j(Q_i) \iint_{\Delta S_i} \frac{\partial G(P_n, Q_i)}{\partial n} dS = -i\omega n_j^*(P) \tag{4.31}$$

where *npanel* is the total number of the fluid panels. Eqs. 4.31 are true for all the fluid panels. Therefore, a total of *npanel* linear equations exist in each equation of Eqs. 4.31. These two equations can be written, in matrix form, as

$$\begin{aligned} [J]\{\bar{\sigma}\} &= \{\dot{u}_n\} \\ \{\phi\} &= [G]\{\bar{\sigma}\} \end{aligned} \tag{4.32}$$

In the first of Eqs. 4.32, [J] is an $npanel \times npanel$ matrix with diagonal equal to $\frac{1}{2}$, while the off-diagonal terms J_{ni} contain the integral in Eq. 4.31, which can be written as

$$J_{ni} = \frac{1}{4\pi} \sum_{\substack{i=1 \\ i \neq n}}^{npanel} \iint_{\Delta S_i} \frac{\partial G(P_n, Q_i)}{\partial n} dS \tag{4.33}$$

$\{\bar{\sigma}\}$ is an $npanel \times 1$ vector that contains the source densities on each panel; $\{\dot{u}_n\}$ is an $npanel \times 1$ vector that contains the prescribed normal velocity in terms of the normal modal velocity on each panel. It can be seen that matrix [J] depends on the

Green function, mean body-surface shape, discretization, and the wave frequency, but not on the body motion. [J] is called the influence coefficient matrix. In the second equation of Eqs. 4.32, [G] is called the Green function coefficient matrix, which contains the integral term in the first equation of Eqs. 4.31, which is also not motion related.

To solve the three-dimensional radiation velocity potential by the Green function method, first one needs to form the influence coefficient matrix [J] for each wave frequency. Then for each structural mode, $npanel \times npanel$ algebraic equations are solved to obtain the source density $\{\bar{\sigma}\}$ at each fluid panel. The Green function coefficient matrix [G] is formed for each wave frequency, and multiplied by $\{\bar{\sigma}\}$ to obtain the velocity potential at each fluid panel.

The remaining problems are the selection of the Green function and the calculation of the influence coefficient and the Green function coefficient matrices. Fortunately, much work has been done on these two problems. Wehausen and Laitone (1960) presented significant work on the Green functions. Some forms of the Green functions also can be found in Wu (1984). It can be seen, from Eq. 3.79, the Green function has a singularity when the source point Q approaches the field point P. Therefore, the integration for influence and the Green function coefficients need special consideration. A pioneering study on this subject can be found in Newman (1986).

The diffraction wave potential also can be obtained by the Green function method. Instead of using normal modal velocity at the structural mean surface, the boundary conditions for the diffraction potential in Eq. 3.69 are used to solve the source density. The jth modal diffraction wave force can be obtained by using the radiation potential and the incident potential by the Haskind-Hanaoka relationship. It should be mentioned here

that the Haskind-Hanaoka relationship cannot provide the pressure distribution. This relationship is used here to calculate the modal diffraction wave force.

4.2.4 Hydrodynamic force vectors and matrices

After obtaining the incident, diffraction, and radiation velocity potentials, the linear generalized (modal) hydrodynamic forces can be calculated by using Eq. 3.104. The generalized incident wave force can be calculated by substituting the incident wave potential ϕ_I into Eq. 3.104:

$$\{F_I\}^* = \sum_{n=1}^{npanel} i\omega\rho \iint_{S_e} \{n\}^* \phi_I dS \tag{4.34}$$

Similarly, the generalized diffraction wave force can be calculated by substituting the diffraction wave potential ϕ_D into Eq. 3.104:

$$\{F_D\}^* = \sum_{n=1}^{npanel} i\omega\rho \iint_{S_e} \{n\}^* \phi_D dS \tag{4.35}$$

As mentioned before, the diffraction wave force can be obtained by using the Haskind-Hanaoka relationship. The jth modal diffraction wave force becomes

$$f_{Dj} = \rho \iint_{S_b} \phi_j \frac{\partial \phi_I}{\partial n} dS \tag{4.36}$$

Finally, the generalized radiation wave force can be calculated by substituting the radiation wave potentials ϕ_R into Eq. 3.104, which can be written as

$$\{F_R\}^* = \sum_{n=1}^{npanel} i\omega\rho \iint_{S_e} \{n\}^* \phi_R dS = \sum_{n=1}^{npanel} i\omega\rho \iint_{S_e} \{n\}^* \phi_j \; p_j dS \tag{4.37}$$

where summation convention is used in Eq. 4.37. The generalized radiation wave force is related to the structural motion. Therefore, Eq. 4.37 can be written in the form of the hydrodynamic coefficient matrix and the principal coordinates as

$$\{F_R\}^* = \sum_{n=1}^{npanel} i\omega\rho \iint_{S_e} \{n\}^* \phi_j \; p_j dS = (\omega^2 [M_f^*] + i\omega [C_f^*]) \{p\} \tag{4.38}$$

where $[M_{fjk}]$ and $[C_{fjk}]$ are added mass and damping matrices, respectively; the subscript j and k represent, the jth modal force caused by the kth modal displacement. The element M_{fjk}^* of the added mass matrix is

$$M_{fjk}^* = \sum_{n=1}^{npanel} \frac{\rho}{\omega^2} Re\left\{ i\omega \iint_{S_e} n_j^* \phi_k dS \right\} \tag{4.39}$$

and the element C_{fjk}^* of the hydrodynamic damping matrix is

$$C_{fjk}^* = \sum_{n=1}^{npanel} \frac{\rho}{\omega} Im\left\{ i\omega \iint_{S_e} n_j^* \phi_k dS \right\} \tag{4.40}$$

where *Re* and *Im* denote the real and imaginary parts of the complex functions, respectively.

4.3 Hydrostatic restoring coefficients in the three-dimensional model

"Hydrostatics is the oldest and most elementary topic of naval architecture and fluid mechanics" (Newman, 1977). The hydrostatic restoring coefficients for rigid body

motion of floating structures have been studied very well. However, the hydroelastic restoring forces which result from flexible deformations of very large flexible structures may be significant compared with elastic forces. Therefore, the study of hydrostatics becomes an important topic for very large floating structures.

The formulation for generalized hydrostatic restoring coefficients is discussed in this section. The formulation discussed here is based on the mode-superposition and panel methods. The general formulation for hydrostatic restoring coefficients is discussed first. The traditional hydrostatic restoring coefficients then become a special case of the general formulation presented here. The consistent formulation of hydrostatic restoring coefficients for single beams and frame structures can be found in Chapters 5 and 6, respectively.

4.3.1 Generalized hydrostatic restoring coefficients

The term $-\rho g z'$ in Euler's integral of Eq. 3.55 is the hydrostatic pressure, which gives rise to the hydrostatic restoring forces. Again, ρ is the water density; g is the gravitational acceleration; $z' = z - z_w$; and z_w is the vertical coordinate of the still-water plane. Fig. 4.6 shows the definition for the hydrostatics.

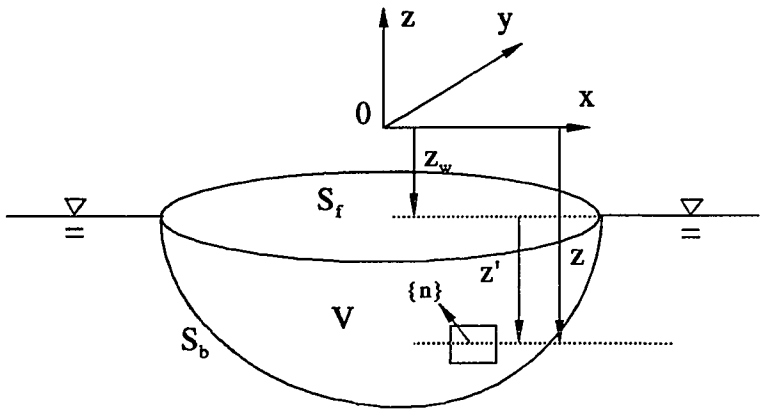

Figure 4.6 The definition for hydrostatics

When a structure floats, from Archimedes' principle, the buoyancy force is equal to the structural weight. If the weight is $\{W\}=[0, 0, F_W]^T$, then Archimedes' principle gives

$$\{W\} = \iiint_V \rho g \{k\} dV \tag{4.41}$$

where V is the water volume displaced by the structure and $\{k\}=[0, 0, 1]^T$ This volume is surrounded by the wetted structural surface S_b and still water plane surface S_f.

The hydrostatic force can also be calculated by integrating the hydrostatic pressure, $-\rho gz'$, in the normal direction over the mean-wetted surface, which can be written as

$$\{W\} = -\iint_{S_b} \rho gz' \{n\} dS \tag{4.42}$$

where the normal vector $\{n\}$, as before, points out of the fluid domain. If the still-water-plane surface S_f is added to this integral of Eq. 4.42, from Gauss's divergence theorem, this surface integral can be converted to a volume integral

$$-\iint_{S_b} \rho gz' \{n\} dS - \iint_{S_f} \rho gz' \{n\} dS = \iiint_V \rho g \{k\} dV = \{W\} \tag{4.43}$$

where the minus sign in the front of the surface integral is canceled with the minus sign implicit in the normal vector. On the still water plane surface S_f, the hydrostatic pressure is equal to zero. Therefore, Archimedes' principle can be also expressed as

$$\{W\} = -\iint_{S_b} \rho gz' \{n\} dS \tag{4.44}$$

In this case, the structure is in the equilibrium position. Hydrostatic pressure tends to restore the structure to this equilibrium position from a disturbed position. In other

words, a disturbance of the structure will modify the hydrostatic pressure acting on the structure, and the resulting pressure forces and moments are called hydrostatic restoring forces.

Suppose that the disturbance in the vertical direction is w, which is a function of the position. Then, after disturbance, the vertical coordinates $\hat{z}$ of each position is given by

$$\hat{z} = z' + w \tag{4.45}$$

and the hydrostatic pressure at this position becomes

$$-\rho g\hat{z} = -\rho gz' - \rho gw \tag{4.46}$$

The hydrostatic force $\{F_{hyst}\}$ acting on the wetted surface can be obtained by

$$\{F_{hyst}\} = -\iint_{S_b} \rho gz' \{n\}\, dS - \iint_{S_b} \rho gw \{n\}\, dS \tag{4.47}$$

The first term of Eq. 4.47 is equal to the structural weight from Eq. 4.44. Only the second term results in hydrostatic restoring force, which can be written as

$$\{F_r\} = -\rho g \iint_{S_b} w \{n\}\, dS \tag{4.48}$$

where $\{n\}$ is the wetted surface normal vector in the global coordinate system. The jth modal hydrostatic restoring force can be calculated by

$$F_{r_j}^* = \{\psi_j\}^T \{F_r\} = -\rho g \iint_{S_b} w \{\psi_j\}^T \{n\}\, dS = -\rho g \iint_{S_b} w n_j^*\, dS \qquad j = 1, 2, \ldots, q \tag{4.49}$$

in which $\{\psi_j\}$ is the jth mode shape vector at a point in the global coordinate system, which contains three translational displacements only; n_j^* is the jth generalized normal.

From the above discussion, it is possible to determine the modal hydrostatic restoring forces for displacements associated with any mode. The vertical displacement w at any point on the wetted surface is

$$w = \{\psi_w\}^T \{p\} \tag{4.50}$$

where $\{\psi_w\}$ is the vertical modal displacement vector at the point, which can be extracted from the mode shape $[\Psi]$; and $\{p\}$ is the principal coordinate vector. When the first q mode shapes are used in mode superposition, $\{\psi_w\}$ is a $q \times 1$ vector and it can be expressed as $\{\psi_w\}^T = \{\psi_{w1}, \psi_{w2}, \ldots, \psi_{wq}\}$. Thus generalized hydrostatic restoring force vector $\{F_r^*\}$ can be written as

$$\{F_r^*\} = -\left[\rho g \iint_{S_b} \{\psi\}^T \{n\} \{\psi_w\}^T dS\right] \{p\} = -[K_f^*] \{p\} \tag{4.51}$$

where $\{\psi\}$ is the mode shape matrix at a point which has column j equal to $\{\psi_j\}$ and $[K_f^*]$ is the newly defined generalized restoring coefficient matrix. The elements of $[K_f^*]$ are given by

$$K_{fjk}^* = \rho g \iint_{S_b} \{\psi_j\}^T \{n\} \psi_{wk} dS = \rho g \iint_{S_b} n_j^* \psi_{wk} dS \qquad j, k = 1, 2, \ldots, q \tag{4.52}$$

Eq. 4.52 is the general formulation for the generalized restoring coefficients.

4.3.2 Rigid body hydrostatic restoring coefficients

The conventional hydrostatic restoring coefficients for rigid body displacements are a special case of Eq. 4.52. For rigid body motion, if the surface integral in Eq. 4.52 is extended to include the still-water plane surface, then it becomes a closed surface integral. Gauss's divergence theorem can be applied to this integral and it can be written as

$$\rho g \iint_{S_b} \{\psi_j\}^T \{n\} \psi_{wk} dS + \rho g \iint_{S_f} \{\psi_j\}^T \{n\} \psi_{wk} dS = -\rho g \iiint_V \nabla (\{\psi_j\} \psi_{wk}) dV \quad (4.53)$$

where ∇ is the gradient operator as defined in Eq. 3.62, and the minus sign in the front of the volume integral, again, is because the normal vector points into the body. So the hydrostatic restoring coefficients can be written as

$$\begin{aligned} K_{fjk}^* &= \rho g \iint_{S_b} \{\psi_j\}^T \{n\} \psi_{wk} dS \\ &= -\rho g \iiint_V \nabla (\{\psi_j\} \psi_{wk}) dV - \rho g \iint_{S_f} \{\psi_j\}^T \{n\} \psi_{wk} dS \end{aligned} \quad (4.54)$$

For heave restoring coefficient K_{f33}^*, $\psi_{w3} = 1$ and $\{\psi_3\} = \{0, 0, 1\}$, and therefore $\nabla (\{\psi_3\} \psi_{w3}) = 0$. The volume integral in Eq. 4.54 is equal to zero. On the still water plane, the generalized normal vector $n_3^* = \{\psi_3\}^T \{n\} = -1$, which points into the structure, so $\{\psi_3\}^T \{n\} \psi_{w3} = -1$. Hence

$$K_{f33}^* = 0 - \rho g \iint_{S_f} (-1) dS = \rho g A_f \quad (4.55)$$

where A_f is the still-water-plane area. Eq. 4.55 can be recognized as the heave restoring coefficient in naval architecture.

For roll restoring coefficient K_{f44}^*, $\psi_{w4} = y - y_G$ and $\{\psi_4\}^T = \{0, -(z - z_G), (y - y_G)\}$. Therefore, $\nabla(\{\psi_4\}^T \psi_{w4}) = -(z - z_G)$, and $n_4^* = \{\psi_4\}^T \{n\} = -n_2(z - z_G) + n_3(y - y_G)$. On the still-water-plane, $n_2 = 0$ and $n_3 = -1$, so $n_4^* = -(y - y_G)$ and $\psi_{w4} n_4^* = -(y - y_G)^2$. Hence

$$K_{f44}^* = -\rho g \iiint_V [-(z - z_G)]\, dV - \rho g \iint_{S_f} [-(y - y_G)^2]\, dS \tag{4.56}$$

The hulls of most ocean structures, such as ships, exhibit port-starboard symmetry, and, in this case, y_G is equal to zero. In such a case, Eq. 4.56 becomes

$$K_{f44}^* = \rho g [V(z_B - z_G) + S_{xx}] \tag{4.57}$$

in which z_B is the center of the displaced water volume (or the center of buoyancy), and S_{xx} is the second moment of the water-plane area about the axis which is parallel to the x-axis (in Fig. 4.6) and in the still-water-plane. Noting that

$$\overline{GM}_T = \frac{S_{xx}}{V} + (z_B - z_G) \tag{4.58}$$

where $\overline{GM}_T$ is the transverse metacentric height, the restoring coefficient for roll motion can be written as

$$K_{f44}^* = \rho g V \overline{GM}_T \tag{4.59}$$

which is the conventional expression in naval architecture.

By using similar steps, the hydrostatic restoring coefficient for pitch, K_{f55}^*, can also be obtained as

$$K_{f55}^* = \rho g [V(z_B - z_G) + S_{yy}] \tag{4.60}$$

where S_{yy} is the second moment of the water plane area about the axis which is parallel to the y-axis (in Fig. 4.6) and in the still-water-plane. By noting that

$$\overline{GM_L} = \frac{S_{yy}}{V} + (z_B - z_G) \tag{4.61}$$

where $\overline{GM_L}$ is the longitudinal metacentric height, then

$$K_{f55}^{*} = \rho g V \overline{GM_L} \tag{4.62}$$

The off-diagonal rigid-body restoring coefficient K_{f35}^{*} can be obtained as follows. In this case, $\{\psi_3\} = \{0, 0, 1\}$ and $\psi_{w5} = -(x - x_G)$. Therefore, $\nabla(\{\psi_3\}\psi_{w5}) = 0$, and so the volume integral in Eq. 4.54 is equal to zero. On the still-water plane, the generalized normal $n_3^{*} = n_3 = -1$, so $\{\psi_3\}^T\{n\}\psi_{w5} = (x - x_G)$. Hence,

$$K_{f35}^{*} = 0 - \rho g \iint_{S_f} (x - x_G)\, dS \tag{4.63}$$

If the center of gravity of the structure is located at $x_G = 0$, then

$$K_{f35}^{*} = -\rho g S_x \tag{4.64}$$

where

$$S_x = \iint_{S_f} x\, dS \tag{4.65}$$

The off-diagonal rigid-body restoring coefficient K_{f53}^{*} can be obtained as follows. In this case, $\{\psi_5\} = \{(z - z_G), 0, -(x - x_G)\}$ and $\psi_{w3} = 1$. Therefore, $\nabla(\{\psi_3\}\psi_{w5}) = 0$, and so the volume integral in Eq. 4.54 is equal to zero. On the still-

water plane, the generalized normal $n_5^* = n_1(z-z_G) - n_3(x-x_G) = (x-x_G)$, so $\{\psi_3\}^T\{n\}\psi_{w5} = (x-x_G)$. As a result,

$$K_{f53}^* = K_{f35}^* \tag{4.66}$$

Similarly, it can be proved that for a structure with $y_G = 0$

$$K_{f34}^* = K_{f43}^* = \rho g S_y \tag{4.67}$$

where

$$S_y = \iint_{S_f} y dS \tag{4.68}$$

For K_{f45}^*, $\{\psi_4\} = \{0, -(z-z_G), -(y-y_G)\}$ and $\psi_{w5} = -(x-x_G)$. Therefore, $\nabla(\{\psi_4\}\psi_{w5}) = 0$, and so the volume integral in Eq. 4.54 is equal to zero. On the still-water plane, the generalized normal $n_4^* = -n_2(z-z_G) - n_3(y-y_G) = (y-y_G)$, so $n^*\psi_{w5} = -(x-x_G)(y-y_G)$. Similarly, $n^*\psi_{4w5} = -(x-x_G)(y-y_G)$. Therefore, for a structure with $x_G = 0$ and $y_G = 0$,

$$K_{f45}^* = K_{f54}^* = -\rho g S_{xy} \tag{4.69}$$

where

$$S_{xy} = \iint_{S_f} xy dS \tag{4.70}$$

From Eqs. 4.64, 4.67, and 4.69, if a structure is double symmetric, the off-diagonal terms are all equal to zero.

4.4 Hydrostatic restoring coefficients by panel method

Even though the hydrostatic restoring coefficients can be calculated by evaluating a volume integral and water plane surface integral, in practical cases, the formulation in Eq. 4.52, which involves an integral on the mean-wetted surface, is more convenient for the hydrostatic restoring coefficient calculation. As described in Section 4.2.1, the panel method has been used in the velocity potential calculation. The same panels can be used to calculate the hydrostatic restoring coefficients. Thus Eq. 4.52 can be written as

$$K_{fjk}^{*} = \rho g \sum_{n=1}^{npanel} \int\int_{\Delta S_n} n_j^{*} \psi_{wk} dS \tag{4.71}$$

in which *npanel* is the total number of fluid panels and ΔS_n is the area of panel n. If the fluid panel is small enough, the integrand can be assumed constant on each panel, and thus Eq. 4.71 becomes

$$K_{fjk}^{*} = \rho g \sum_{n=1}^{N} n_j^{*} \psi_{wk} \Delta S_n \tag{4.72}$$

4.5 Equations of motion of three-dimensional hydroelasticity

The modal equations of motion are

$$\left[-\omega^2 \left([M_s^{*}] + [M_f^{*}]\right) - i\omega \left([C_s^{*}] + [C_f^{*}]\right) + \left([K_s^{*}] + [K_f^{*}]\right)\right] \{p\} = \{F_I^{*}\} + \{F_D^{*}\} \tag{4.73}$$

in which $[M_s^{*}]$, $[C_s^{*}]$, and $[K_s^{*}]$ are the modal structural mass, damping, and stiffness matrices, respectively; M_{fjk} and C_{fjk} are the elements of the modal added-mass and damping matrices, $[M_f^{*}]$ and $[C_f^{*}]$, respectively; $[K_f^{*}]$ is the hydrostatic

stiffness matrix, which results from the changes in hydrostatic pressure as discussed in Sections 4.3 and 4.4; and $\{F_I^*\}$ and $\{F_D^*\}$ are the modal hydrodynamic forces, which represent incident and diffraction forces, respectively.

Eq. 4.73 represents q modal equations. Upon solutions of Eq. 4.73 for the principle coordinates {p}, the nodal displacements {D} can be calculated by Eq. 3.45. The other structural responses required by engineering design can be calculated, and internal forces and stresses can be obtained from Eqs. 3.46 and 3.47.

CHAPTER 5

TWO-DIMENSIONAL HYDROELASTICITY

5.1 Overview

The difficulty of applying general three-dimensional hydroelasticity to a VLFS is the large computational resources that would be required. Although it may be technically possible to carry out a three-dimensional hydroelastic analysis of a VLFS, it would appear that such an analysis may be most appropriate as a final step in the design process, rather than during the intermediate design phases. Hence, there is a need for alternative, less computationally demanding methods of analysis which can provide the basic data for design of VLFSs. Two-dimensional hydroelasticity offers one such method.

Two-dimensional hydroelasticity was developed originally based on strip theory for hydrodynamic force calculations. Strip theory is most applicable to long structures with relatively constant cross-sectional geometry because two-dimensional flow is assumed. In strip theory, The structure is assumed as a single rigid 'beam'. In two-dimensional hydroelasticity, the slender structure is modeled as an elastic, nonuniform beam to satisfy the two-dimensional flow assumption. Therefore, the beam-like structural deformations and internal forces, such as vertical and horizontal bending moments and shear force, can be predicted by two-dimensional hydroelasticity. Two-dimensional hydroelasticity has been applied extensively to ships (Bishop and Price, 1979), bridges (Langen and Sigbjornsson, 1980; Georgiadis, 1981; Luft, 1981; Hartz and Georgiadis, 1982), and other slender structures (Okamoto et al., 1985; Masuda et al., 1987; Che et al., 1990; Ertekin et al., 1990; Riggs et al., 1991).

The two-dimensional hydroelasticity developed by Bishop and Price (1979) models a

slender structure as a nonuniform Timoshenko beam to describe the beam deformation, and the fluid forces are determined by strip theory. This approach employs the mode-superposition method. This theory is reviewed first. An alternate two-dimensional hydroelasticity developed herein is based on the finite element method. The ubiquitous 'frame' element is used to model the slender structure below the water line. Above the water line, a general three-dimensional model of the structure can be used. The hydrodynamic coefficients, wave exciting forces, and hydrostatic restoring coefficients are formed in a consistent manner with the beam finite element model. The direct solution method is used to solve the equations of motion. This method is very efficient for hydroelastic analysis of very large floating structures. This chapter will discuss this approach for two-dimensional hydroelasticity.

5.2 Two-dimensional hydroelasticity of Bishop and Price

Based on the well-developed strip theory, Bishop and Price (1979) developed a two-dimensional hydroelasticity theory for ships. Unlike the traditional strip theory, a slender structure is modeled as an elastic beam. Bishop and Price (1979) have illustrated that for ships (which have a very large cross section compared to most other applications), shear deformation can have a measurable effect on the response. Hence, they used Timoshenko beam theory.

In this approach, the whole structure is modeled as a Timoshenko beam. Mode superposition is used to solve the equations of motion, and therefore an eigenvalue problem must be solved. The hydrodynamic coefficients and wave exciting forces for each section are obtained from strip theory. They are then transformed to the modal hydrodynamic coefficients and fluid forces. The modal equations of motion are solved and the physical displacement and beam-like internal forces can be obtained by superposition.

5.3 Alternative approach

As discussed in Section 5.2, the mode-superposition method has been used in two-dimensional hydroelasticity by Bishop and Price (1979). Since the structure is modeled as a beam, the total displacement-degrees-of-freedom are not large, and it is trivial to solve the equations of motion directly. In addition, since strip theory is used, there is no advantage to use mode superposition for the hydrodynamic calculations as there is in three-dimensional hydroelasticity. For these reasons, an alternate approach of two-dimensional hydroelasticity is developed. In this approach, the structure below the still-water line is modeled by beam finite elements. The part of the structure above the still-water line can be modeled as a general three-dimensional structure. The hydrodynamic and hydrostatic loads are formed in a manner consistent with the finite element model.

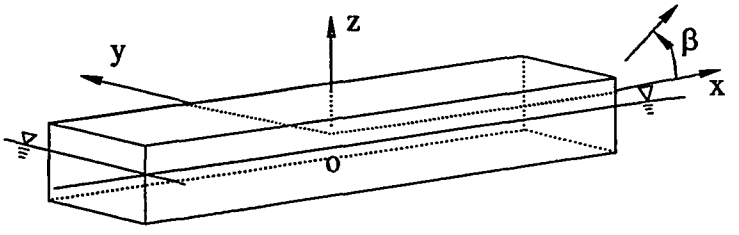

Figure 5.1 Schematic of a beam-like VLFS

Fig. 5.1 shows schematically a nonuniform beam. This beam model can be used to determine basic structural motion response and cross sectional internal forces. To describe the beam element, the global coordinate system x-y-z is defined in Fig. 5.1. The global longitudinal axis, x, is located such that it passes through the center of mass of the structure, and the z-axis is directed upward.

A 2-node, three-dimensional beam element is used to discretize the beam model of the submerged structure. Each node has six displacement-degrees-of-freedom, three

translations and three rotations. The element local coordinate system $\bar{x}-\bar{y}-\bar{z}$ is defined such that $\bar{x}$ is parallel to the global x-axis; $\bar{y}$ and $\bar{z}$ are the principal axes of the beam cross-section. The element local coordinate $\bar{x}-\bar{y}-\bar{z}$ typically corresponds to the global x-y-z system, except for $\bar{x}$ and (possibly) $\bar{z}$ translations. This local coordinate system has been shown in Fig. 3.1.

The formulation for the element mass matrix and the equivalent nodal forces will be used often in this chapter, and are therefore repeated for convenience. The element mass matrix is given by

$$[m] = \int_{L_e} [N]^T [\bar{m}] [N] \, dL \tag{5.1}$$

in which $[N]$ is the 6×12 matrix of interpolation functions from Eq. 3.27, which includes all interpolations for axial, torsional, and transverse displacements; $[\bar{m}]$ is the 6×6 matrix of mass densities per unit length given by Eq. 3.28, which is assumed constant within an element; and L_e is the length of the beam element. This formulation is also valid for other beam element matrices which have distributed properties similar to mass density.

The forces distributed along an element are replaced by equivalent nodal forces, which in local coordinates are given by

$$\{r^{ext}\} = \int_{L_e} [N]^T \{F_c\} \, dL \tag{5.2}$$

in which $\{F_c\}$ is the 6×1 vector of distributed forces and moments, and $\{r^{ext}\}$ is a 12×1 nodal force vector.

The Euler-Bernoulli beam element mass matrix is given in Eq. A.10, and stiffness matrix is given in Eq. A.11 in Appendix A. As mentioned previously, if a beam model is used to model a slender structure, the shear deformation should be considered. The

element stiffness matrix that includes the shear deformation can be found in Eq. A.12 in Appendix A. The structural mass, damping, and stiffness matrices, $[M_s]$, $[C_s]$, and $[K_s]$, respectively, can then be assembled by using the procedure described in Section 3.2.2.

5.4 Distributed hydrodynamic forces

Strip theory was originally developed to predict the rigid motion of slender structures, such as ships. It was first developed by Korvin-Kroukovsky (1955 and 1957) for predicting heave and pitch motions. It is the first motion theory which is suitable for numerical computations with adequate accuracy for engineering applications. Even today, strip theory is still used to predict motions in ship design. Tasai (1967) extended the theory first to obtain the sway, roll and yaw motions of a ship in oblique waves. Since then, many researchers have made significant contributions to this theory which include numerical improvements (Frank, 1967; Gerritsma and Beukelman, 1967; Smith, 1967; Smith and Salvesen, 1970). In 1970, Salvesen, Tuck, and Faltinsen (1970) revised the new strip theory of Ogilvie and Tuck (1969) for head seas to predict the heave, pitch, sway, roll, and yaw motions, as well as the wave-induced vertical and horizontal shear forces, bending and torsional moments for a ship advancing at constant forward speed in regular waves.

Strip theory has the following assumptions. First, an inviscid and incompressible fluid undergoing irrotational flow is assumed. Second, the fluid disturbance induced by the motion of a strip of the structure only propagates in the plane of the strip, perpendicular to the longitudinal axis of the body. The first assumption results in a potential problem, and the second assumption results in two-dimensional flow. The derivation of the two-dimensional flow problem based on the above assumptions can be found in many references, for example, Wang (1991).

The hydrodynamic forces obtained from strip theory have been used to excite rigid body motions. Actually, the hydrodynamic forces for each strip also can be taken as the distributed forces for hydroelastic analysis. For this reason, strip theory is reviewed here and the formulation of the distributed hydrodynamic forces are given.

In strip theory, the fluid forces are calculated for each cross-section. Each section has three rigid body modes: sway, heave, and roll. The two-dimensional radiation potential ϕ_j for the jth mode (j= 2, 3, 4), in infinitely deep water, satisfies the following boundary-value problem, which is illustrated in Fig. 5.2,

$$\left(\frac{\partial^2}{\partial y^2}+\frac{\partial^2}{\partial z^2}\right)\phi_j = 0 \qquad \text{in } D \tag{5.3}$$

$$\left(\frac{\partial}{\partial z}-k\right)\phi_j = 0 \qquad \text{on } z = z_w \tag{5.4}$$

$$\frac{\partial \phi_j}{\partial n} = \dot{u}_{nj} = -i\omega n_j^* \qquad \text{on } C_b \tag{5.5}$$

$$\lim_{z\to-\infty}\frac{\partial}{\partial z}(\phi_j) = 0, \qquad \lim_{y\to\pm\infty}\left[\frac{\partial \phi_j}{\partial y}\mp ik\phi_j\right] = 0 \tag{5.6}$$

where D is the two-dimensional fluid domain; $k = \omega^2/g$ is the wave number in deep water; C_b is the immersed contour of the strip cross-section; $\partial/\partial n$ is the derivative in the normal direction where the normal is determined from the normal to the contour of the cross-section and is directed out of the fluid; $\dot{u}_{nj}$ is the normal velocity of the wetted strip surface, and j=2, 3 and 4 represent sway, heave, and roll motion, respectively; $n_j^* = \{\psi_j\}^T\{n\}$ is the jth generalized normal for rigid-body motion given by Eq. 3.101. Similarly, the two-dimensional diffraction potential problem can be written.

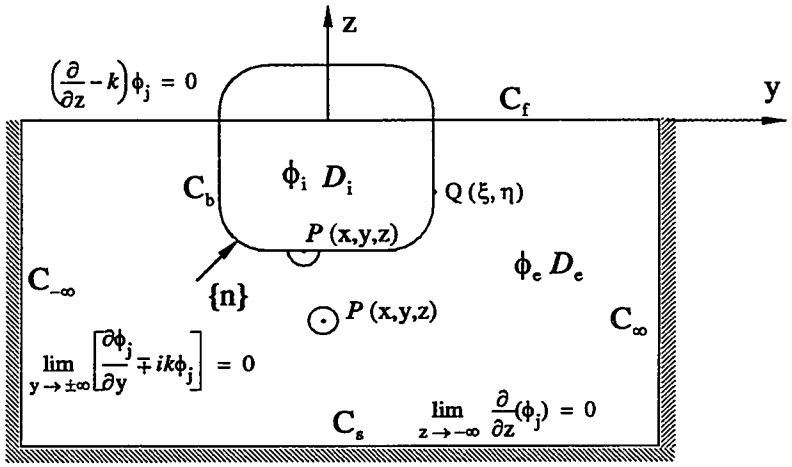

Figure 5.2 Two-dimensional domain for velocity potential

The two-dimensional flow described in Eqs. 5.3 - 5.6 can be solved with the Green function method (sometimes known as Frank's method; Frank, 1967). For the two-dimensional boundary-value problem, Green's third identity can be written as

$$\phi(P) = \alpha\int_C\left(\phi(Q)\frac{\partial G(P,Q)}{\partial n} - G(P,Q)\frac{\partial\phi(Q)}{\partial n}\right)dC \tag{5.7}$$

where C represents the entire two-dimensional boundary, which includes the still-water line, C_f; the sea floor boundary, C_s; the control boundary at $\pm\infty$, $C_{\pm\infty}$; and the mean body surface below the still-water line, C_b. G(P, Q) is the Green function.

The Green function G(P, Q) can be chosen by the same consideration as described in Section 3.3.3. The two-dimensional potential at point P(y, z) caused by a source located at $Q(\xi, \eta)$ can be expressed by a simple source:

$$\phi_2 = \ln(r) \tag{5.8}$$

where $r = \sqrt{(y-\xi)^2 + (z-\eta)^2}$. This two-dimensional potential ϕ_2 can be taken as a part of the two-dimensional radiation potential.

It can be shown that if one can choose a function $H(P, Q)$ such that the Green function

$$G(P, Q) = \ln(r) + H(P, Q) \tag{5.9}$$

satisfies

$$\nabla^2 G = \delta(P - Q) \qquad \text{in} \quad D \tag{5.10}$$

$$\left(\frac{\partial}{\partial z} - k\right) G = 0 \qquad \text{on} \quad z = z_w \tag{5.11}$$

$$\lim_{z \to -\infty} \frac{\partial}{\partial z}(G) = 0 \tag{5.12}$$

$$\lim_{y \to \pm\infty} \left[\frac{\partial G}{\partial y} \mp ikG\right] = 0 \tag{5.13}$$

then the integral in Eq. 5.7 need be evaluated only on the body wetted surface C_b, and can therefore be written as

$$\phi(P) = -\frac{1}{2\pi} \int_{C_b} \left(\phi(Q) \frac{\partial G(P, Q)}{\partial n} - G(P, Q) \frac{\partial \phi(Q)}{\partial n}\right) dC \tag{5.14}$$

Considering the interior and exterior problems which are illustrated in Fig. 5.2, the source distribution method, as described in Eq. 3.3.3, can be applied to this problem. The velocity potential can be written as

$$\phi(P) = \frac{1}{2\pi} \int_{C_b} G(P, Q)\, \sigma(Q)\, dC \qquad P \in C_b \tag{5.15}$$

where $\sigma(Q)$ is the source density at the source point Q.

One very efficient method for solving the two-dimensional potential problem is the so-called Frank's "Close-Fit" method (Frank, 1967). This method considers not only the interior and exterior problems but also the upper imaginary part which is mirrored from the strip contour line about the still-water line. The integral Eq. 5.15 is carried out over a

closed contour line. The name of "Close-Fit" comes from this closed contour line. The Green function for this problem was given earlier by Wehausen and Laitone (1960):

$$G(P,Q) = \ln(r) - \ln(r_1) + 2PV\cdot\int_0^{\infty} e^{z+\eta}\frac{\cos m(y-\xi)}{m-k}dm - ie^{k(z+\eta)}\cos k(y-\xi) \quad (5.16)$$

where $k = \omega^2/g$; $r = \sqrt{(y-\xi)^2+(z-\eta)^2}$; $r_1 = \sqrt{(y-\xi)^2+(z+\eta)^2}$; and PV denotes the Cauchy principal value integral.

By using the body boundary condition of Eq. 5.12 and taking the normal derivative of Eq. 5.15, one has

$$\frac{1}{2}\sigma(P) + \frac{1}{4\pi}\int_{C_b}\sigma(Q)\frac{\partial G(P,Q)}{\partial n}dC = \frac{\partial\phi(P)}{\partial n} = \dot{u}_{nj} \quad (5.17)$$

where $\dot{u}_n$ is the normal velocity of the mean-wetted surface. The source density can be determined from Eq. 5.17. and the radiation potential follows from Eq. 5.15.

A numerical method is needed to calculate these two integral equations. Since it is a two-dimensional problem, 'line' panels are used to discretize the cross section. The potential is solved for each cross section, so the number of the two-dimensional panels is not very large. Therefore, this method is very efficient.

The dynamic fluid pressures p can be calculated by using Euler's integral. The sectional modal fluid forces (moments) f_j can be calculated by integrating the pressures along the contour of the cross section in the generalized normal direction:

$$f_j = \int_C p n_j^* dC \qquad j = 2, 3, 4 \quad (5.18)$$

These sectional modal fluid forces are the distributed forces acting on a beam element.

5.5 Direct solution for two-dimensional hydroelasticity

The purpose of this section is to develop expressions for the distributed hydrodynamic forces acting on a beam model. Structural analysis typically requires that the six distributed generalized forces (forces and moments) which potentially act along the beam be defined. However, in two-dimensional hydroelasticity, these forces are obtained from strip theory. In strip theory, only the distributed "sway" and "heave" forces and "roll" moment in the y-z plane are defined. The other force and two moments cannot be obtained by using strip theory. Hence, they are assumed to be zero in the structural analysis.

The structure (Figure 5.1) is freely floating and it is assumed to be stationary (i.e., with zero forward speed). The hydrodynamic forces result from a train of regular waves with a crest at x = 0 (at time t=0) and an incidence angle of β, and from the resultant motion of the structure. The structure is partially submerged in an incompressible fluid undergoing irrotational flow in infinitely deep water. To determine the fluid flow, in linear theory, the total velocity potential, Φ_T, can be decomposed as in Eq. 3.63, and rewritten here

$$\Phi_T = (\phi_I + \phi_D + \phi_R)\, e^{-i\omega t} = \left(\phi_I + \phi_D + \sum_{j=1}^{q} p_j \phi_j\right) e^{-i\omega t} = \Phi e^{-i\omega t} \tag{5.19}$$

The incident wave potential is given in Eq. 3.71, which can be written for two-dimensional theory as

$$\phi_I = -\frac{ig\alpha}{\omega} e^{ikx\cos\beta} e^{iky\sin\beta} e^{kz'} \tag{5.20}$$

Once the potentials have been determined, the distributed forces acting on a beam element can be determined by integrating the hydrodynamic pressure for each cross

section obtained from Euler's integral. The sectional modal forces as a result of the incident, diffraction, and radiation potentials can be written, respectively, as

$$f_{Ij} = i\omega\rho\int_C \phi_I n_j^* dC \qquad j = 2, 3, 4 \tag{5.21}$$

$$f_{Dj} = i\omega\rho\int_C \phi_D n_j^* dC \qquad j = 2, 3, 4 \tag{5.22}$$

$$f_{Rj} = i\omega\rho p_k\int_C \phi_k n_j^* dC \qquad k, j = 2, 3, 4 \tag{5.23}$$

where summation convention is used in Eq. 5.23. Substitution of the body boundary-condition in Eq. 5.5 into Eq. 5.23 results in the modal sectional radiation wave force for mode j:

$$f_{Rj} = -\rho p_k\int_C \frac{\partial\phi_j}{\partial n}\phi_k dC = a_{jk}p_k \tag{5.24}$$

$$a_{jk} = \mu_{jk} + \frac{i}{\omega}\lambda_{jk} = -\rho\int_C \frac{\partial\phi_j}{\partial n}\phi_k dC \tag{5.25}$$

The a_{jk} are the (complex) modal sectional hydrodynamic coefficients, and μ_{jk} and λ_{jk} are the (real) modal sectional added mass and damping coefficients, respectively.

The diffraction force given by Eq. 5.22 requires the calculation of the diffraction wave potential. However, with the Haskind-Hanaoka relationship, the diffraction wave force f_{Dj} can be obtained from the incident and radiation wave potentials:

$$f_{Dj} = \rho\int_C \phi_j \frac{\partial\phi_I}{\partial n} dC \tag{5.26}$$

The physical meaning of the sectional modal forces is very clear. They are exactly the same as the distributed forces acting along the beam element, which is shown in Fig. 5.3.

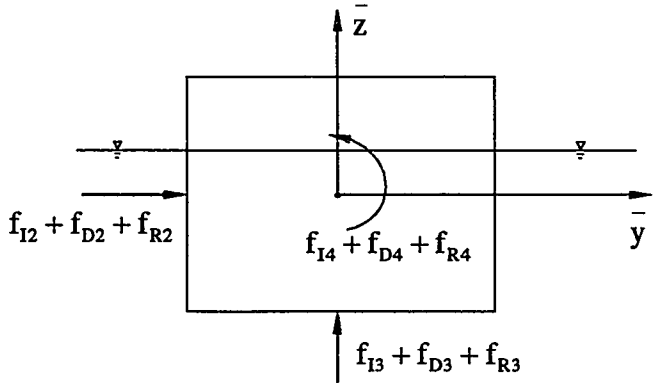

Figure 5.3 Distributed hydrodynamic forces on the slice of beam

It is assumed that the distributed fluid forces acting on each element are constant. Therefore, the surface distributed force vector for each element can be formed by sectional incident and diffraction wave exciting forces as

$$\{F_c\} = \begin{bmatrix} 0 \\ f_{I2} + f_{D2} \\ f_{I3} + f_{D3} \\ f_{I4} + f_{D4} \\ 0 \\ 0 \end{bmatrix} \tag{5.27}$$

The radiation wave forces are related to the structural motion. They can be used to form the added mass and damping matrices. The added mass "density" can be formed by the sectional added mass coefficients, for the port-starboard symmetric section, as

$$[\bar{m}_f] = \begin{bmatrix} 0 & 0 & 0 & 0 & 0 & 0 \\ 0 & \mu_{22} & 0 & \mu_{24} & 0 & 0 \\ 0 & 0 & \mu_{33} & 0 & 0 & 0 \\ 0 & \mu_{42} & 0 & \mu_{44} & 0 & 0 \\ 0 & 0 & 0 & 0 & 0 & 0 \\ 0 & 0 & 0 & 0 & 0 & 0 \end{bmatrix} \tag{5.28}$$

The damping "density" matrix can be formed by sectional damping coefficients as

$$[\bar{c}_f] = \begin{bmatrix} 0 & 0 & 0 & 0 & 0 & 0 \\ 0 & \lambda_{22} & 0 & \lambda_{24} & 0 & 0 \\ 0 & 0 & \lambda_{33} & 0 & 0 & 0 \\ 0 & \lambda_{42} & 0 & \lambda_{44} & 0 & 0 \\ 0 & 0 & 0 & 0 & 0 & 0 \\ 0 & 0 & 0 & 0 & 0 & 0 \end{bmatrix} \tag{5.29}$$

Since the sway and heave (or mode 2 and mode 3) are orthogonal to each other, $\mu_{23} = \mu_{32} = \lambda_{23} = \lambda_{32} = 0$. The port-starboard symmetry results in $\mu_{34} = \mu_{43} = \lambda_{34} = \lambda_{43} = 0$.

The distributed surface force vector in Eq. 5.27 can be used to form the equivalent nodal forces by using Eq. 5.2. The added mass "density" and damping "density" matrices can be used to form the element added-mass and damping matrices, respectively, by using Eq. 5.1.

5.6 Hydrostatic restoring coefficients of a beam element

To use the consistent formulation in Section 5.5 to perform two-dimensional hydroelasticity, corresponding hydrostatic restoring coefficients need to be formed. When a structure floats in water, the hydrostatic restoring forces can be represented by a Winkler-type foundation of vertical and rotational 'springs.' The Winkler foundation (see for example, Cook et al. 1989) consists of uncoupled, distributed springs to form a

continuous base. For each element, it is then possible to define a 6×6 'density' matrix $[\bar{k}_f]$ of distributed spring stiffnesses. This density matrix can be used in Eq. 5.1 in place of the mass density matrix $[\bar{m}]$ to form the element hydrostatic stiffness matrix.

Consider a unit strip of the beam and a corresponding cross section, shown in Fig. 5.4. The local x-axis of the element passes through the center of gravity of the structure, which is located a distance KG from the bottom (or keel) of the cross section, denoted by K. The $\bar{z}$ axis is along the center line of the beam. The center of gravity of the strip is located a distance KG_s from the keel. The weight of the strip is W_s. The center of buoyancy of the strip is located a distance KB_s and the buoyancy force is Δ_s.

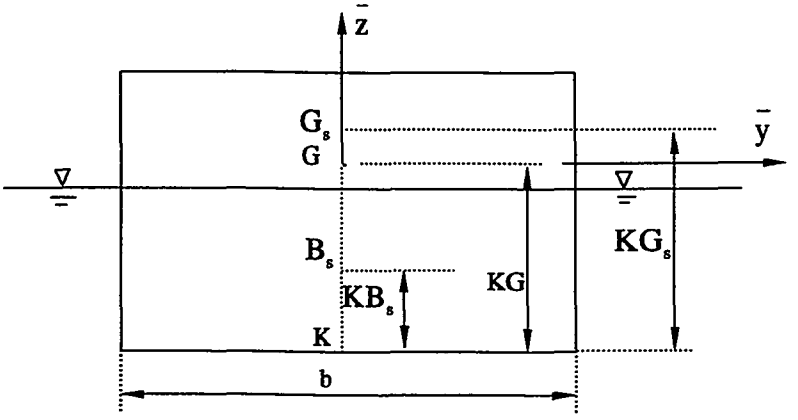

Figure 5.4 Definition for hydrostatic stiffness of a beam element

Because no horizontal restoring forces exist, $\bar{k}_{f11} = \bar{k}_{f22} = 0$, where the subscript 1 refers to the $\bar{x}$-direction and 2 refers to the $\bar{y}$-direction. A unit vertical displacement of the strip results in a change in distributed hydrostatic force equal to $\rho g b$, where $b = b(\bar{x})$ is the width of the water plane; that is,

$$\bar{k}_{f33} = \rho g b \tag{5.30}$$

For a non surface-piercing section, b=0, and therefore, $\bar{k}_{f33} = 0$.

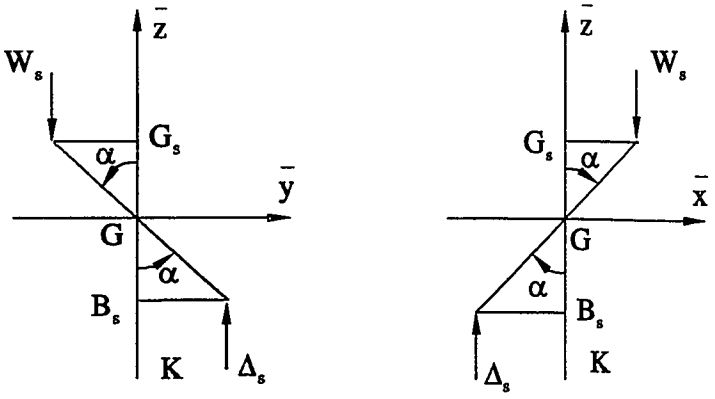

(a) Rotation about the $\bar{x}$ – axis (b) Rotation about the $\bar{y}$ – axis

Figure 5.5 Restoring moments

From Fig. 5.5a, a rotation α about the $\bar{x}$-axis of the unit strip results in the following moments. The upward buoyancy force Δ_s results in a negative restoring moment, which is equal to $-\Delta_s(KG - KB_s)\alpha$. The weight of the unit strip also results in a negative restoring moment, which is equal to $-W_s(KG_s - KG)\alpha$. The water plane area of the unit strip has the contribution of $\rho g S_{\bar{x}\bar{x}}$ to the rotational restoring moment as described in Section 4.3, where $S_{\bar{x}\bar{x}}$ is the second moment of the water plane area of the unit strip about the $\bar{x}$-axis. The total restoring moment for a unit rotation about the $\bar{x}$-axis can be written as

$$\bar{k}_{f44} = -\Delta_s(KG - KB_s) - W_s(KG_s - KG) + \rho g S_{\bar{x}\bar{x}} \tag{5.31}$$

The first term in Eq. 5.31 is typically negative.

From Fig. 5.5b, a unit rotation about the $\bar{y}$-axis results in a restoring moment identical to the first two terms in Eq. 5.31. In addition, the water plane area also has the contribution of $\rho g S_{\bar{y}\bar{y}}$ to rotational hydrostatic restoring force, where $S_{\bar{y}\bar{y}}$ is the second moment of the unit strip area about the $\bar{y}$-axis. The total rotational hydrostatic restoring

'density' for the unit rotation about the $\bar{y}$-axis is

$$\bar{k}_{f55} = -\Delta_s(KG - KB_s) - W_s(KG_s - KG) + \rho g S_{\bar{y}\bar{y}} \tag{5.32}$$

If each element has a uniform symmetric cross section, the element hydrostatic restoring 'density' matrix $[\bar{k}_f]$ can then be written as

$$[\bar{k}_f] = \begin{bmatrix} 0 & 0 & 0 & 0 & 0 & 0 \\ 0 & 0 & 0 & 0 & 0 & 0 \\ 0 & 0 & \bar{k}_{f33} & 0 & 0 & 0 \\ 0 & 0 & 0 & \bar{k}_{f44} & 0 & 0 \\ 0 & 0 & 0 & 0 & \bar{k}_{f55} & 0 \\ 0 & 0 & 0 & 0 & 0 & 0 \end{bmatrix} \tag{5.33}$$

where off-diagonal terms are equal to zero because of symmetry. Substitution of Eq. 5.33 into Eq. 5.1, the consistent hydrostatic restoring matrix for each element can be formed.

The above formulations are not only for the application of strip theory in hydroelasticity. They are also applicable to any horizontal beam element, whether it is partially submerged or totally submerged. When a horizontal beam-like structure is submerged in water, the water plane area is equal to zero. Therefore, $\bar{k}_{f33}$, $S_{\bar{x}\bar{x}}$, and $S_{\bar{y}\bar{y}}$ are equal to zero. Only the rotational restoring coefficients may not be equal to zero, which is the case for a submarine. The magnitudes of the rotational restoring forces can be designed based on KG, KB, KG_s and KB_s.

These formulations of hydrostatic restoring forces may be useful for design of slender ships, slender structures, submarines, horizontal pipelines, towing cables, and horizontal beam elements in three-dimensional frames.

5.7 Equations of motion in two-dimensional hydroelasticity

Following the procedure described in Section 3.2.2, the element added-mass and damping matrices, and nodal forces can be transformed to the global element matrices and forces; finally, the global structural added-mass and damping matrices, $[M_f]$, $[C_f]$, and force vector, $\{F_f\}$ can be assembled. The element hydrostatic stiffness can be used to form the global hydrostatic stiffness matrix, $[K_f]$. Together with the structural mass, damping, and stiffness matrices, the resulting equations of motion are

$$\{-\omega^2([M_s]+[M_f]) - i\omega([C_s]+[C_f]) + ([K_s]+[K_f])\}\{D\} = \{F_f\} \quad (5.34)$$

in which $\{D\}$ is the (complex) vector of the physical nodal displacements. The fluid terms, $[M_f]$, $[C_f]$, and $\{F_f\}$, are dependent on the wave frequency ω, and hence, they must be formed for each frequency.

The response of a stationary structure to regular waves (transfer functions) are obtained through the solution of Eq. 5.34 for a range of wave frequencies. Since the nodal displacements $\{D\}$ have been solved directly from Eq. 5.34, any sectional structural internal force can be obtained from nodal displacements.

CHAPTER 6

MORISON'S EQUATION METHOD

6.1 Overview

Morison's equation (Morison, et al., 1950), which includes the effects of fluid acceleration and viscous form drag in terms of empirically determined coefficients, has been successfully used in the offshore industry to determine the motion response of floating structures, especially during the preliminary design stage. Morison's equation was introduced originally to calculate the wave exciting forces on vertical piles of circular cross section. Since then, this equation has been used by many to obtain the dynamic forces on fixed tubular structures, as well as the motion response of floating structures, such as semi-submersibles. The earliest applications of Morison's equation, in the frequency domain, to rigid semisubmersibles can be found in Burke (1969) and Paulling (1970). This approach has been extended by Paulling and Tyagi (1991) to multiple rigid modules flexibly connected to each other; however, it appears that Morison's equation has not been used in conjunction with elastic body motion of very large floating structures.

The main reason for introducing Morison's equation to analyze very large floating structures is due to the large computational cost of using three-dimensional hydroelasticity. Morison's equation avoids the calculation of velocity potentials. Since it is not limited to a two-dimensional model, the method also overcomes the disadvantages of using two-dimensional hydroelasticity. Of course, Morison's equation is only applicable to structures which have tubular structural elements below the still-water plane.

In this chapter, the consistent hydrodynamic formulation for Morison's equation based on the finite element method will be introduced. The formulation includes hydrodynamic added-mass, damping matrices and wave exciting forces. The formulation of hydrostatic restoring coefficients for the frame element is also discussed.

6.2 Three-dimensional frame model of a structure

Since hydrodynamic loading will be based on Morison's equation, the structure below the still-water plane is modelled by frame finite elements. The formulation of the two-node frame element has been described in Section 3.1.3. The element local coordinates $\bar{x}-\bar{y}-\bar{z}$ and global coordinates x-y-z has been shown in Fig. 3.1. Each node has 6-displacement degrees of freedom, three translational and three rotational displacements. The displacements within an element can be represented by the nodal displacements through interpolation functions, which can be written as

$$\{u\} = ([N_{at}+N_b])\{d\} = [N]\{d\} \tag{6.1}$$

in which $\{u\}$ is the 6×1 displacement vector at a point of the element; the axial and torsional displacement interpolation function matrix $[N_{at}]$ and the transverse displacement interpolation function $[N_b]$ are given in Eq. II.2 and Eq. II.4 in Appendix II; and $\{d\}$ is a 12×1 vector of nodal displacements which has been shown in Fig. 3.1.

The forces distributed along an element can be replaced by equivalent nodal forces. The equivalent nodal forces acting at the two nodes of a frame element are given by

$$\{r^{ext}\} = \int_{L_e} [N]^T \{F_c\}\, dS \tag{6.2}$$

in which $\{F_c\}$ is the 6×1 vector of distributed forces and moments, which are calculated from Morison's equation, $\{r^{ext}\}$ is the corresponding 12×1 vector of

equivalent nodal forces in the element local coordinate system, and L_e is the element length.

The structural mass and stiffness matrices, $[M_s]$ and $[K_s]$, for frame structures can be formed by using the formulations in Eqs. II.10 and II.11 in Appendix II for the element mass and stiffness matrices, transforming to global coordinates, and then assembling to the global matrices. If the frame elements below the still-water plane do not have a circular cross section, they will be modelled as circular cylinders for hydrodynamic force calculations, such that the displaced volumes of the elements remain the same.

6.3 Morison's equation

The two important hydrodynamic forces on a circular cylinder are the inertia and form drag forces. The domination of these two forces depends on the ratio of the diameter of the cylinder (D) to the wave length (L). When this ratio is relatively large, the wave diffraction is relatively important. Therefore, the inertia force will be dominant. On the other hand, when this ratio is relatively small, the wave diffraction may be negligible, flow will be separated and the form drag force becomes important. The frictional drag force is generally too small to have an appreciable effect on the overall forces.

When D/L is relatively small such that the cylinder is regarded as a slender cylinder, the drag force can not be neglected. Morison et al. (1950) suggested an empirical relationship for a fixed vertical cylinder:

$$\{F_{cp}\} = \frac{1}{2}\rho C_D D \| \{\dot{u}_{fn}\} \| \{\dot{u}_{fn}\} + \frac{1}{4}\rho\pi D^2 C_M \{\ddot{u}_{fn}\} \tag{6.3}$$

where $\{F_{cp}\}$ is the distributed normal pressure force vector; C_D is the drag coefficient; $\{u_{fn}\}$ is the 3×1 water particle displacement vector, normal to the element; ρ is the water density; C_M $(=1+C_m)$ is the inertia coefficient, where C_m is the added-mass coefficient; and the superposed dot denotes the local time derivative. The first term on the right hand side of Eq. 6.3 represents the drag forces, and the second term represents the inertia forces.

Because of the importance of cylindrical piles in offshore engineering and coastal engineering, there have been many investigations on the proper coefficients after Morison et al. proposed Eq. 6.3. When structural motions and deformations are considered, the inertia and drag forces are dependent not only on the fluid motion but also on the structural motion and deformation. Morison's equation can then be written, in terms of the relative motion between the fluid and structure, as

$$\{F_{cp}\} = \frac{1}{2}\rho C_D D \| \{\dot{u}_{fn}\} - \{\dot{u}_n\} \| (\{\dot{u}_{fn}\} - \{\dot{u}_n\}) + \frac{1}{4}\rho\pi D^2 (C_M \{\ddot{u}_{fn}\} - (C_M - 1) \{\ddot{u}_n\}) \tag{6.4}$$

where u_n is the 3×1 normal displacement vector of a point on the element.

The drag term in Morison's equation contains the product of the unknown displacement (velocity) vector, and therefore, is nonlinear. The usual practice is to linearize this term. Among the several available linearization methods, the method of equal energy dissipation per wave cycle, (Blagoveshchensky 1962) is chosen. The equal energy dissipation can be expressed as

$$E_D = E_{DL} \tag{6.5}$$

where E_D is the energy dissipated by drag forces, while E_{DL} is the energy dissipated by the linearized drag forces. The nonlinear drag term can be written, in the linearized form, as

$$\{F_{cpD}\} = \frac{1}{2}\rho C_{DL} D (\{\dot{u}_{fn}\} - \{\dot{u}_n\}) \tag{6.6}$$

where C_{DL} is called the equivalent linear drag coefficient. Mathematically, the equivalent linear drag coefficient can be obtained from the relationship in Eq. 6.5:

$$C_{DL} = \frac{8}{3}\pi C_d (\dot{u}_{fn0} - \dot{u}_{n0}) \tag{6.7}$$

in which $\dot{u}_{fn0}$ is the amplitude of the water particle velocity and $\dot{u}_{n0}$ is the amplitude of velocity of a point on the element, in the normal direction. Note that C_{DL} is a dimensional coefficient. Drag forces in Eq. 6.6 requires an iterative scheme for the determination of the relative velocity on which the equivalent linear drag coefficient depends. By substitution of Eq. 6.6 into 6.3, the linearized Morison's equation becomes

$$\begin{aligned}\{F_{cp}\} &= \frac{1}{2}\rho C_{DL} D (\{\dot{u}_{fn}\} - \{\dot{u}_n\}) \\ &+ \frac{1}{4}\rho\pi D^2 (C_M \{\ddot{u}_{fn}\} - (C_M - 1) \{\ddot{u}_n\})\end{aligned} \tag{6.8}$$

Eq. 6.8 can be decomposed into four parts. The first part involves the water particle acceleration:

$$\{F_{cIf}\} = \frac{1}{4}\rho\pi D^2 C_M \{\ddot{u}_{fn}\}_6 \tag{6.9}$$

in which $\{F_{cIf}\}$ is a 6×1 distributed normal force vector; the subscript I and f denote the inertia and fluid, respectively; $\{\ddot{u}_{fn}\}_6$ is the 6×1 water particle acceleration vector,

which is obtained by including 3×1 subvector $\{\ddot{u}_{fn}\}$ and three zero rotational components.

The second part involves the water particle velocity:

$$\{F_{cDf}\} = \frac{1}{2}\rho C_{DL} D \{\dot{u}_{fn}\}_6 \tag{6.10}$$

in which $\{F_{cDf}\}$ is a 6×1 distributed normal force vector; the subscript D denotes drag; $\{\dot{u}_{fn}\}_6$ is 6×1 water particle velocity vector, which is obtained by including 3×1 subvector $\{\dot{u}_{fn}\}$ and three zero rotational components.

The third part involves the structural acceleration:

$$\{F_{cIs}\} = \frac{1}{4}\rho\pi D^2 (C_M - 1) \{\ddot{u}_n\}_6 \tag{6.11}$$

in which $\{F_{cIs}\}$ is a 6×1 distributed normal force vector; the subscript s denotes structure; $\{\ddot{u}_n\}_6$ is 6×1 structural acceleration vector, which is obtained by including 3×1 subvector $\{\ddot{u}_n\}$ and three zero rotational components.

The last part involves the structural velocity:

$$\{F_{cDs}\} = \frac{1}{2}\rho C_{DL} D \{\dot{u}_n\}_6 \tag{6.12}$$

in which $\{F_{cDs}\}$ is a 6×1 distributed force vector; $\{\dot{u}_n\}_6$ is 6×1 structural velocity vector, which is obtained by including 3×1 subvector $\{\dot{u}_n\}$ and three zero rotational components.

From the above decomposition, the fluid forces from Eq. 6.9 contribute to the fluid inertia forces; the fluid forces from Eq. 6.10 contribute to the fluid damping forces; the fluid forces from Eq. 6.11 contribute to the fluid added mass; and the fluid forces from Eq. 6.12 contribute to the fluid damping.

The water particle velocity and acceleration is calculated from the incident wave potential Φ_I

$$\Phi_I = -\frac{ig\alpha}{\omega} e^{ik(x\cos\beta + y\sin\beta)} e^{kz'} e^{-i\omega t} = \phi_I e^{-i\omega t} \tag{6.13}$$

6.4 Hydroelastic formulations for Morison's equation

Eqs. 6.9, 6.10, 6.11 and 6.12 give the distributed normal forces acting on an element. The distributed forces are replaced by equivalent nodal loads in the finite element model via Eq. 6.2. Because the distributed forces involve both the fluid and structural motion, the result will be expressions for added mass, damping, and wave exciting forces. Since no axial forces are involved in these fluid forces, only the interpolation functions for transverse displacements are considered.

For each element, substitution in Eq. 6.2 of Eq. 6.9 results in the element nodal inertia exciting forces, which are dependent on the water particle acceleration

$$\{F_I\} = \int_{L_e} [N_b]^T \{F_{cIf}\} d\bar{x} \tag{6.14}$$

These wave exciting forces can be directly calculated from the water particle acceleration at each point, if C_M is given. The water particle acceleration can be calculated from the incident wave potential. The wave exciting forces in Eq. 6.14 are the Froude-Krylov forces.

Substitution in Eq. 6.2 of Eq. 6.10 results in the element nodal drag exciting forces, which are dependent on the water particle velocity:

$$\{F_D\} = \int_{L_e} [N_b]^T \{F_{cDf}\} d\bar{x} \tag{6.15}$$

Eq. 6.15 involves the equivalent linear drag coefficient C_{DL}, which is a function of the unknown relative velocity. Hence, this exciting force must be calculated iteratively.

Substitution in Eq. 6.2 of Eq. 6.11 results in the element nodal inertial exciting forces, which are dependent on the structural acceleration:

$$\{F_{Is}\} = \int_{L_e} [N_b]^T \{F_{cIs}\} \, d\bar{x} \tag{6.16}$$

$\{F_{Is}\}$ depends on the structural displacements. Eq. 6.11 can be used to form a distributed inertia density matrix $[\bar{m}_f]$. Since only distributed normal forces are considered, the only nonzero terms of the 6×6 matrix $[\bar{m}_f]$ are $\bar{m}_{f22} = \bar{m}_{f33} = \pi D^2 \rho (C_M - 1)/4$. Therefore, Eq. 6.11 can be written as

$$\{F_{cIs}\} = [\bar{m}_f] \{\ddot{u}_n\} = [\bar{m}_f] [N_b] \{\ddot{d}\} \tag{6.17}$$

Thus, Eq. 6.16 becomes

$$\{F_{Is}\} = \int_{L_e} [N_b]^T [\bar{m}_f] [N_b] \, d\bar{x} \{\ddot{d}\} = [m_f] \{\ddot{d}\} \tag{6.18}$$

where

$$[m_f] = \int_{L_e} [N_b]^T [\bar{m}_f] [N_b] \, d\bar{x} \tag{6.19}$$

Similarly, the distributed forces in Eq. 6.12 can be written, either in force format, as

$$\{F_{Ds}\} = \int_{L_e} [N_b]^T \{F_{cDs}\} \, d\bar{x} \tag{6.20}$$

or in element damping-matrix format, as

$$\{F_{Ds}\} = [c_f] \{\dot{d}\} \tag{6.21}$$

where

$$[c_f] = \int_{L_e} [N_b]^T [\bar{c}_f] [N_b] \, d\bar{x} \tag{6.22}$$

in which $[\bar{c}_f]$ is 6×6 damping-density matrix whose only nonzero terms are $c_{f22} = c_{f33} = \rho C_{DL} D/2$.

An additional force exists due to the presence of the end planes of a structural member exposed to direct wave action. The end planes of a structural member can be taken as the element nodes. Therefore, the nodal Froude-Krylov forces can be calculated by considering the wave pressure due to the incident wave (in Eq. 6.13) alone. For an end of area A, the end plane force can be approximated by

$$\{F_{fend}\} = -i\rho\omega\phi_I A \{n\} \tag{6.23}$$

where $\{n\}$ is the 3×1 unit normal to the end plane in the local coordinate system. The end plane force vector $\{F_{fend}\}$ also can be extended to the 6×1 nodal vector $\{F_{fend}\}_6$ by adding rotational components, so it is consistent with the general definition.

The element added-mass matrix in Eq. 6.19 and damping matrix in Eq. 6.22 can be transferred to the global coordinate system, and then assembled to form the structural added-mass matrix $[M_f]$, and damping matrix $[C_f]$, following the procedures used for structural matrices. The element local nodal forces $\{F_I\}$ and $\{F_D\}$ can be transformed to global coordinates and assembled to form the structural nodal forces $\{F_{fI}\}$ and $\{F_{fD}\}$, respectively. If one prefers to form the nodal drag-force-vector which involves the structural velocity instead of forming the damping matrix, the structural nodal force $\{F^s_{fD}\}$ can be formed from Eq. 6.12 by the same procedure as for other nodal force vectors.

6.5 Hydrostatic restoring coefficients for frame element

It is convenient to use a direct solution method to deal with the hydroelastic problem by using Morison's equation. Therefore, it is necessary to form the hydrostatic restoring matrix for three-dimensional frame elements. Only horizontal and vertical frame elements are discussed here.

Before considering the hydrostatic restoring coefficients for each element, consider first the stability of the structure. For a semisubmersible structure, the water-plane area of the members which pierce the still-water plane will resist any disturbance from its equilibrium position, which is the stabilizing component in hydrostatic restoring forces. The structural weight may be another factor to keep the structure in its equilibrium position in the case the center of weight is in the proper position. However, when the center of the net buoyancy forces of the structure shifts from the equilibrium position, the net buoyancy force will overturn the structure. The net buoyancy forces become the destabilizing component in hydrostatic restoring forces, leading to negative stiffness. If a structure is stable, the contribution to the hydrostatic restoring forces from the stabilizing component must be larger than that from the destabilizing component.

6.5.1 Stabilizing components

The stabilizing components which result from the water-plane area can be treated as in the following. For a horizontal beam which is semi-submerged in the water, the formulations in Section 5.6 can be used directly to form the element hydrostatic stiffness for each element. For a vertical beam which pierces the still-water surface, the hydrostatic stiffness is modeled as follows. A node of the beam element is located at each intersection of the still-water surface and the vertical beam, and discrete vertical

and rotational springs are attached to these nodes. The vertical and rotational nodal spring stiffnesses are given, in local coordinates, $\bar{x} - \bar{y} - \bar{z}$, by

$$k_{f\bar{z}\bar{z}} = \rho g A_v \qquad k_{f\bar{x}\bar{x}} = \rho g S_{v\bar{x}\bar{x}} \qquad k_{f\bar{y}\bar{y}} = \rho g S_{v\bar{y}\bar{y}} \tag{6.24}$$

where A_v is the water-plane area of the vertical element, $S_{v\bar{x}\bar{x}}$ and $S_{v\bar{y}\bar{y}}$ are the second moments of water-plane area of the column about $\bar{x}$ and $\bar{y}$ axes, respectively. The location of the springs at the still-water surface means that the effects of the change in hydrostatic forces will be accurately represented in the structure above the still-water surface, but not necessarily below. That is, the change in the distributed hydrostatic pressures on the submerged members is not modelled directly. Note also that implicit in Eq. 6.24 is the assumption that $\bar{x}$ and $\bar{y}$ are the principal axes of the vertical beam cross-section.

6.5.2 Destabilizing components

The destabilizing components of the hydrostatic stiffness is caused by the change of the positions of the center of buoyancy and the center of gravity. For a completely submerged horizontal circular cylinder, with its center of buoyancy located at the center of gravity and the center of gravity located on the local $\bar{x}$-axis, from Section 5.6, the cylinder will not contribute to the hydrostatic restoring forces. However, to support the part of the structure above the still-water plane, the buoyancy force on a submerged horizontal cylinder is usually larger than the weight of the cylinder, and the center of buoyancy of the cylinder is usually below the center of gravity of the structure. Clearly, a shift in the center of buoyancy such that it is no longer vertically aligned with the center of gravity tends to overturn, or destabilize, the structure and causes an overturning moment on the structure. This overturning moment, which is caused by the buoyancy forces of the lower elements, is transmitted to the upper elements through

compression in the vertical elements. Hence, this component of the hydrostatic stiffness is incorporated in the structural model by the geometric stiffness of the frame elements, which was discussed in Section 3.2.3.

The geometric stiffness of a frame element is given by Eq. 3.31

$$[k_{eg}] = \int_0^{L_e} f_a [N']^T [N'] \, dx \tag{6.25}$$

and f_a is the axial force (tension positive) in the element and $\{N'_b\}$ is the derivatives with respect to $\bar{x}$ of the corresponding transverse displacement interpolation matrix. In this case, f_a is negative because the buoyancy from the lower elements will compress the vertical elements.

The hydrostatic pressure acting on the vertical elements and the pressure inside the cylinder will affect the geometric stiffness. This effect can be included by using the effective tension in Eq. 6.25. The effective tension of a cylinder is well-known in riser mechanics (see for example, Spark, 1984), and is given by

$$f_{eff} = f_a + p_o A_o - p_i A_i \tag{6.26}$$

in which p_o and p_i are the external and internal pressures, respectively, and A_o and A_i are the external and internal areas of the element cross sections, respectively. In the case no internal pressure exists, $p_i = 0$. The axial forces within the element, for simplification, may be assumed constant and they are determined based on the hydrostatic buoyancy forces and the weight of the structure.

6.5.3 Net buoyancy-force contribution

Since a floating structure is semi-submerged, the buoyancy force for a completely submerged horizontal element may be larger than its weight. The horizontal elements

are connected to the other horizontal elements or vertical columns and this buoyancy force causes the compression in the columns, which can be calculated from statics.

The element hydrostatic stiffness matrices are assembled, together with the nodal spring stiffness, to form the global hydrostatic stiffness $[K_f]$ in the same manner as described in assembling the structural element matrix.

6.6 Solution methods

The equations of motion in the frequency domain can be formed

$$\{-\omega^2([M_s]+[M_f])-i\omega([C_s]+[C_f])+([K_s]+[K_f])\}\{D\} = \{F_{fI}\}+\{F_{fD}\} \tag{6.27}$$

Because $[C_s]$ and $\{F_{fD}\}$ include the drag coefficient C_{DL}, which is dependent on the unknown structural velocity, the equations of motion must be solved iteratively until the value of C_{DL} for each element converges.

The relative error between successive iterations can be used to control the iteration procedure. First, the relative velocity between the fluid and structure is used to form the relative error (er_{rel}). The structural velocity at iteration i-1 is $\{\dot{D}\}^{i-1}$ and at iteration i is $\{\dot{D}\}^{i}$. The fluid velocity during the iteration does not change within the assumption of linearity (small motions). The relative error (er_{rel}) is defined as

$$(er_{rel}) = \frac{\left\| \left(\{\dot{u}_f\} - \{\dot{D}^i\}\right) - \left(\{\dot{u}_f\} - \{\dot{D}^{i-1}\}\right) \right\|}{\left\| \{\dot{u}_f\} - \{\dot{D}^i\} \right\|} \tag{6.28}$$

As a second measure, the relative error (er_s) of the structural displacements between two adjacent iterations is defined as

$$(er_s) = \frac{\left\| \{D^i\} - \{D^{i-1}\} \right\|}{\left\| \{D^i\} \right\|} \tag{6.29}$$

Since the displacements {D} can be directly obtained by solving the equations of motion, it is easy to use (er_s) for convergence. The convergence criterion is

$$(er_{rel}) < \varepsilon, \qquad (er_s) < \varepsilon \tag{6.30}$$

where ε is an input tolerance.

At iteration i, the linearized equations of motion can be written as

$$\{-\omega^2([M_s] + [M_f]) - i\omega([C_s] + [C_f]^{i-1}) + ([K_s] + [K_f])\}\{D\}^i = \{F_{fM}\} + \{F_{fD}\}^{i-1} \tag{6.31}$$

in which $[C_f]^{i-1}$ and $\{F_{fD}\}^{i-1}$ are based on $\{D\}^{i-1}$ for $i > 1$. By definition, $D_i^0 = \alpha\omega/\pi$ for translational displacement components of $\{D^0\}$.

This iteration strategy is stable and few iterations are required for convergence. However, at each iteration, $[C_f]$ must be reformed and therefore Eq. 6.31 must be solved completely. Because the coefficient matrices in Eq. 6.31 are complex, re-factoring this matrix and then solving Eq. 6.31 is time consuming.

A potentially attractive alternative to this scheme results if all the drag-dependent terms are kept on the right-hand-side of Eq. 6.31. That is

$$\{-\omega^2([M_s] + [M_f]) - i\omega[C_s] + ([K_s] + [K_f])\}\{D\}^i = \{F_{fI}\} + \{F_{fD}\}^{i-1} + i\omega[C_f]^{i-1}\{D\}^{i-1} \tag{6.32}$$

or, alternatively,

$$\{-\omega^2([M_s] + [M_f]) - i\omega[C_s] + ([K_s] + [K_f])\}\{D\}^i = \{F_{fI}\} + \{F_{fDu}\}^{i-1} \tag{6.33}$$

in which the drag forces included in $\{F_{fDu}\}^{i-1}$ are based on the relative velocity and not the fluid velocity. The advantage to this approach is that the coefficient matrix of Eq. 6.33 is constant for each wave frequency; hence it need be formed and factored only

once for each frequency. Furthermore, if there is no or negligible structural damping, Eq. 6.33 can be written as

$$\{-\omega^2([M_s] + [M_f]) + ([K_s] + [K_f])\}\{D\}^i = \{F_{fI}\} + \{F_{fDu}\}^{i-1} \tag{6.34}$$

Eq. 6.34 has a real coefficient matrix with a complex right-hand vector. The solution of Eq. 6.34 is computationally less involved. In addition, the damping matrix $[C_f]$ need never be formed, and the effort to form $\{F_{fDu}\}$ is the same as required to form $\{F_{fD}\}$. The potential disadvantage of this approach is that a few more iterations will be required for convergence. However, for an inertia dominated structure, any increase in the number of iterations likely would be overcome by the previously mentioned advantages. Both iterative strategies in Eqs. 6.31 and 6.34 have been implemented in the program **HYDRAS-MORISON**.

CHAPTER 7

A COMPOSITE 2-D/3-D METHOD FOR HYDROELASTICITY

7.1 Introduction

Two-dimensional hydroelasticity, discussed in Chapter 5, uses strip theory to determine the fluid forces and a nonuniform beam model to represent a floating structure. Hence, this approach is numerically efficient especially for very large floating structures. In this model, the 'cross-section' of the structure is assumed rigid (at least below the still-water plane) and this primitive structural model means that only 'beam' deformational modes are considered. Therefore, it is limited to the evaluation of motions and force resultants along the longitudinal axis of the structure. In particular, the method cannot provide the more detailed results which are useful for engineering design. For example, in the case of a twin-hull structure, such as a SWATH ship shown schematically in Fig. 7.1, no information about the 'prying' forces on the struts are obtained from such an analysis. These forces are of course important in designing not only the struts but also the connections between the deck and struts.

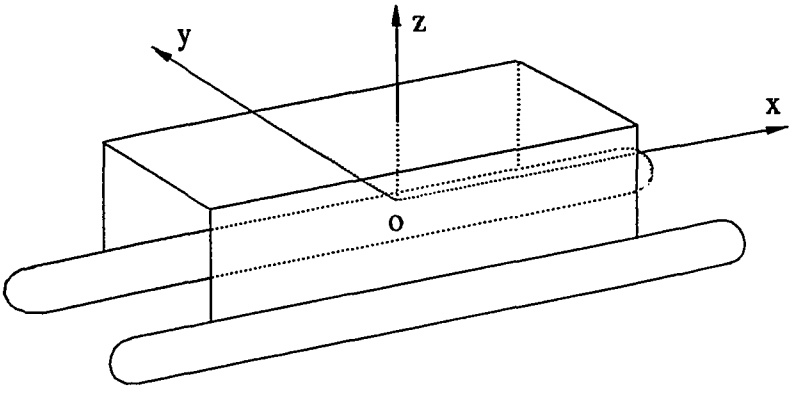

Figure 7.1 Schematic view of a SWATH ship

Three-dimensional hydroelasticity, discussed in Chapter 4, avoids the limitations of a two-dimensional theory by using the three-dimensional potential theory to model the fluid forces and a three-dimensional finite element model of the structure. It therefore represents the most general and accurate theory to date, and information on the detailed response is provided by such an analysis. However, it is computationally intensive, primarily because of the three-dimensional fluid model. As such, it is probably most useful as a final design tool.

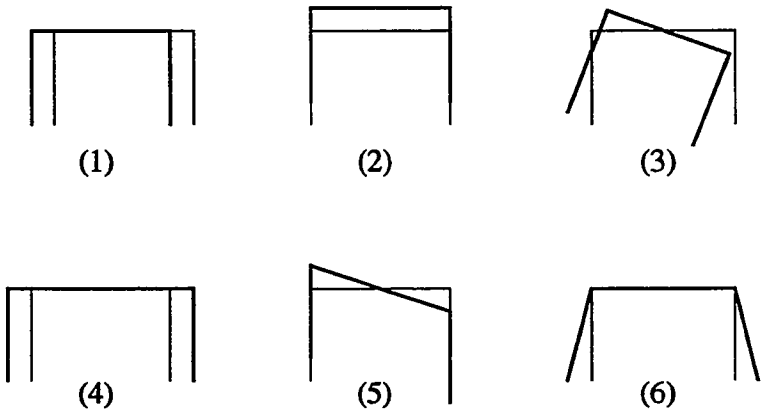

Figure 7.2 'Basic modes' of a cross-section

To avoid the limitations of a beam model and the computational requirements of a three-dimensional fluid model, a hybrid approach for twin-hull structures has been proposed in Wang (1991) and Wang et al. (1991). In this approach, the structure is represented by a three-dimensional finite element model, while the fluid forces are still calculated from strip theory. However, the 'basic modes' of deformation in Fig. 7.2 are used to represent the actual deformation. A very approximate procedure was used to represent the three-dimensional finite element deformational response by the 'basic modes.'

Recently, Che et al. (1992a) presented preliminary results of an effort to develop the

composite 2D/3D method so that the three-dimensional finite element results are used directly in the hydroelastic analysis. In this approach, the mode shapes predicted by a three-dimensional finite element model of the structure are used. Because two-dimensional strip theory is used to calculate the fluid forces, the method retains a fundamental assumption of strip theory; that is, flow at one cross-section is assumed to be independent of flow at any other section. Hence, the method is primarily applicable to slender structures. However, there is no other restriction on the structure, that is it can be monohull or multi-hull.

In this chapter, the feasibility of using a composite 2D/3D approach for hydroelasticity is discussed first. Then, the formulation of this approach is given for general structures and twin-hull symmetric structures. In addition, the three-dimensional incident wave force and a revised two-dimensional normal are used to improve the method. Finally, a more rigorous approach for representing the finite element response by the basic modes is presented.

7.2 3-D model of structure and 2-D model of fluid

Two-dimensional hydroelasticity has primarily two disadvantages. First, the structure is limited to have only beam motion and deformation. Second, the motion and fluid action in the direction of the longitudinal axis are not considered. The limitations come from the two-dimensional structural and fluid models. To overcome these disadvantages, the structural model or fluid model, or both structural and fluid models must be changed. Changing only the fluid model cannot solve the first problem. In addition, using a three-dimensional fluid model will tremendously increase the computational effort.

The two-dimensional Green function method requires the solution of Eq. 5.17 to obtain the source densities. Note that in this equation, the body-boundary conditions

affect only the right-hand side. Therefore, application of Eq. 5.17 to deformable cross-section affects only the right hand side.

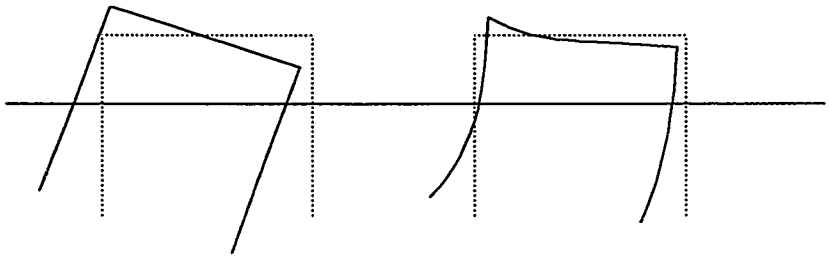

(a) Rigid cross-section (b) Flexible cross-section

Figure 7.3 Cross-sectional motion

Fig. 7.3 shows possible cross sectional motion for a rigid cross-section and a flexible cross-section. The rigid cross-sectional motion is considered in traditional strip theory and two-dimensional hydroelasticity. The flexible cross-sectional motion is considered in this approach. The basic difference between the composite 2D/3D approach and three-dimensional hydroelasticity is that, in the former, two-dimensional flow is assumed.

The three-dimensional structural model described in Chapter 4 is used here to describe the structural motions and deformations. Mode superposition is used for the three-dimensional structural dynamic analysis. The first q 'dry' modes are assumed to be sufficient to represent the structural response. The actual nodal displacements $\{D\}$ can be expressed in terms of the mode shapes $[\Psi]$ as

$$\{D\} = [\Psi]\{p\} \tag{7.1}$$

where $\{p\}$ is the $q \times 1$ vector of principle coordinates. The modal equations of motion can be written as

$$\left[-\omega^2 [M_s^*] - i\omega [C_s^*] + [K_s^*]\right] \{p\} = \{F_f^*\} + \{F_r^*\} \tag{7.2}$$

where $[M_s^*]$, $[C_s^*]$, and $[K_s^*]$ are structural modal mass, damping, and stiffness matrices, respectively; and $\{F_f^*\}$ and $\{F_r^*\}$ are modal hydrodynamic and hydrostatic forces, respectively.

The two-dimensional fluid model described in Chapter 5 is used to solve for the radiation velocity potentials. The coupling of the three-dimensional structural model and the two-dimensional fluid model and some special modifications will be described in the following sections.

7.3 Formulations for composite 2-D/3-D method

The generalized wave forces acting on the whole structure can be obtained, as described before, by integrating the distributed force over the mean wetted-surface S:

$$\{F^*\} = i\omega\rho \iint_S \Phi [\psi]^T \{n\} dS \tag{7.3}$$

where ω is the wave frequency; ρ is the water density; Φ is the velocity potential; the $3 \times q$ matrix $[\psi]$ contains the modal translational displacements at a point (x,y,z) on S, which can be obtained from the global mode shapes, $[\Psi]$; and $\{n\}$ is the normal vector at a point (x,y,z). The term $[\psi]^T \{n\}$ is defined as the generalized normal vector, $\{n^*\}$.

In infinitely deep water, the boundary-value problem of the jth radiation potential ϕ_j has been given in Eqs. 5.3 through 5.6, they are repeated for convenience:

$$\left(\frac{\partial^2}{\partial y^2} + \frac{\partial^2}{\partial z^2}\right)\phi_j = 0 \qquad \text{in } D \tag{7.4}$$

$$\left(\frac{\partial}{\partial z} - k\right)\phi_j = 0 \qquad \text{on } z = z_w \tag{7.5}$$

$$\frac{\partial \phi_j}{\partial n} = -i\omega n_j^* \qquad \text{on } C_b \tag{7.6}$$

$$\lim_{z \to -\infty} \frac{\partial}{\partial z}(\phi_j) = 0 \qquad \lim_{y \to \pm\infty} \left[\frac{\partial \phi_j}{\partial y} \mp ik\phi_j \right] = 0 \tag{7.7}$$

where D is the two-dimensional fluid domain; $k = \omega^2/g$ is the wave number in deep water; C_b is the immersed contour of the cross-section; $\partial/\partial n$ is the derivative in the normal direction; and $\{n_j^*\}$ is the generalized normal on the wetted surface, and j=1 to q. It should be emphasized that the normal vector {n} in Eq. 7.6 may be determined from either the normal to the cross section, C_b, as is typical in strip theory, or directly from the three-dimensional normal vector obtained from a three-dimensional structural model.

It is convenient to write Eq. 7.3 as an integration along the structural length, L, and the contour of the cross-section of the wetted surface, C_b:

$$\{F^*\} = i\omega\rho \int_L \left\{ \int_{C_b} \Phi \{n^*\} \, dC \right\} dx \tag{7.8}$$

Consistent with strip theory, the integral on C_b can be interpreted as the modal sectional fluid forces, denoted {f}. Eq. 7.8 is similar to the formulation in strip theory for the hydrodynamic wave forces with zero forward speed (Salvesen et al., 1970). However, in the present formulation, the three-dimensional structural mode shapes are used, whereas in traditional two-dimensional hydrodynamics, only sway, heave, and roll of the 'rigid' cross-section are used.

Decomposing the total velocity potential Φ into incident, diffraction, and radiation potentials and substitution of them into Eq. 7.8 results in the sectional modal forces as a result of the incident, diffraction, and radiation potentials:

$$f_{Ij} = i\omega\rho\int_C \phi_I n_j^* \, dC \tag{7.9}$$

$$f_{Dj} = i\omega\rho\int_C \phi_D n_j^* \, dC \tag{7.10}$$

$$f_{Rj} = i\omega\rho p_k \int_C \phi_k n_j^* \, dC \tag{7.11}$$

where summation convention is used in Eq. 7.11. The total jth sectional modal hydrodynamic forces are

$$f_j = f_{Ij} + f_{Dj} + f_{Rj} \tag{7.12}$$

The force from the incident wave is determined from the incident wave potential, which for deep water is

$$\phi_I = -\frac{ig\alpha}{\omega} e^{ikx\cos\beta} e^{iky\sin\beta} e^{kz'} \tag{7.13}$$

where α is the wave amplitude. With Eq. 7.13, Eq. 7.9 becomes

$$f_{Ij} = \rho g\alpha e^{ikx\cos\beta} \int_{C_b} n_j^* e^{iky\sin\beta} e^{kz'} \, dC \tag{7.14}$$

which can be termed the Froude-Krylov sectional modal force.

The diffraction force requires additional consideration. With Eqs. 7.6 and 7.10, the modal sectional diffraction wave force can be written as

$$f_{Dj} = -\rho \int_{C_b} \phi_D \frac{\partial \phi_j}{\partial n} dC \tag{7.15}$$

By using the well-known Haskind-Hanaoka relationship, the diffraction wave force f_{Dj} can be obtained from the incident and radiation wave potentials:

$$f_{Dj} = \rho \int_{C_b} \phi_j \frac{\partial \phi_I}{\partial n} dC \tag{7.16}$$

From Eq. 7.13, one has

$$\frac{\partial \phi_I}{\partial n} = k(n_z + i n_y \sin\beta)\, \phi_I \tag{7.17}$$

so that the modal sectional diffraction force can be written as

$$f_{Dj} = -\alpha\omega\rho e^{ikx\cos\beta} \int_{C_b} (i n_z - n_y \sin\beta)\, e^{iky\sin\beta} e^{kz'} \phi_j dC \tag{7.18}$$

The modal sectional radiation wave force for mode j can be obtained by substitution of Eq. 7.6 into 7.11:

$$f_{Rj} = -\rho p_k \int_{C_b} \frac{\partial \phi_j}{\partial n} \phi_k dC = a_{jk} p_k \tag{7.19}$$

where

$$a_{jk} = \mu_{jk} + \frac{i}{\omega} \lambda_{jk} = -\rho \int_{C_b} \frac{\partial \phi_j}{\partial n} \phi_k dC \tag{7.20}$$

The a_{jk} are the modal sectional hydrodynamic coefficients, μ_{jk} and λ_{jk} are the modal sectional added-mass and damping coefficients, respectively.

It should be emphasized, again, that j and k can be larger than 6 in Eqs. 7.14, 7.18, and 7.20. That is, these equations for the generalized incident, diffraction, and radiation wave forces are valid for the rigid-body modes as well as the deformational modes.

7.4 Twin-hull symmetric structure

For a twin-hull structure, which is symmetric about its center plane, the contour integration in the above equations can be simplified (Wang et al., 1991; Che et al., 1992b). For port to starboard symmetric modes

$$n_j^*(x, y, z) = n_j^*(x, -y, z) \tag{7.21}$$

$$\phi_j(x, y, z) = \phi_j(x, -y, z) \tag{7.22}$$

and for port to starboard anti-symmetric modes

$$n_j^*(x, y, z) = -n_j^*(x, -y, z) \tag{7.23}$$

$$\phi_j(x, y, z) = -\phi_j(x, -y, z) \tag{7.24}$$

With these relations, the integrations in Eqs. 7.14, 7.18 and 7.20 around the sectional contour need only be carried out along a single hull, for example, the port hull. If R is used to denote the cross-sectional wetted surface of the port hull, the modal sectional incident and diffraction wave forces in Eqs. 7.14 and 7.18 can be written for symmetric modes as

$$f_{Ij} = \rho g \alpha e^{ikx\cos\beta} \int_R 2 n_j^* \cos(ky\sin\beta)\, e^{kz'}\, dR \tag{7.25}$$

$$f_{Dj} = -\alpha\omega\rho e^{ikx\cos\beta} \int_R 2\,[in_z\cos(ky\sin\beta) - in_y\sin\beta\sin(ky\sin\beta)]\, e^{kz'}\phi_j\, dR \tag{7.26}$$

and for anti-symmetric modes as

$$f_{Ij} = \rho g \alpha e^{ikx\cos\beta} \int_R 2 n_j^* i\sin(ky\sin\beta)\, e^{kz'}\, dR \tag{7.27}$$

$$f_{Dj} = -\alpha\omega\rho e^{ikx\cos\beta} \int_R 2\,[-n_z\sin(ky\sin\beta) - n_y\sin\beta\cos(ky\sin\beta)]\, e^{kz'}\phi_j\, dR \tag{7.28}$$

The sectional hydrodynamic coefficients a_{jk} in Eq. 7.20 can be written as

$$a_{jk} = -2\rho \int_R \frac{\partial \phi_j}{\partial n} \phi_k dR \tag{7.29}$$

when both ϕ_k and ϕ_j correspond to either symmetric or antisymmetric modes. The corresponding terms in Eq. 7.29 for coupling of symmetric and antisymmetric modes are zero.

The structural modal hydrodynamic forces are obtained by integrating the sectional modal hydrodynamic forces along the structural length:

$$\{F_I^*\} = \int_L \{f_I\}\, dx \tag{7.30}$$

$$\{F_D^*\} = \int_L \{f_D\}\, dx \tag{7.31}$$

$$\{F_R^*\} = \int_L \{f_R\}\, dx \tag{7.32}$$

where the components of $\{F_R^*\}$ are given by

$$F_{Rj}^* = p_k \int_L a_{jk} dx = (\omega^2 M_{fjk} + i\omega C_{fjk})\, p_k \tag{7.33}$$

In the above equations, $\{F_I^*\}$ is the vector of modal incident wave forces; $\{F_D^*\}$ is the vector of modal diffraction wave forces; $\{F_R^*\}$ is the vector of modal radiation wave forces; and M_{fjk} and C_{fjk} are modal added-mass and damping, respectively.

7.5 Consistent two-dimensional normal

A two-dimensional fluid model is used in the composite 2-D/3-D approach for hydroelasticity. Therefore, Frank's method is applied on each cross-section. The normal vector {n}, in traditional strip theory, is determined from the normal to the cross section

C. Each cross section is represented by two-dimensional line elements along the contour line.

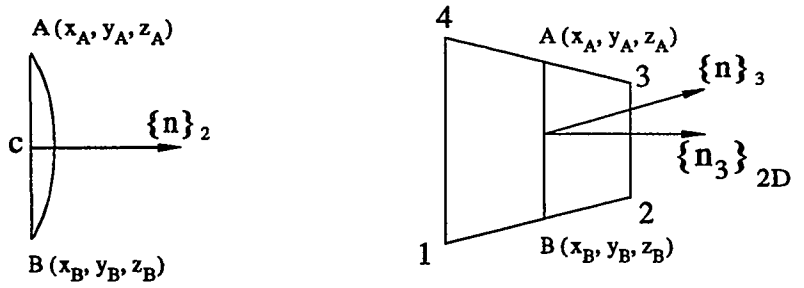

Figure 7.4 Two-dimensional normal vector $\{n\}_2$ and $\{n_3\}_{2D}$

The body boundary condition for the radiation potential problem involves the component of normal velocity in the y-z plane. Therefore, from Fig. 7.4, the two-dimensional normal vector should be obtained by assuming $n_x = 0$ in the three-dimensional normal $\{n\}_3$. This "consistent two-dimensional normal vector" is denoted by $\{n_3\}_{2D}$. The traditional normal vector $\{n\}_2$ is not equal to the consistent two-dimensional normal $\{n_3\}_{2D}$ except when the normal to the body surface is normal to the x-axis.

The difference between the consistent two-dimensional normal $\{n_3\}_{2D}$ and the normal $\{n\}_2$ which is used in traditional strip theory may result in differences in hydrodynamic force calculations. Since the two-dimensional normal $\{n\}_2$ is always larger than or equal to the consistent two-dimensional normal $\{n_3\}_{2D}$, it may be one of the reasons that the quantities in strip theory are always larger than or equal to those in three-dimensional potential theory.

A three-dimensional structural model is used in the composite 2-D/3-D approach. Therefore, it is possible to calculate the consistent two-dimensional normal $\{n_3\}_{2D}$ for this approach. For example, if the structural surface below the still-water plane is

modeled by quadrilateral thin shell elements, one possible way to calculate the consistent normal is as follows.

The four node three-dimensional shell element can be used to calculate the three-dimensional normal vector $\{n\}_3$ in such a way that the center of the two neighbor nodes $A(x_A, y_A, z_A)$ and $B(x_B, y_B, z_B)$ of a two-dimensional panel is located at the same position as the center c of the three-dimensional element. The three-dimensional normal vector $\{n\}_3$ can be obtained as described in Section 3.4.1. After the three-dimensional normal vector $\{n\}_3$ is obtained, set the component $n_x = 0$. Thus, the consistent two-dimensional normal vector is

$$\{n_3\}_{2D} = \{0, n_y, n_z\} \tag{7.34}$$

The consistent two-dimensional normal vector can then be used to form the generalized normal vector, $\{n^*\}$:

$$\{n^*\} = [\psi]^T \{n_3\}_{2D} \tag{7.35}$$

The generalized normal vector $\{n^*\}$ can be used in the equations in Sections 7.3 and 7.4. The implementation of this consistent normal vector concept is left for future work.

7.6 Modification of two-dimensional fluid forces

It is well known that two-dimensional strip theory and two-dimensional hydroelasticity has some serious limitations. For example, pitch response cannot be predicted very well. The incorrect pitch response results from neglecting the fluid action in the longitudinal direction. Some work has been done to improve two-dimensional strip theory by considering longitudinal fluid forces. For example, Riggs and Ertekin (1993) have proposed augmenting the forces from strip theory by surge forces calculated from Morison's equation.

The same idea can be applied in the composite 2-D/3-D approach to improve the motion responses. Two components of the fluid forces may be calculated by a three-dimensional model without much more computational effort. They are the three-dimensional hydrostatic restoring forces and the incident wave forces.

Hydrostatic restoring coefficients calculated by a three-dimensional model for the rigid body motion are the same as those by the two-dimensional model because in both cases, the structure is treated as a rigid body. However, three-dimensional hydrostatic restoring coefficients for flexible motions of a structure are different from those obtained by traditional two-dimensional hydroelasticity. The generalized three-dimensional hydrostatic restoring coefficients have been discussed in Section 4.3; they can be calculated by

$$K_{fjk}^{*} = \rho g \iint_{S_b} n_j^{*} \psi_{wk} dS \qquad j,k = 1,2,\ldots,q \tag{7.36}$$

in which n_j^{*} is the three-dimensional generalized normal at the point (x,y,z) on the mean wetted-surface corresponding to the jth mode shape, and ψ_{wk} is the vertical displacement at the point (x,y,z) on the mean-wetted surface in the kth mode shape.

The incident wave potential which was given in Eq. 7.13 can be used to calculate the three-dimensional incident wave force. Unlike Eq. 7.14, the integral will be carried out by using three-dimensional generalized normal. The incident wave force for the jth mode shape can be written as

$$f_{Ij} = \rho g \alpha \iint_{S_b} n_j^{*} e^{ikx\cos\beta} e^{iky\sin\beta} e^{kz'} dS \tag{7.37}$$

Since two-dimensional potential theory is used to calculate the radiation potentials, the horizontal motion in the x-direction cannot be predicted by the composite 2-D/3-D approach. The objective in introducing the three-dimensional incident wave force here is

to include the component of the pitch moment which results from the incident wave forces in the x-direction.

7.7 Simplified method using "basic modes"

The integrations in Eqs. 29 must be carried out numerically. Because the mode shapes $\{\psi\}$ vary, in general, along the x-axis, the modal sectional hydrodynamic coefficients and forces must be calculated for each cross-section at which the integrand is evaluated, even if the geometry of the cross section does not change along the length.

To reduce further the computations, Wang (1991) proposed for twin-hull structures to approximate the cross-sectional deformation in the mode shapes by a small number of 'basic modes,' which include the three rigid modes (modes 1-3 in Fig. 7.2) used in two-dimensional hydrodynamics, as well as three additional deformational modes (modes 4-6 in Fig. 7.2). The basic modes assume that the deformation can be expressed as extensional deformation of the deck (mode 4) and rigid rotation of each hull about some point, typically at the connection of the strut and deck (modes 5 and 6). With this simplification, the same basic modes can be used for all cross-sections, and the velocity potentials for the basic modes need only be determined once for geometrically identical sections. These can then be used to approximate the forces and hydrodynamic coefficients for the actual modes. A more rigorous approach to approximate the actual mode shapes with the basic modes has been used for the present work. This approach is developed below.

From Fig. 7.2, a 3×6 matrix, [D], which contains the translational displacements associated with the basic modes at any point (y,z) on the mean wetted-surface at the cross-section with longitudinal coordinate x can be written as

$$[D] = \begin{bmatrix} 0\,0 & 0 & 0\,0 & 0 \\ 1\,0 & -(z-z_G) & 1\,0 & -(z-z_P^*) \\ 0\,1 & (y-y_G) & 0\,1 & (y-y_P^*) \end{bmatrix} \quad \text{on port hull} \tag{7.38}$$

$$[D] = \begin{bmatrix} 0\,0 & 0 & 0\,0 & 0 \\ 1\,0 & -(z-z_G) & -1\,0 & (z-z_S^*) \\ 0\,1 & (y-y_G) & 0\,-1 & -(y-y_S^*) \end{bmatrix} \quad \text{on starboard hull} \tag{7.39}$$

where y_G and z_G are the y and z coordinates of the center of gravity of the structure; and y_P^*, z_P^* and y_S^*, z_S^* are the coordinates of the center of rotation between the deck and the port and starboard hulls, respectively.

Only the structural motion below the still-water line affects the fluid motion, and therefore, the basic modes are only used to represent the motion of the mean wetted-surface. For a given cross-section, suppose there are m_s nodes in the structural model below or at the still-water line. If there are no nodes at the still-water line, m_s will also include the nodes which are just above the still-water line. Then the modal translational displacements of the m_s nodes can be used to form an $n_s \times q$ matrix $[\psi_s]$, with $n_s = m_s \times 3$. The modal displacements can be approximated by the basic modes as

$$[\psi_s] \approx [D_s]\,[S_s] \tag{7.40}$$

in which $[D_s]$ is an $n_s \times 6$ matrix formed by the basic mode shape matrices for the m_s nodes; and $[S_s]$ is a $6 \times q$ matrix. Using the method of least squares, $[S_s]$ for each cross-section can be obtained by solving the following equation:

$$[D_s]^T[\psi_s] = [D_s]^T[D_s]\,[S_s] \tag{7.41}$$

$[D_s]^T[D_s]$ only needs to be factored once for each different cross-section.

The use of the basic modes introduces a significant simplification of the deformational motion. To estimate how well Eq. 7.40 is satisfied, the following indicators are defined:

$$\gamma^j = \frac{\left\| \left([\psi_s] \right)^j \right\|}{\left\| \left([D_S]\ [S_S] \right)^j \right\|} \tag{7.42}$$

$$\cos\theta^j = \frac{\left\| \left([\psi_s]^T \right)^j \left([D_S]\ [S_S] \right)^j \right\|}{\left\| \left([\psi_s] \right)^j \right\| \left\| \left([D_S]\ [S_S] \right)^j \right\|} \tag{7.43}$$

in which $\left([\ ] \right)^j$ is the jth column of the matrix $\left([\ ] \right)$ and $\| \bullet \|$ represents the L_2 norm. Here γ^j is the ratio of the length of the actual displacements $\left([\psi_s] \right)^j$ to the length of the approximation $\left([D_S]\ [S_S] \right)^j$. Accordingly, θ^j is the angle between these two vectors. For an exact representation, $\gamma^j = 1$ and $\theta^j = 0$.

If $\{\xi\}$ is used to represent the principal coordinates for basic modes, the two principal coordinates $\{\xi\}$ and $\{p\}$ have the following approximate relationship:

$$\{\xi\} \approx [S_S]\ \{p\} \tag{7.44}$$

The generalized normal vector $\{n_b^*\}$ for the basic modes can be found, similar to $\{n^*\}$, as

$$\{n_b^*\} = [D]^T \{n\} \tag{7.45}$$

which does not vary as a function of x for geometrically identical cross-sections. Therefore, the radiation potentials only need to be solved once for similar cross-sections. The generalized normal vector $\{n_b^*\}$ can be written as

$$\{n_b^*\} = \begin{bmatrix} n_2 \\ n_3 \\ -(z-z_G)\,n_2 + (y-y_G)\,n_3 \\ n_2 \\ n_3 \\ -(z-z_p^*)\,n_2 + (y-y_p^*) \end{bmatrix} \quad \text{on port hull} \tag{7.46}$$

$$\{n_b^*\} = \begin{bmatrix} n_2 \\ n_3 \\ -(z-z_G)\,n_2 + (y-y_G)\,n_3 \\ -n_2 \\ -n_3 \\ (z-z_S^*)\,n_2 - (y-y_S^*) \end{bmatrix} \quad \text{on starboard hull} \tag{7.47}$$

By substituting Eq. 7.40 into Eq. 7.3, the modal wave forces for basic modes, noting that the matrix $[S_s]$ is a function of x only, can be written as

$$\begin{aligned} \{F^*\} &= i\omega\rho \int_L [S_s]^T \left\{ \int_{C_b} [\Phi]\,[D]^T \{n\}\, dC \right\} dx \\ &= \int_L [S_s]^T \left\{ i\omega\rho \int_{C_b} [\Phi]\,\{n_b^*\}\, dC \right\} dx \end{aligned} \tag{7.48}$$

which has the same terms as Eq. 7.8 except for $[S_s]^T$. Note that the quantity in braces in Eq. 7.48 is the sectional force which can be decomposed into incident, diffraction, and radiation terms as in Eqs. 7.9, 7.10 and 7.11. Eq. 7.48 illustrates that the 2-D potential problem can be solved only for the basic modes for each cross-section to obtain the sectional modal forces. Then, the generalized wave forces for principal modes in terms of the forces for the basic modes become

$$\{F_I^*\} = \int_L [S_s]^T \{f_I\}\, dx \tag{7.49}$$

$$\{F_D^*\} = \int_L [S_s]^T \{f_D\}\, dx \tag{7.50}$$

$$F_{Rj}^* = \left(\int_L [S_s]^T a_{jk} dx\right)\xi_k = \left(\int_L [S_s]^T a_{jk} [S_s]\, dx\right) p_k = (\omega^2 M_{fjk} + i\omega C_{fjk})\, p_k \tag{7.51}$$

in which it is understood that $\{f_I\}$, $\{f_D\}$, and a_{jk} are the result of the term in braces in Eq. 7.48.

The generalized hydrodynamic forces from either Eqs. 7.30, 7.31, and 7.32 or Eqs. 7.49, 7.50, and 7.51 can be substituted into Eq. 7.2 to obtain

$$\begin{aligned}\left[-\omega^2([M_s^*] + [M_f^*]) - i\omega([C_s^*] + [C_f^*]) + ([K_s^*] + [K_f^*])\right]\{p\} \\ = \{F_I\}^* + \{F_D\}^*\end{aligned} \tag{7.52}$$

in which $\{F_I^*\}$ and $\{F_D^*\}$ have the same definitions as before; M_{fjk} and C_{fjk} are the elements of the modal added-mass and damping matrices, $[M_f^*]$ and $[C_f^*]$, respectively; and $\{F_r^*\}$ is written as $-[K_f^*]\{p\}$, where $[K_f^*]$ is the hydrostatic restoring stiffness which results from the hydrostatic pressure.

After solving Eq. 7.52 for the principle coordinates, the nodal displacements {D} can be calculated with Eq. 7.1, and internal forces or stresses can be calculated with nodal displacements {D}.

The computer programs have been implemented based on both methods described in Sections 7.3 and 7.7. They are named **HYDRAS-COMPOSITE** and **HYDRAS-BASIC**, respectively (Che, 1993).

CHAPTER 8

STRUCTURAL MODELS

Three models of floating structures are developed primarily to apply and verify the approaches described in Chapter 5 to 7 for determining hydroelastic response of floating structures. They are: a 100 m × 100 m module, which is used to 'assemble' a multi-module VLFS; an idealized twin-hull structure; and a SWATH ship.

8.1 VLFS module

The single VLFS module used here was designed by Winkler et al. (1990). The overall geometry of a single module, which is their 'revised design No. 2', is shown in Fig. 8.1. The cross-bracings prevent deformation in the transverse plane (prying deformations). However, since the bracings have minimal influence on the hydrodynamic loading to which the system is subject, they are ignored in the present study. Such a simplification reduces the single module to a 4-column, 2-pontoon structure. The principal characteristics of a single module is given in Table 8.1. Further details on the module design may be found in Winkler et al. (1990).

This single module can function individually. Therefore the dynamic behavior is one important consideration (among many others) for the design. Therefore, a structural dynamic analysis was performed by Winkler et al. (1990) for the single module. In present study, the module was modeled as a frame structure. That is, the pontoons and columns were modeled by frame elements and the deck was represented by a grid of frame elements, as shown in Fig. 8.2. The section properties of the pontoon, column, and deck are shown in Table 8.2, in which $I_{\bar{y}\bar{y}}$, $I_{\bar{z}\bar{z}}$, and J are the mass moment of inertia about the local $\bar{y}$-axis and $\bar{z}$-axis, and the torsional constant of the section, respectively. In addition, the hydrodynamic forces acting on the module will be calculated by

Morison's equation. Therefore, any non-tubular member of the structure below the still-water plane is approximately modeled as a circular cylinder based on the equivalent underwater volume, which is shown in Fig. 8.3.

The other option for single module design is to consider various arrangements of modules to construct multi-module VLFSs. In this case, the single module must function both individually and as part of a VLFS with respect to floating stability, strength, and motions induced by environmental forces. Functional arrangements for airfield, OTEC power plant, and offshore mining facilities can be made by connecting single modules. Fig. 8.4 shows a multi-module VLFS connected in tandem.

An important aspect for multi-module VLFS design is the connections. It is difficult enough to connect together two relatively light floating structures in a calm sea. To connect two VLFS modules will increase the difficulty many times. The objective of the research here is not to explore what the physical connectors should be and how the modules are connected. Rather, it is limited to determining the response for hinged, elastic, and rigid connections. These results can be used for further preliminary design of the VLFS connections.

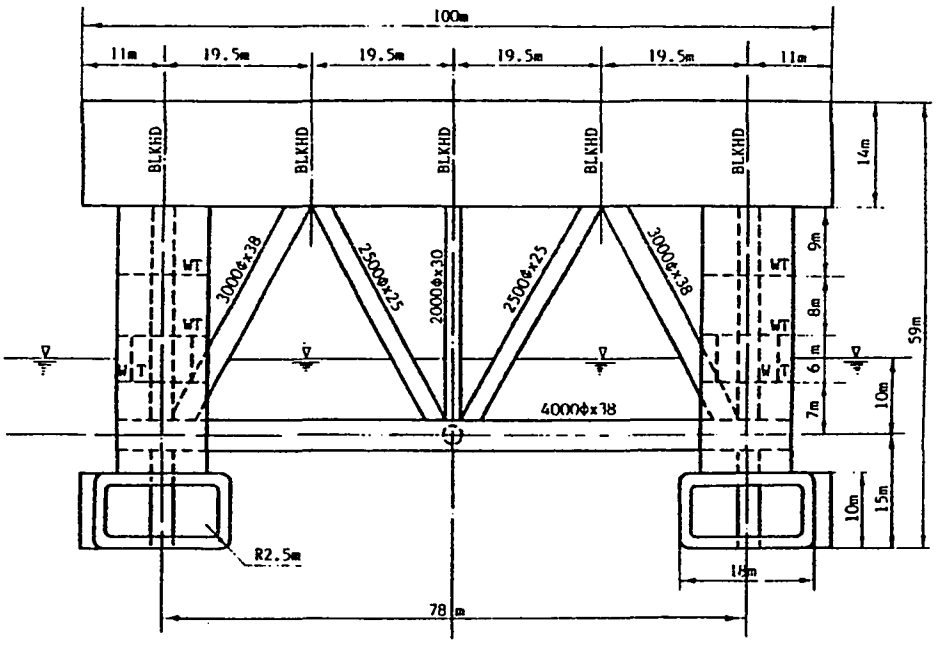

(a) Forward elevation of the single module

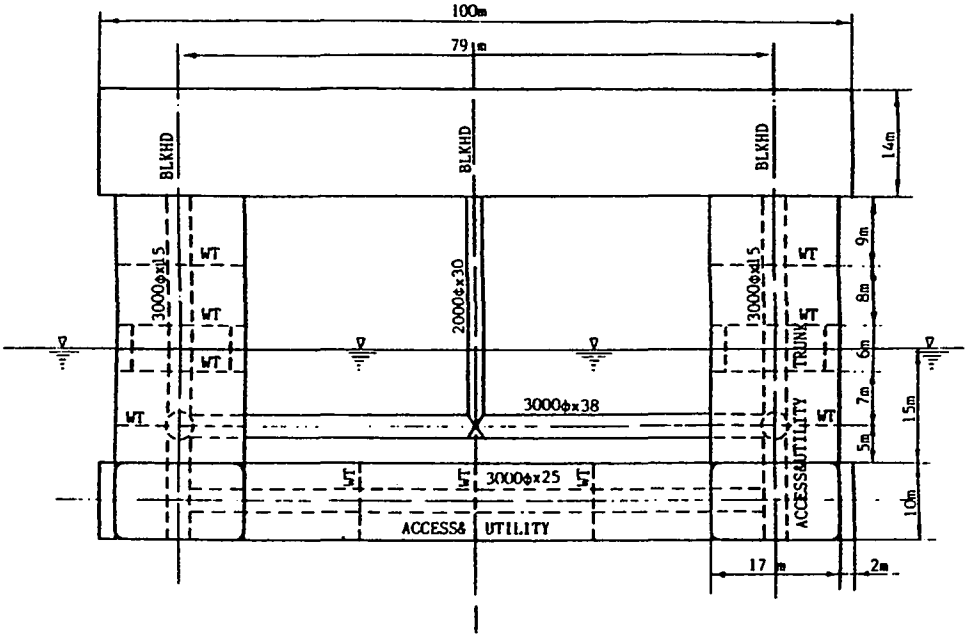

(b) Starboard elevation of the single module

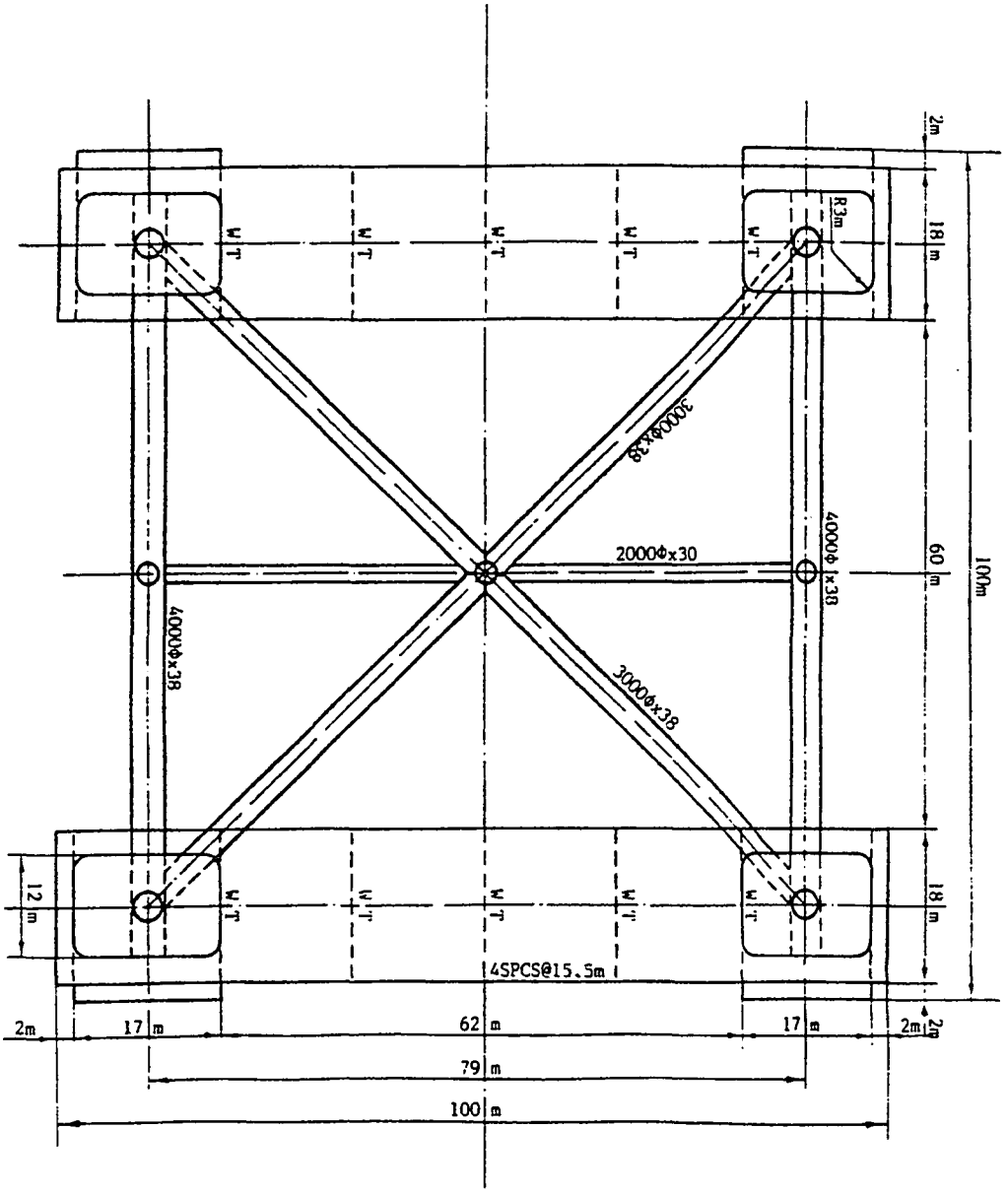

(c)Plan view of the single module

Figure 8.1 Configuration of a single module (Winkler et al. 1990)

Table 8.1 Principle characteristics of a single module

Description	Value
Displacement (mass) (kg)	$46,440 \times 10^3$
Water-plane area A (m^2)	816
Length (m)	100
Width (m)	100
Operating draft (m)	25
Height (m)	59
Column Width × Depth × Length (m)	12 × 17 × 35
Pontoon Width × Height × Length (m)	18 × 10 × 96
KG (m)	30.67
KB (m)	8.25
GM_L (m)	5.01
GM_T (m)	4.13
Mass moment of inertia I_{xx} ($kg \cdot m^2$)	7.19×10^{10}
Mass moment of inertia I_{yy} ($kg \cdot m^2$)	6.49×10^{10}
Mass moment of inertia I_{zz} ($kg \cdot m^2$)	9.53×10^{10}

Table 8.2 Section structural properties

Modulus of Elasticity: 2.07×10^{11} (N/m^2)
Shear Modulus: 8.0×10^{10} (N/m^2)

Member	Steel area (m^2)	I_{yy} (m^4)	I_{zz} (m^4)	J (m^4)	$\bar{m}$ (kg/m)
Pontoon	2.8	40	90	60	57290
Column	2.21	70	40	70	39230
Deck					
Longitudinal	0.80	25	25	50	23400
Transverse	0.25	20	40	50	23400

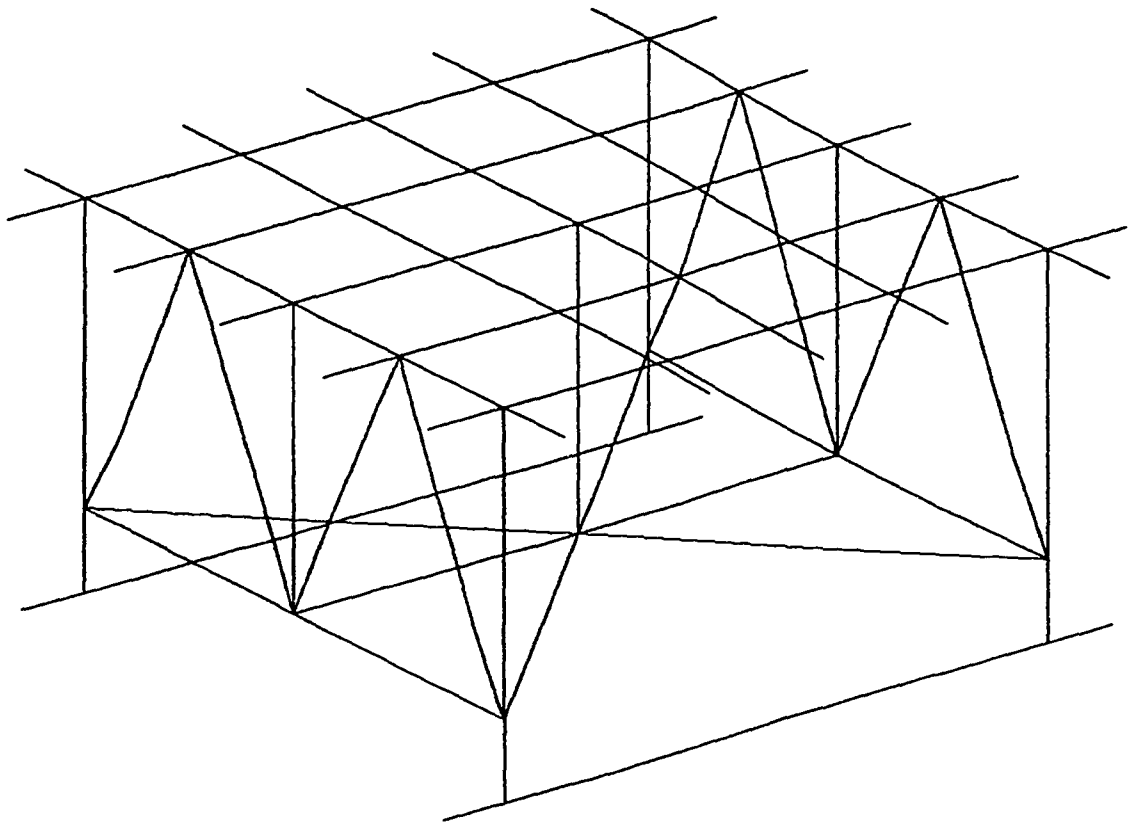

Figure 8.2 Frame model of a single module

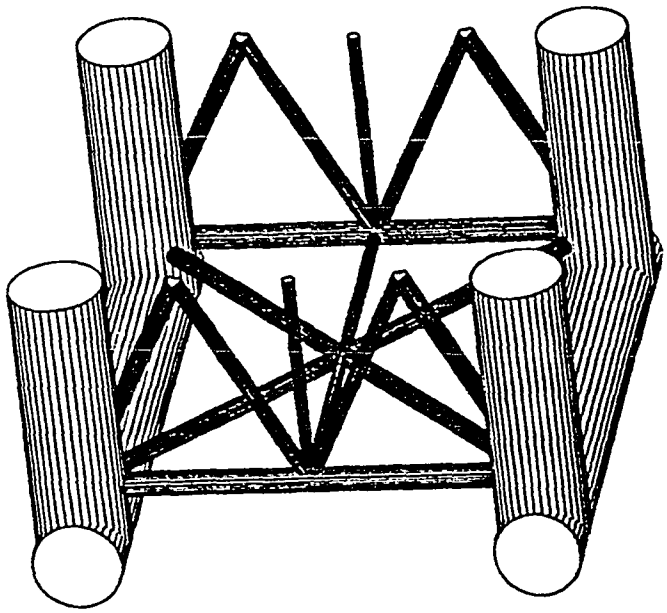

Figure 8.3 Idealization of a single module by tubular members (Ertekin et al. 1991)

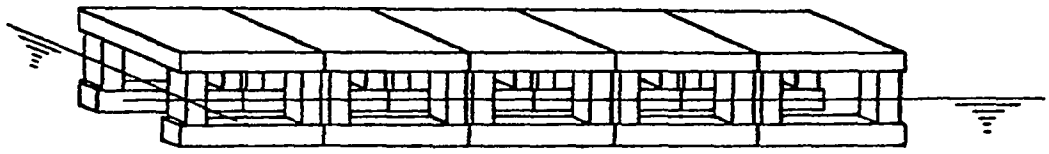

Figure 8.4 Schematic of a five module VLFS

8.2 Simple twin-hull structure

A simple, idealized, very long and slender twin-hull floating structure, shown in Fig. 8.5, has been designed to verify the composite 2-D/3-D hydroelasticity theory. A uniform cross-section, as shown in Fig. 8.6, was assumed. Additional properties of this simple twin-hull floating structure are given in Table 8.3. It should be noted that this simple structure is not meant to represent a realistic structure and neither is the calculated response realistic. Rather, the structure is simple and highly idealized, and it has been developed to demonstrate application of the theory. The other purpose of using this simple structure is to validate the new methods and corresponding computer implementation. It is difficult to find a computational model with sufficient geometric and property description to validate and compare the results of newly developed methods. This simple structural model also can be used for comparison in future work.

To simplify the analysis and verification, the deck and struts are assumed to be rigid with the only flexibility represented by rotational springs joining the deck and struts. The cross-section of the structure model, therefore, is represented by the line diagram. The exact, dry modes for this simple structure are readily obtained by hand calculation. If the structure is assumed fixed at the center of gravity, there are only two modes, which involve symmetric (mode 7) and antisymmetric (mode 8) 'swinging' of the struts. The natural frequencies of these two modes, which can be calculated based on the rotational stiffness of the strut-deck connection, are 0.6 rad/sec.

When the structure is freely-floating, there are eight displacement degrees of freedom. The first six dry modes are the usual rigid body motions. Mode 7 is identical to mode 7 for the fixed structure, with a corresponding dry natural frequency of 0.6 rad.sec. Mode 8 is a combination of mode 8 for the fixed structure and sway and roll, and it has a natural frequency of 1.16 rad/sec.

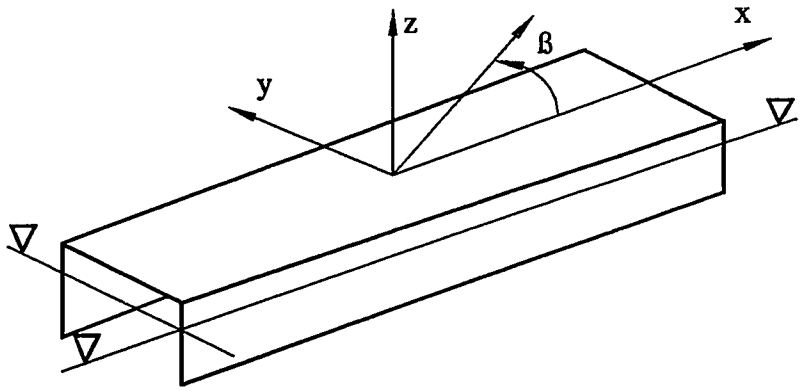

Figure 8.5 Schematic view of a twin-hull structure

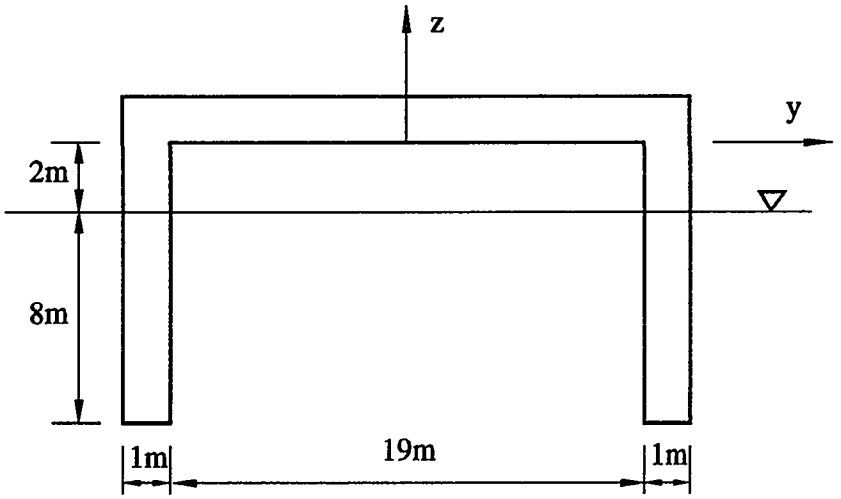

Figure 8.6 Geometry of cross-section of a simple twin-hull structure

Table 8.3 Principle characteristics of simple twin-hull structure

Description	Value
Length (m)	300
Displaced volume (m^3)	4800
Distance between struts (m)	20
Draft (m)	8
Strut	
Dimensions	
Thickness × Height × Length (m)	$1 \times 10 \times 300$ m
Mass density kg/m^3	300
Rotational stiffness of strut-deck connection $N \cdot m/m$	3.6×10^4
Roll mass moment of inertia $kg \cdot m^2$	1.31×10^8
Heave restoring stiffness MN/m	6.03
Roll restoring stiffness $MN \cdot m$	314

8.3 SWATH model

The Small Waterplane Area Twin Hull (SWATH) ship concept began to be recognized in the 1970s and the technology has since developed rapidly (Kalloi et al., 1976; Curphey et al., 1977). The majority of the SWATH's buoyancy comes from hulls submerged well below the sea surface and hence the hulls are away from the location of the largest wave excitation forces. Therefore, SWATH ships have superior seakeeping characteristics. Another advantage is that they have a minimum speed degradation when operated in the seas. However, because very few SWATH vessels exist, there is still insufficient information available on the motion, loading, and structural responses of SWATH ships. For example, one of the structural strength problems is transverse wave

'prying moment' on struts. Hence, a SWATH model is developed here to study these.

Fig. 8.7 schematically shows the geometry of the SWATH model. The principle characteristics of the SWATH model can be found in Table 8.4. The resonant frequencies for rigid body motion of the SWATH ship in water are estimated, by assuming constant added mass, as 0.62 rad/sec, 0.42 rad/sec, and 0.32 rad/sec for heave, roll, and pitch motion, respectively.

Fig. 8.8 shows the finite element model, developed with the general purpose finite element code COSMOS/M, which is used for structural analysis. The structural model consists entirely of shell elements. The properties of the shell elements are shown in Table 8.5. For dynamic analysis, the mass of all nonstructural components has been incorporated in the mass densities of the shell elements. The inside girder elements are assumed massless to simplify the problem. Because of port-starboard (x-z plane) symmetry, only one-half of the structure was modeled, using a total of 922 elements, many of which are used for inside stiffeners. To simplify the coupling of the structural model with the fluid models, the fore-aft symmetry was not exploited. The structural dry modes are calculated by using the finite element code COSMOS/M and the first 14 'dry' mode shapes are considered (q=14). The first 6 modes involve rigid body motion, while the remaining 8 consist of 4 symmetric and 4 antisymmetric deformational modes. The deformational modes and corresponding natural frequencies are shown in Fig. 8.9. To increase the responses in the deformation modes and thereby more readily compare the results of the composite method and three-dimensional hydroelasticity, the structure has been designed such that these frequencies are lower than they would be for a practical design. This is why the thickness of the inside stiffener is only 0.0015 m.

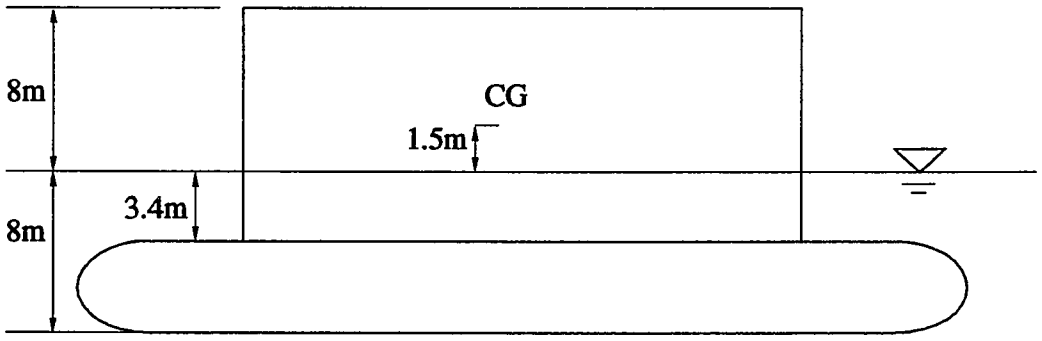

(a)

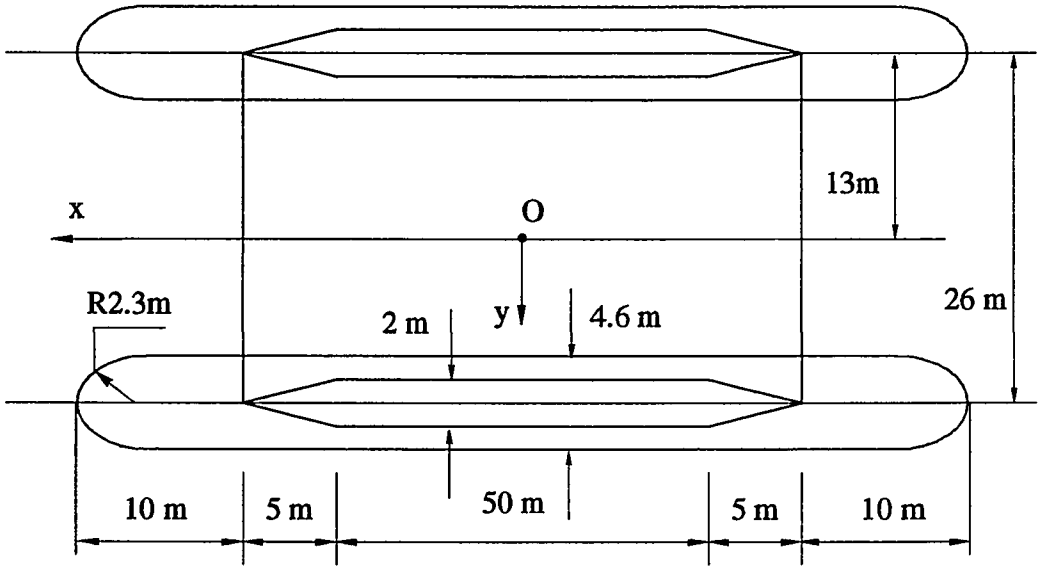

(b)

Figure 8.7 Geometry of SWATH ship, (a) side view, (b) top view

Table 8.4 Principle characteristics of SWATH ship

Parameter	Value
Length (m)	80 m
Displaced Volume (m^3)	3356.1 m^3
Distance between struts (m)	26 m
Draft (m)	8 m
KB (m)	3.192 m
KG (m)	9.5 m
Height of the deck above still water line (m)	8 m
GM_T (m)	4.79 m
GM_L (m)	10.37 m
Roll mass moment of inertia $kg \cdot m^2$	2.303×10^8
Pitch mass moment of inertia $kg \cdot m^2$	1.529×10^9
Roll restoring stiffness $N \cdot m$	1.454×10^9

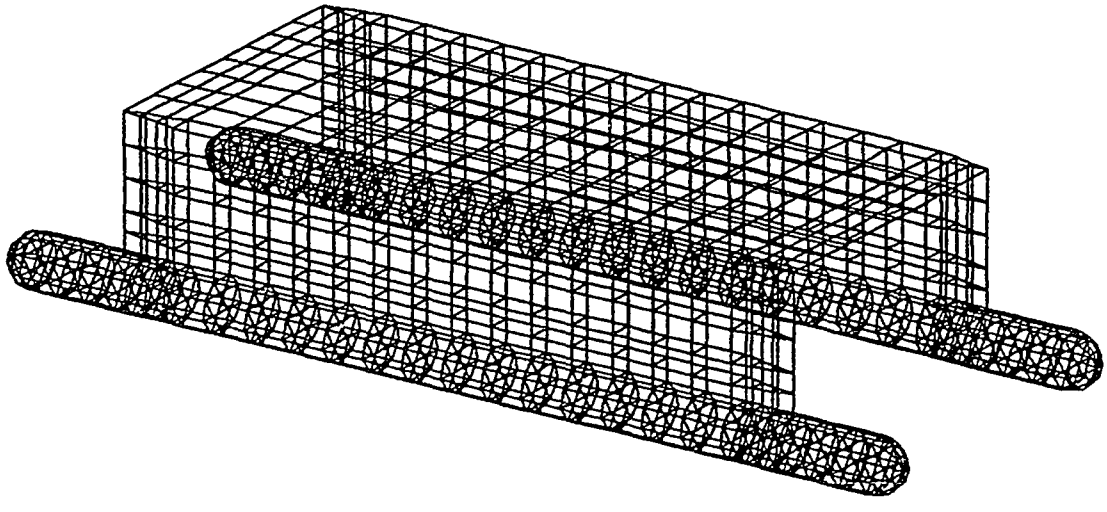

Figure 8.8 Finite element model of the SWATH ship

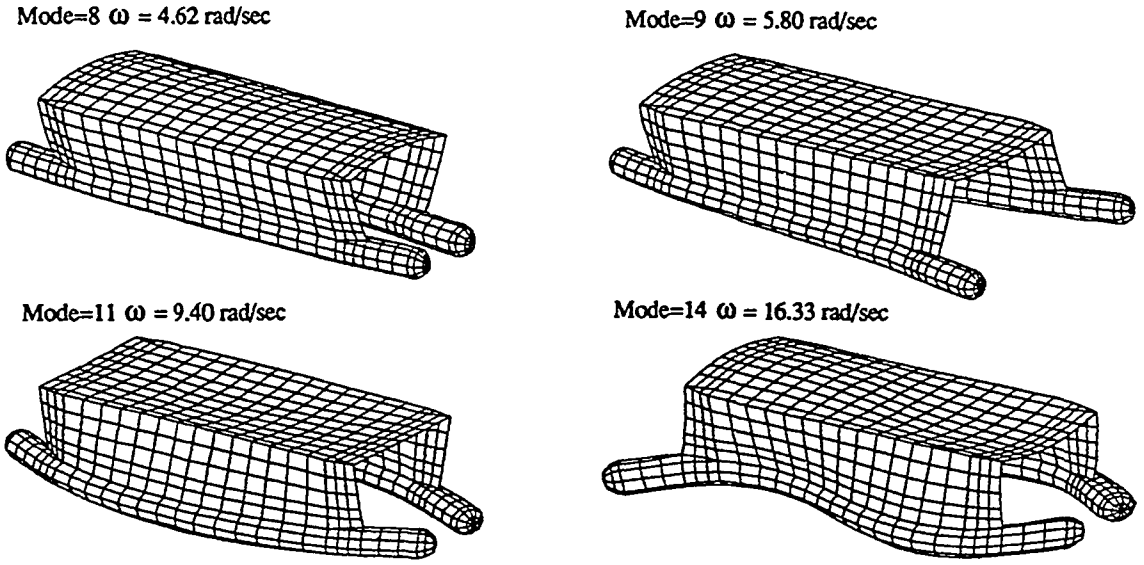

Symmetric modes

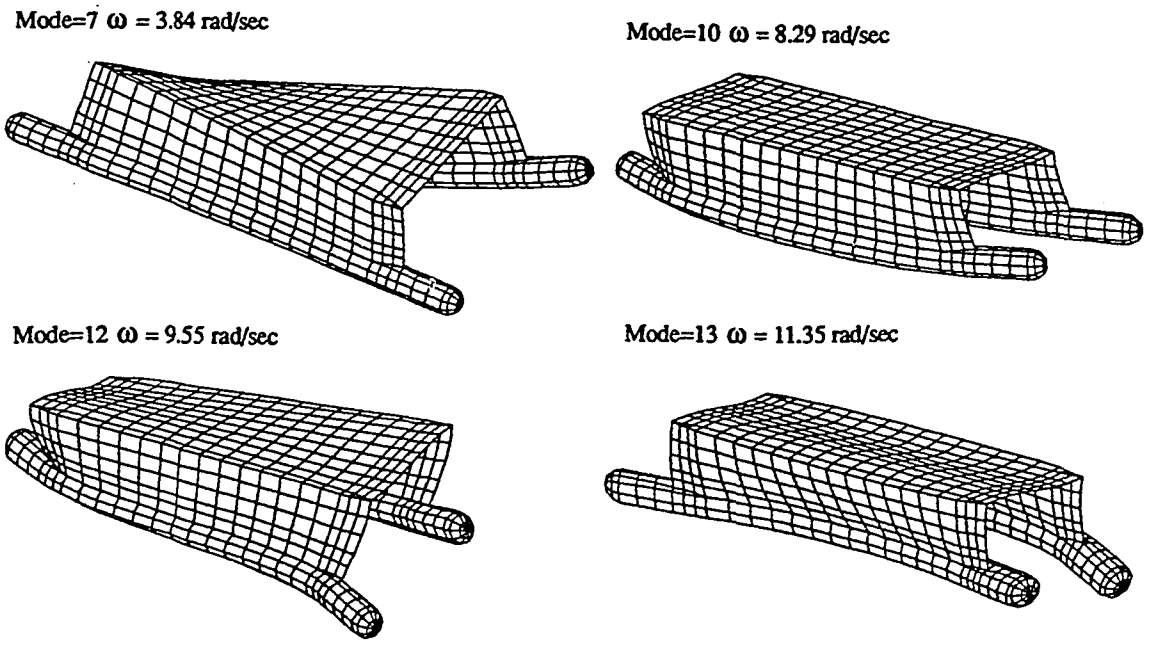

Antisymmetric modes

Figure 8.9 Flexible mode shapes of SWATH ship

Table 8.5 Section structural properties

Modulus of Elasticity: $2.0 \times 10^{11} N/m^2$, Shear Modulus: $8.0 \times 10^{10} N/m^2$		
Member	Thickness (m)	Density kg/m^3
Element for pontoon	0.0025	2.557×10^5
Element for strut	0.0025	5.288×10^4
Element for deck	0.4	2.380×10^3
Element for stiffener	0.0015	0

CHAPTER 9

NUMERICAL RESULTS AND DISCUSSIONS

9.1 Application of two-dimensional hydroelasticity

The approach for two-dimensional hydroelasticity described in Section 5.3 has been used to determine the motions of the single module described in Section 8.1. The geometry of the 4-column, 2-pontoon single module has been shown in Fig. 8.1, and the module properties have been given in Table 8.1. For the two-dimensional hydroelastic analysis, the structure must be modeled as a beam. To determine the equivalent beam properties of the structure, a detailed 3–D frame model of a single module was developed. This model, together with 'engineering judgement,' was used to determine the beam stiffness and mass properties shown in Table 9.1 for the three cross sections considered: pontoon, column-pontoon, and deck overhang. In Table 9.1, I_{yy} and I_{zz} are the second moment of the cross-section area about the y-axis and the z-axis, respectively; J is the torsional constant of the cross-section; A_{sy} and A_{sz} are the shear area about the y-axis and the z-axis, respectively; m_{ii} are the mass densities, for i=1,2,3, and mass moment of inertia densities, for i=4,5,6, per unit length. The latter results from the fact that the pontoons are 96 m long, while the deck is 100 m long. Structural damping is assumed to be zero, and, for simplicity, it is assumed that the centers of mass and shear for each section are located on the x axis.

The hydrodynamic coefficients and wave exciting forces were determined based on a column-pontoon section and a pontoon section (Fig. 9.1). Twenty sections are used for two-dimensional hydrodynamic and wave exciting force calculations. The bracing was ignored in these calculations.

The response of a single module to regular head ($\beta = 180°$), quartering

($\beta = 135°$), and beam seas ($\beta = 90°$) has been determined for a range of wave frequencies between 0.2 and 1.25 rad/s. The results are compared in Fig. 9.5 with the results obtained from 3-D potential theory (Wang et al., 1991). As can be seen, the results of the 2–D analysis agree favorably with the 3–D results, especially for heave, sway, and roll. The pitch response is clearly less accurate. The discrepancy is likely due to ignoring the hydrodynamic forces in the x direction on the pontoon ends and the column face in strip theory. This error presumably should be less for a multi-module, 'linear' structure. Similar difficulties in using strip theory for semisubmersibles were reported by Kim and Chou (1973) and Carlsen and Mathisen (1980).

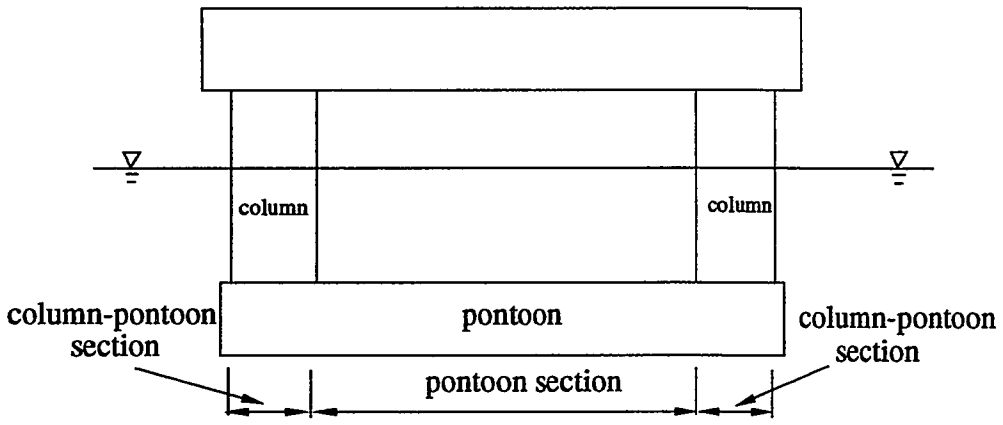

Figure 9.1 Two sections of a single VLFS

Two-dimensional hydroelasticity is also applied to a five module VLFS which consists of five identical single modules. Two models for the module connectors were investigated: a "hinge" connector, for which the three relative rotations between modules are unrestrained, and a "rigid" connector, which ensures both displacement and rotational continuity at the module interfaces. Practical connector designs would fall between these two extremes.

The response of the five module VLFS to regular head and quartering seas has been

determined for a range of wave frequencies between 0.2 and 1.25 rad/s. The absolute value of the vertical displacements per unit wave amplitude is shown in Fig. 9.6 as a function of position and wave frequency. For the hinge connector, the presence of the individual modules is quite clear. For the rigid connector, however, the individual modules are not obvious because the motion is predominantly that of a rigid body. The vertical deflection for the hinge model is shown in Fig. 9.7 as a function of time for a frequency of 0.5 rad/s. It is clear that there is significant pitching of the individual modules. From Fig. 9.6a it may be observed that the displacements are not symmetric for low frequencies. The unsymmetry is likely due to the inaccuracies in the pitch motion of a single module. For the rigid connection model, the results are unsymmetric only very close to the heave resonant frequency of a single module, possibly a result of numerical sensitivity. These results indicate that the inaccuracies in the pitch response determined from strip theory are less important for large structures which behave as a 'single' structure, rather than one whose response is primarily composed of connected smaller structures.

The vertical and rotational displacements at the bow are compared for the two models in Figs. 9.8 and 9.9. The motion of the hinged model is nearly always larger than the motion of the rigid model. That is, flexible connections allow greater motion than stiff connections, as expected.

Fig. 9.10 shows the absolute value of the rotations of the four hinge-connectors in head seas, and Fig. 9.11 shows the moments in the rigid connectors. Whereas the displacement transfer functions are a maximum at low wave frequencies, the force transfer functions are maximum at intermediate frequencies. Also, the response is nearly symmetric, with the connections at 100 m and 200 m responding nearly identically to those at 400 m and 300 m, respectively. Fig. 9.12 shows the corresponding moment at

the center of the VLFS. Again, the maximum moment response occurs at intermediate frequencies. Also, the moment in the rigid connection model is significantly larger than the moment in the hinge-connection model. This increase in moment may have a major impact not only on the connector design, but also on the module design.

Table 9.1 Equivalent beam properties

Table 9.1 (a) Pontoon section	
I_{yy}	5500 m^4
I_{zz}	12000 m^4
J	480 m^4
A_{sy}	5.1 m^2
A_{sz}	1.6 m^2
$m_{11} = m_{22} = m_{33}$	416700 kg/m
m_{44}	7.12×10^8 kg-m
m_{55}	2.36×10^8 kg-m
m_{66}	4.73×10^8 kg-m

Table 9.1 (b) Column section	
I_{yy}	7500 m^4
I_{zz}	2800 m^4
J	550 m^4
A_s	N/A
$m_{11} = m_{22} = m_{33}$	1578500 kg/m
m_{44}	9.76×10^8 kg-m
m_{55}	2.63×10^8 kg-m
m_{66}	7.19×10^8 kg-m

Table 9.1 (c) Deck overhang section	
I_{yy}	5500 m^4
I_{zz}	12000 m^4
J	480 m^4
A_{sy}	5.1 m^2
A_{sz}	1.6 m^2
$m_{11} = m_{22} = m_{33}$	234000 kg/m
m_{44}	2.96 x 10^8 kg-m
m_{55}	1.05 x 10^8 kg-m
m_{66}	1.95 x 10^8 kg-m

9.2 Application of Morison's equation method

Three-dimensional hydroelasticity by Morison's equation method is applied to the same 4-column, 2-pontoon VLFS model which has been analyzed by two-dimensional hydroelasticity (Fig. 8.1). The columns and pontoons below the still-water surface are modeled as circular cylinders as shown in Fig. 8.3. The entire structure, including the deck, are modeled by frame elements (Fig. 8.2). There are a total of 171 frame elements for a single module, of which 56 are below the still-water surface, with a maximum length of 5 m each. In Morison's equation, the inertia coefficient C_M = 2.0 and drag coefficient C_D = 1.0 are used for all cases studied in this work as representative values. However, one needs to use more accurate values in actual design studies by using experimental data.

The rigid motion responses of a single module are calculated first. To compare the motion responses of a rigid module obtained by Morison's equation and three-dimensional potential theory, the module was made rigid in the finite element

model by substantially increasing the elastic modulus and shear modulus. The transfer function of 6 rigid-body motions (per unit wave amplitude) obtained by Morison's equation method and three-dimensional potential theory (Wang et al., 1991) are shown in Figs. 9.13 a-f. Considering the rough estimate of the inertia and drag coefficients and large diameters of pontoon and column cross-sections, the overall agreement between the two methods for wave heading angles of $\beta = 180°$ (head seas), 135° (quartering seas), and 90° (beam seas) seems to be good except for the yaw response in quartering seas. Therefore, Morison's equation method may be useful for analyzing VLFSs with pontoons and columns.

With good comparison for a single module, Morison's equation method is then used to predict the responses of a 16 module, 100 m by 1600 m VLFS (Fig. 9.2). A total of 2464 nodes and 1872 frame elements are used for the entire 16 module VLFS. The module connectors, which are 4 m long, are located at the deck level, and their structural properties are the same as the properties of the longitudinal deck elements given in Table 8.2. Therefore, the structure consists of elastic modules and flexible connectors (EMFC model). Because each node has 6 degrees-of-freedom, the complex matrix equation to be solved contains a coefficient matrix of more than 218 million elements. To reduce this matrix to a manageable size, a profile-storage scheme, which exploits the sparsity of the coefficient matrix, is used. The resultant matrix then contains about 2.2 million elements. The CPU time for the complete solution by Morison's equation method for 20 frequencies, and 3 wave headings was about 4 hours on an IBM/RS/6000/530 workstation. This CPU time includes the complete re-assembly of the coefficient matrix required for each iteration on the relative velocity used in the drag term. About 3-4 iterations were required to obtain convergence within a 1% tolerance.

The 16 module VLFS is also analyzed by three-dimensional potential theory. In this

case, the module is assumed to be rigid with flexible connections (RMFC model), and double symmetry of the structure is exploited. As a result, the solution for 20 wave frequencies and 3 wave heading requires about 13 hours of CPU time on a Cray YMP8/ 864 super computer, which is about 5 times faster than the IBM/RS/6000/530 workstation. This means that by using Morison's equation method to determine the hydroelastic response of a 16-module VLFS, one needs about one-sixteenth CPU time compared with the RMFC method even though the entire structure is modeled as an elastic body.

Table 9.2 Natural frequencies of the 16 module VLFS (rad/sec)

Mode No.	1	2	3	4	5	6	7	8	9	10	11	12
Dry mode	0	0	0	0	0	0	0.17	0.47	0.90	1.20	1.46	2.13
wet mode	0	0	.11	.27	.27	0	.29	.43	.65	.71	1.00	1.51

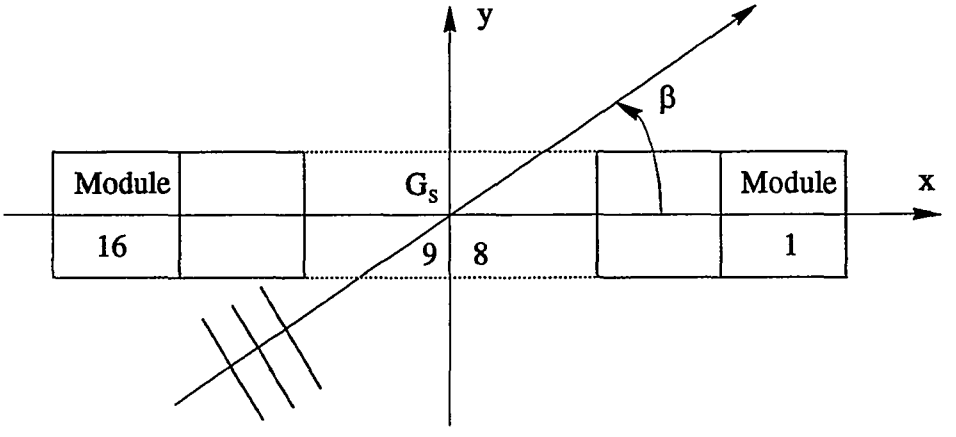

Figure 9.2 Schematic view of a multi-module VLFS

The natural frequencies for the 16 module VLFS are calculated for dry modes and wet modes (for wet modes, the added mass coefficients in Morison's equation method are constant), and they are listed in Table 9.2. The comparison of the transfer functions

of the response amplitude of module 1 and 8, in head seas, are shown in Figs. 9.14a-f obtained by both methods. From Fig. 9.2, module 1 is located at the bow and module 8 is located near the origin, in the middle of the VLFS. It is interesting to note, in Figs. 9.14a and b, different surge responses for modules 1 and 8. This is due to the flexibility of the connectors used between neighboring modules. Due to the very small damping present at around $\omega = 0.3$ rad/s, the RMFC model, indicated in these figures by 'GFM', predicts very large responses. On the other hand, the EMFC model, which includes viscous form drag, exhibits smaller responses at this frequency. However, the overall agreement for surge, heave and pitch responses is acceptable. Note that the EMFC model, indicated by 'Morison' in these figures, consistently predicts large peaks around $\omega = 0.5$ rad/s and 0.8 rad/s. These frequencies, as well as $\omega = 0.3$ rad/s correspond to flexible-mode natural frequencies shown in Table 9.2.

Figs. 9.15a-i show the transfer functions for the case of quartering seas. The agreement for surge, heave and pitch is better than sway and roll transfer functions. The explanation for this discrepancy is related to the fact that in the RMFC model, where the Green function method is used, the hydrodynamic interaction between multiple modules is included. This interaction becomes more important in quartering seas than in head seas, as expected, since in quartering seas, the pontoon end-planes of two neighboring modules are exposed more to wave action and, therefore, wave-scattering interaction is very strong. Obviously, Morison's equation cannot incorporate such effects. Note that the fluid velocity between the columns and pontoons of two neighboring modules is much greater in magnitude than the fluid velocity in the middle of a pontoon, resulting in reduced fluid pressure in these areas. This, in turn, causes the overall forces to reduce and, thus, the response predicted by the Green function method becomes significantly smaller than Morison's equation results. The transfer functions of response for other

modules show similar trends and, therefore, they are not shown here. The transfer functions presented here can be easily used to predict the responses in irregular seas by using measured or analytic wave spectra.

9.3 Application of composite 2-D/3-D hydroelasticity

The composite 2-D/3-D hydroelasticity method has been applied to two structures. The first is a simple, idealized, very long and slender twin-hull structure as described in Section 8.2 and shown in Figs. 8.5 and 8.6. To obtain results for the composite 2-D/3-D method, the two-dimensional potential problem has been solved by the 'close-fit' method. Because of port-starboard (x-z plane) symmetry, only one-half of the structure was modeled. A total of 149 sections at 2 meter intervals were used, and the trapezoidal integration rule was used to evaluate the hydrodynamic coefficients and wave exciting forces in the longitudinal direction. The mean wetted-surface of the port hull of each section was discretized by 10 two-dimensional fluid panels. The discretization is schematically shown in Fig. 9.3.

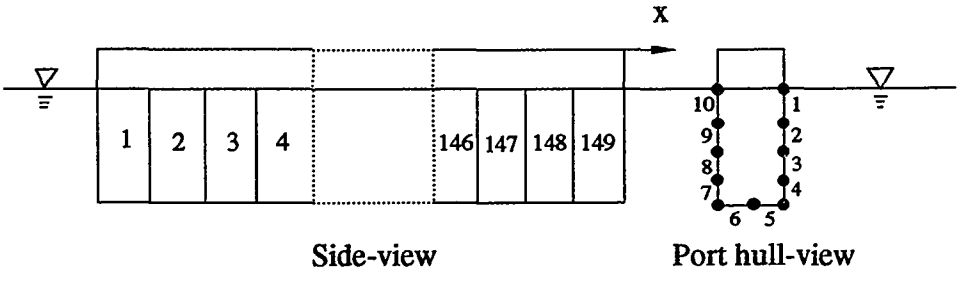

Figure 9.3 Schematic view of discretization of a twin-hull structure

For comparison, the response was also determined by three-dimensional hydroelasticity. A total of 1506 fluid panels, each 2m × 2m, except at the ends and the

bottom, were used in this case. Therefore, the two-dimensional fluid panels and the three-dimensional panels have the same size.

If only the first 6 modes are considered (q=6), then the results from the composite method are identical to those from traditional two-dimensional hydrodynamics based on a rigid structure. The resonant frequencies for rigid-body motion of a structure in water depend on the structural mass, added mass, and hydrostatic restoring coefficients. They are approximately 1.05 rad/sec, 0.38 rad/sec, and 1.04 rad/sec for heave, roll and pitch, respectively. Fig. 9.16 compares the rigid motions for three wave headings based on the composite method (2-D) and three-dimensional (3-D) potential theory. Zero responses for some wave headings have been removed from these figures (e.g., sway in head seas). The agreement is very good, with the primary differences in heave and pitch at resonant frequencies. These differences may result from the different hydrodynamic damping obtained from two-dimensional and three-dimensional flow problems. The maximum roll response occurs not at the resonant frequency, but at a wave frequency of approximately 0.87 rad/sec. This frequency corresponds to a wave length which is equal to four times the width of the structure. At the natural roll frequency, the wave length is too long to create significant roll motion. The maximum sway response occurs at the same frequency as does maximum roll. The correspondence between the 2-D and 3-D results indicate that the two-dimensional flow assumption of strip theory is likely to be acceptable for this structure.

Flexible cross-sectional motion is considered next, which cannot be treated by either traditional two-dimensional hydrodynamics or two-dimensional hydroelasticity. As mentioned in Section 8.2, if the structure is assumed fixed at the deck, there are only two dry modes, which involve symmetric and antisymmetric 'swinging' of the struts. The symmetric 'prying' mode, identical to the basic mode 6 in Fig. 7.2, is labeled mode 7,

while the antisymmetric 'torsional' mode is labeled mode 8. (Mode 8 involves antisymmetric rotation of the struts.) Both modes have a dry natural frequency of 0.6 rad/sec. For both of these flexible modes, the associated hydrostatic restoring stiffness is negligibly small and is ignored in the calculations. Note that the actual modes in this simple example can be represented exactly by the 'basic modes' in Fig. 7.2.

Figs. 9.17, 9.18, and 9.19 compare, for the fixed-deck case, the modal added mass, hydrodynamic damping and exciting forces determined by the composite 2-D/3-D approach and three-dimensional hydroelasticity. In these three figures, M_{fjj}^* and M_{sjj}^* are the jth modal added mass and the jth structural modal mass; C_{fjj}^* are the jth modal damping; F_{fjj}^* are the jth modal wave exciting forces; α is the wave amplitude. M_{fjj}^*/M_{sjj}^* is the ratio between the jth modal added mass and the jth structural modal mass, $C_{fjj}^*/2\varpi_j(M_{sjj}^* + M_{fjj}^*)$ (ϖ_j is the jth natural frequency) is the ratio between the jth modal hydrodynamic damping and the jth critical damping, and $F_{fjj}^*/\alpha\rho g\nabla$ is the ratio between the jth modal wave exciting force for unit wave amplitude and the structural weight. M_{fjj}^*/M_{sjj}^*, $C_{fjj}^*/2\varpi_j(M_{sjj}^* + M_{fjj}^*)$ and $F_{fjj}^*/\alpha\rho g\nabla$ are non-dimensional quantities. The agreement is quite good. It is interesting to note that for some wave frequencies, the modal hydrodynamic damping is greater than critical damping. In this case, the system is overdamped. For such systems, the free vibration response will not be oscillatory. The response in these modes, as measured by the relative rotation between the deck and strut, is shown in Fig. 9.20. Only beam sea results for wave exciting forces and relative rotation are plotted here since they are significant for these two modes. The distributed moment at the joint between deck and strut is simply the rotational stiffness, 36 kN-m/m (from Table 8.3), multiplied by the rotation in Fig. 9.20.

When the simple twin-hull structure, whose deck and struts are connected by hinges,

is freely floating, there are a total of eight displacement degrees-of-freedom. The responses of the freely floating structure in beam seas is shown in Figs. 9.21a-d. Figs. 9.21a-c show the horizontal and vertical displacements and 'roll' rotation of the center of gravity. The agreement between the results obtained by two-dimensional and three-dimensional fluid models is reasonably good, with the major differences occurring at the resonant frequencies. Fig. 9.21c shows that roll has the largest discrepancy between the two approaches. In particular, resonant response of mode 8 results in substantial deviation at high frequencies, which is due primarily to a shift in the 'wet' natural frequency of this mode. The deformational responses, that is, the relative rotation of the deck joint, are in substantially better agreement (Fig. 9.21d). The 'prying' forces, that is, the bending moment at the deck joint, is simply the product of the rotational stiffness (in Table 8.3) and the rotation in Fig. 9.21d.

It has already been mentioned that the motivation to use a two-dimensional fluid model is to reduce the computer time so that hydroelastic analysis of very large structures is more readily accomplished. For the hydrodynamic coefficient and wave exciting force calculations of this simple twin-hull structure, in which 6-rigid body modes and two flexible modes were used, the CPU computer time required by full 3-D hydroelasticity, on an IBM RS/6000/550, is 16 minutes and 24 seconds. The total time is 12 hours and 20 minutes, which consists primarily of disk I/O for intermediate files. The composite 2D/3D approach, however, took only 3.85 seconds CPU time, with a total time of 1 minute and 26 seconds. Hence, the composite method requires just a fraction of the time that three-dimensional hydroelasticity requires. As long as the accuracy is sufficient, it therefore represents a more useful tool for design, especially if small computers are used.

The previous structure was artificial, having been designed solely to test and validate

the composite method. For further validation, a more realistic SWATH ship, Fig. 8.7, has been designed and analyzed with the composite 2-D/3-D method and three-dimensional hydroelasticity. The rigid and flexible responses and internal forces are calculated by the composite method and 'full' three-dimensional hydroelasticity.

Again, because of symmetry, only half the structure was modeled to determine the hydrodynamic coefficients and wave exciting forces. The structure has been modeled entirely by shell elements, as shown in Fig. 8.8. For the three-dimensional hydroelastic analysis, a one-to-one correspondence was used between the quadrilateral shell elements below the mean water line and the fluid panels. A total of 372 fluid panels were used. The surface elements of the SWATH ship are shown in Fig. 9.4, in which the fluid panels are those surface elements below the still water plane. For the composite 2D/3D analysis, each vertical line in Fig. 9.4 was taken as a section, and structural nodes below the mean water line were taken as sectional nodes for the two-dimensional fluid model. Therefore, a total of 31 sections were used, and the trapezoidal rule was used for the integration in the longitudinal axis direction to evaluate the hydrodynamic coefficients and wave exciting forces.

First, the rigid body motions are compared. Figs. 9.22 and 9.23 show the comparison of added-mass coefficients and wave exciting forces, respectively, for rigid-body mode shapes between 2-D/3-D composite method and three-dimensional hydroelasticity. A comparison of the rigid-body motions are shown in Figs. 9.24. Again the results compare favorably with the primary differences resulting from resonance.

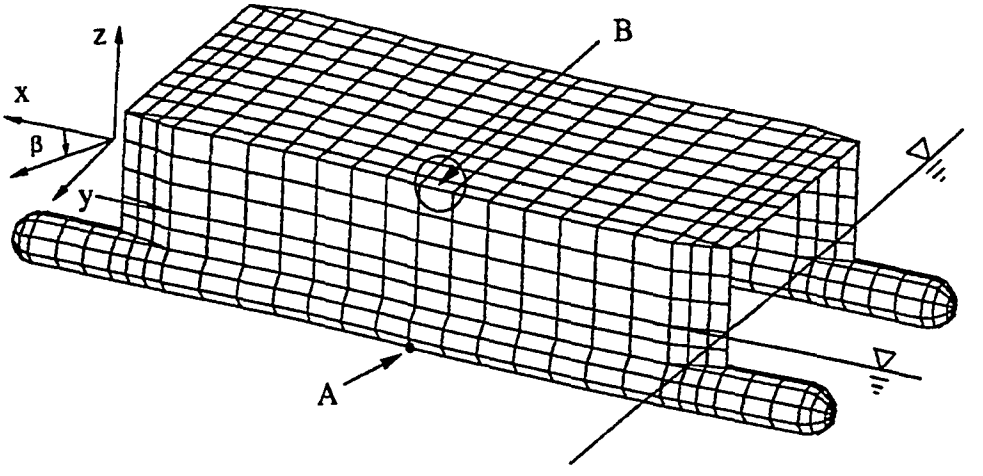

Figure 9.4 Surface elements of the SWATH ship

Figs. 9.25 and 9.26 show the comparison of added-mass coefficients and wave exciting forces between three-dimensional hydroelasticity and 2D/3D composite method for flexible mode shapes. In these two figures, M_{fjj}^*, M_{sjj}^*, and F_{fjj}^*, j=7,8,...,14, have the same definition as before. The comparisons for some mode shapes are not very good, although they demonstrate the same tendencies. The reasons for these differences are not clear at this stage and need to be studied.

To compare the predicted deformational responses obtained by the two methods, the 'deformational' motion (excluding rigid-body motion) at point 'A' (Fig. 9.4) and the moment at the strut-deck interface at point 'B' have been determined. Figs. 9.27a-b show the horizontal u_y and vertical u_z displacements. Since point A is taken at midship, the response for head seas is expected to be small from the symmetry. From the figures, it can be seen that the results from the composite method compare favorably with those

from three-dimensional hydroelasticity.

Fig. 9.28 shows the internal forces at the point B. N_x and N_y represent the deck 'membrane' forces per unit length in the x-direction and y-direction, respectively, and M_x and M_y represent the bending moment per unit length about the x-axis and y-axis, respectively. The forces are calculated at the edge of the deck where it is connected to the strut, so that they can be used to design the connection. It can be seen that the comparison of the internal forces between the composite method and three-dimensional hydroelasticity is good.

The simplified composite method which uses basic modes to represent the actual modes has also been applied to the same SWATH model. Fig. 9.29 represents the ratios of the lengths and angles between the actual four symmetric flexible modes and approximations obtained with the basic modes (Eqs. 7.42 and 7.43). From Fig. 9.29, the ratios of the 'length' and the angles between those two modes at most cross-sections are close to 1 and 0, respectively. These indicate that the real modes for the SWATH ship can be well represented by the basic modes. Fig. 9.30 shows the horizontal flexible displacement u_y at point A, and Fig. 9.31 shows the comparison of bending moment M_x, at the element B, between the composite method and the simplified composite method, for beam seas. These results indicate that, at least for this structure, the basic modes can be used to estimate the flexible response.

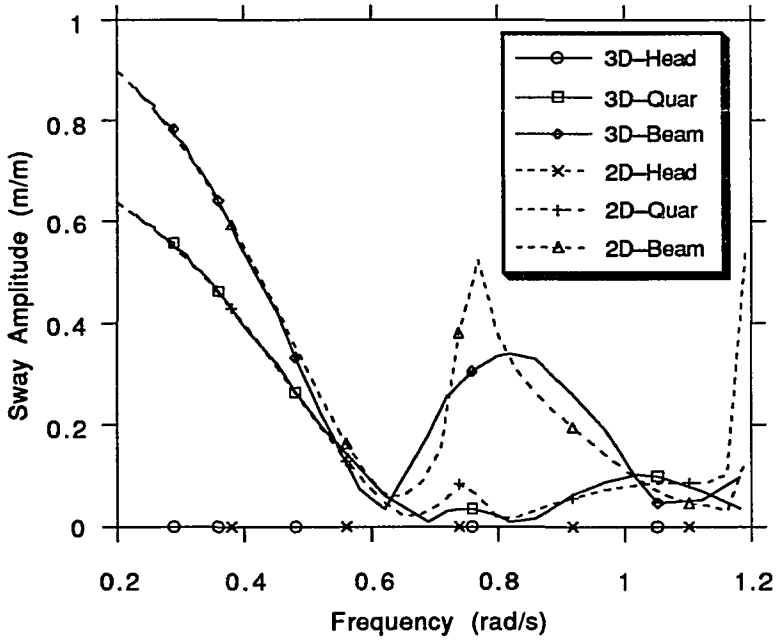
Sway Amplitude (m/m)
Frequency (rad/s)
3D–Head
3D–Quar
3D–Beam
2D–Head
2D–Quar
2D–Beam

(9.5a)

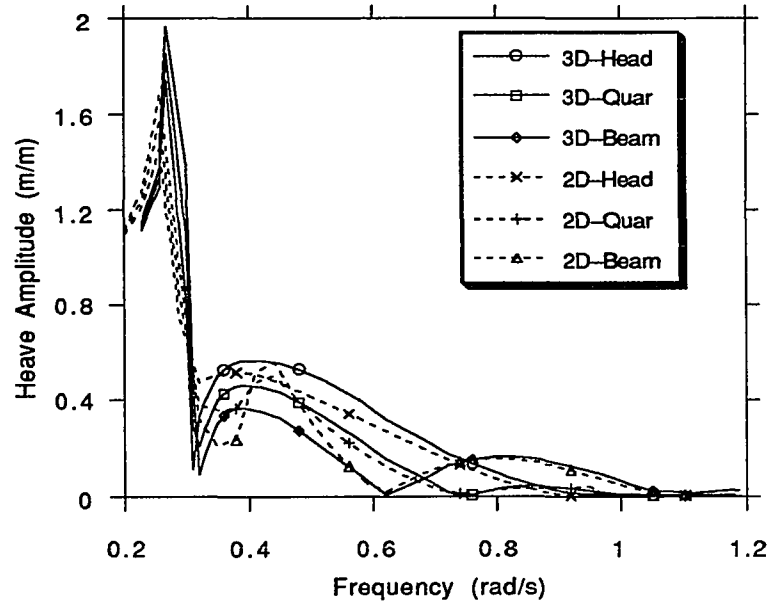
Heave Amplitude (m/m)
Frequency (rad/s)
3D–Head
3D–Quar
3D–Beam
2D–Head
2D–Quar
2D–Beam

(9.5b)

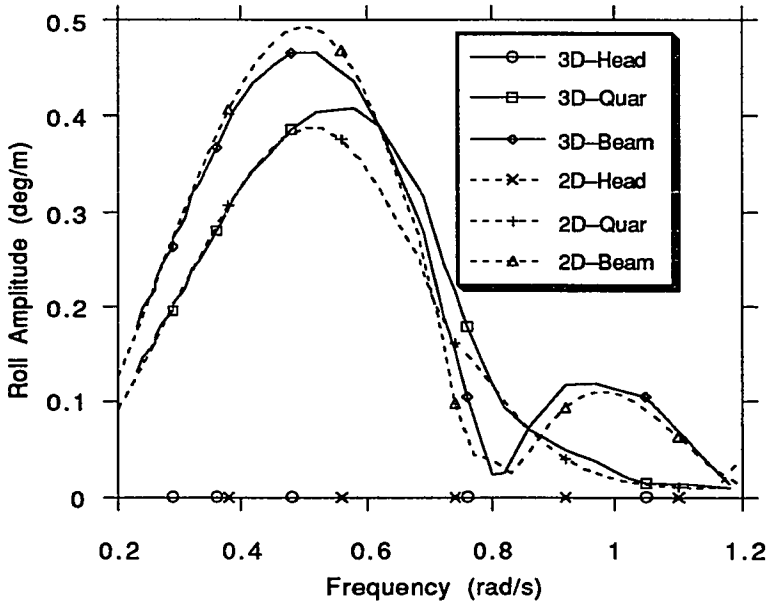

(9.5c)

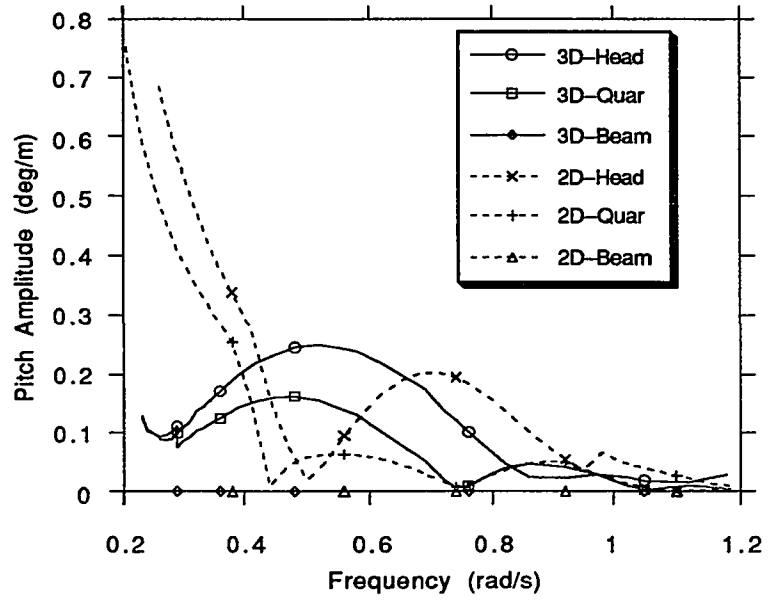

(9.5d)

Figure 9.5 Comparison of single module motions based on 2-D and 3-D hydroelasticity, (a) sway, (b) heave, (c) roll, (d) pitch

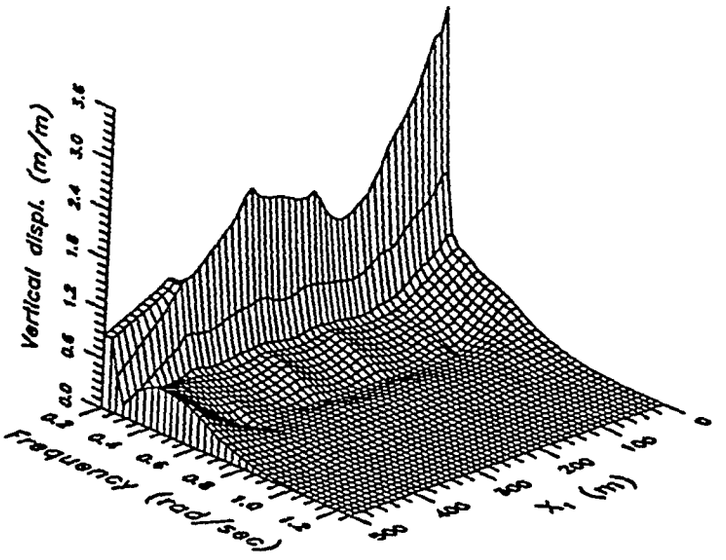

Head Sea

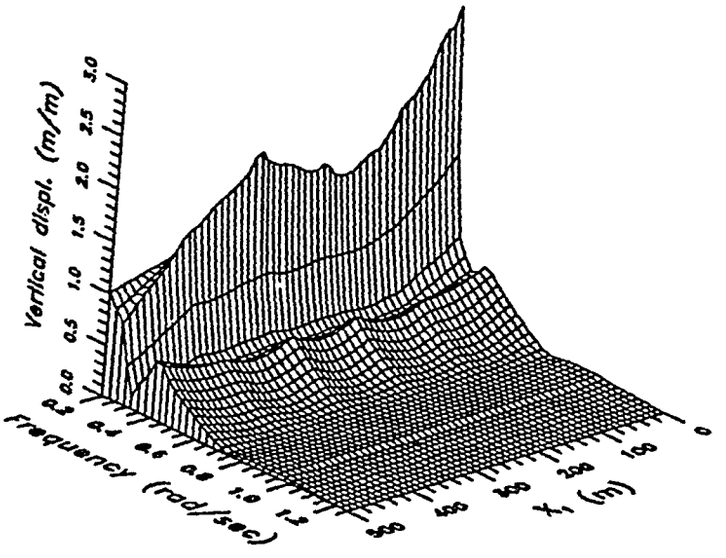

Quartering Sea

(9.6a) Hinge model

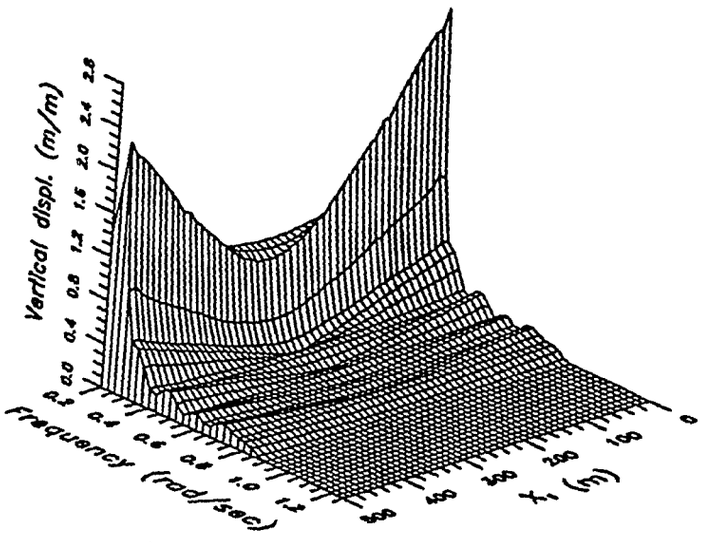

Head Sea

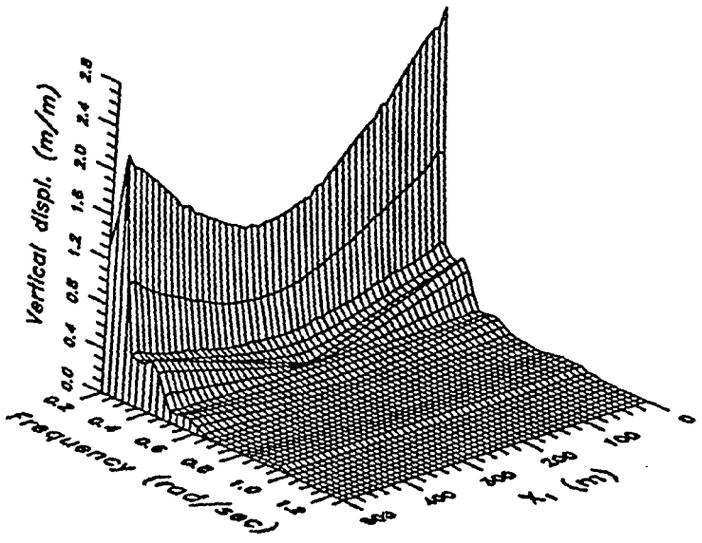

Quartering Sea

(9.6b) Rigid model

Figure 9.6 Absolute value of the vertical displacement as a function of potion and wave frequency

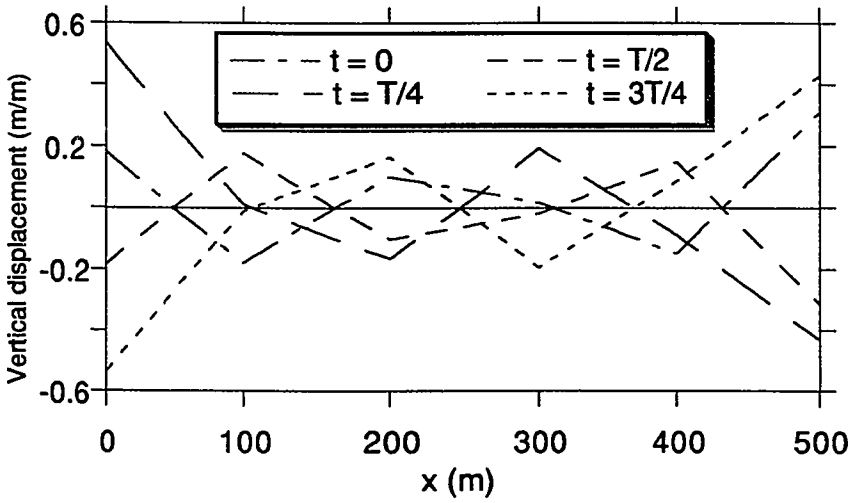

Figure 9.7 Vertical motion of hinge model during one wave cycle (ω = 0.5 rad/s, T=12.6 s)

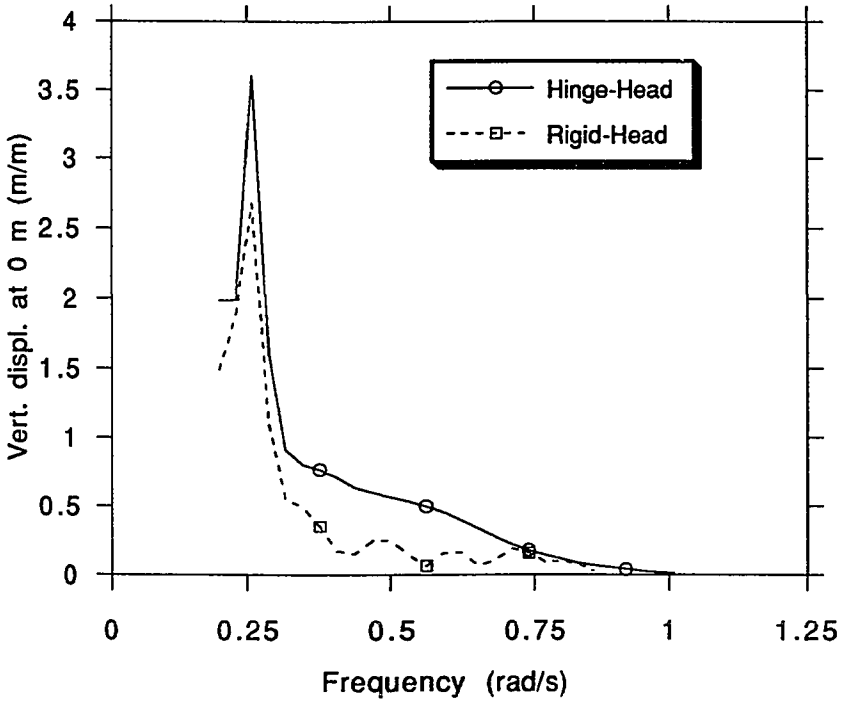

(9.8a) Head Sea

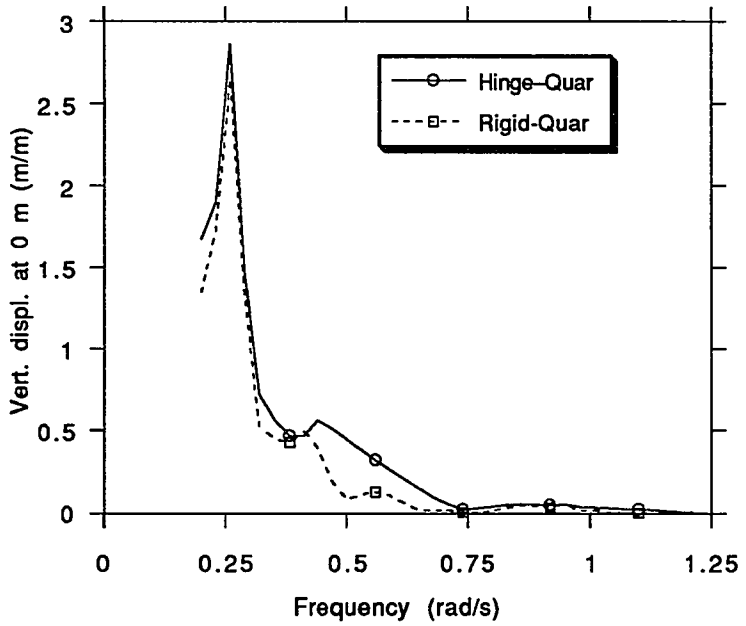

(9.8b) Quartering Sea

Figure 9.8 Absolute value of the vertical displacement at x=0 m for head and quartering seas

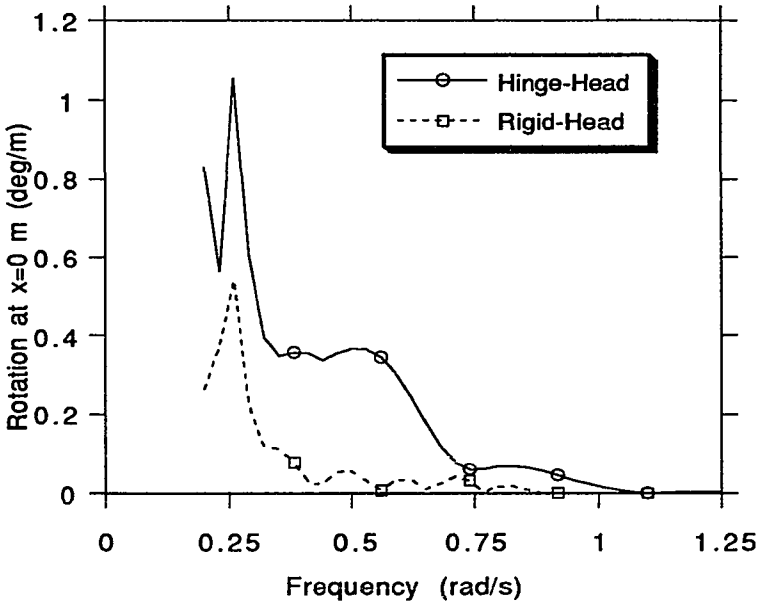

(9.9a) Head Sea

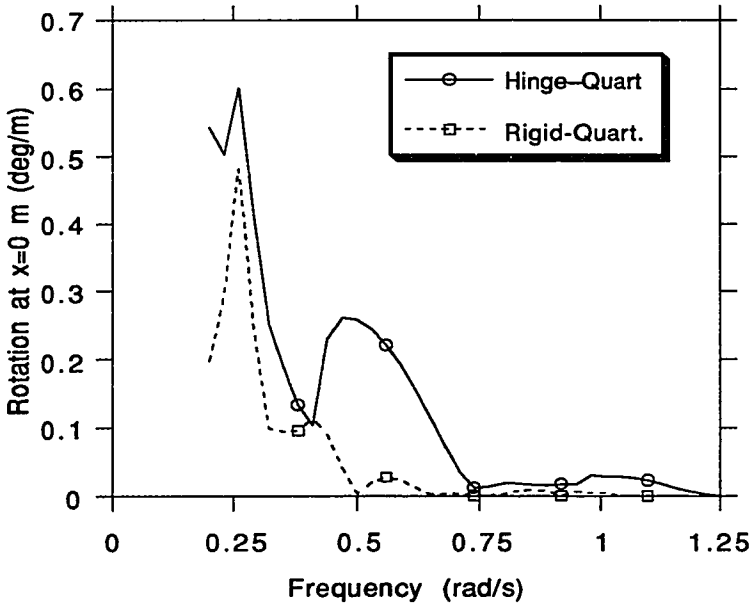

(9.9b) Quartering Sea

Figure 9.9 Absolute value of the rotation about y-axis at x=0 m

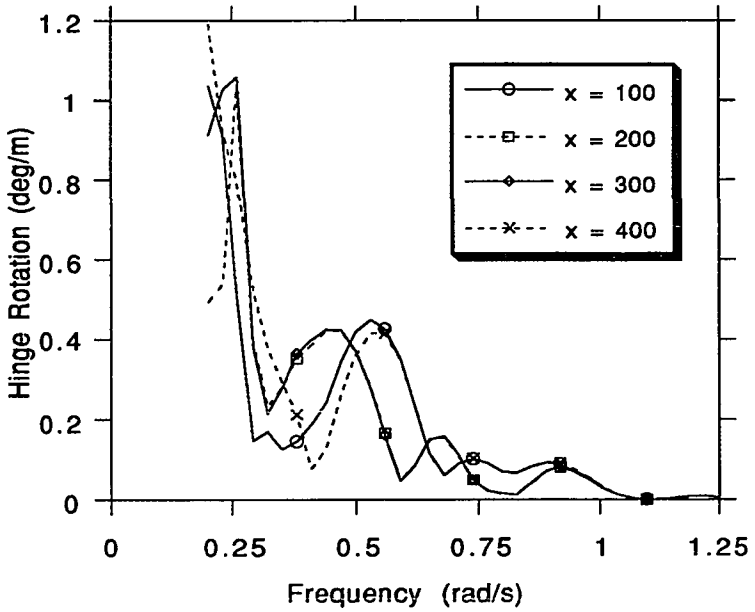

Figure 9.10 Absolute value of hinge rotation about the y-axis for head sea

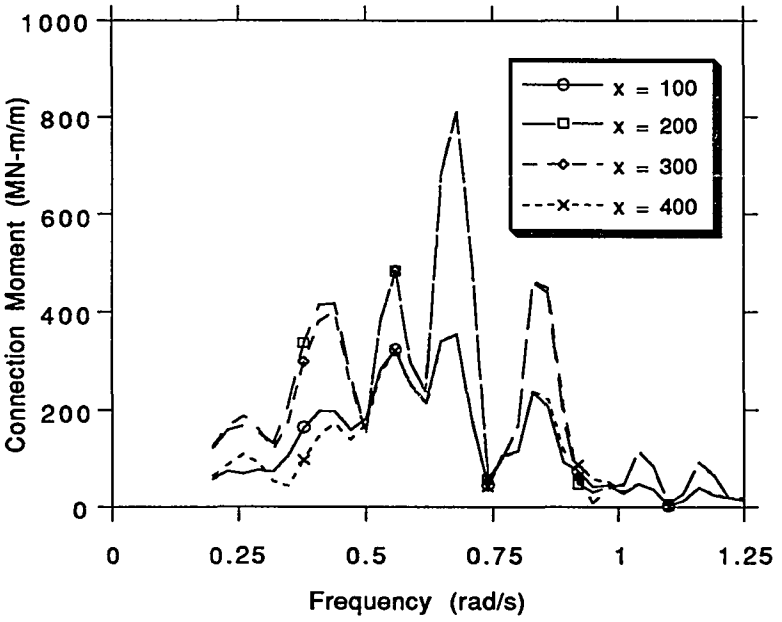

(9.11a) Moment (head sea)

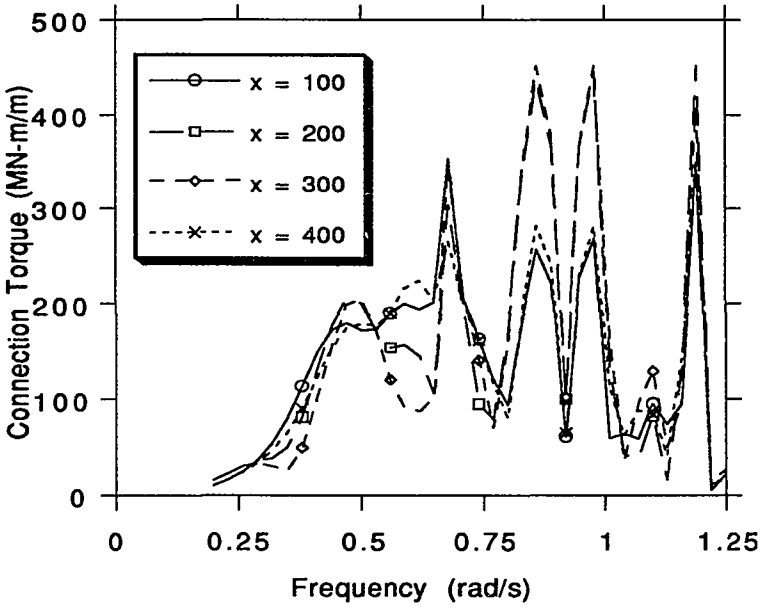

(9.11b) Torque (quartering sea)

Figure 9.11 Absolute value of the connection moment (head sea) and torque (quartering sea)

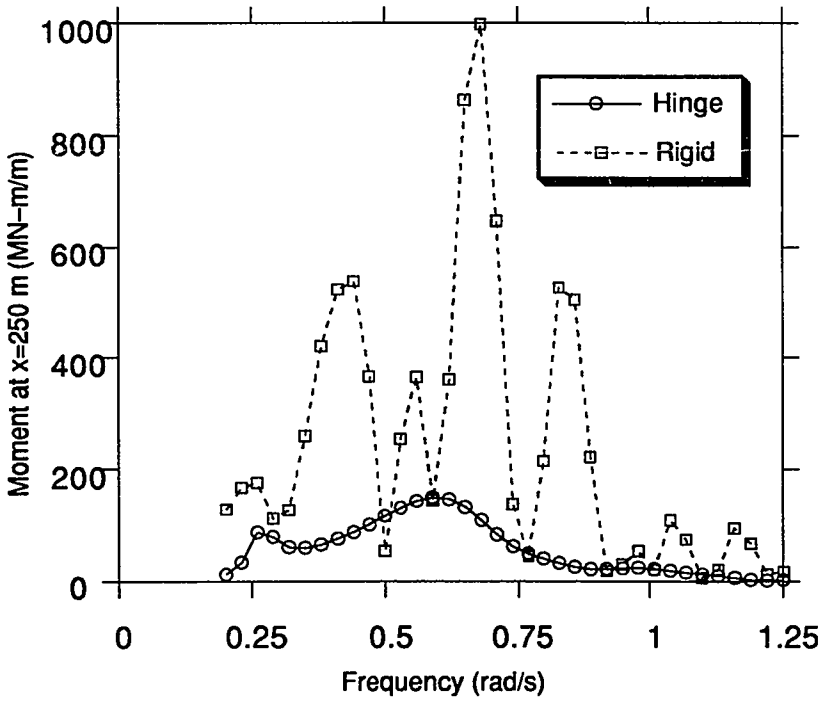

Figure 9.12 Absolute value of the moment about the y-axis at x= 250 m for head sea

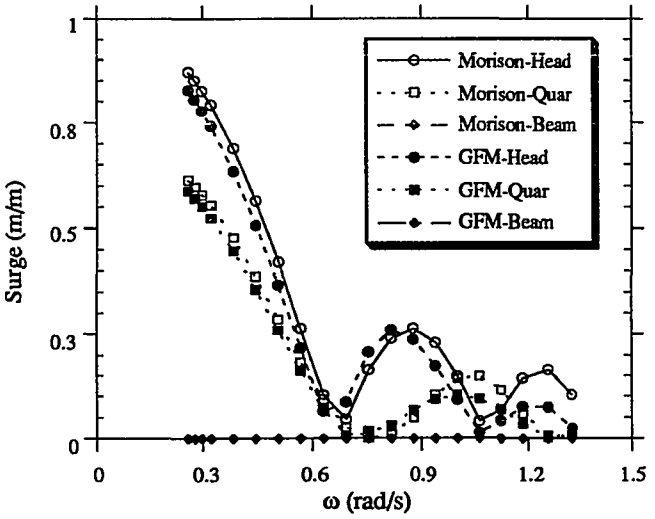
Morison-Head
Morison-Quar
Morison-Beam
GFM-Head
GFM-Quar
GFM-Beam
Surge (m/m)
ω (rad/s)
0
0.3
0.5
0.8
1
0.6
0.9
1.2
1.5

(9.13a)

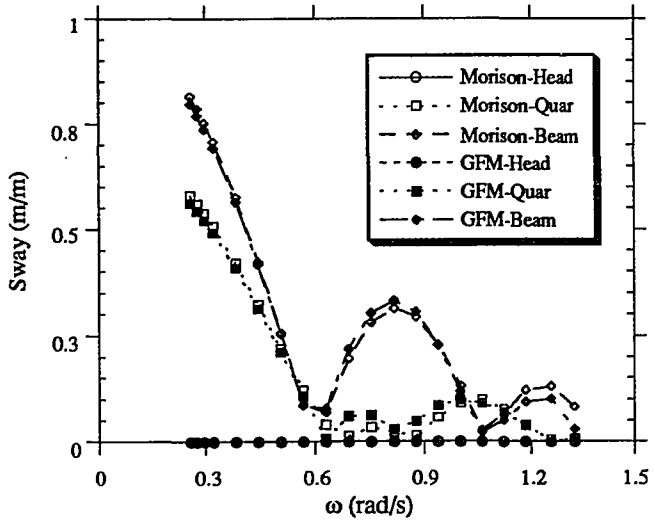
Morison-Head
Morison-Quar
Morison-Beam
GFM-Head
GFM-Quar
GFM-Beam
Sway (m/m)
ω (rad/s)
0
0.3
0.5
0.8
1
0.6
0.9
1.2
1.5

(9.13b)

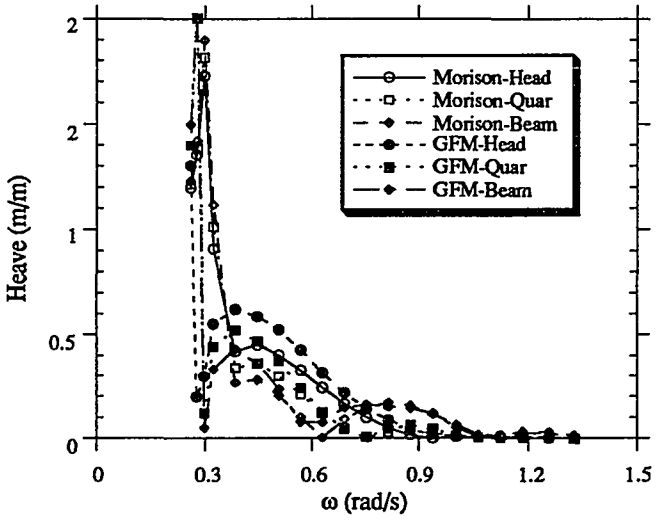
Heave (m/m)
ω (rad/s)
Morison-Head
Morison-Quar
Morison-Beam
GFM-Head
GFM-Quar
GFM-Beam

(9.13c)

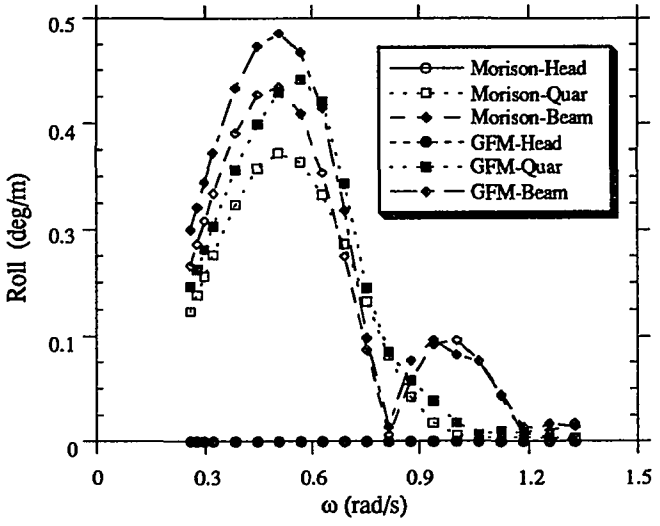
Roll (deg/m)
ω (rad/s)
Morison-Head
Morison-Quar
Morison-Beam
GFM-Head
GFM-Quar
GFM-Beam

(9.13d)

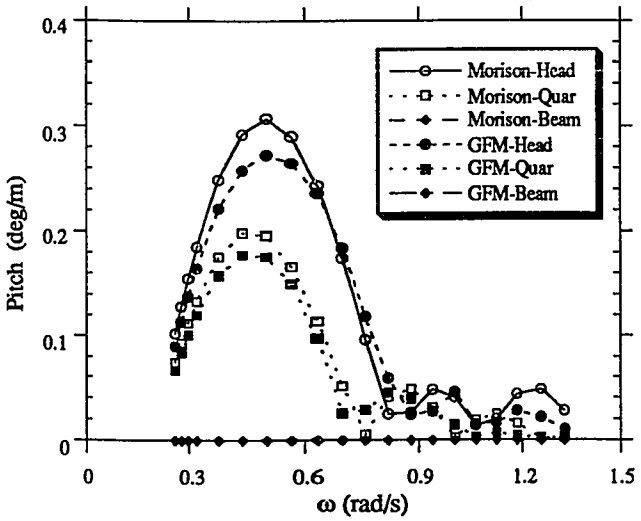

(9.13e)

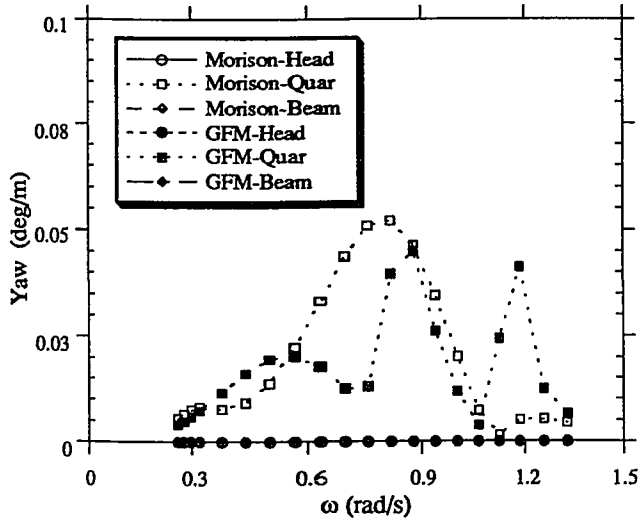

(9.13f)

Figure 9.13 Comparison of the motion transfer functions of a single module obtained by the Green Function and Morison's equation method for head, quartering and beam seas

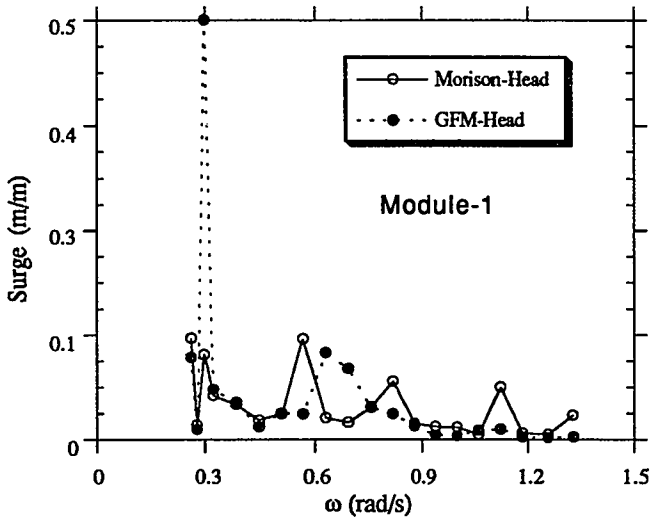
Morison-Head
GFM-Head
Module-1
Surge (m/m)
ω (rad/s)
0.5
0.4
0.3
0.1
0
0.3
0.6
0.9
1.2
1.5

(9.14a)

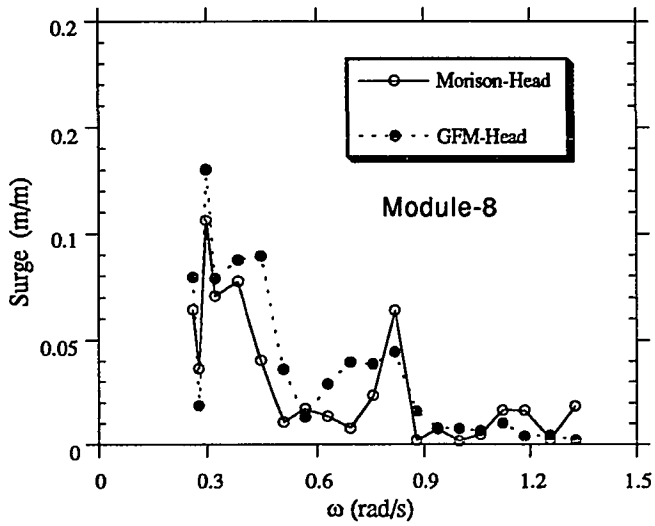
Morison-Head
GFM-Head
Module-8
Surge (m/m)
ω (rad/s)
0.2
0.2
0.1
0.05
0
0.3
0.6
0.9
1.2
1.5

(9.14b)

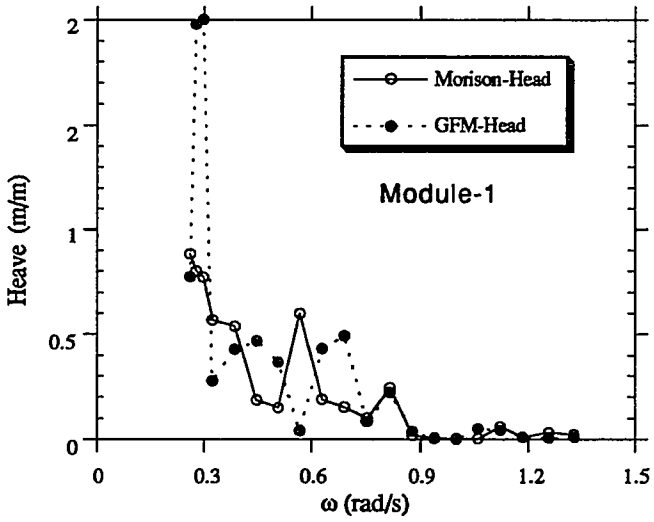
Morison-Head
GFM-Head
Module-1
Heave (m/m)
ω (rad/s)
0
0.5
1
2
0.3
0.6
0.9
1.2
1.5

(9.14c)

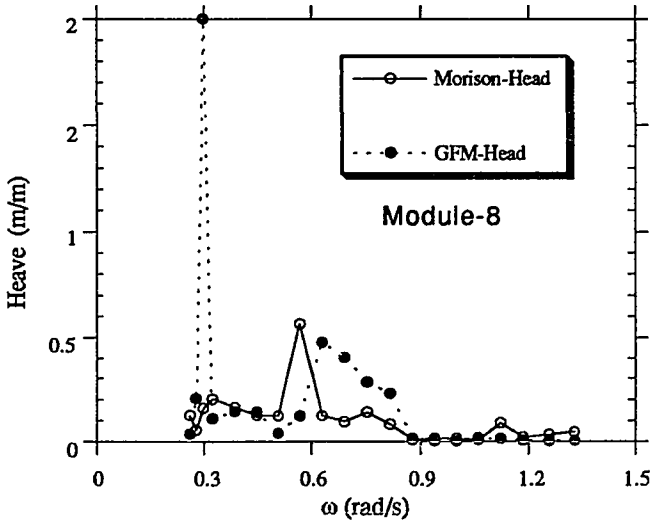
Morison-Head
GFM-Head
Module-8
Heave (m/m)
ω (rad/s)
0
0.5
1
2
0.3
0.6
0.9
1.2
1.5

(9.14d)

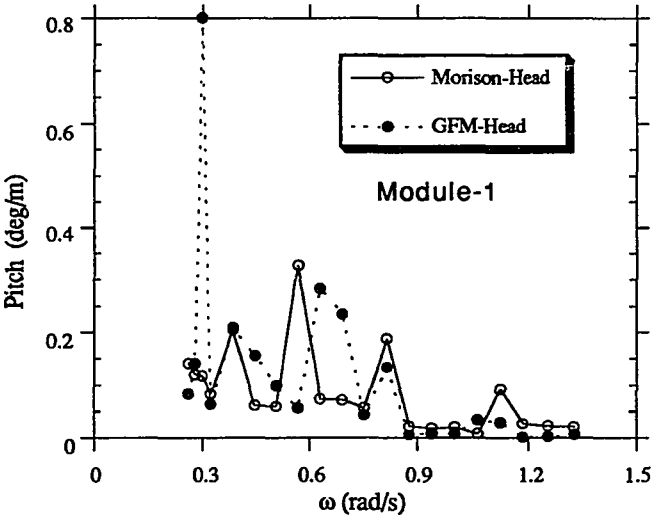

(9.14e)

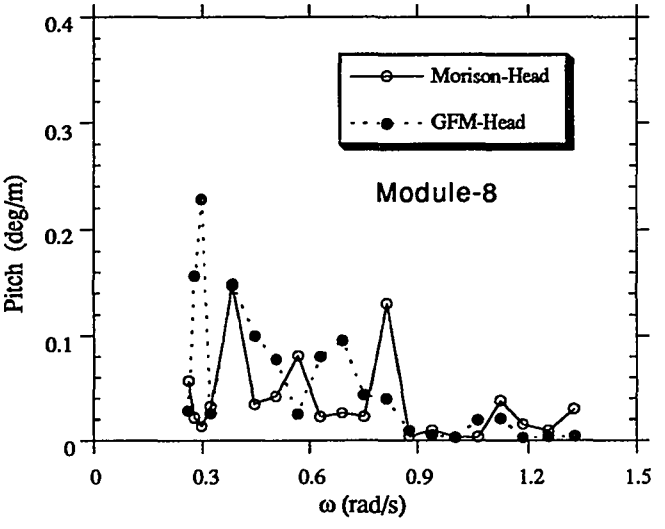

(9.14f)

Figure 9.14 Comparison of the motion transfer function of module 1 and 8 obtained by the Green Function and Morison's equation method for head seas

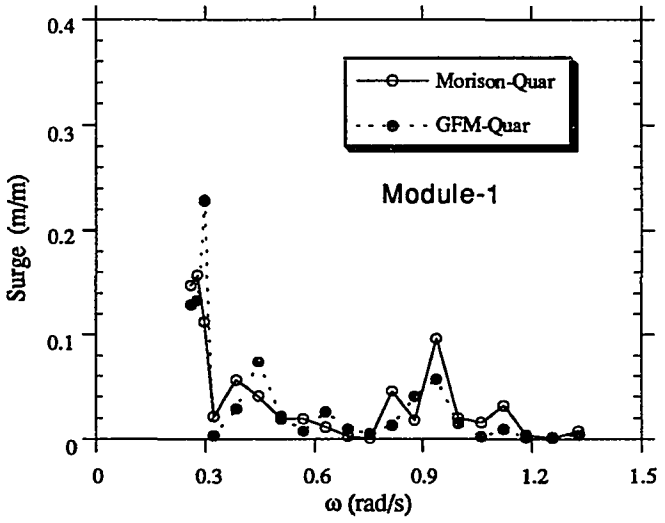
Morison-Quar
GFM-Quar
Module-1
Surge (m/m)
ω (rad/s)
0.4
0.3
0.2
0.1
0
0
0.3
0.6
0.9
1.2
1.5

(9.15a)

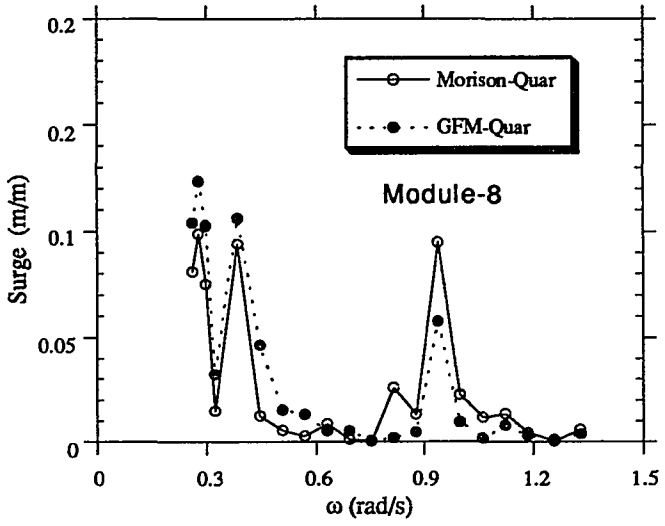
Morison-Quar
GFM-Quar
Module-8
Surge (m/m)
ω (rad/s)
0.2
0.2
0.1
0.05
0
0
0.3
0.6
0.9
1.2
1.5

(9.15b)

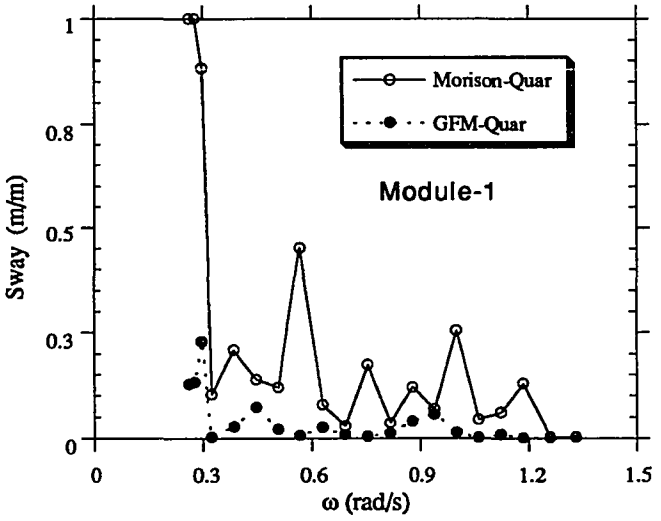
Morison-Quar
GFM-Quar
Module-1
Sway (m/m)
ω (rad/s)
0
0.3
0.6
0.9
1.2
1.5
0.8
0.5

(9.15c)

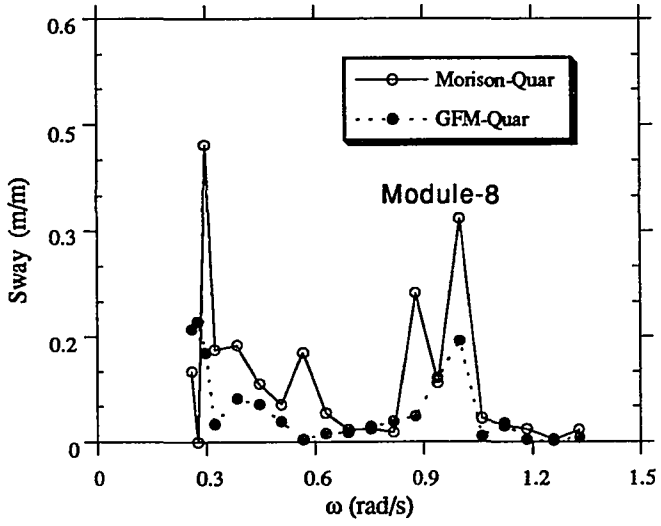
Morison-Quar
GFM-Quar
Module-8
Sway (m/m)
ω (rad/s)
0
0.2
0.3
0.5
0.6
0.9
1.2
1.5

(9.15d)

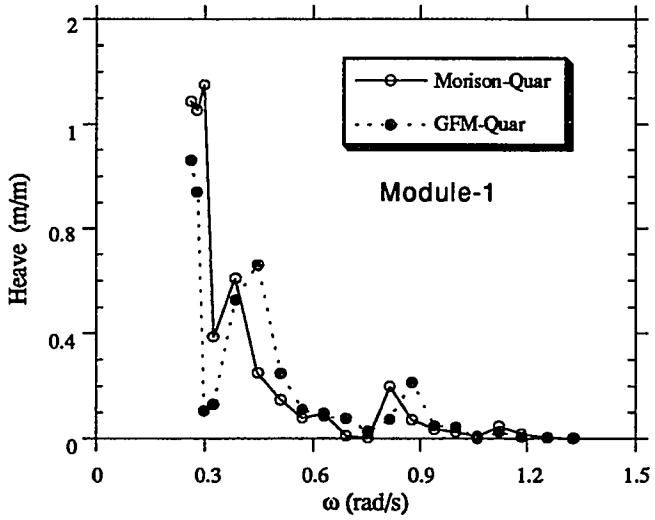
Morison-Quar
GFM-Quar
Module-1
Heave (m/m)
ω (rad/s)
0
0.4
0.8
1
2
0.3
0.6
0.9
1.2
1.5

(9.15e)

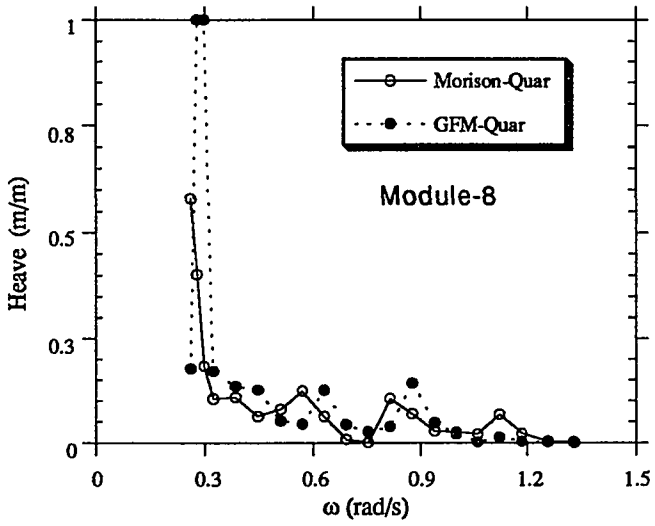
Morison-Quar
GFM-Quar
Module-8
Heave (m/m)
ω (rad/s)
0
0.3
0.5
0.8
1
0.3
0.6
0.9
1.2
1.5

(9.15f)

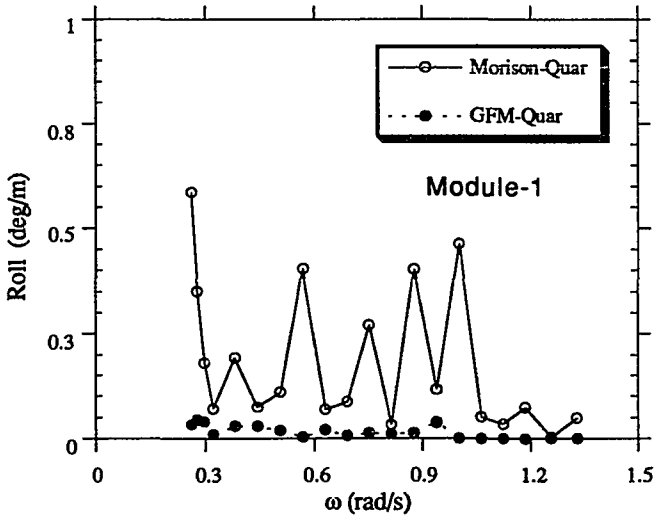
Morison-Quar
GFM-Quar
Module-1
Roll (deg/m)
ω (rad/s)
0
0.3
0.6
0.9
1.2
1.5
0.5
0.8
1

(9.15g)

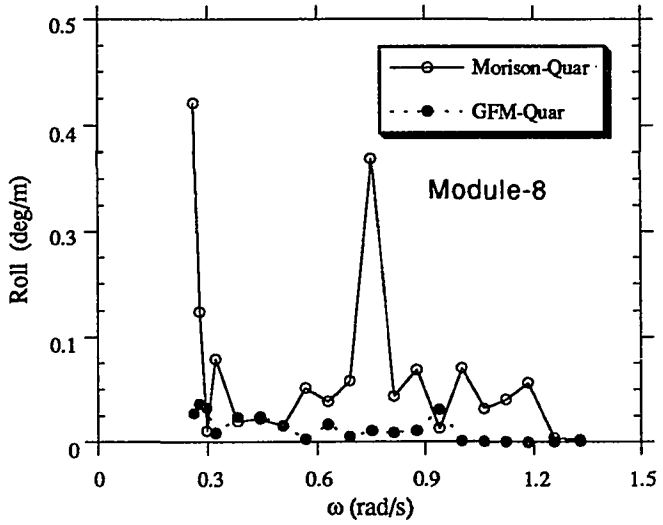
Morison-Quar
GFM-Quar
Module-8
Roll (deg/m)
ω (rad/s)
0
0.3
0.6
0.9
1.2
1.5
0.1
0.4
0.5

(9.15h)

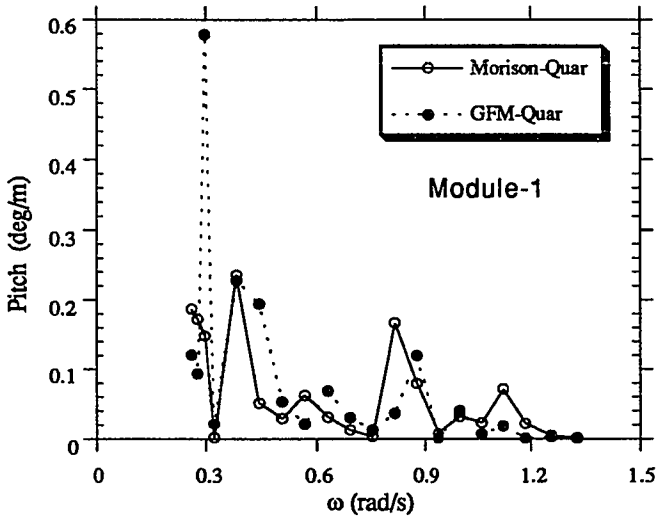

(9.15i)

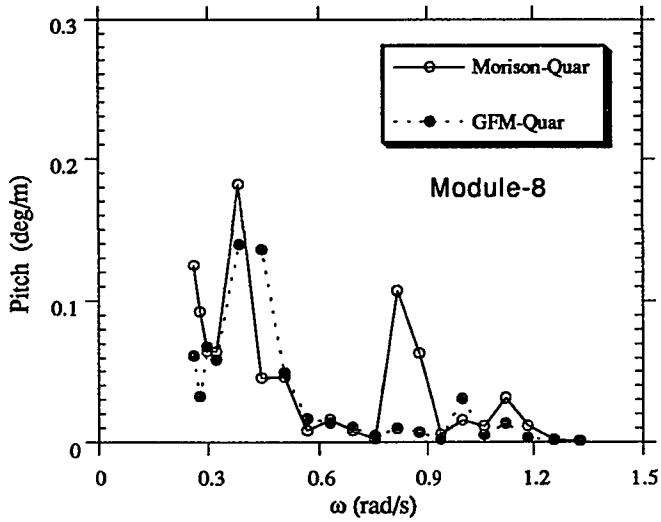

(9.15j)

Figure 9.15 Comparison of the motion transfer function of module 1 and 8 obtained by the Green Function and Morison's equation method for quartering seas

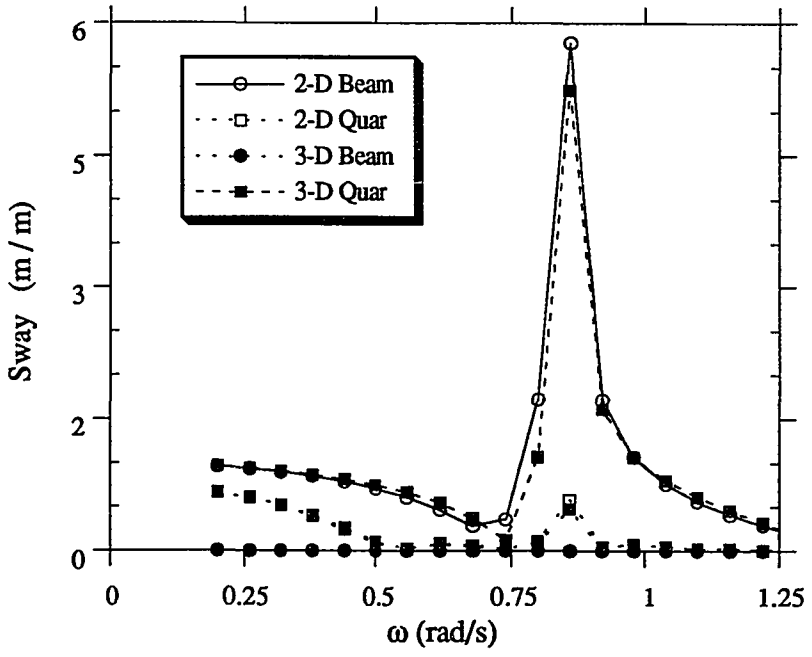
2-D Beam
2-D Quar
3-D Beam
3-D Quar
Sway (m / m)
ω (rad/s)
0
2
3
5
6
0.25
0.5
0.75
1
1.25

(9.16a)

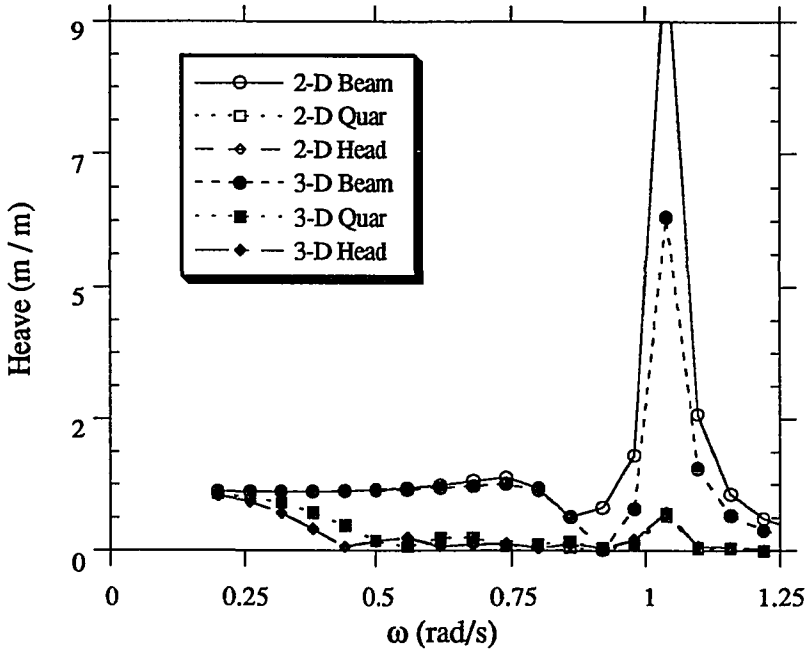
2-D Beam
2-D Quar
2-D Head
3-D Beam
3-D Quar
3-D Head
Heave (m / m)
ω (rad/s)
0
2
5
7
9
0.25
0.5
0.75
1
1.25

(9.16b)

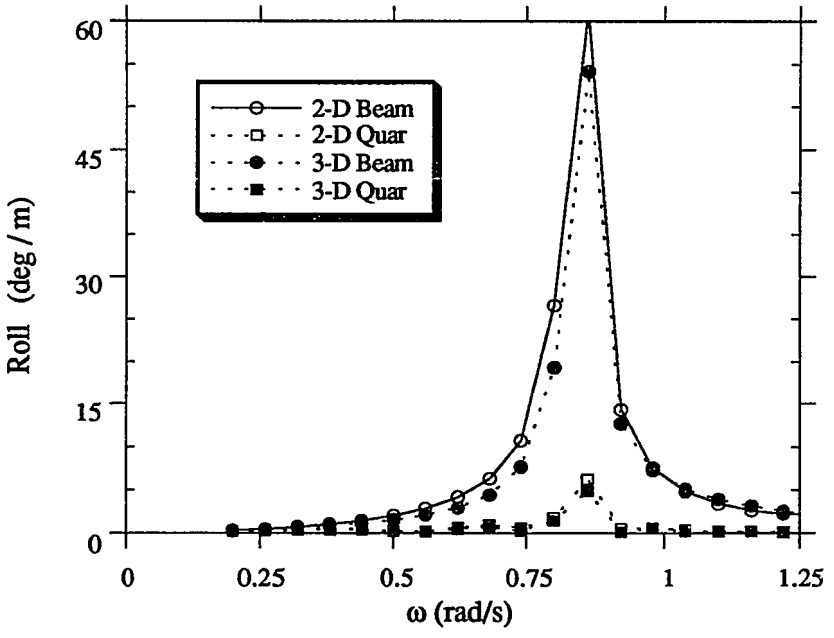

(9.16c)

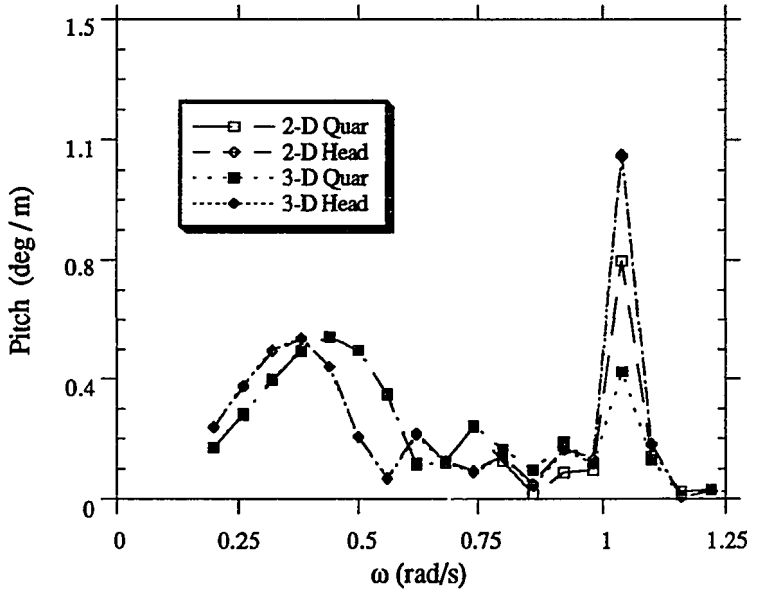

(9.16d)

Figure 9.16 Rigid body motions based on 2-D (present results) and 3-D potential theory (a) sway, (b) heave, (c) roll, and (d) pitch

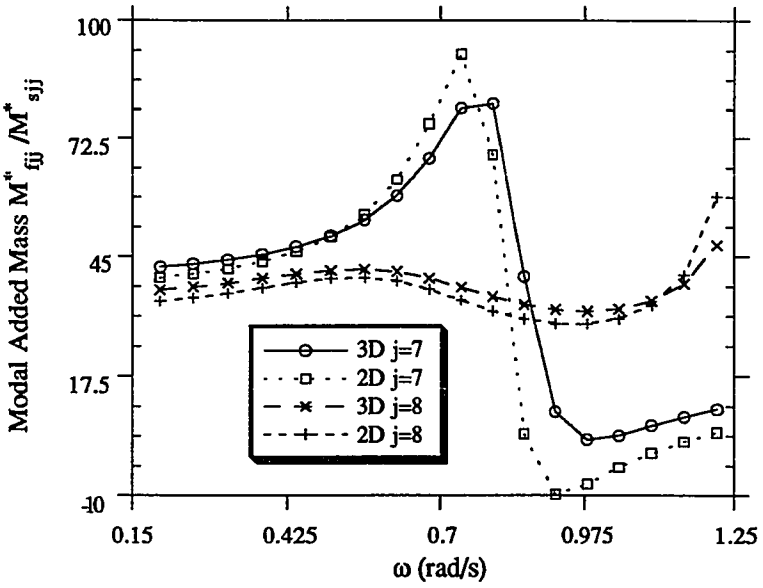

Figure 9.17 Modal added mass (j=7 and 8) based on composite 2D/3D method and 3-D hydroelasticity

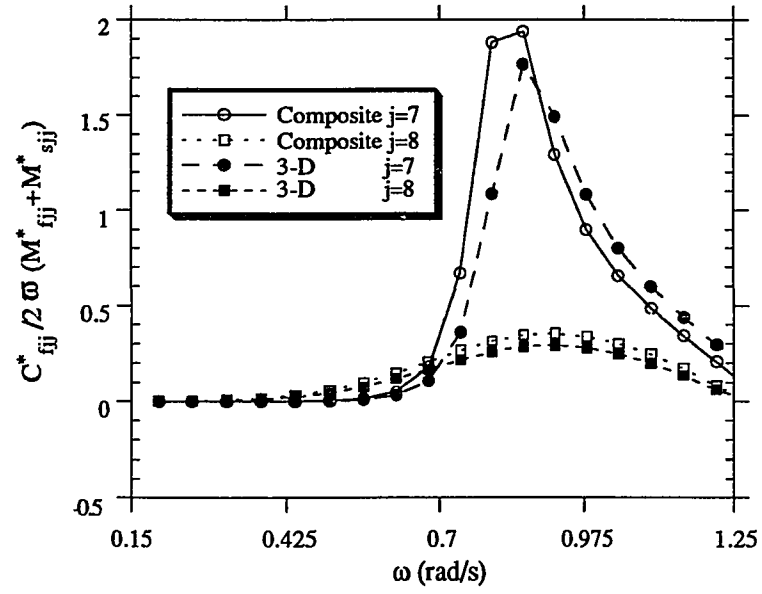

Figure 9.18 Modal hydrodynamic damping (j=7 and 8) based on composite 2D/3D method and 3-D hydroelasticity

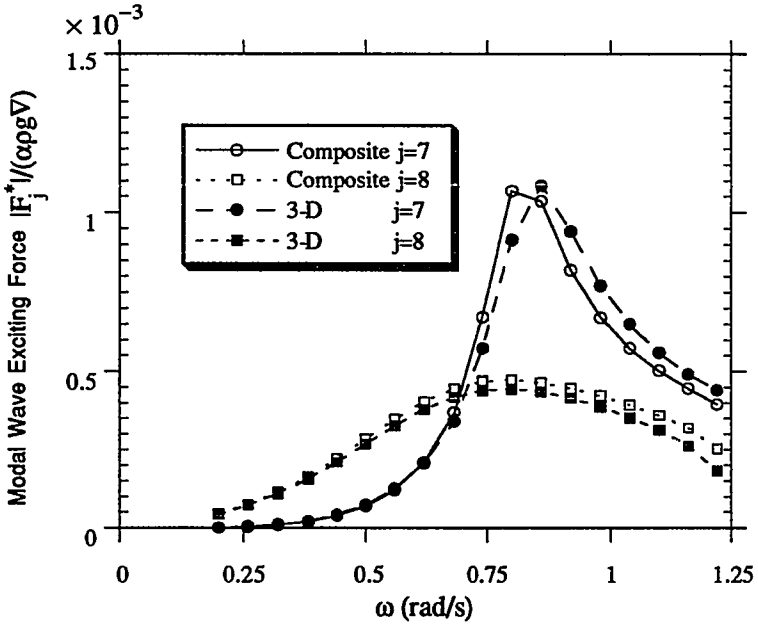

Figure 9.19 Modal exciting forces (j=7 and 8) based on composite 2D/3D method and 3-D hydroelasticity

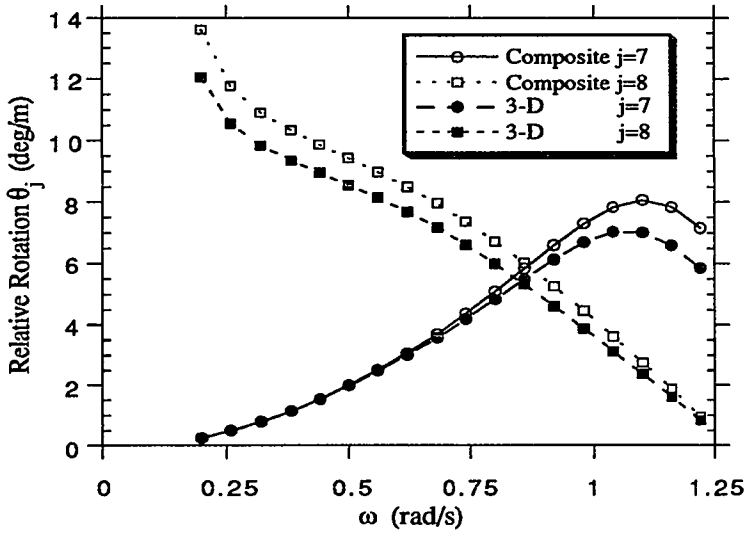

Figure 9.20 Amplitude of the relative rotation between deck and strut for modes 7 and 8 based on composite 2D/3D method and 3-D hydroelasticity

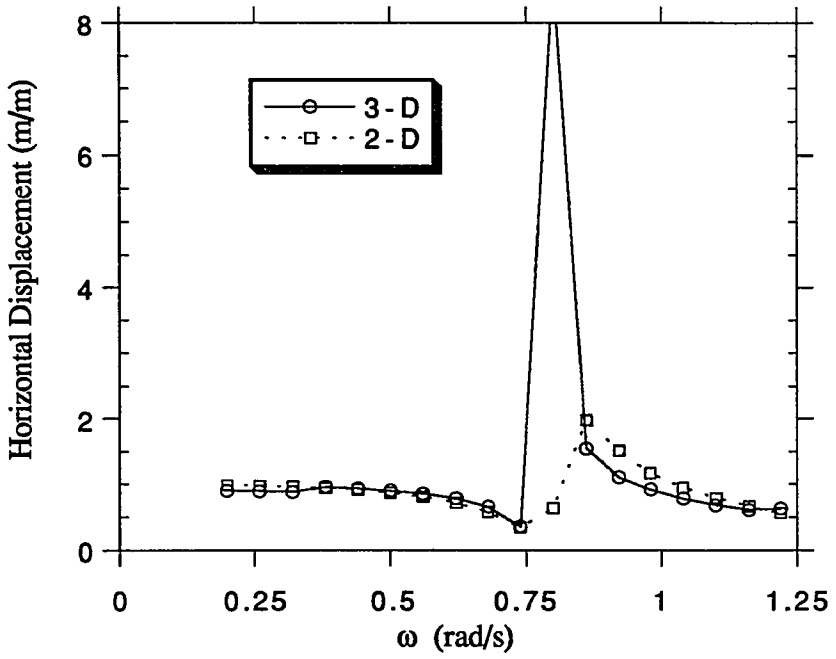
Horizontal Displacement (m/m)
8
6
4
2
0
3 - D
2 - D
0
0.25
0.5
0.75
1
1.25
ω (rad/s)

(9.21a)

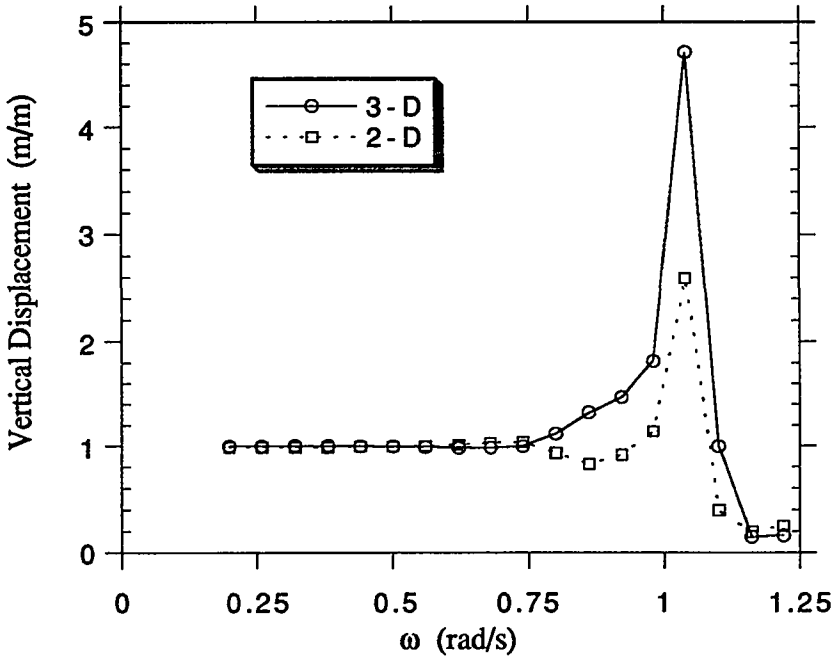
Vertical Displacement (m/m)
5
4
3
2
1
0
3 - D
2 - D
0
0.25
0.5
0.75
1
1.25
ω (rad/s)

(9.21b)

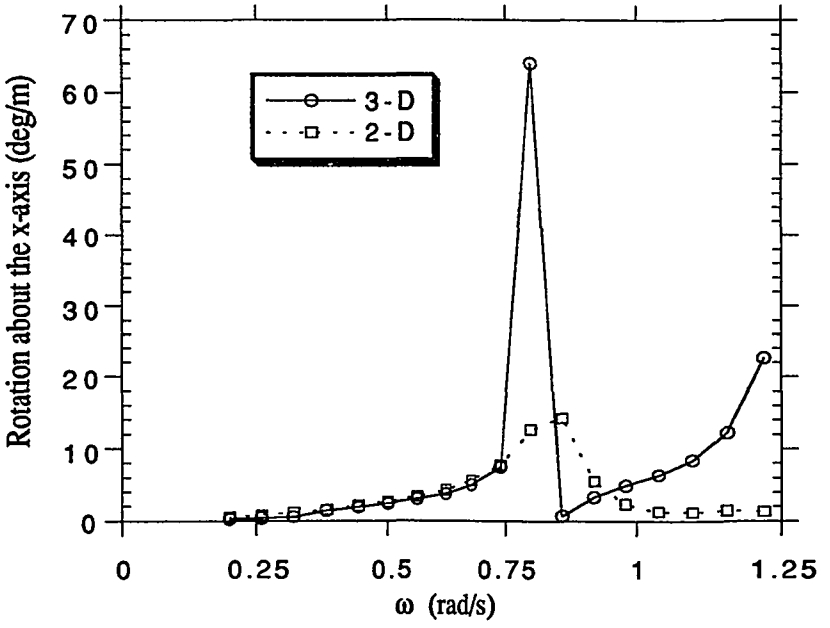

(9.21c)

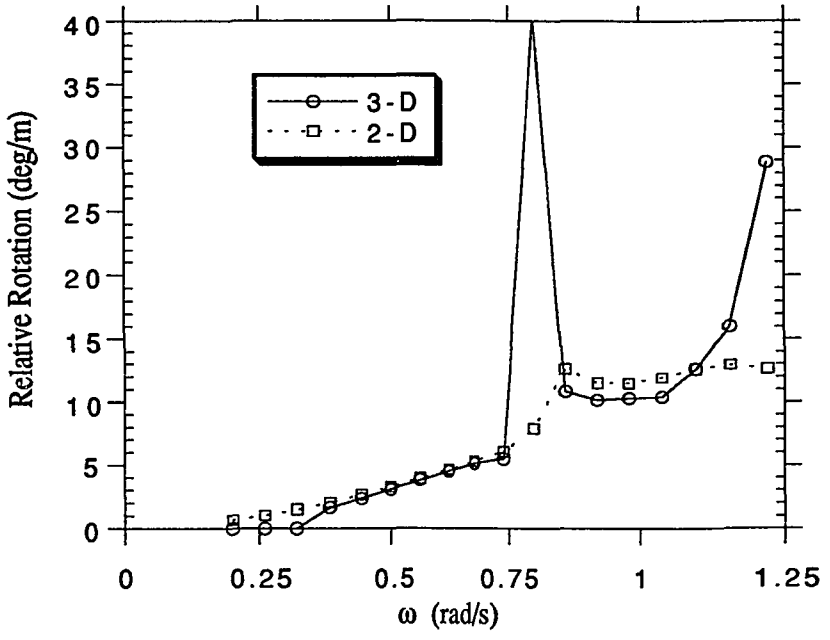

(9.21d)

Figure 9.21 Response of the freely floating structure computed with 2-D and 3-D fluid models (a) Horizontal displacement, (b) Vertical displacement, (c) Rotation about the x-axis, and (d) Relative rotation between the deck and strut

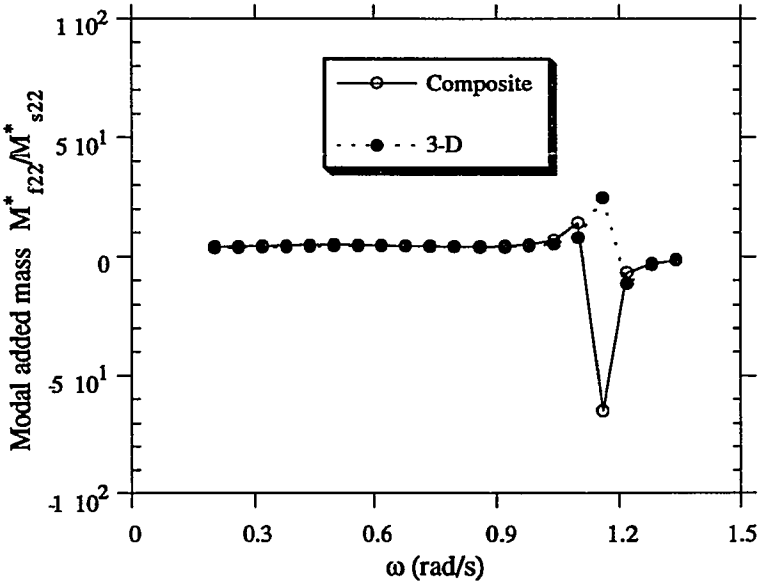
Composite
3-D
Modal added mass M^*_{f22}/M^*_{s22}
1 10^2
5 10^1
0
-5 10^1
-1 10^2
0
0.3
0.6
0.9
1.2
1.5
ω (rad/s)

(9.22a)

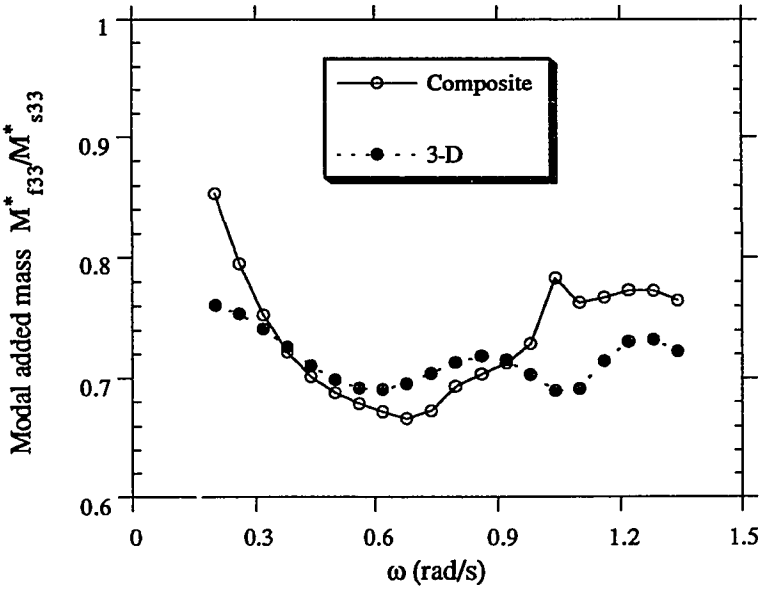
Composite
3-D
Modal added mass M^*_{f33}/M^*_{s33}
1
0.9
0.8
0.7
0.6
0
0.3
0.6
0.9
1.2
1.5
ω (rad/s)

(9.22b)

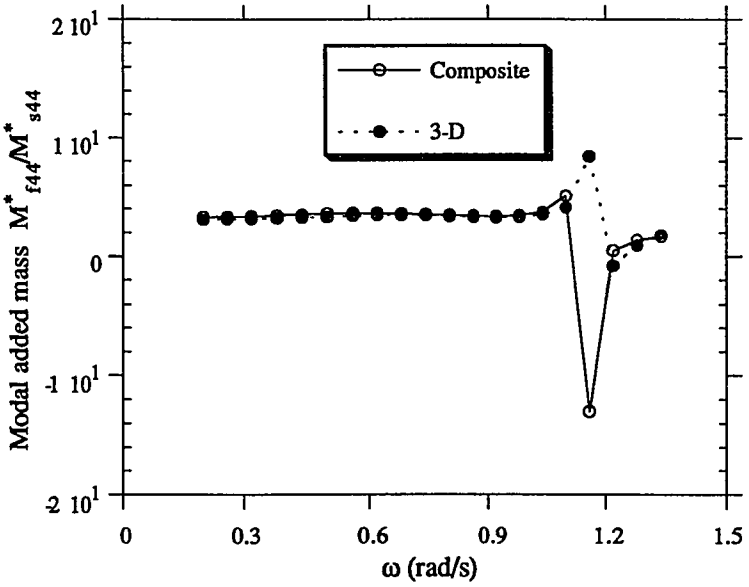

(9.22c)

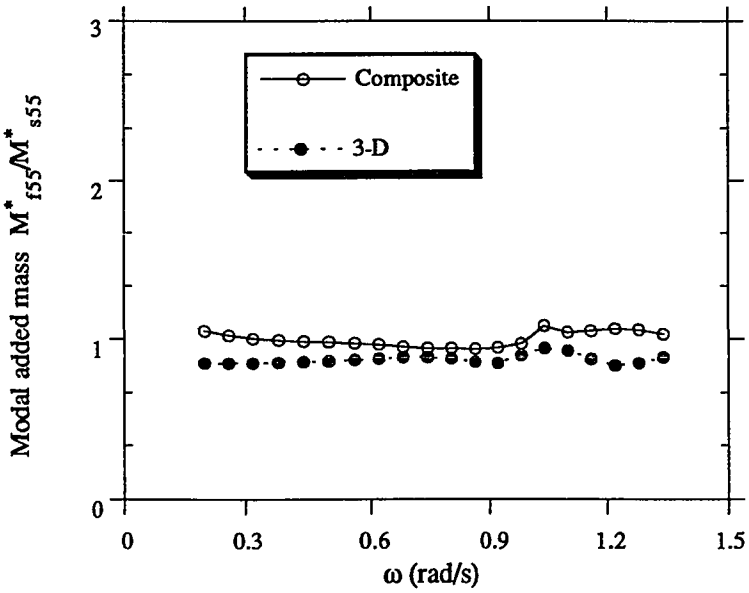

(9.22d)

Figure 9.22 Modal added mass for rigid body motion of SWATH ship based on composite 2-D/3-D method and 3-D hydroelasticity

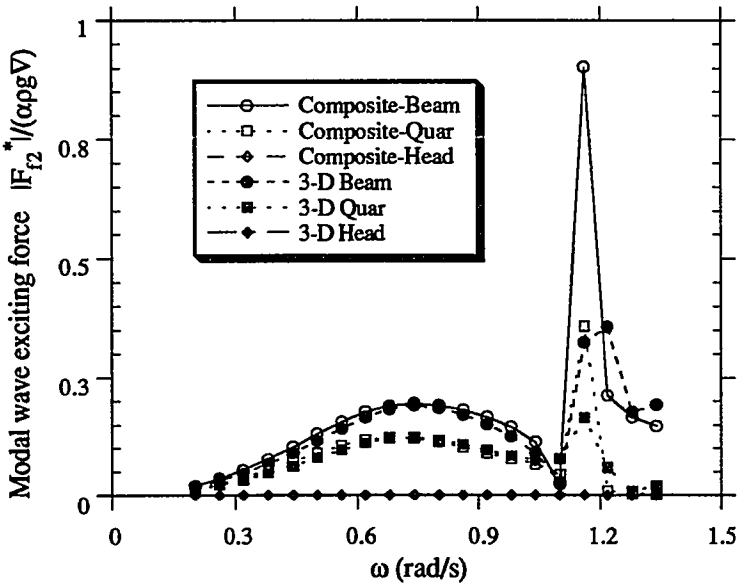
Modal wave exciting force $|F_{f2}^*|/(\alpha\rho gV)$
ω (rad/s)
Composite-Beam
Composite-Quar
Composite-Head
3-D Beam
3-D Quar
3-D Head
0
0.3
0.5
0.8
1
0.6
0.9
1.2
1.5

(9.23a)

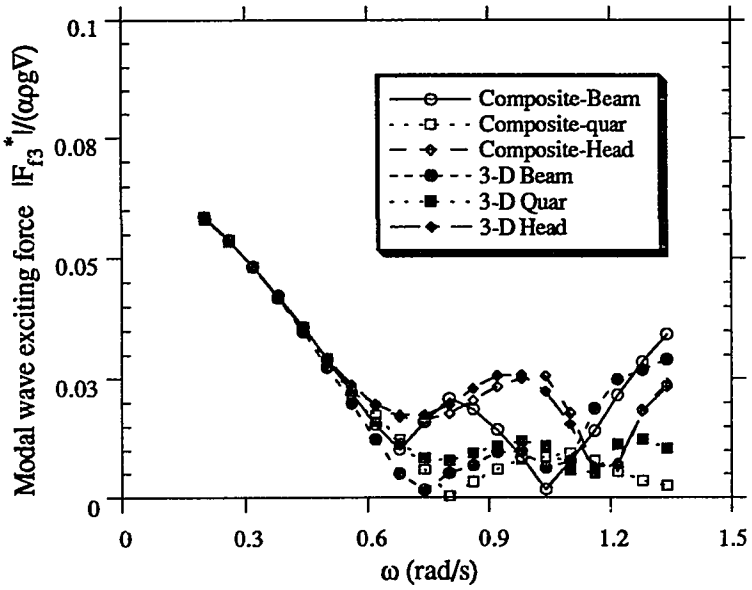
Modal wave exciting force $|F_{f3}^*|/(\alpha\rho gV)$
ω (rad/s)
Composite-Beam
Composite-quar
Composite-Head
3-D Beam
3-D Quar
3-D Head
0
0.03
0.05
0.08
0.1
0.3
0.6
0.9
1.2
1.5

(9.23b)

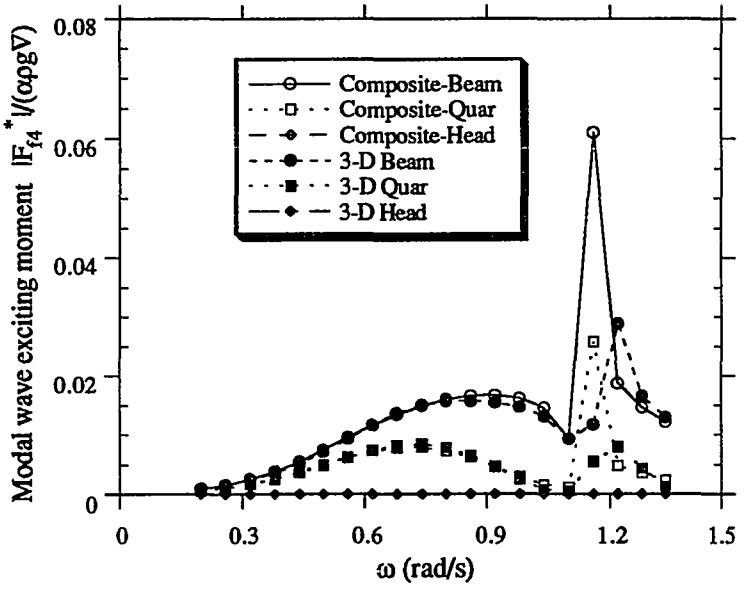

(9.23c)

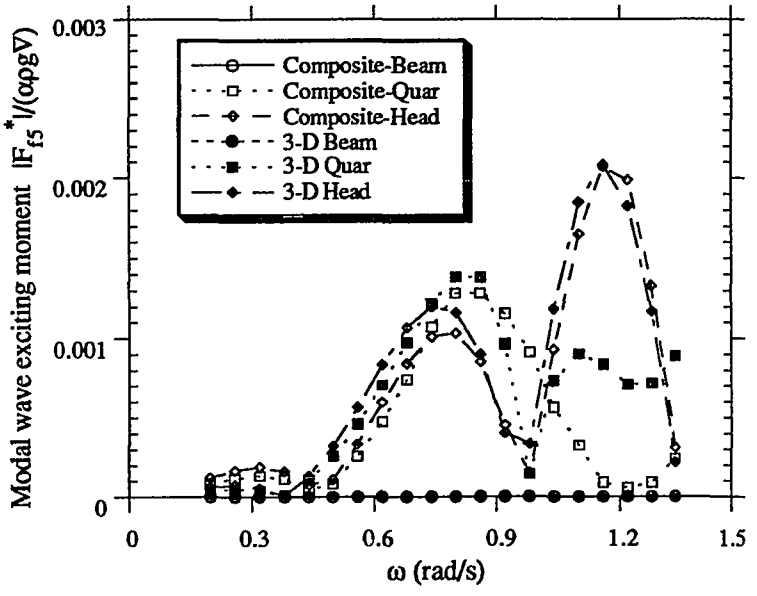

(9.23d)

Figure 9.23 Modal wave exciting forces and moments for rigid body motion of SWATH ship based on composite 2-D/3-D method and 3-D hydroelasticity

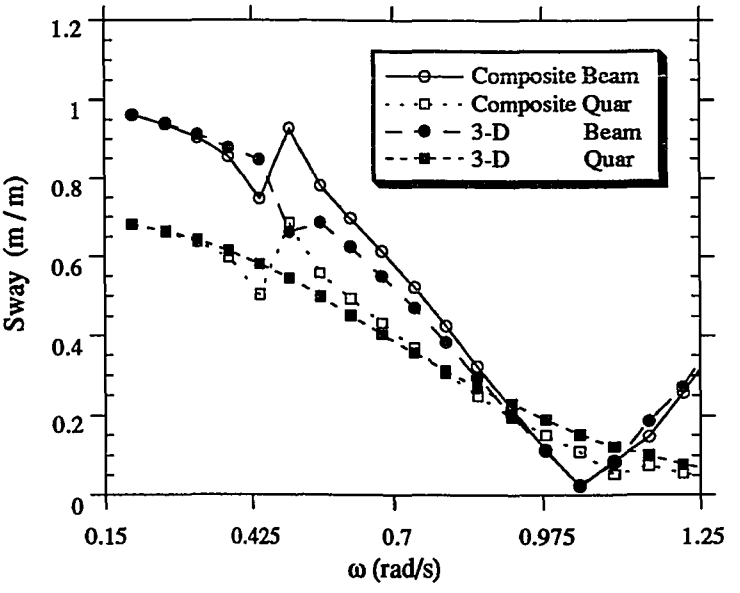
Composite Beam
Composite Quar
3-D Beam
3-D Quar
Sway (m / m)
ω (rad/s)
1.2
1
0.8
0.6
0.4
0.2
0
0.15
0.425
0.7
0.975
1.25

(9.24a)

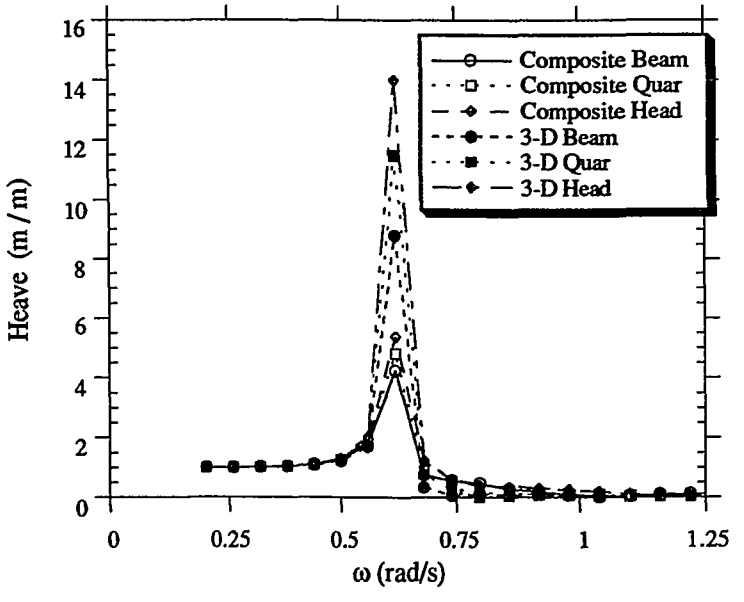
Composite Beam
Composite Quar
Composite Head
3-D Beam
3-D Quar
3-D Head
Heave (m / m)
ω (rad/s)
16
14
12
10
8
6
4
2
0
0
0.25
0.5
0.75
1
1.25

(9.24b)

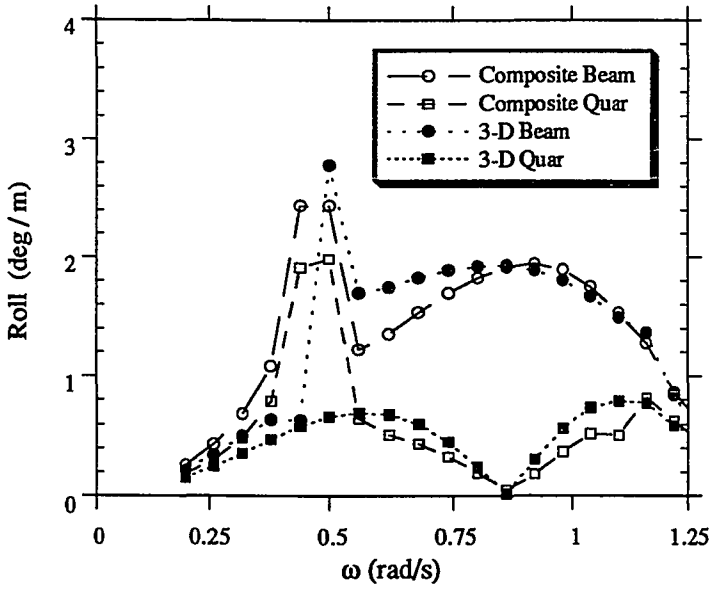

(9.24c)

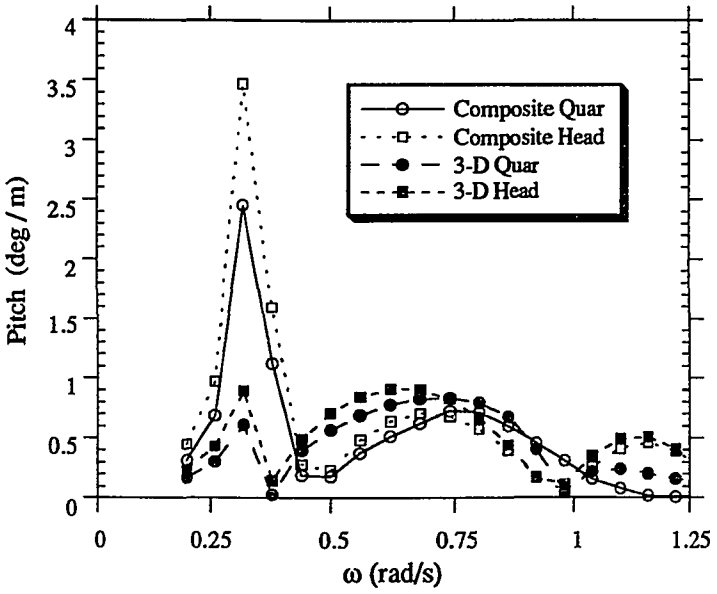

(9.24d)

Figure 9.24 Rigid body motions of SWATH based on 2-D (composite method) and 3-D potential theory, (a) sway, (b) heave, (c) roll, and (d) pitch

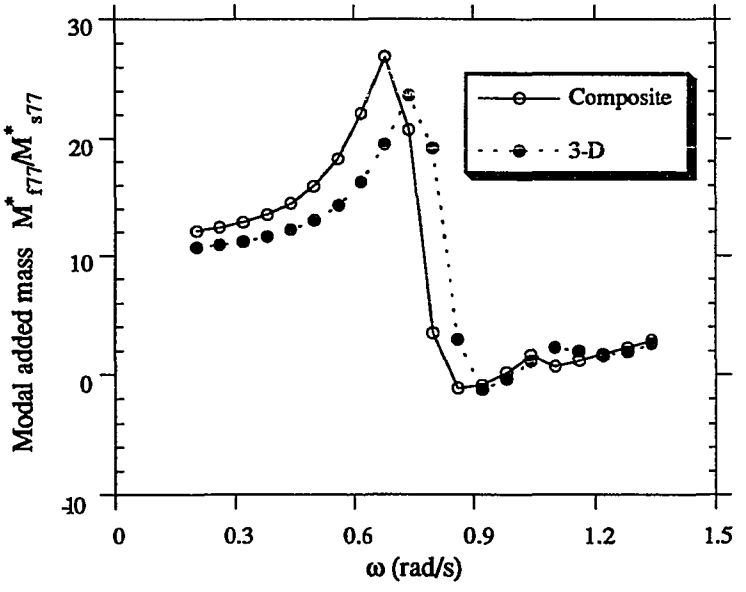
Modal added mass M^*_{f77}/M^*_{s77}
30
20
10
0
-10
0
0.3
0.6
0.9
1.2
1.5
ω (rad/s)
Composite
3-D

(9.25a)

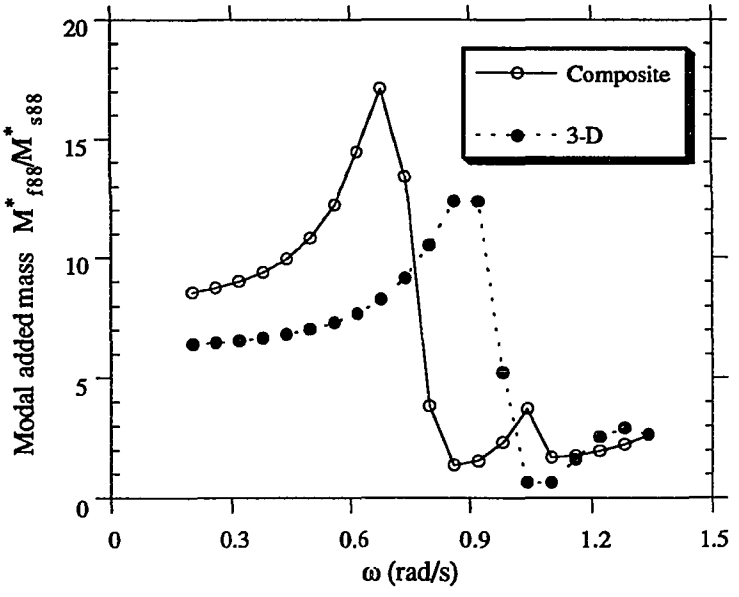
Modal added mass M^*_{f88}/M^*_{s88}
20
15
10
5
0
0
0.3
0.6
0.9
1.2
1.5
ω (rad/s)
Composite
3-D

(9.25b)

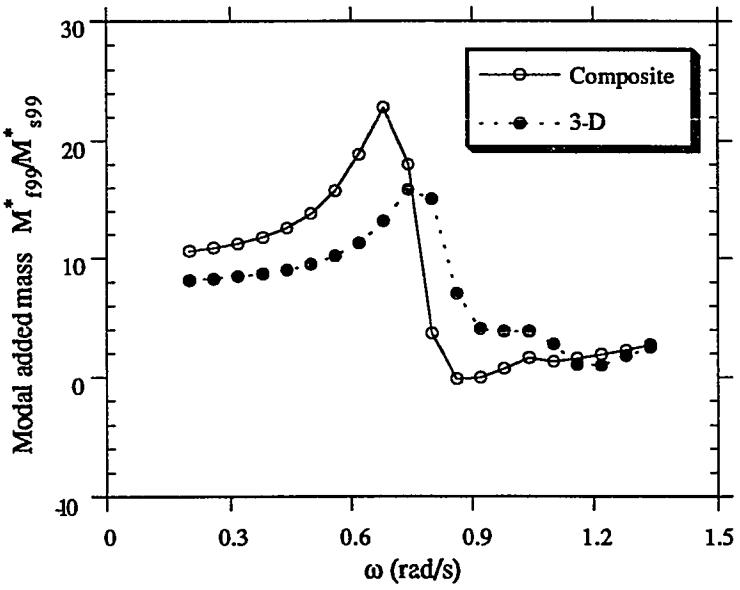
Composite
3-D
Modal added mass M^*_{f99}/M^*_{s99}
ω (rad/s)
30
20
10
0
-10
0
0.3
0.6
0.9
1.2
1.5

(9.25c)

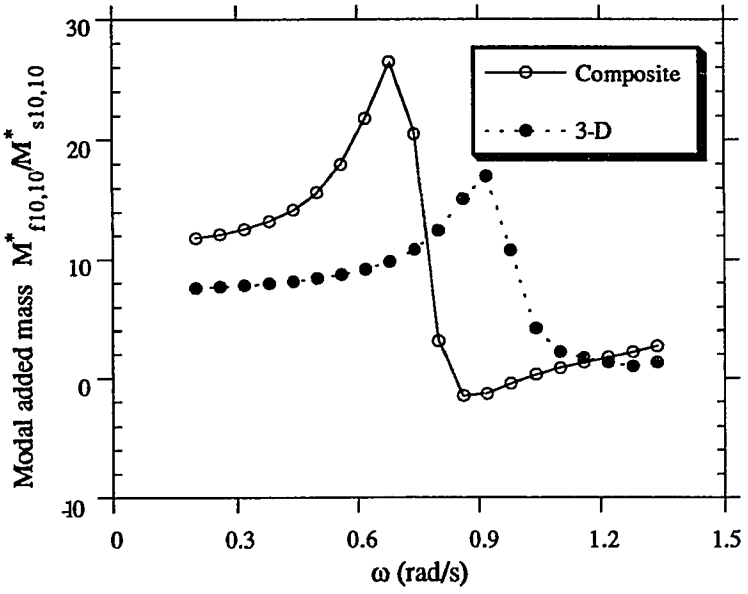
Composite
3-D
Modal added mass $M^*_{f10,10}/M^*_{s10,10}$
ω (rad/s)
30
20
10
0
-10
0
0.3
0.6
0.9
1.2
1.5

(9.25d)

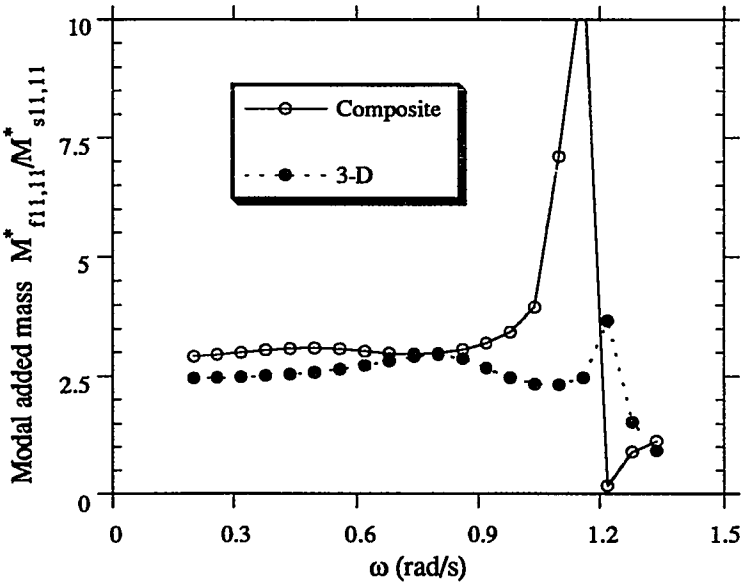
Composite
3-D
Modal added mass $M^*_{f11,11}/M^*_{s11,11}$
ω (rad/s)
10
7.5
5
2.5
0
0
0.3
0.6
0.9
1.2
1.5

(9.25e)

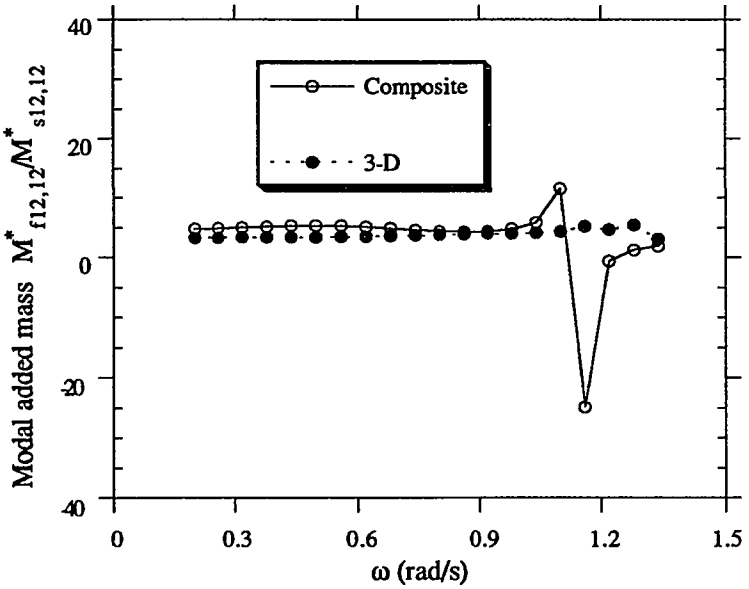
Composite
3-D
Modal added mass $M^*_{f12,12}/M^*_{s12,12}$
ω (rad/s)
40
20
0
-20
-40
0
0.3
0.6
0.9
1.2
1.5

(9.25f)

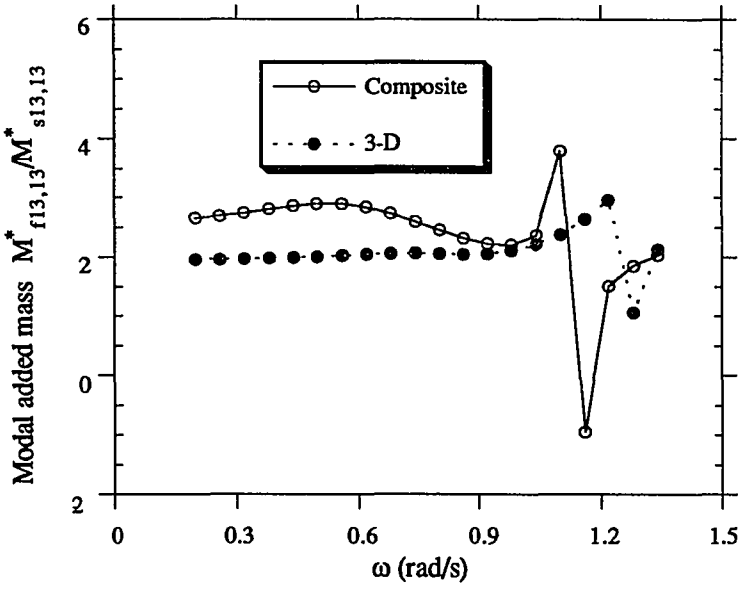

(9.25g)

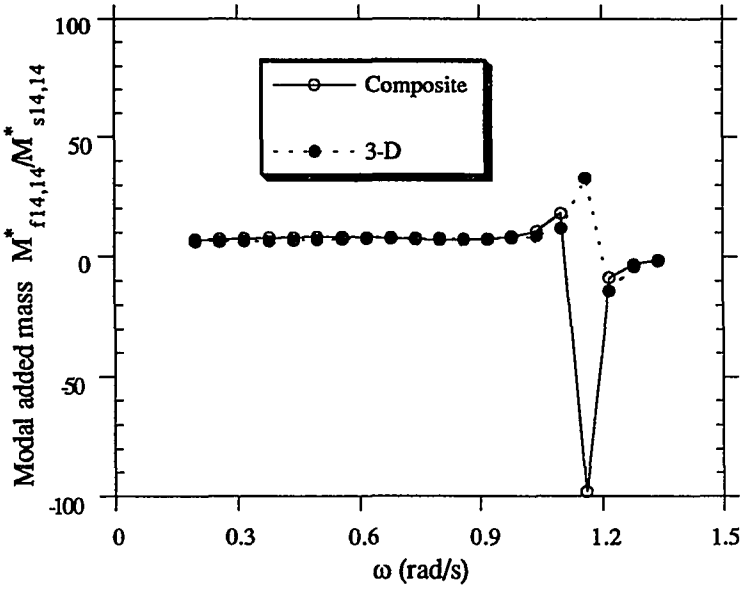

(9.25h)

Figure 9.25 Modal added mass for flexible motion of SWATH ship based on composite 2-D/3-D method and 3-D hydroelasticity

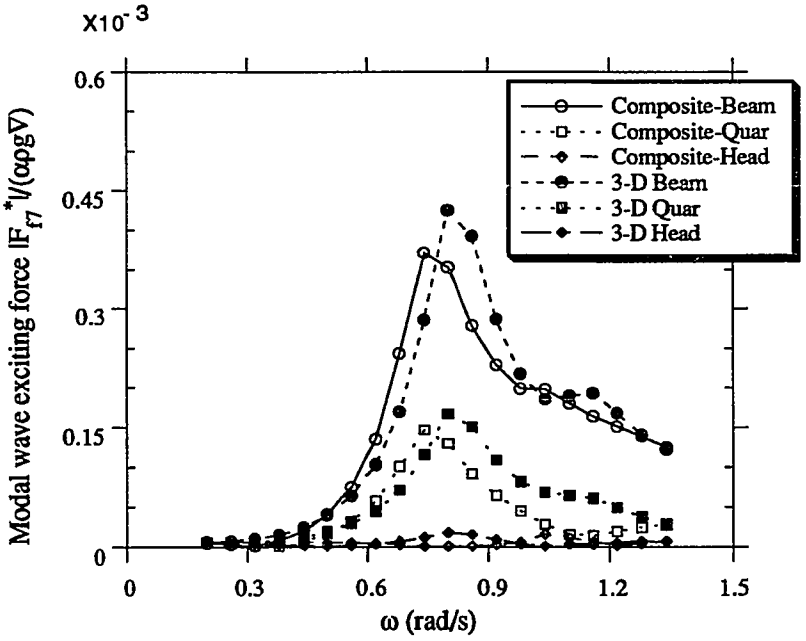
X10^-3
0.6
0.45
0.3
0.15
0
0
0.3
0.6
0.9
1.2
1.5
ω (rad/s)
Modal wave exciting force |F_f7*|/(αρgV)
Composite-Beam
Composite-Quar
Composite-Head
3-D Beam
3-D Quar
3-D Head

(9.26a)

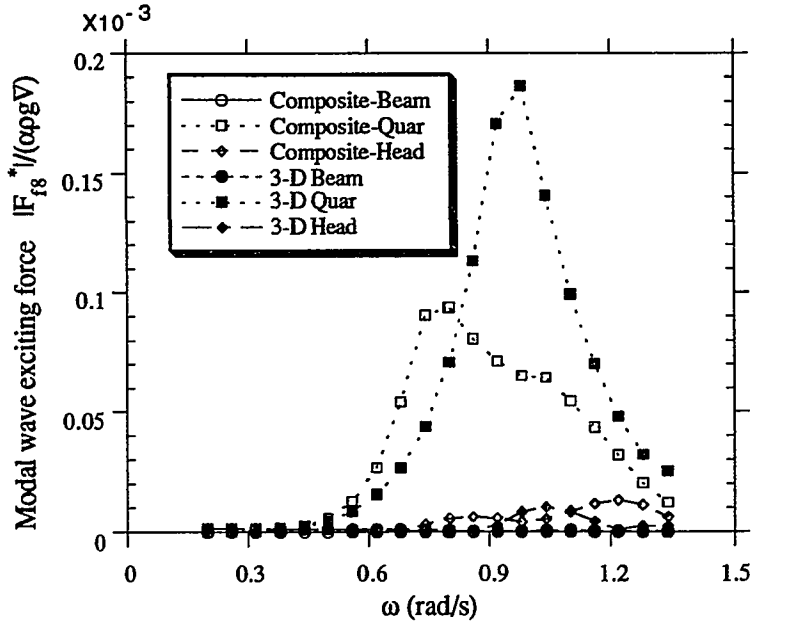
X10^-3
0.2
0.15
0.1
0.05
0
0
0.3
0.6
0.9
1.2
1.5
ω (rad/s)
Modal wave exciting force |F_f8*|/(αρgV)
Composite-Beam
Composite-Quar
Composite-Head
3-D Beam
3-D Quar
3-D Head

(9.26b)

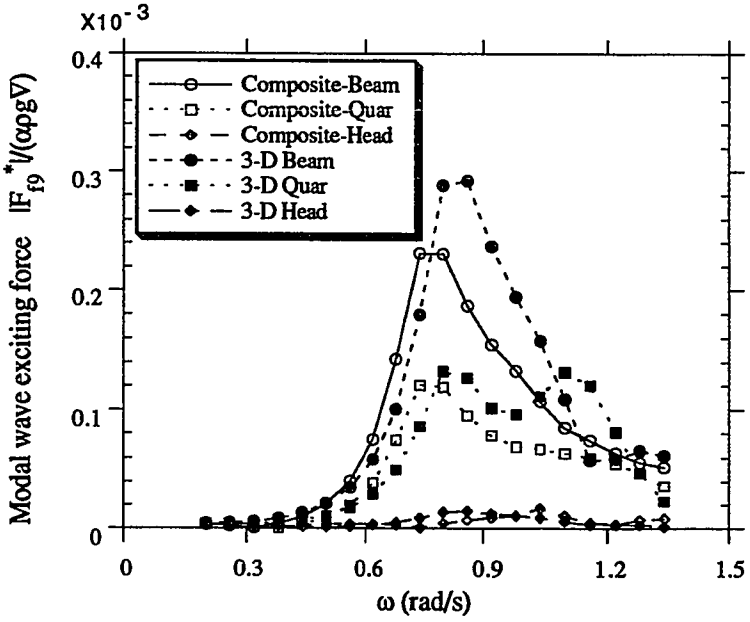
X10^-3
0.4
0.3
0.2
0.1
0
Modal wave exciting force |F_f9*|/(αρgV)
Composite-Beam
Composite-Quar
Composite-Head
3-D Beam
3-D Quar
3-D Head
0
0.3
0.6
0.9
1.2
1.5
ω (rad/s)

(9.26c)

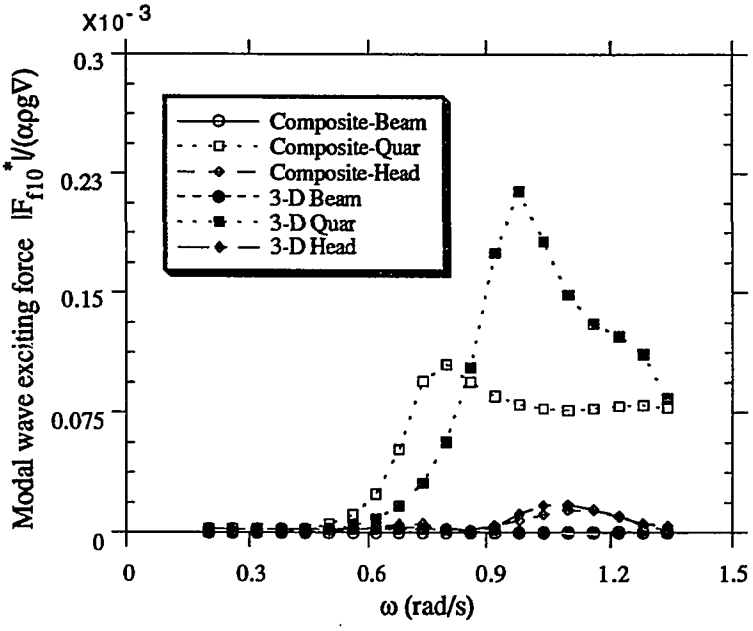
X10^-3
0.3
0.23
0.15
0.075
0
Modal wave exciting force |F_f10*|/(αρgV)
Composite-Beam
Composite-Quar
Composite-Head
3-D Beam
3-D Quar
3-D Head
0
0.3
0.6
0.9
1.2
1.5
ω (rad/s)

(9.26d)

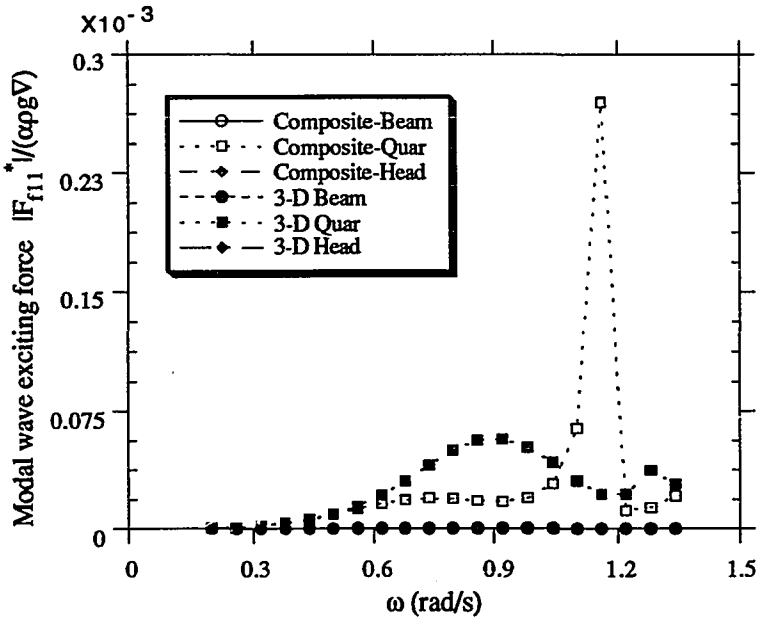
X10⁻³
0.3
0.23
0.15
0.075
0
Modal wave exciting force |F*f11|/(αρgV)
Composite-Beam
Composite-Quar
Composite-Head
3-D Beam
3-D Quar
3-D Head
0
0.3
0.6
0.9
1.2
1.5
ω (rad/s)

(9.26e)

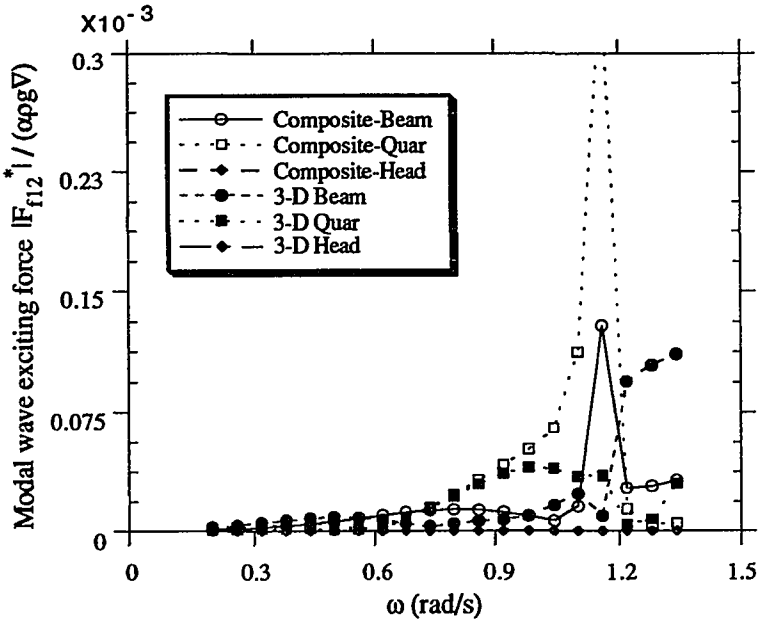
X10⁻³
0.3
0.23
0.15
0.075
0
Modal wave exciting force |F*f12|/(αρgV)
Composite-Beam
Composite-Quar
Composite-Head
3-D Beam
3-D Quar
3-D Head
0
0.3
0.6
0.9
1.2
1.5
ω (rad/s)

(9.26f)

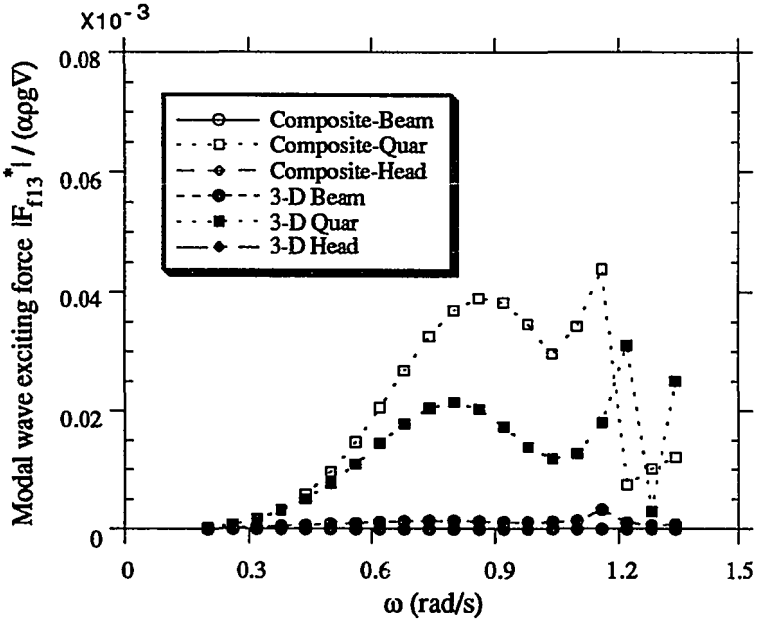

(9.26g)

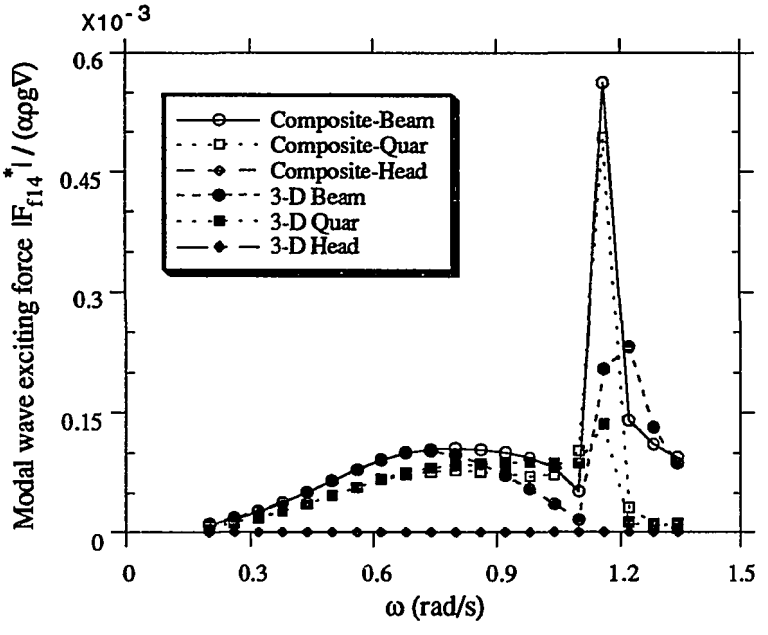

(9.26h)

Figure 9.26 Modal wave exciting forces for flexible motion of SWATH ship based on composite 2-D/3-D method and 3-D hydroelasticity

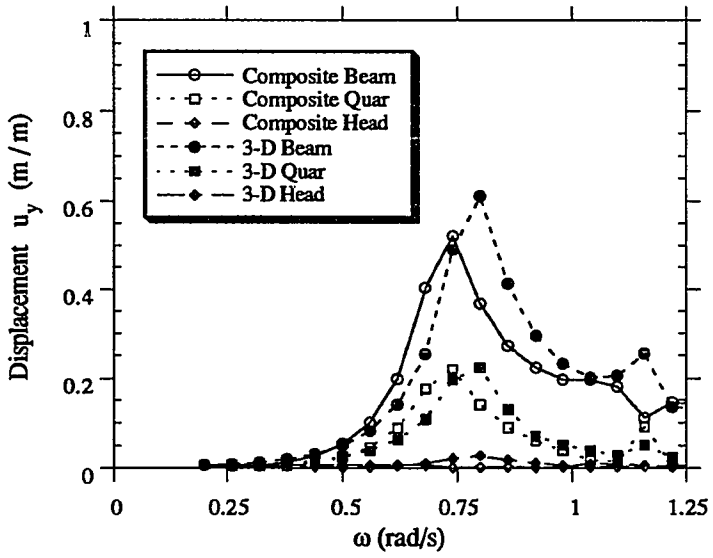
Composite Beam
Composite Quar
Composite Head
3-D Beam
3-D Quar
3-D Head
Displacement u_y (m / m)
ω (rad/s)
0
0.2
0.4
0.6
0.8
1
0.25
0.5
0.75
1.25

(9.27a)

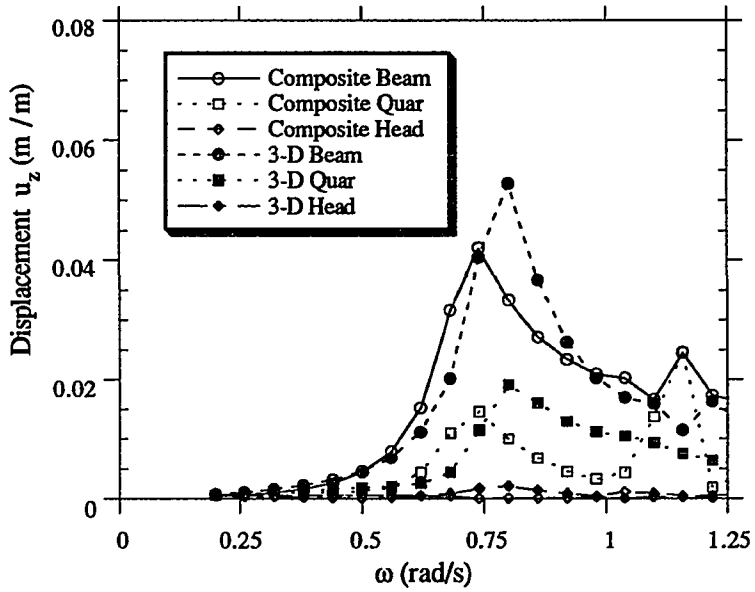
Composite Beam
Composite Quar
Composite Head
3-D Beam
3-D Quar
3-D Head
Displacement u_z (m / m)
ω (rad/s)
0
0.02
0.04
0.06
0.08
0.25
0.5
0.75
1
1.25

(9.27b)

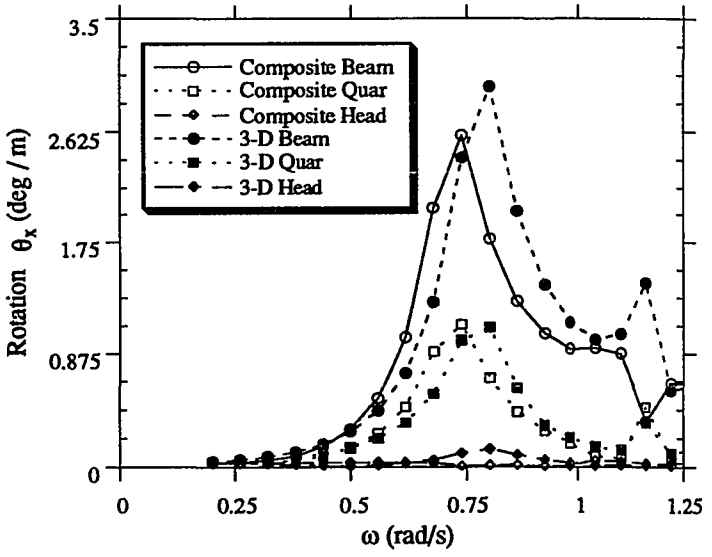

(9.27c)

Figure 9.27 Deformational motions of SWATH ship at point A based on composite 2-D/3-D method and 3-D hydroelasticity, (a) horizontal u_y, (b) vertical u_z, and (c) rotational θ_x

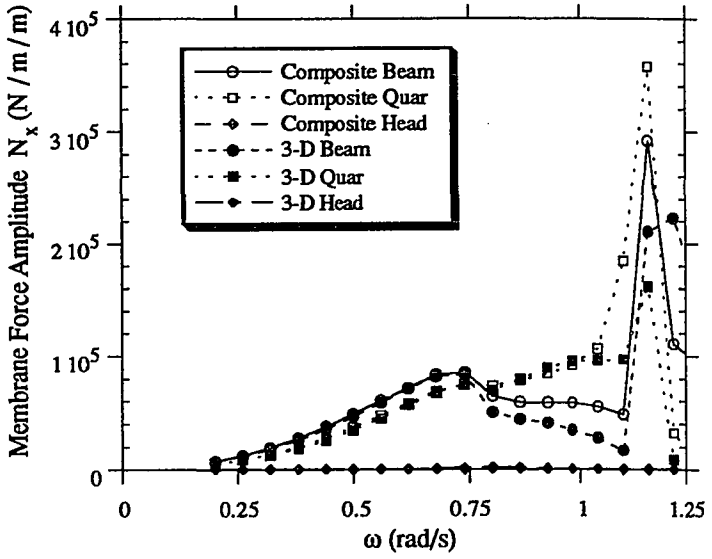

(9.28a)

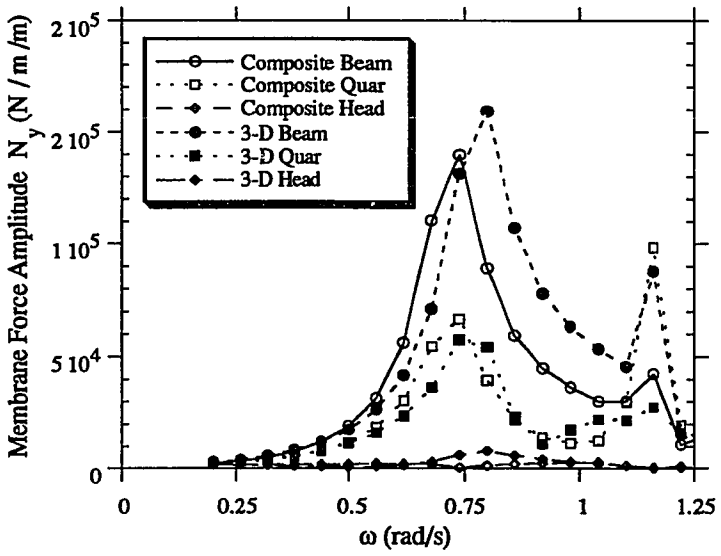
Membrane Force Amplitude N_y (N / m /m)
2 10^5
2 10^5
1 10^5
5 10^4
0
0
0.25
0.5
0.75
1
1.25
ω (rad/s)
Composite Beam
Composite Quar
Composite Head
3-D Beam
3-D Quar
3-D Head

(9.28b)

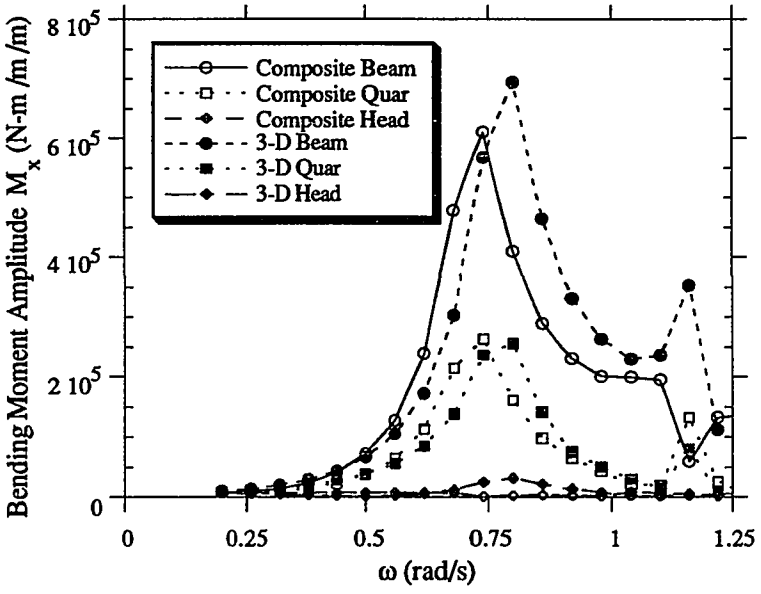
Bending Moment Amplitude M_x (N-m /m /m)
8 10^5
6 10^5
4 10^5
2 10^5
0
0
0.25
0.5
0.75
1
1.25
ω (rad/s)
Composite Beam
Composite Quar
Composite Head
3-D Beam
3-D Quar
3-D Head

(9.28c)

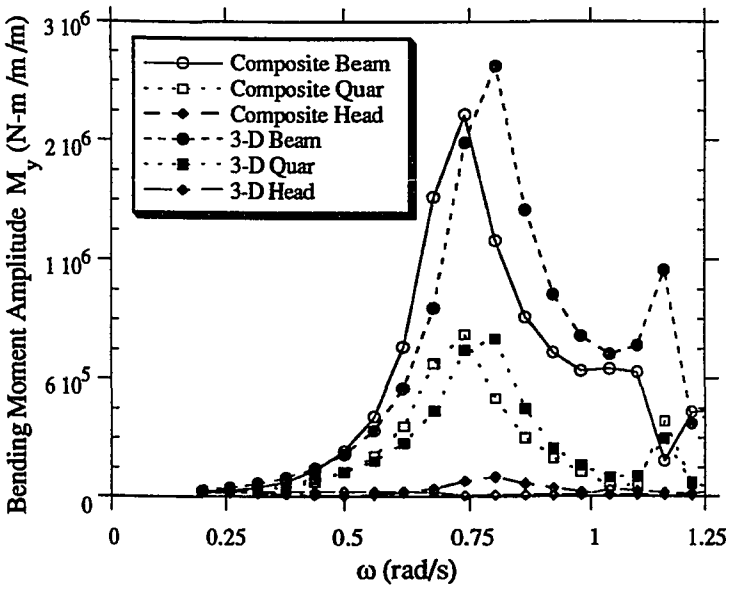

(9.28d)

Figure 9.28 Internal forces of SWATH ship at connection B based on composite 2-D/ 3-D method and 3-D hydroelasticity, (a) N_x, (b) N_y, (c) M_x, and (d) M_y

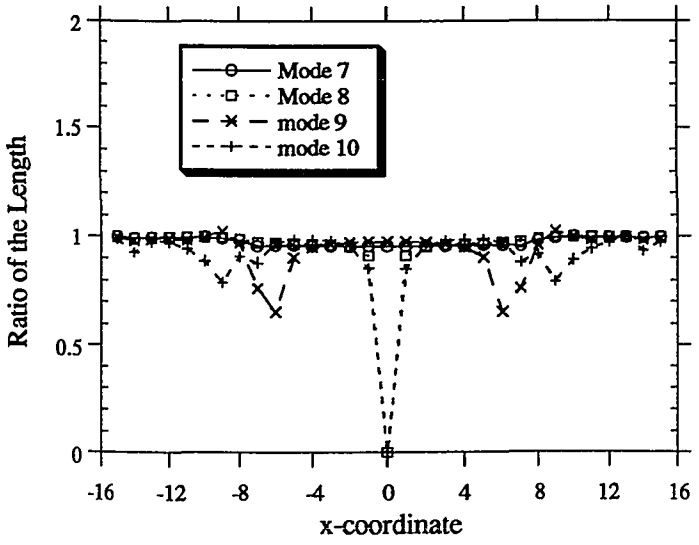

(9.29a)

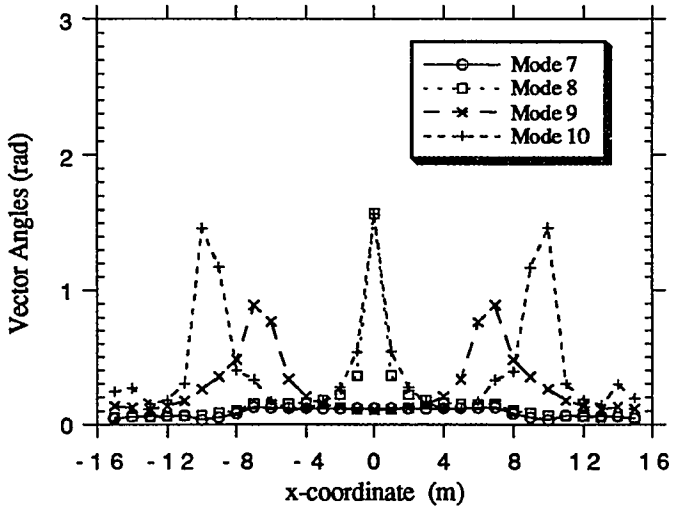

(9.29b)

Figure 9.29 (a) The ratio of the length, and (b) the angle between actual symmetric modes and the approximate modes

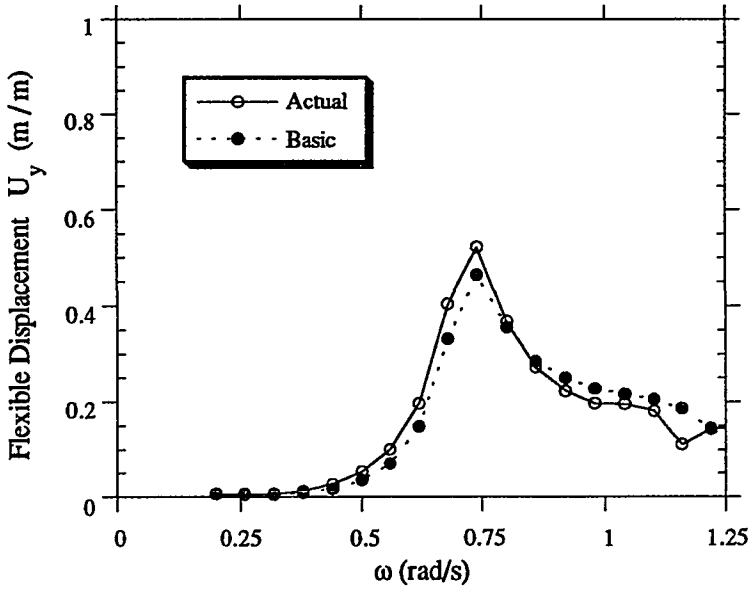

Figure 9.30 Deformational motion at A in beam seas based on composite method for actual modes and basic modes

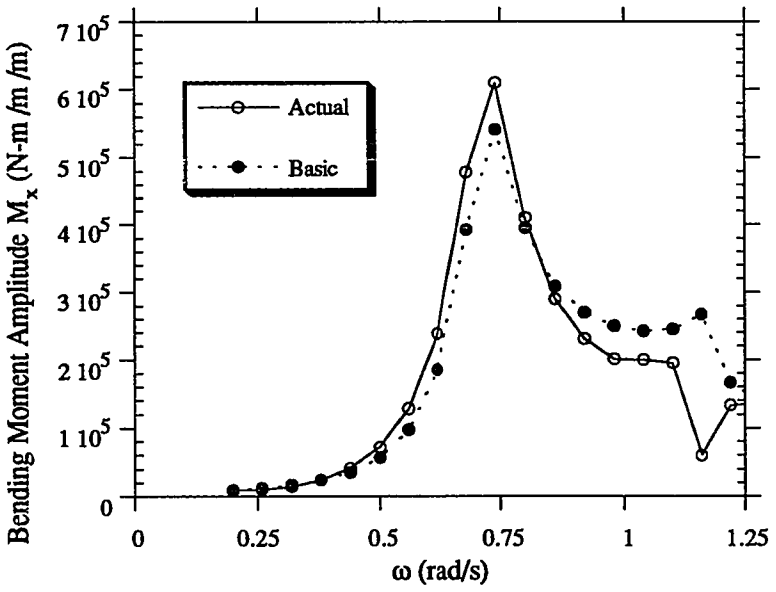

Figure 9.31 Bending Moment M_x at B in beam seas based on composite method for actual modes and basic modes

CHAPTER 10

CONCLUSIONS AND RECOMMENDATIONS

10.1 Conclusions

Three methods for the hydroelastic analysis of very large floating structures have been developed. They are an improved two-dimensional hydroelastic method, a three-dimensional hydroelastic method incorporating frame elements with Morison's equation, and a composite 2-D/3-D hydroelastic method. All the methods are developed to apply to very large floating structures. However, the methods are also applicable to other offshore structures.

A common characteristic of all three methods is efficiency. The methods avoid three-dimensional potential theory to calculate hydrodynamic coefficients and wave exciting forces, which is a computationally time consuming part of hydroelastic analysis of VLFSs. Another common characteristic is that structural responses and forces are an integral result of the analysis.

The two-dimensional hydroelastic method is based on strip theory and a nonuniform beam model for the structure below the still-water line. A general three-dimensional structural model is possible for the structure above the water surface. Therefore, modeling the fluid is very simple and the method is very efficient. The deficiency of this method is that the fluid interaction between the beam cross-section and the longitudinal fluid forces are ignored and only the beam-like responses and forces can be predicted. Two-dimensional hydroelasticity has been used to analyze the motions and forces in a long, relatively slender 5-module VLFS which is 100 m wide and 500 m long. The results are useful to develop an understanding of the fundamental modes of displacement and force magnitudes for which multi-module VLFSs must be designed.

Ignoring the longitudinal forces in two-dimensional hydroelasticity results in inaccuracies, especially for pitch motion of a single module. However, the results indicate that the inaccuracies are less important for large structures which behave as a 'single' structure, rather than one whose response is primarily composed of connected smaller structures.

Frame finite elements for modeling the structure and Morison's equation for calculating the fluid forces have been incorporated in a three-dimensional hydroelastic analysis method. The advantages of this method are that a three-dimensional structural model is used to provide detailed information of the structure and the very efficient Morison's equation is adopted to calculate the fluid force. One of the deficiencies of this method is that fluid interaction is not taken into account since Morison's equation is used. Another is that the method is limited to structures which can be modeled by circular cylinders below the still water line. Moreover, one needs to have accurate inertia and drag coefficients in this analysis.

Despite the limitation of Morison's equation and the relatively large diameters of the circular members, somewhat acceptable results, especially for a single module, in comparison with the three-dimensional potential theory, are obtained. Based on the present results, it appears the method can be used to predict the hydroelastic response of a VLFS during, at least, the preliminary design stage. This is especially true when one considers that the method requires very little computational time in comparison with three-dimensional potential theory.

To reduce the computational time required for a full, three-dimensional hydroelastic analysis, but to improve the results of two-dimensional hydroelasticity, a composite 2-D/ 3-D hydroelastic method has been developed. The method combines a three-dimensional structural model and a two-dimensional fluid model to compute the wave-

induced, hydroelastic response. The advantages of this method are that three-dimensional structural motions and deformations are used with two-dimensional potential theory to obtain the hydrodynamic coefficients and wave exciting forces, and the deformation and internal forces of each individual structural element can be obtained. However, because the fluid forces are determined from two-dimensional potential theory, the method is applicable to slender structures.

To demonstrate the composite method and to verify the implementation, a simple, twin-hull structure with two flexible modes has been analyzed. The comparison of results between the composite method and three-dimensional analysis is good. In addition to this highly idealized, 'two-dimensional' structure, the method is also applied to a more realistic SWATH-like structure. Again the results of the composite method compare well with those from a full, three-dimensional analysis. From the results, we conclude that the composite 2-D/3-D method represents an effective alternative to a full three-dimensional hydroelastic analysis in the preliminary design of large, floating structures which can be characterized as slender. For large structures, the savings in computer time is substantial with the composite method, and the accuracy is sufficient for many design purposes. To calculate hydrodynamic coefficients and wave exciting forces for the simple, twin-hull structure, three-dimensional potential theory requires 255 times the CPU computer time that the composite 2-D/3-D method does.

The results clearly indicate that a VLFS will experience substantial deformations as a result of wave loading. Therefore, conventional motion analysis methodology for floating structures, in which the structure is assumed rigid, does not apply to VLFSs. Hydroelasticity must be considered to determine both the force in the structure and the overall motion response.

10.2 Recommendations

1. Since three-dimensional hydroelasticity using potential theory is the most general and accurate linear theory to date, an efficient three-dimensional hydroelasticity theory should be developed for VLFS design. Three aspects should be considered for this development: exploiting the symmetry of the structure (Wu et al., 1993); using an efficient vector basis to replace the 'dry modes'; and developing more efficient numerical techniques to determine the three-dimensional fluid potential.

2. Since VLFSs may have large motions and deformations, non-linearities may have to be considered to obtain more accurate results. An efficient second-order theory which is suitable for VLFS analysis should ideally be developed. However, such a decision should be based on a comparison between experimental data and predictions.

3. The connection design is a very important aspect for multi-module VLFS design. It has been seen from this study that different connections used in multi-module VLFSs affect the response. Further study on the connection design should be done to provide design information for physical connector design.

4. For final VLFS design, an experimental study should be carried out to verify the analytical methodology and provide final design criteria.

APPENDIX A. FRAME ELEMENT

The shape function for a frame element, [N], can be written as

$$[N] = [N_{at}] + [N_b] \tag{A.1}$$

where $[N_{at}]$ is a 6×12 matrix of interpolation functions for axial and torsional degrees of freedom:

$$[N_{at}] = \begin{bmatrix} N_1 & 0 & 0 & 0 & 0 & 0 & N_7 & 0 & 0 & 0 & 0 & 0 \\ 0 & 0 & 0 & 0 & 0 & 0 & 0 & 0 & 0 & 0 & 0 & 0 \\ 0 & 0 & 0 & 0 & 0 & 0 & 0 & 0 & 0 & 0 & 0 & 0 \\ 0 & 0 & 0 & N_4 & 0 & 0 & 0 & 0 & 0 & N_{10} & 0 & 0 \\ 0 & 0 & 0 & 0 & 0 & 0 & 0 & 0 & 0 & 0 & 0 & 0 \\ 0 & 0 & 0 & 0 & 0 & 0 & 0 & 0 & 0 & 0 & 0 & 0 \end{bmatrix} \tag{A.2}$$

in which $N_4 = N_1$ and $N_{10} = N_7$. N_1 and N_7 are for axial effects, and are given by

$$N_1 = 1 - \frac{x}{L}; \qquad N_7 = \frac{x}{L} \tag{A.3}$$

where L is the beam element length, and x is the local x-coordinate.

N_b is a 6×12 matrix of interpolation functions for transverse displacements:

$$[N_b] = \begin{bmatrix} 0 & 0 & 0 & 0 & 0 & 0 & 0 & 0 & 0 & 0 & 0 & 0 \\ 0 & N_2 & 0 & 0 & 0 & N_6 & 0 & N_8 & 0 & 0 & 0 & N_{12} \\ 0 & 0 & N_3 & 0 & N_5 & 0 & 0 & 0 & N_9 & 0 & N_{11} & 0 \\ 0 & 0 & 0 & 0 & 0 & 0 & 0 & 0 & 0 & 0 & 0 & 0 \\ 0 & N'_2 & 0 & 0 & 0 & N'_6 & 0 & N'_8 & 0 & 0 & 0 & N'_{12} \\ 0 & 0 & N'_3 & 0 & N'_5 & 0 & 0 & 0 & N'_9 & 0 & N'_{11} & 0 \end{bmatrix} \tag{A.4}$$

where the components N_2, N_3, N_5, N_6, N_8, N_9, N_{11}, and N_{12} are for deflection effects,

and are

$$N_2 = N_3 = 1 - 3\left(\frac{x}{L}\right)^2 + 2\left(\frac{x}{L}\right)^3 \tag{A.5}$$

$$N_6 = 3\left(\frac{x}{L}\right)^2 - 2\left(\frac{x}{L}\right)^3 \qquad N_5 = -N_6 \tag{A.6}$$

$$N_8 = N_9 = x\left(1 - \frac{x}{L}\right)^2 \tag{A.7}$$

$$N_{12} = \frac{x^2}{L}\left(\frac{x}{L} - 1\right) \qquad N_{11} = -N_{12} \tag{A.8}$$

Therefore [N] can be written as

$$[N] = \begin{bmatrix} N_1 & 0 & 0 & 0 & 0 & 0 & N_7 & 0 & 0 & 0 & 0 & 0 \\ 0 & N_2 & 0 & 0 & 0 & N_6 & 0 & N_8 & 0 & 0 & 0 & N_{12} \\ 0 & 0 & N_3 & 0 & N_5 & 0 & 0 & 0 & N_9 & 0 & N_{11} & 0 \\ 0 & 0 & 0 & N_4 & 0 & 0 & 0 & 0 & 0 & N_{10} & 0 & 0 \\ 0 & N'_2 & 0 & 0 & 0 & N'_6 & 0 & N'_8 & 0 & 0 & 0 & N'_{12} \\ 0 & 0 & N'_3 & 0 & N'_5 & 0 & 0 & 0 & N'_9 & 0 & N'_{11} & 0 \end{bmatrix} \tag{A.9}$$

The frame element mass [m] suitable for displacement field {u} in Eq. 3.28 is given in Eq. II.10. The frame element damping matrix [c] can be obtained in the same manner. The frame element stiffness matrix [k] is given in Eq. II.11. The frame element stiffness matrix $[k^s]$ that includes the shear deformation is written in Eq. II.12.

$$
[m] = \begin{bmatrix}
\frac{\bar{m}_{11}L}{3} & & & & & & & & & & & & \\
0 & \frac{13\bar{m}_{22}L}{35}+\frac{6\bar{m}_{66}}{5L} & & & & & & & & & & & \\
0 & 0 & \frac{13\bar{m}_{33}L}{35}+\frac{6\bar{m}_{55}}{5L} & & & & & & & & & & \\
0 & \frac{7\bar{m}_{24}L}{20} & 0 & \frac{\bar{m}_{44}L}{3} & & & & & & & & & \\
0 & 0 & \frac{11\bar{m}_{22}L^2}{210}+\frac{\bar{m}_{55}}{10} & 0 & \frac{\bar{m}_{33}L^3}{105}+\frac{2\bar{m}_{55}L}{15} & & & & & & & & \\
0 & \frac{11\bar{m}_{22}L^2}{210}+\frac{\bar{m}_{66}}{10} & 0 & \frac{\bar{m}_{42}L^2}{20} & 0 & \frac{\bar{m}_{22}L^3}{105}+\frac{2\bar{m}_{66}L}{15} & & & & & & & \\
\frac{\bar{m}_{11}L}{6} & 0 & 0 & 0 & 0 & 0 & \frac{\bar{m}_{11}L}{3} & & & & & & \\
0 & \frac{9\bar{m}_{22}L}{70}-\frac{6\bar{m}_{66}}{5L} & 0 & \frac{3\bar{m}_{42}L}{20} & 0 & \frac{13\bar{m}_{22}L^2}{420}-\frac{\bar{m}_{66}}{10} & 0 & \frac{13\bar{m}_{22}L}{35}+\frac{6\bar{m}_{66}}{5L} & & & & & \\
0 & 0 & \frac{9\bar{m}_{33}L}{70}-\frac{6\bar{m}_{55}}{5L} & 0 & \frac{-13\bar{m}_{33}L^2}{420}+\frac{\bar{m}_{55}}{10} & 0 & 0 & 0 & \frac{13\bar{m}_{33}L}{35}+\frac{6\bar{m}_{55}}{5L} & & & & \\
0 & \frac{3\bar{m}_{24}L}{20} & 0 & \frac{\bar{m}_{44}L}{6} & 0 & \frac{\bar{m}_{4}L^2}{30} & 0 & \frac{7\bar{m}_{24}L}{20} & 0 & \frac{\bar{m}_{44}L}{3} & & & \\
0 & 0 & \frac{13\bar{m}_{33}L^2}{420}-\frac{\bar{m}_{55}}{10} & 0 & \frac{-\bar{m}_{33}L^3}{140}-\frac{\bar{m}_{55}L}{30} & 0 & 0 & 0 & \frac{-11\bar{m}_{22}L^2}{210}-\frac{\bar{m}_{55}}{10} & 0 & \frac{\bar{m}_{33}L^3}{105}+\frac{2\bar{m}_{55}L}{15} & & \\
0 & \frac{-13\bar{m}_{22}L}{420}+\frac{\bar{m}_{66}}{10} & 0 & \frac{-\bar{m}_{42}L^2}{30} & 0 & \frac{-\bar{m}_{22}L^3}{140}-\frac{\bar{m}_{66}L}{30} & 0 & \frac{-11\bar{m}_{22}L^2}{210}-\frac{\bar{m}_{66}}{10} & 0 & \frac{\bar{m}_{42}L^2}{20} & 0 & \frac{\bar{m}_{22}L^3}{105}+\frac{2\bar{m}_{66}L}{15}
\end{bmatrix}
$$

Symmetric

(A.10)

$$
[k] = \begin{bmatrix}
\frac{EA}{L} & & & & & & & & & & & \\
0 & \frac{12EI_z}{L^3} & & & & & & & \text{Symmetric} & & & \\
0 & 0 & \frac{12EI_y}{L^3} & & & & & & & & & \\
0 & 0 & 0 & \frac{GJ}{L} & & & & & & & & \\
0 & 0 & \frac{-6EI_y}{L^2} & 0 & \frac{4EI_y}{L} & & & & & & & \\
0 & \frac{6EI_z}{L^2} & 0 & 0 & 0 & \frac{4EI_z}{L} & & & & & & \\
\frac{-EA}{L} & 0 & 0 & 0 & 0 & 0 & \frac{EA}{L} & & & & & \\
0 & \frac{-12EI_z}{L^3} & 0 & 0 & 0 & \frac{-6EI_z}{L^2} & 0 & \frac{12EI_z}{L^3} & & & & \\
0 & 0 & \frac{-12EI_y}{L^3} & o & \frac{6EI_y}{L^2} & 0 & 0 & 0 & \frac{12EI_y}{L^3} & & & \\
0 & 0 & 0 & \frac{-GJ}{L} & 0 & 0 & 0 & 0 & 0 & \frac{GJ}{L} & & \\
0 & 0 & \frac{-6EI_y}{L^2} & 0 & \frac{2EI_y}{L} & 0 & 0 & 0 & \frac{6EI_y}{L^2} & 0 & \frac{4EI_y}{L} & \\
0 & \frac{6EI_z}{L^2} & 0 & 0 & 0 & \frac{2EI_z}{L} & 0 & \frac{-6EI_z}{L^2} & 0 & 0 & 0 & \frac{4EI_z}{L}
\end{bmatrix} \qquad \text{(A.11)}
$$

$$
\left[k^{e}\right] = \begin{bmatrix}
\frac{EA}{L} & & & & & & & & & & & \\
0 & \frac{12EI_z}{L^3(1+\varphi_2)} & & & & & & & & & & \\
0 & 0 & \frac{12EI_y}{L^3(1+\varphi_3)} & & & & & & & & & \\
0 & 0 & 0 & \frac{GJ}{L} & & & & & & & & \\
0 & 0 & \frac{-6EI_y}{L^2(1+\varphi_3)} & 0 & \frac{(4+\varphi_3)EI_y}{L(1+\varphi_3)} & & & & & & & \\
0 & \frac{6EI_z}{L^2(1+\varphi_2)} & 0 & 0 & 0 & \frac{(4+\varphi_2)EI_z}{L(1+\varphi_2)} & & & & & & \\
\frac{-EA}{L} & 0 & 0 & 0 & 0 & 0 & \frac{EA}{L} & & & & & \\
0 & \frac{-12EI_z}{L^3(1+\varphi_2)} & 0 & 0 & 0 & \frac{-6EI_z}{L^2(1+\varphi_2)} & 0 & \frac{12EI_z}{L^3(1+\varphi_2)} & & & & \\
0 & 0 & \frac{-12EI_y}{L^3(1+\varphi_3)} & o & \frac{6EI_y}{L^2(1+\varphi_3)} & 0 & 0 & 0 & \frac{12EI_y}{L^3(1+\varphi_3)} & & & \\
0 & 0 & 0 & \frac{-GJ}{L} & 0 & 0 & 0 & 0 & 0 & \frac{GJ}{L} & & \\
0 & 0 & \frac{-6EI_y}{L^2(1+\varphi_3)} & 0 & \frac{(2-\varphi_3)EI_y}{L(1+\varphi_3)} & 0 & 0 & 0 & \frac{6EI_y}{L^2(1+\varphi_3)} & 0 & \frac{(4+\varphi_3)EI_y}{L(1+\varphi_3)} & \\
0 & \frac{6EI_z}{L^2(1+\varphi_2)} & 0 & 0 & 0 & \frac{(2-\varphi_2)EI_z}{L(1+\varphi_2)} & 0 & \frac{-6EI_z}{L^2(1+\varphi_2)} & 0 & 0 & 0 & \frac{(4+\varphi_2)EI_z}{L(1+\varphi_2)}
\end{bmatrix}
$$

Symmetric

(A.12)

In the above equations, A is the cross-sectional area of the beam; E is the elastic modulus; G is the shear modulus; I_y and I_z are the second moment of the cross-sectional area about local y and z axes, respectively; $\varphi_2 = \frac{12EI_z}{GA_yL^2}$ and $\varphi_3 = \frac{12EI_y}{GA_zL^2}$, $A_y = \frac{A}{K_y}$ and $A_z = \frac{A}{K_z}$; K_y and K_z are the cross-section shear coefficients in y and z direction, respectively.

In general, geometric stiffness coefficients may be expressed as

$$k_{Gij} = \int_{L_e} f_a(x)\, N'_i N'_j dL \qquad \text{for } i,j = 2,3,5,6,8,9,11,12 \tag{A.13}$$

The beam element geometric stiffness matrix, for the case where the axial force is constant, can be written as

$$[k_{eG}] = \frac{N}{30L}\begin{bmatrix}
0 & & & & & & & & & & & \\
0 & 36 & & & & & & & & & & \\
0 & 0 & 36 & & & & & & & & & \\
0 & 0 & 0 & 0 & & & & & & & & \\
0 & 0 & -3L & 0 & 4L^2 & & & & & & & \\
0 & 3L & 0 & 0 & 0 & 4L^2 & & & & & & \\
0 & 0 & 0 & 0 & 0 & 0 & 0 & & & & & \\
0 & -36 & 0 & 0 & 0 & -3L & 0 & 36 & & & & \\
0 & 0 & -36 & 0 & 3L & 0 & 0 & 0 & 36 & & & \\
0 & 0 & 0 & 0 & 0 & 0 & 0 & 0 & 0 & 0 & & \\
0 & 0 & -3L & 0 & -L^2 & 0 & 0 & 0 & 3L & 0 & 4L^2 & \\
0 & 3L & 0 & 0 & 0 & -L^2 & 0 & -3L & 0 & 0 & 0 & 4L^2
\end{bmatrix} \tag{A.14}$$

Symmetric

APPENDIX B. COMPUTER PROGRAMS

The methods developed in this work have been implemented in the **HYDRAS** series of computer programs. The program **HYDRAS** performs the linear Hydroelastic Response Analysis of Structures in the frequency domain. **HYDRAS** includes five programs **HYDRAS-2D**, **HYDRAS-MORISON**, **HYDRAS-COMPOSITE**, **HYDRAS-BASIC**, and **HYDRAS3D-I**. The program user's guide can be found in a separate report (Che, 1993).

B.1 HYDRAS-2D

The program **HYDRAS-2D** is the part of program **HYDRAS-I**, which is for linear two-dimensional hydroelastic analysis of floating structures in the frequency domain. This two-dimensional hydroelasticity is developed by using a consistent formulation based on the finite element method. The structure below the still water plane is modeled, by the finite element method, as a nonuniform beam subjected to hydrodynamic forces. Above the water surface, a three-dimensional model of the structure is possible. Strip theory is used to calculate the hydrodynamic coefficients and wave exciting forces. Hydrodynamic matrices for added mass and damping, and wave exciting force vectors are formed directly in the same manner as the structural mass matrix and structural force vector. The resulting coupled equations of motion are solved directly. The detailed description of this method can be found in Chapter 5. The method is applicable to slender floating structures with any stiffness distribution.

B.2 HYDRAS-MORISON

The program **HYDRAS-MORISON** is the part of program **HYDRAS-I**, which is for linear three-dimensional hydroelastic analysis of floating structures in the frequency domain. A three-dimensional frame model is used to represent the elasticity of the

structure. Morison's equation (Morison et al., 1950) is used to determine the fluid loading. This approach is applicable to structures which can be modeled by tubular members below the still water line. There is no restriction on the upper part of the structure. Morison's equation includes the effects of fluid acceleration and viscous form drag in terms of empirically determined coefficients. Since the three-dimensional potential problem is avoided, Morison's equation is an efficient method for VLFSs which use columns and pontoons below the still water line. In addition, the hydrostatic restoring stiffness matrices for frame element is also included in this method. The detailed description of this method can be found in Chapter 6.

B.3 HYDRAS-COMPOSITE

The program **HYDRAS-COMPOSITE** is for linear 2-D/3-D hydroelastic analysis of floating structures in the frequency domain. This approach uses a three-dimensional structural model and a two-dimensional fluid model. The method includes an accurate description of the structure by a three-dimensional structural model and the computational efficiency of a two-dimensional fluid model. Therefore, the responses are not limited to the beam-like response of traditional two-dimensional hydroelasticity. The detailed description of this method can be found in Chapter 7.

B.4 HYDRAS-BASIC

The program **HYDRAS-BASIC** is for linear 2-D/3-D hydroelastic analysis of floating structures in the frequency domain. This approach is identical to the one implemented in **HYDRAS-COMPOSITE**, except the deformations of the three-dimensional structural model is represented by 'basic modes' for the fluid potential calculations. The computational efficiency of a two-dimensional fluid model is used in this method. The detailed description of this method can be found in Chapter 7.

B.5 HYDRAS3D-I

The program **HYDRAS3D-I** is the first phase of a program for the three-dimensional hydroelastic analysis of floating structures in the frequency domain. The body-boundary conditions coupling the structure and fluid are calculated in this program. Quadrilateral fluid panels and quadrilateral thin shell elements are used for structural and fluid models, respectively. A one-to-one mapping between structural element and fluid panel is adopted in the program. Further development is necessary. The detailed description of this method can be found in Chapter 4.

REFERENCES

Baschieri, M. and Bellincioni P. (1991). 'Prestressed Concrete Floating Airport,' *Proceedings, First International Workshop on Very Large Floating Structures,* University of Hawaii, Honolulu, pp. 421-436.

Bathe, K. J. and Wilson, E. L. (1976). *Numerical Methods in Finite Element Analysis*, Prentice-hall, Inc., Englewood Cliffs, New Jersey, 528 pp.

Betts, C. V., Bishop, R. E. D., and Price, W. G. (1977). 'The symmetric Generalized Fluid Forces Applied to A Ship in A Seaway,' Phil. Trans. Royal Society, London, A255, pp. 241-280.

Bishop, R. E. D., and Price, W. G. (1974). 'On Modal Analysis of Ship Strength,' Phil. Trans. Royal Society, London, A255, pp. 241-280.

Bishop, R. E. D., and Price, W. G. (1976). 'On the Relationship between 'Dry Modes' and 'Wet Modes' in the Theory of Ship Response,' *J Sound and Vibration*, Vol. 45, No. 2, 157-164.

Bishop, R. E. D., and Price, W. G. (1979). *Hydroelasticity of Ships*, Cambridge University Press, Cambridge, U.K., 423 pp.

Blagoveshchensky, S. N. (1962). *Theory of Ship Motion,* Dover Publications Co., New York.

Bretz, G. McAllister, K. and Vaughters, T. (1991). 'Technological Alternatives to Overseas Basing- Concepts in Naval Offshore Basing,' *Proceedings, First International Workshop on Very Large Floating Structures,* University of Hawaii, Honolulu, pp. 379-395.

Burke, B. G. (1969). 'The Analysis of Semi-submersible Drilling Vessels in Waves,' *Proc. 1st Int. Offshore Tech. Conf.*, Houston, May, pp i-235 to I-241.

Carlsen, C. A. and Mathisen, J. (1980). 'Hydrodynamic Loading for structural Analysis of Twin Hull Semi-submersible,' *Computational Method for Offshore Structures*, ASME, New York, Vol. 37, pp. 35-48.

Chakrabarti S. K. (1987). *Hydrodynamics of Offshore Structures*, Computational Mechanics Publications, Southampton Boston.

Che, X. L., Riggs, H. R., Ertekin, R. C., Wu, Y. S., and Wang, M. L. (1992a). 'Two-Dimensional Analysis of Prying Response of Twin-Hull Floating Structures,' *Proc 2th Int Offshore and Polar Eng Conf*, San Francisco, Vol. 1, 187-194.

Che, X. L., Wang, D. Y., Wang, M. L., and Xu, Y. F. (1992b). 'Two-Dimensional Hydroelastic Analysis of Very Large Floating Structures,' *Marine Technology*, Vol. 29, No. 1, 13-24.

Che, X.L. (1993) 'HYDRAS User Guide: A Computer Program for Hydroelastic analysis of Floating Structures,' Department of Ocean Engineering, University of Hawaii, 79 pp.

Chow, P. Y., Lin, T. Y., Riggs, H. R. and Takahashi P. K. (1991). 'Engineering Concepts for Design and Construction of Very Large Floating Structures,' *Proceedings, First International Workshop on Very Large Floating Structures*, University of Hawaii, Honolulu, pp. 97-106.

Cook, R. D., Malkus D. S., and Flesha M. E. (1989). *Concepts and Applications of Finite Element Analysis*, John Wiley & Sons, Inc. New York, 630 pp.

Cruickshank, M. J. (1991) 'The Application of Very Large Floating Structures in Marine Minerals Development,' *Proceedings, First International Workshop on Very Large Floating Structures*, University of Hawaii, Honolulu, pp. 397-403.

Curphey, R. M. and Lee C. M. (1977). 'Theoretical Prediction of Dynamic Wave Loads on Small-Waterplane-Area, Twin-hull Ship,' Report No. DTNSRDC 77-0061, Naval

Ship R&D Center, Bethesda, Md.

Du, X. S. and Ertekin, R. C. (1991). 'Dynamic Response Analysis of a Flexibly Joined, Multi-Module Very Large Floating Structure,' Proceedings, OCEANS's 91 Conf., IEEE, Honolulu, Oct., 3, 1286-1293.

Ertekin, R. C., Riggs, H. R., Seidl, L. H. and Wu, Y. S. (1990). 'The Design and Analysis of Very Large Floating Structures (VLFS): Vol. 2-Analysis,' Rep. No. UHMOE-90106, Dept. of Ocean Eng., Univ. of Hawaii at Manoa, June, 1990, 89 pp.

Ertekin, R. C., and Riggs, H. R. Editors, (1991). *Proceedings, First International Workshop on Very Large Floating Structures,* University of Hawaii, Honolulu, 436 pp.

Ertekin, R. C. Wang, M. L. and Riggs, H. R. (1991). 'Response of Flexible Floating-Structure Modules in Regular and Irregular Waves,' *Proc. of the Int. Symp. on Marine Structures*, ISMS '91 (ISSC '91 Pre-Congress Symp.) Ed. Xinsen Lu, September, Shanghai, pp. 75-80.

Ertekin, R. C., Riggs, H. R., Che, X. L. and Du, S. X. (1993). 'Efficient Methods for Hydroelastic Analysis of Very Large Floating Structures,' *Journal of Ship Research*, Vol. 37, No. 1, March, pp. 58-76.

Faltinsen, O. M. and Michelsen, F. C. (1974). 'Motions of Large Structures in Waves at Zero Froude Number,' *Proc. Int. Symp. on the Dynamics of Marine Vehicles and Structures in Waves* Univ. College London, pp. 91-106.

Flax, A. H. (1960). 'Aero and hydroelasticity,' in *Structural Mechanics*, Eds. J. N. Goodier & N. J. Hoff, Pergamon Press, New York, 94-159.

Frank, W. (1967). 'Oscillation of Cylinders in or Below the Free Surface of Deep Fluids,' NSRDC Report 2375, Naval Ship R&D Center, Bethesda, Md.

Frank, W. and Salvesen, N. (1970). 'The Frank Close-Fit Ship-Motion Computer

Program,' NSRDC, Washington D.C., Report 3289, June, Vii+131 pp.

Garrison, C. J., 'Hydrodynamic Interaction of Waves with a Large Displacement Floating Body,' Rep. No. NPS-69Gm77091, Naval Postgraduate School, Monterey, August, 157 pp.

Garrison, C. J. (1984). 'Interaction of Oblique Waves with an Infinite Cylinder,' *Applied Ocean Research*, Vol. 6, No. 1, 1984, pp. 4-15.

Garritsma, J. and Beukelman, W. (1964). 'The Distribution of the Hydrodynamic Forces on a Heaving and Pitching Ship Model in Still Water,' *5th Symposium on Naval Hydrodynamics,* Washington D.C., pp. 219-251.

Georgiadis, C. (1981). 'Wave Induced Vibrations of Continuous Floating Structures,' Ph.D. Dissertation, University of Washington, Seattle, WA.

Hamida, M. ben and Webster, W. C. (1991). 'The motion of Large Floating Flexible Structures,' *Proceedings, First International Workshop on Very Large Floating Structures,* University of Hawaii, Honolulu, pp.331a-331p.

Hartz, B. J. and Georgiadis, C. (1982). 'A Finite Element Program for Dynamic Response of Continuous Floating Structures in Short-Crested Waves,' *Proceedings, International Conf. on Finite Element Methods*, Shanghai, pp. 493-498.

Heller, S. R. and Abramson H. N. (1959). 'Hydroelasticity: A New Naval Science,' *J. Am. Soc. Naval Engrs.*, Vol. 71, No. 2, pp. 205-209.

Heller, S. R. (1964). 'Hydroelasticity,' in *Advances in Hydroscience*, Ed. Ven Te Chow, Vol. 1, Academic Press, New York, 1964, 94-159.

Jacobs, W. R. (1958). 'The Analytical Calculation of Ship Bending Moment in Regular Waves,' *J Ship Research.* Vol. 2, 13-57.

Kallio, J. A. and Ricci, J. J. (1976). 'Seaworthiness Characteristics of A Small Waterplane Area Twin Hull (SWATH IV) Part II,' Report No. DTNSRDC SPD 620-

02, Naval Ship R&D Center, Bethesda, Md.

Katory, M. 'On the motion Analysis of Interlinked Articulated Bodies floating Among Sea Waves,' The Naval Architect, No. 1, pp. 28-29.

Kim, C. H. and Chou, F. (1973). 'Motion of Semi-submersible Drilling Platform in Head Seas,' *Marine Technology*, Vol. 1, No. 2, pp. 28-29.

Kito, F., *Principles of Hydroelasticity*, Keio University, Japan, April, 1970, iii+124pp.

Korvin-Kroukovsky, B. V. and Jacobs, W. R. (1957). 'Pitching and Heaving Motion of a Ship in Regular Waves,' *Trans SNAME* Vol. 65, pp. 3-11.

Langen, I. and Sigbjornesson, R. (1983). 'On Stochastic Dynamics of Floating Bridges,' *Engineering Structures*, Vol. 2, pp. 209-216.

Lee, C. K. and Lou, J. Y. K. (1989). 'The hydroelastic effects on three-dimensional structural dynamics,' *Ocean Engng.*, Vol. 16, No. 4, pp.327-342.

Lemke, E. (1987). 'Floating Airport,' Concrete International, May, pp. 37-41.

Luft, R. W. (1981). 'Analysis of Floating Bridges: The Hood Canal Bridge,' *Proceedings, Dynamic Response of Structures*. pp. 1-15.

Morison, J. R., O'Brien, M. P., Johnson, J. W. and Schaff, S. A. (1950) 'The Force Exerted by Surface Waves on Piles,' *Petroleum Transactions, AIME*, Vol. 189, 1950, 149-154.

Masuda, K., Maeda, H., Usui, M., and Kato, W., (1987). 'Dynamic Response by Shallow Draft Floating Elastic Structures in Head Waves,' *Proc. 6th off. Mech. & Arc. Eng. Conf.*, Houston, pp. 337-344.

Newman, J. N. (1977) *Marine Hydrodynamics*, The MIT press, Cambridge, Massachusetts and London, England.

Newman, J. N. (1978) 'The theory of Ship Motions,' *Advance in Applied Mechanics*, Vol. 18, 221-283.

Newman, J. N. (1986) 'Distributions of Sources and Normal Dipoles over A Quadrilateral Panel,' *J. of Engineering Mathematics*, Vol. 20, pp. 113-126.

Nihous, G. C. and Vega L. A. (1993) 'Design of a 100 MWe OTEC-Hydrogen Plantship,' *Marine Structures*, Vol. 6, pp. 207-221.

Ogilvie, T. F. and Tuck, E.O, (1969). 'A Rational Strip Theory of Ship Motions, Part I,' Interim Technical Report No. 013, Dept. of Naval Arch. and Marine Eng., University of Michigan, also AD-682507.

Ogilvie, T. F. (1971). 'On the Computation of Wave-Induced Bending and Torsion Moments,' *J Ship Research*, September, 217-220.

Okamoto, K., Masuda, K., and Kato, W. (1985). 'Hydroelastic Response Analysis for Large Floating Structures,' *Proc. Int. Symp. on Ocean Space Util.*, Tokyo, pp. 275-281.

Paz, M. (1985). *Structural Dynamics,* Van Nostrand Reinhold Company, 561 pp.

Price, W. G., and Wu, Y. S. (1985). 'Hydroelasticity of Marine Structures,' *Theoretical and Applied Mechanics*, F. I. Niordson and N. Olhoff, eds., Elsevier Science Publishers B.V., 311-337.

Paulling, J. R. (1970). 'Wave Induced Forces and Motions of Tubular Structures,' *Proc. 8th Symp. on Naval Hydrodynamics,* Pasadena, California, pp. 1083-1110.

Paulling, J. R. and Tyagi, S. (1991) 'Multi-Module Floating Ocean Structures,' *Marine Structures*, Vol. 6, pp. 187-205.

Rao, S. S. (1989). *The Finite Element Method in Engineering,* 2nd Edition, Pergamon Press, 643 pp.

Riggs, H. R., Che, X. L., and Ertekin, R. C. (1991). 'Hydroelastic Response of Very Large Floating Structures,' *Proc 10th Int Conf Offshore Mech Arctic Eng*, Stavanger, ASME, Vol. 1A, 291-300.

Riggs, H. R. (1991). 'Current Efforts in Technology Development for Very Large Floating Structures,' Proceedings, OCEANS's 91 Conf. IEEE, Honolulu, Oct., 3, 201-206.

Riggs, H. R. and Ertekin, R. C. (1993). 'Approximate Methods for Dynamic Response of Multi-Module Floating Structures,' *Marine Structures*, Vol. 6, 117-141.

Salvesen, N., Tuck, E. O., and Faltinsen, O. (1970). 'Ship Motions and Sea Loads,' *Trans SNAME*, Vol. 78, 250–287.

Seidl, L. H. (1991). 'Iterative Source Distribution Technique,' *Proceedings, First International Workshop on Very Large Floating Structures,* University of Hawaii, Honolulu, pp. 171-190.

Smith, W. E. (1967). 'Computation of Pitch and Heave Motions for Arbitrary Ship forms,' *Int. Shipbldg. Prog.*, Vol. 14, No. 155, pp. 267-291.

Smith, W. E. and Salvesen (1970). 'Comparison of Ship Motion Theory and Experiment for Destroyer with Large Bulb,' *J. of Ship Research*, Vol. 14, No. 1, pp. 67-76.

Spark, C. P. (1984). 'The influence of Tension, Pressure, and Weight on Pipe and Riser Deformation and Stresses,' *J. Energy Resources Tech.*, ASME, 1984, Vol. 106, pp. 46-54.

St. Denis, M. and Pierson, W. J. (1953). 'On the Motion of Ships in Confused Seas,' *SNAME Trans.*, Vol 61, pp. 280-357.

St. Denis, M. (1974). 'The winds, Current and Waves at the Site of the Floating City off Waikiki,' Report Seagrant-CR-75-01, Technical Report No. 1, University of Hawaii at Manoa, Honolulu, HI.

Takarada, N. (1984). 'Technical Study Results of Floating Runway for Night Landing Practice of Carrier-Borne Planes,' Report of the Shipbuilders' Association of Japan.

Tasai, F. (1967). 'On the Swaying, Yawing and Rolling Motions of Ship in Oblique

Waves,' *International Shipbldg. Prog.* Vol. 14, No. 153, pp. 216-228.

Vugts, J. H. (1971). 'The hydrodynamic forces and ship motion in oblique waves,' Netherlands, Ship Research Center TNO, Report No. 15OS.

Wang, D. Y., Riggs, H. R. and Ertekin, R. C. (1991). 'Three-Dimensional Hydroelastic Response of A Very Large Floating Structure,' *International J. of Offshore and Polar Engineering,* Vol. 1, No. 4, December, pp. 307-316

Wang, M. L. (1991). 'A Hybrid Approach to the Hydroelastic Analysis of Very Large Floating Structures,' MS Thesis, Dept. of Ocean Eng, Univ of Hawaii at Manoa, Honolulu, 191 pp.

Wang, M. L., Du, S. X., and Ertekin, R. C. (1991). 'Hydroelastic Response and Fatigue Analyses of a Multi-Module Very Large Floating Structure,' *Fatigue and Fracture in Steel and Concrete Structures,* Proc. of ISFF'91, Vol 2, Oxford & IBH Pub. Co., Bombay, 1277-1291.

Wehausen, J. V. and Laitone, E. V. (1960). 'Surface Waves,' Ed. by S. Flügge, *Handbuch der Physik,* Band 9, Springer Verlag, pp. 446-776.

Wilkins G. A., Ertekin, R. C. and Riggs H. R. editors, (1992). 'Future Directions in VLFS Research and Development,' *Proceedings, First International Workshop on Very Large Floating Structures,* Vol. 2, University of Hawaii, Honolulu, 42 pp.

Winkler, R. S., Seidl, L. H., Riggs, H. R., Ertekin, R. C. and Wilkins, G. A. (1990). 'The Design and Analysis of Very Large Floating Structures (VLFS): Vol. 1 Design,' Rep. No. UHMOE-90105, Dept. of Ocean Engng., University of Hawaii, June, 114 pp.

Wu, Y. S. (1984). 'Hydroelasticity of Floating Bodies,' Ph.D. thesis, Brunel University, 430 pp.

Wu, Y. S., Wang, D. Y., Riggs, H.R. and Ertekin, R. C. (1993). 'Composite Singularity Distribution Method with Application to Hydroelasticity,' *Marine Structures*, Vol. 6,

pp. 143-163.

Yeung, R. W. (1973). 'A Singularity Distribution Method for Free Surface Flow Problem,' Rep. No. NA-73-6, Dept. of Naval Architecture, University of California, Berkeley, vi+124 pp.

Yoshida, K., Arima, T., Goo. J. S. and Oka N. (1991) 'A Conceptual Design of a Huge Ring-Like Semisubmersible,' *Proceedings, First International Workshop on Very Large Floating Structures,* Vol. 1, University of Hawaii, Honolulu, pp. 397-403.